Title

Reconstruction of Ancient Production Technology of Chinese Blue Pigment and Synthesis of Chinese Blue Nanoscrolls as a Novel Optical Material

Author

Lin, Yuan

Publication Date

2018

Peer reviewed|Thesis/dissertation

UNIVERSITY OF CALIFORNIA

Los Angeles

Reconstruction of Ancient Production Technology of Chinese Blue Pigment and Synthesis of Chinese Blue Nanoscrolls as a Novel Optical Material

A thesis submitted in partial satisfaction

of the requirements for the degree Doctor of Philosophy

in Materials Science and Engineering

by

Yuan Lin

2018

ABSTRACT OF THE THESIS

Reconstruction of Ancient Production Technology of Chinese Blue Pigment and Synthesis of Chinese Blue Nanoscrolls as a Novel Optical Material

by

Yuan Lin

Doctor of Philosophy in Materials Science and Engineering

University of California, Los Angeles, 2018

Professor Ioanna Kakoulli, Chair

Technological inventions and innovations in ancient societies can be unmasked through the systematic study of surviving artifacts. Through the application of materials science and engineering principles and probing at the atomic and submicron scale, this research has a twofold goal: 1) to re-evaluate the production technology and raw material selection for the manufacture of the oldest synthetic blue pigment in China's history, Chinese blue (CB) with major crystal phase $BaCuSi_4O_{10}$, in order to infer materials and technological choices and

determination of production events, as well as the relationships of these choices to the social and craft organization of ancient societies, and 2) to harness the unique stable visible-induced near infrared (NIR) luminescence properties of $BaCuSi_4O_{10}$ at the nanoscale through hydrothermal synthesis of $BaCuSi_4O_{10}$ nanoscrolls, and to explore its potential application as novel optical material and fluorescent marker.

Results from the analysis of Chinese blue at the micron to submicron level with scanning transmission electron and transmission electron microscopy coupled with energy dispersive X-ray spectroscopy (STEM/TEM-EDS) revealed the presence of micron or submicron-sized $BaSO_4$, $(Ba,Pb)SO_4$ solid solution, Pb_3O_4, and amorphous SiO_2 inclusions whose formation are closely related to raw materials selection and manufacturing processes. Based on possible formation mechanisms and systematic laboratory-based reproduction experiments of Chinese blue and Chinese purple, the rarer mineral witherite ($BaCO_3$) seems to have been used as the source of Ba, though the presence of $BaSO_4$, a more abundant mineral, as an impurity in the witherite deposits could not be ruled out. For the Pb and S accounted in the ancient pigment samples, galena (PbS) and/or anglesite ($PbSO_4$) may have been used as sources. The direct use of galena (PbS) has shown to pose difficulty in the production of Chinese blue and purple, requiring a pre-treatment step. The ancient contemporary bronze and $PbO\text{-}BaO\text{-}SiO_2$ glass production as well as alchemical and medicinal practices based on Pb-containing compounds, may have provided the technological bases for the transformation of galena into other Pb-compounds such as $PbSO_4$, PbO, or $PbCO_3$ that could lead to the successful production of

Chinese blue or Chinese purple pigments.

Pb stable isotope analysis by laser ablation inductively multi-collector coupled plasma mass spectrometry (LA-MC-ICP/MS) suggested that the Pb-source used in the production of the Chinese blue and Chinese purple faience beads analyzed, is the same or similar to other Chinese blue and Chinese purple pigment samples analyzed previously, as well as to contemporary PbO-BaO-SiO_2 glasses.

$BaCuSi_4O_{10}$ nanoscrolls with length < 500 nm have been synthesized under hydrothermal conditions. The purity and morphology of the $BaCuSi_4O_{10}$ nanoscrolls was strongly dependent on the synthesis temperature and time, as well as the pH of the precursor mixture. Visible light induced near infrared (Vis-induced NIR) imaging indicated that the $BaCuSi_4O_{10}$ nanoscrolls preserve the characteristic NIR luminescence of the bulk materials. The nanoscrolls are likely to have formed through a rolling mechanisms of $BaCuSi_4O_{10}$ nanosheets during the hydrothermal synthesis, affected by the heat treatment conditions and the pH of the precursor mixture.

The dissertation of Yuan Lin is approved.

Bruce S. Dunn

Katherine Faber

Mark S. Goorsky

Timothy Mark Harrison

Ioanna Kakoulli, Committee Chair

University of California, Los Angeles

2018

To my family and friends

TABLE OF CONTENTS

LIST OF TABLES

LIST OF FIGURES

ACKNOWLEDGEMENTS

First of all, I would like to express my gratitude to my advisor Prof. Ioanna Kakoulli for her expertise guidance and continual encouragement, which has made my doctoral studies at UCLA so fruitful and enjoyable. I am deeply grateful for all the time that she has dedicated to me, for all the support that she has offered to me, and for all the rigorous academic knowledge and research skills she has taught me. I would also like to express my gratitude to Prof. Bruce S. Dunn, Prof. Katherine Faber, Prof. Mark S. Goorsky and Prof. Timothy Mark Harrison for serving on my committee and providing me valuable and insightful comments and suggestions.

I would like to thank the co-directors of the Archaeomaterials Group and the Molecular and Nano Archaeology Laboratory, Prof. Christian Fischer and Prof. Sergey Prikhodko, as well as my current and former group members, Dr. Magdalena Balonis-Sant, Vanessa Muros, Dr. Xiao Ma, Roxanne Radpour, Karime Castillo, Krystal Cunningham, Xuanyi Wu, Thomas Tran, Vivian Ly, Haroula Kyriacou, Lindsey Perry, Moupi Mukhopadhyay, Aileen Shin, Tianchi Liu, and Xinghong Tang. I would also like to thank visiting scholars, Prof. Xiaoqi Wang from Nanjing University (China), Prof. Guofeng Wei from Anhui University (China), Prof. Pujun Jin from Shaanxi Normal University (China), Prof. Celestino Grifa from Università degli Studi del Sannio (Italy), and Prof. Santiago Sanchez-Cortes from Institute of Structure of the Matter in CSIC (Spain), for their insightful research discussions and suggestions.

I would like to thank Dr. Qiulong Wei, David Ashby, Christopher Choi, and Dr. Matt Chunhan Lai from Prof. Bruce S. Dunn's group for their help with the hydrothermal synthesis

of Chinese blue nanoscrolls. I would like to thank Dr. Patrick Boehnke from the UCLA Earth, Planetary, and Space Sciences (EPSS) Department for introducing me to stable isotope analysis, as well as Dr. Rosario Esposito from the Electron Microprobe Laboratory (EPSS) for his help with the SEM-WDS analysis.

I would like to thank the administrative staff of the UCLA Materials Science and Engineering Department, especially Lili Bulhoes. I would also like to thank Amber Cordts-Cole, the former administrative staff of the UCLA/Getty Conservation Interdepartmental Program.

I would like to thank Laboratoire d'Archéologie Moléculaire et Structurale (LAMS), CNRS-Sorbonne Universités-UMR 8220, and Centre for Nanosciences and Nanotechnology (C2N), CNRS/Paris Sub University-UMR 9001, for supporting part of my Ph.D. research during my stay in Paris as a Chateaubriand Fellow. I am deeply grateful to Prof. Philippe Walter (LAMS) and Dr. Gilles Patriarche (C2N) for their research supervision and guidance. I would also like to thank Prof. Maguy Jaber (LAMS) for her help on the hydrothermal synthesis. I would like to thank my friends and colleagues at LAMS, Dr. Matthias Alfeld, Dr. Silvia Pedetti, Dr. Marlène Aubin, Dr. David Guillermin, Leila Galai, and Hélèn Glanville, for their support, as well as all the fun we had in Paris.

I would like to thank the Center for Materials Research in Archaeology and Ethnology (CMRAE) and the Materials Science and Engineering Department at Massachusetts Institute of Technology (MIT), for supporting part of my Ph.D. research during my stay at MIT as a

visiting research student. I am deeply grateful to Prof. Heather Lechtman, Dr. William Gilstrap, Michael Tarkanian, and Matthew Chastain for their research support on the reconstruction experiment of Chinese blue and Chinese purple.

I would like to thank my friends at UCLA, especially Dr. Dian Yu, Dr. Noah Bodzin, Dr. Chilan Ngo, Dr. Dean Cheikh, Fangyi Guan, Tingyu Bai, as well as my roommate, Xinke Yu, and her dog, Stony, for their support. I would also like to thank my friends outside UCLA, especially Dr. Zhihong Tan, Dr. Zhihao Zhang, Minqian Liang, Doreen Zhiyu Dong, Nora Xiaobo Luo, Tingting Zhang, and Jessie Yuan-Chun Han, for their long-term support and encouragement.

I will be ever grateful to Bobbie Saenz, not only for her support during my difficult time as a new immigrant in the United States, but also for her encouragement during my undergraduate and graduate studies. Her memory will be with me always.

Finally, I would like to thank my parents, my grandparents, as well as my boyfriend, Dr. Chao Li, for their love, support and encouragement.

VITA

2011	Bachelor of Science in Chemistry, University of California, Berkeley
2011-2013	Lab technician, Research and Development, Behr Process Corporation
2013-present	Graduate student researcher, Materials Science and Engineering Department, UCLA
2015-2016	Chateaubriand Fellowship for STEM for 2015-2016 year, Embassy of France in the United States
2017	John Anson Kittredge Fund
2017-2018	Dissertation Year Fellowship, UCLA
2018	Student presentation contest, 2nd place, Southern California Society for Microscopy and Microanalysis Symposium, Spring 2018

PUBLICATIONS

1. **Lin, Y.,** T. Liu, M.K. Toumazou, D. Counts, I. Kakoulli, “Chemical analyses and production technology of archaeological glass from Athienou-*Malloura*, Cyprus.” *Journal of Archaeological Science, Reports*, 23 (2019):700-713.
2. Castillo, K. and **Y. Lin**, “Glass and Faience” in *The SAS Encyclopedia of Archaeological Sciences*, editor-in-chief: Sandra L. López Varela, Wiley: Blackwell 2018.
3. Kakoulli, I, R. Radpour, **Y. Lin**, M. Svoboda, C, Fischer, “Application of forensic photography for the detection and mapping of Egyptian blue and madder lake in Hellenistic polychrome terracottas based on their photophysical properties.” *Dyes and Pigments*, 13 (2017):104-115.
4. Muros, V., N. Little, **Y. Lin**, and P. Boehnke. “Down in the dumps: Analysis of glass production debris from Petrie’s excavations at Amarna.” In: Owczarek, N., M. Gleeson and L. Grant. *Engaging Conservation: Collaboration Across Disciplines.* London: Archetype Books, 2017.

Chapter 1. Introduction and thesis outline

Chinese blue, the earliest synthetic blue pigment in China's history, emerged for the first time in the Warring States Period (475-221 BC) and was used until the Eastern Han Dynasty (AD 25-220) [7-10]. Chinese blue is a highly stable synthetic barium copper silicate pigment, composed of different compounds (**Figure 1-1**), each of which is associated with its raw materials and production process: 1) a crystalline barium copper tetrasilicate phase with chemical formulas of $BaCuSi_4O_{10}$; 2) unreacted quartz from the silica source; 3) Pb-rich crystalline or amorphous compounds resulting from the use of Pb-containing flux materials to lower the melting temperature of silica and other raw materials; and 4) Ba-rich crystalline or amorphous phases [8].

Despite its importance and value, there are no surviving recipes for the production of Chinese blue and the original raw materials selection and synthesis conditions remain unknown. Besides its archaeological significance, $BaCuSi_4O_{10}$, the main crystalline component of Chinese blue, also shows a high luminescence yield in the near infrared (NIR) region with emission centered at ~980 nm when excited by red light (~600 nm) [11]. With emission in the biomedical imaging window (650-1450 nm) where tissue penetration is the greatest, this material presents itself as a potential fluorescent marker. Recent studies have shown that

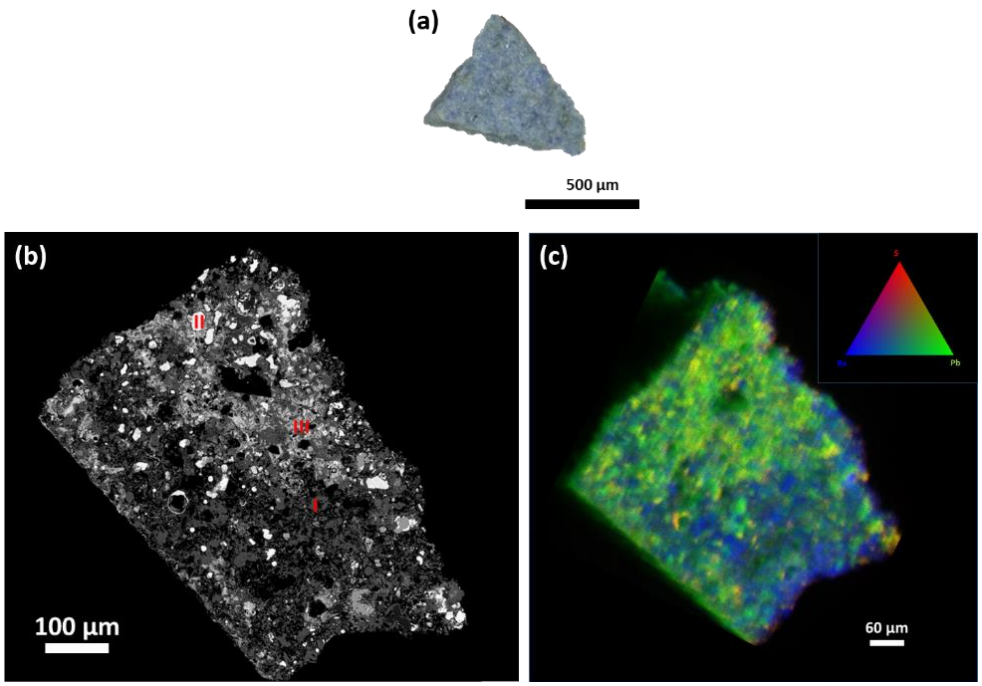

Figure 1-1. (a) A photomicrograph of a Chinese blue sample from a pigment stick, Han Dynasties, courtesy: Freer and Sackler Galleries. (b) A BSE micrograph of the cross section of the Chinese blue sample, showing compositional heterogeneity. I: $BaCuSi_4O_{10}$ crystals. II: $PbO\text{-}SiO_2$ glass. III: $PbO\text{-}BaO\text{-}SiO_2$ glass. (c) A tri-color synchrotron radiation-based X-ray fluorescence (SR-XRF) elemental mapping of the Chinese blue sample with distribution of Ba, Pb and S, showing compositional heterogeneity.

$BaCuSi_4O_{10}$ can be delaminated into monolayer nanosheets [12], which renders it suitable for applications as optical nanomaterials. Owing to these new determinations, the second part of this research explores the synthesis of nanoscrolls of $BaCuSi_4O_{10}$ and its potential as a novel NIR luminescent optical material and fluorescent marker.

From the materials science perspective this research aims to reconstruct ancient production technology of Chinese blue to reveal raw materials selection and synthesis conditions. This is achieved through: 1) the analysis of archaeological Chinese blue pigments; 2) reproduction experiments to re-create the pigment using modern methods and 3) geosourcing of the raw materials. From a materials engineering perspective and harnessing the stable visible light-

induced NIR photoluminescence property of Chinese blue pigment, this research aims to synthesize nanoscale $BaCuSi_4O_{10}$ as optical materials for biomedical and other applications. As such, the research goals are addressed in the various chapters as described below.

In Chapter 2, a systematic literature review on the production technology and photophysical properties as well as the state of the art on studies of Chinese blue and the chemically related Chinese purple are presented. In Chapter 3, current analytical challenges are discussed and results from the analysis of ancient Chinese blue samples at the micron and submicron scale using aberration corrected scanning transmission electron microscopy and transmission electron microscopy (STEM/TEM) coupled with energy dispersive X-ray spectroscopy (EDS) are presented. This chapter presents new data on the atomic arrangement and elemental composition of very small crystallites (< 2 μm) and polymorphs (byproducts of the pigment's production) through electron diffraction patterns and EDS, inferring materials and technological choices. Chapter 4, presents and discusses the results from systematic reproduction experiments of Chinese blue and Chinese purple, with a focus on testing the effects of different combinations of Ba-sources ($BaSO_4$ and $BaCO_3$) and Pb-sources (PbO, $PbCO_3$, $PbSO_4$ and PbS) as raw materials for the synthesis of the pigments. In order to establish the boundary of synthesis conditions for each combination of raw materials, heat treatments were performed in the range of 800-1000 ˚C with every 50 ˚C increment, for 6 hours to obtain the kinetic products, and 24 hours to obtain the most thermodynamically stable products. In Chapter 5, geosourcing of the Pb-source used in the original production of a Late Warring

Chinese blue faience bead will be performed based on Pb stable isotope analysis with laser ablation multi-collector inductively coupled plasma mass spectrometry (LA-MC-ICP/MS). In Chapter 6, the hydrothermal synthesis of $BaCuSi_4O_{10}$ nanoscrolls is presented. Factors affecting the growth and morphology of the $BaCuSi_4O_{10}$ nanoscrolls and the possible formation mechanisms are discussed.

Chapter 2. State of the art on studies of Chinese blue and Chinese purple

2.1 Early studies on $BaCuSi_4O_{10}$ and $BaCuSi_2O_6$

Early studies of $BaCuSi_4O_{10}$, the main crystalline phase in Chinese blue, compared to its chemically analogue $CaCuSi_4O_{10}$, the principle component of Egyptian blue, is much less abundant. The latter is the earliest known synthetic pigment of which production can be traced back to the fourth millennium BC and was used extensively as the main blue pigment until the Late Antiquity [8, 13-23]. In 1899, in an effort to make green, blue and purple barium silicates, Le Chatelier successfully synthesized $BaCuSi_4O_{10}$ by firing a mixture of $BaCO_3$, CuO, SiO_2, (with Ba:Cu:Si = 1:1:4) and Na_2O-based flux at 1050 ˚C [24]. Following, in 1959, in a study on structures of $CaCuSi_4O_{10}$ together with other members in the $MCuSi_4O_{10}$ (M=Ca, Ba, Sr) family, Pabst made crystals of $BaCuSi_4O_{10}$ by sintering pellets of $BaCO_3$, CuO and amorphous silica in the proportions of 1:1:4 with 10% of borax flux at 800 ˚C for one day and determined its crystal structure [25]. The crystal structure of $BaCuSi_4O_{10}$ was further refined by various other scholars [26-28]. In 1975, based on the successful synthesis of $CaCuSi_4O_{10}$, G. Bayer and H. G. Wiedemann produced $BaCuSi_4O_{10}$ crystals using CuO, SiO_2 and $BaCO_3$, using different fluxes such as borax, $NaNO_3$, Na_2CO_3 and Li_2CO_3 and firing conditions at a temperature between 850 and 900 ˚C [29]. In 1994, a new mineral, named ‘effenbergerite’, was discovered in the Kalahari Manganese Field in South Africa, and was determined as the natural analog to the synthetic $BaCuSi_4O_{10}$ [30].

While there are only a few studies on Chinese blue, there are numerous publications on the analysis of the structure and properties of $BaCuSi_2O_6$, the main component in Chinese purple, another Chinese ceramic pigment. It seems that its study began with its accidental formation and discovery in the search of superconductors in the Tl-Ca-Ba-Cu-O system [31-34]. During initial attempts to form the desired Tl-Ba-Ca-Cu-O superconductors, oxide precursors of Cu and Ba reacted with the silica sample container, forming a thin coating of two silicate phases, one of which was determined as $BaCuSi_2O_6$, a cyclosilicate with four-membered tetrahedral rings [34]. In another study on the chemical reactivity of the '1-2-3' type superconductors, crystals of $BaCuSi_2O_6$ (referred to as '$Ba_2Cu_2[Si_4O_{12}]$' by the authors) were also formed with the reaction of $YBa_2Cu_3O_{7-x}$, PbO and Na_2O_2 and the quartz tube walls when fired at high temperatures [35]. In 2013, a new mineral from the Kalahari Manganese Field in South Africa, whose crystal structure was later determined to be identical to $BaCuSi_2O_6$ [36] was identified and named 'colinowensite' [37, 38].

2.2 Reconstruction of production technology of Chinese blue and Chinese purple

Despite the early production and structural studies of $BaCuSi_4O_{10}$ and $BaCuSi_2O_6$ within a context of modern materials chemistry and geology, these two crystals were first mentioned on archaeological objects in 1983 and 1992, respectively [39, 40]. FitzHugh and Zycherman confirmed the presence of these compounds by XRD as the major crystalline phases of Chinese blue and Chinese purple, respectively [39, 40]. Since then, owing to their archaeological and

historical importance and technological significance, a lot of research was conducted on Chinese blue and Chinese purple, in order to reconstruct their production technology and social context associated with their invention and manufacture. Most studies involved characterization of archaeological samples and laboratory-based reproduction experiments.

2.2.1 Identification and characterization of archaeological Chinese blue and Chinese purple samples

The identification and characterization of Chinese blue and Chinese purple found on archaeological objects have mainly been carried out using laboratory-based instruments that have spatial resolution from the macro to micron scale. Elemental composition has been commonly determined by energy dispersive X-ray spectroscopy (EDS) [9, 22, 39, 41-52], electron probe micro analyzer (EPMA) [39, 40, 49, 50], X-ray fluorescence (XRF) [44, 53-58], laser ablation inductively coupled plasma mass spectrometry (LA-ICP-MS) [49, 50] and emission spectrographic analysis [59]. Structural and molecular information has been obtained by micro-Raman spectroscopy (μRS) [7, 9, 22, 41, 42, 44-51, 53-58, 60, 61], powder or micro X-ray diffraction (μXRD) [22, 39, 40, 46, 47, 49, 51, 58, 59, 62, 63] and Fourier-transform infrared (FTIR) spectroscopy [44, 49]. A few studies used polarized light microscopy (PLM) [7, 42, 45, 54] to identify the presence of these two pigments based on their specific optical appearance. Some studies also employed microstructure investigation, carried out by secondary emission scanning electron microscopy (SE-SEM) and back scattered emission scanning

electron microscopy (BSE-SEM) [9, 39, 41, 43-51]. Synchrotron radiation-based X-ray techniques with high specificity has also been performed on a Chinese purple sample from a Terracotta Warrior, from the famous site of the Terracotta Army in X'ian, China, in an attempt to obtain compositional and structural data that yielded information related to its invention and production [43].

Besides Chinese blue and Chinese purple, on archaeological samples, Chinese dark blue, $BaCu_2Si_2O_7$, another stoichiometric ternary member in the barium copper silicate system [64, 65], has been found to be present in small amounts [7, 45-47, 55, 57, 58]. Its natural analog, mineral scottyite, was also found in the Kalahari Manganese Field in South Africa [66]. $BaCuSi_4O_{10}$ (Chinese blue, CB), $BaCuSi_2O_6$ (Chinese purple, CP), $BaCu_2Si_2O_7$ (Chines dark blue, CDB), together with $Ba_2CuSi_2O_7$ [67, 68], a compound that has not yet been identified on archaeological objects, are four stoichiometric ternary phases confirmed to exist in the BaO-CuO-SiO_2 system. A progressive silicate condensation model has been proposed for the formation sequence of the three archaeologically significant barium copper silicates, from orthosilicate, SiO_4^{4-}, the basic tetrahedral structural unit, to disilicate, $Si_2O_7^{6-}$, the silicate building block for Chinese dark blue ($BaCu_2Si_2O_7$), to cyclotetrasilicate, $Si_4O_{12}^{8-}$, the silicate building block for Chinese purple ($BaCuSi_2O_6$), and to the eight-membered ring units $Si_8O_{20}^{8-}$, the silicate framework for Chinese blue ($BaCuSi_4O_{10}$) [9]. Based on this model, Chinese dark blue and $Ba_2CuSi_2O_7$ are expected to be formed as initial kinetic products, then Chinese purple as an intermediate product, and finally Chinese blue as the most thermodynamically stable

product of this silicate condensation process [9]. Therefore, the final product(s) from the synthesis of barium copper silicate depend on multiple factors, such as the relative proportions among the precursors for Ba, Cu and Si, the firing temperature, and the duration of firing. In fact, Chinese blue and Chinese purple are often found to coexist, with one of them being the predominant crystalline phase and the other as a minor phase. Chinese dark blue has been found to be present in very small amounts, together with Chinese blue and/or Chinese purple on archaeological objects. Thus far, it has not been identified as an individual pigment [49].

In addition to the major crystalline phases that are responsible for the color of the pigment, the archaeological blue and purple compounds contain reaction residues and production byproducts, both crystalline and amorphous, depending on the raw materials and synthesis conditions. These vary across time periods and geographical locations. Unreacted SiO_2 [9, 41, 43, 45, 47-50, 53, 57, 58] are often found in archaeological Chinese blue or Chinese purple samples. Sometimes identified are Ba-rich crystalline phases such as $BaSO_4$ [7, 9, 22, 41, 47-49, 51, 57, 60], $BaSi_2O_5$ [7, 41, 48, 49, 57], $BaSiO_3$ [41, 48, 49], or $BaCO_3$ [9, 22, 60].

Notwithstanding of the variability in Si- and Ba-rich reaction residues and byproducts, in all archaeological Chinese blue and Chinese purple samples, Pb has also been detected. Pb amounts vary from a few wt% to over 90 wt% (expressed in PbO). Pb-containing precursors resulted in the formation of PbO-BaO-SiO_2, PbO-SiO_2, or PbO-CuO-SiO_2 glass, as well as in Pb-rich crystalline phases, either as byproducts from the synthesis or weathering products due to prolonged burial environments. These include $PbCO_3$ [7, 9, 22, 40, 41, 48, 49, 53, 57], $PbSO_4$

[9, 22, 60], $PbSiO_3$ [48, 57], $PbSO_4 \cdot PbO$ [51], PbO [7, 22, 60], $PbCO_3 \cdot PbCl_2$ [41], $Pb_5(PO_4)_3OH$ [40], or $Pb_9(PO_4)_6$ [40]. The prominent presence of Pb points to the possible use of Pb-containing flux to lower the melting temperature of SiO_2 [9, 22, 69]. The variability in the concentration of Pb found in archaeological samples might be due to the differences in the analytical techniques employed with various detection limits and accuracies, the differences in the forms of the archaeological samples (octagonal sticks, pigment on polychrome ceramics, glaze layer on faience beads, etc.), and the differences in the mode of analysis (spot analysis or bulk analysis) and the locations on the samples where Pb has been detected.

Studies by 夏寅, et al., and Berke et al. [45, 47], showed significant amounts of Sn, ranging from a few wt% to ~20 wt%, suggesting the use of slags of bronze as source of Cu in the production. In all other published data on Chinese blue and Chinese purple, Sn or Sn-containing phases were either not detected or were found in trace amounts (< 1%), pointing to the use of different sources of Cu. Other minor elements through elemental analyses that are often detected are Al, Fe, Ca, and P, most likely to be introduced into the final products as impurities associated with the major raw materials and/or contaminants from the burial environment [42, 43, 46, 51, 55, 56]. Minor phases such as $CaCO_3$ [53, 57], $CaSO_4$ [57], albite ($NaAlSi_3O_8$) [57], Al_2O_3 [57], and amorphous carbon [58] have also been identified in some studies of archaeological materials. Na was detected to be ~2.55% in one Chinese blue faience bead from the Late Warring States period, whereas, another sample does not contain any Na [50]. The authors suggested the possible intentional addition of Na-containing raw materials to

facilitate the formation of final product with less porosity and higher content of $BaCuSi_4O_{10}$, and argued a similar trend was also observed in Chinese purple faience beads samples, however without available data.

2.2.2 Laboratory-based reproduction experiments of Chinese blue and Chinese purple

Before the identification of $BaCuSi_4O_{10}$ [39] and $BaCuSi_2O_6$ [40] on archaeological objects, modern reproductions of these two pigments were mainly achieved by introducing various fluxes in modern ceramic and glass production that did not replicate ancient production technology [29]. Within an archaeological context, laboratory-based reproductions of $BaCuSi_4O_{10}$ have started within a scientific investigation of ancient Chinese PbO-BaO-SiO_2 glasses, which were manufactured about the same time as Chinese blue. Mixtures of $BaCuSi_4O_{10}$ and $BaCuSi_2O_6$ were successfully made either by devitrification of a glass having the stoichiometry of $CuO{\cdot}BaO{\cdot}4SiO_2$ or by heating dry batch materials though no information on the exact nature of the starting materials was reported [1, 70]. In this study, the presence and stoichiometry of $BaCuSi_2O_6$ was determined by EPMA in the end-products [1, 70], and later it was identified by XRD on archaeological objects [40]. In another study, the two pigments were reproduced using $BaSO_4$ or $BaCO_3$ as Ba-source, CuO or Cu_2S as Cu-source, SiO_2 as Si-source, with stoichiometry of Ba:Cu:Si to be 1:1:2, 1:1:4, 1:2:2, or 2:1:2, together with 3% Na_2CO_3, 5% PbO, or 10% NaCl as flux, fired at 900 ˚C, 1000 ˚C, or 1100 ˚C for 20 hours [69]. However, only selected results on some trials were presented, in which multiple phases in the end-

products were characterized only by XRD with no information on their microstructure or relative abundance.

In another study, reproduction experiments of Chinese blue and Chinese purple were performed using $BaSO_4$, $BaCO_3$ or BaO as Ba-source, malachite ($Cu_2(OH)_2CO_3$) or CuO as Cu-source, SiO_2 as Si-source, and orthorhombic PbO (massicot) as flux [71]. SiO_2 powder was put in between mixtures and corundum (Al_2O_3) crucibles in order to prevent formation of Al-containing phases. XRD was applied to characterize samples taken from the surface of the end-products. Starting materials, synthesis conditions, and characterization results on the end-products are summarized in **Table 2-1**. It was concluded that it was more difficult to obtain pure $BaCuSi_2O_6$ compared to pure $BaCuSi_4O_{10}$, mainly due to the higher chemical stability of $BaCuSi_4O_{10}$. It was also noted that a difference of 50 ˚C or 100 ˚C could result in the failure to obtain the desired copper barium silicate pigment and thus careful control of temperature was suggested.

Table 2-1. Summary of starting materials, synthesis conditions, and characterization results on the end-products of reproduction experiments reported by Zhang, et al. [71]. CP: Chinese purple ($BaCuSi_2O_6$); CB: Chinese blue ($BaCuSi_4O_{10}$).

Target pigment	Ba source	Cu source	Si source	Ba:Cu:Si	PbO (wt%)	T (ºC)	t (hrs)	Color	Main phases	Minor phases
CP	$BaSO_4$	$Cu_2(OH)_2CO_3$	SiO_2	1:1:2	19	1000	24	Purple	CP, $BaSO_4$	-
CP	$BaCO_3$	$Cu_2(OH)_2CO_3$	SiO_2	1:1:2	19	900	24	Dark purple	CP	$BaSi_2O_5$
CP	BaO	CuO	SiO_2	1:1:2	39	1000	24	Bluish purple	CP	-
CB	$BaSO_4$	$Cu_2(OH)_2CO_3$	SiO_2	1:1:2	19	900	24	Bluish green	CB, $BaSO_4$, CuO	-
CB	$BaCO_3$	$Cu_2(OH)_2CO_3$	SiO_2	1:2:4	25	1000	24	Bluish purple	CB	-

CB	BaO	CuO	SiO_2	1:1:4	32	1000	24	Bluish purple	CB, SiO_2	-

The effect of different raw materials and synthesis conditions on production of Chinese purple has also been investigated [48]. With 10 wt% of PbO, PbS, or $PbCO_3$ added, mixtures of malachite, $BaCO_3$ or $BaSO_4$, and quartz powder (Cu:Ba:Si=1:1:2) were heated at 900 ˚C for 4 hours, cooled to room temperature, repeated for another two times, with a total firing time to be 12 hours. End-products produced with $BaCO_3$ were bluish purple while those produced with $BaSO_4$ resulted in mainly transparent crystals with very few blue particles. Under such synthesis condition, it was concluded under heat treatment of 1100 ˚C, $BaCO_3$ is a more suitable source for Ba than $BaSO_4$. The effect of Pb additives was also investigated [72]. Mixtures of malachite, $BaCO_3$, quartz powder (Cu:Ba:Si=1:1:2) were heated at 900 ˚C for 12 hours with 10 wt% of PbO, PbS or $PbCO_3$. XRD results on final products showed that with PbO and PbS, the main product was $BaCuSi_4O_{10}$ while with $PbCO_3$, the main product was $BaCuSi_2O_6$. Coupled with results obtained from thermal analysis using TG/DTG, it was suggested that such difference resulted from the better catalysis effect of $PbCO_3$ over PbS, and the smaller particle size of $PbCO_3$ (~2 μm) than that of PbO (10-20 μm). Similarly, in order to reproduce Chinese blue and to investigate effect of different synthesis conditions on its production, mixtures of malachite, $BaCO_3$, quartz powder (Cu:Ba:Si=1:1:4) with 10% $PbCO_3$ were heated at 950 ˚C for 3 hours, 5 hours, and 10 hours [48]. As time prolonged, amounts of SiO_2 and CuO diminished, and a mixture of $BaCuSi_4O_{10}$ and $BaCuSi_2O_6$ was determined to be the final

product after 10 hours of heat treatment by XRD. Different amounts of $PbCO_3$ (0%, 3%, 5%, or 10%) were also added into mixtures of malachite, $BaCO_3$, quartz powder (Cu:Ba:Si=1:1:4) and heated at 980 ˚C for 4 hours for two times. It was noted that as amount of $PbCO_3$ increased, the final product became bluer in color with higher hardness. However, no further discussion was made on the comparison of the results. The effect of excess SiO_2 was also studied. When heated at 950 ˚C for 4 hours, excess SiO_2 (5% or 10% in excess) in the Chinese blue formula with addition of 10% of $PbCO_3$ could promote the formation of $BaCuSi_4O_{10}$ and drive the reaction to be more complete.

Reproduction experiment of Chinese blue and Chinese purple has also been performed using natural minerals obtained from mines in China as precursors, with or without pre-treatment [73]. Natural barite ($BaSO_4$), witherite ($BaCO_3$), tenorite (CuO), quartz (SiO_2) and massicot (PbO) were employed. Mixtures of stoichiometric compositions of 1:1:2 and 1:1:4 for Ba:Cu:Si with barite or witherite as the source for Ba, with or without 25 wt% of PbO as flux, and with or without calcination pre-treatment when barite was used, were synthesized at selected temperatures between 850 ˚C and 1100 ˚C and heat treatment periods of 2 hours, 6 hours, and 10 hours. The calcination of barite was performed at 1200 ˚C. End-products were characterized by XRF, powder XRD and μRS. However, due to its high decomposition temperature and thermal stability, when barite or its calcined dust was used, even with the addition of PbO, large amounts of $BaSO_4$ slag residues were found in the end-products with very small amounts of $BaCuSi_2O_6$ or $BaCuSi_4O_{10}$ formed. When witherite was used, even

without the addition of PbO, $BaCuSi_2O_6$ could be easily synthesized.

Further to the reproduction experiments, thermal analysis by thermogravimetry/differential thermogravimetry (TG/DTG) has also been performed to better understand the starting temperatures of the decomposition of the raw materials and the formation of new phases. The analysis has shown that $BaCO_3$ started to decompose at ~800 ˚C and completed at ~950 ˚C when mixtures of $BaCO_3$, CuO and SiO_2 (with either 1:1:2 or 1:1:4 stoichiometry for Ba:Cu:Si) were heated to 1000 ˚C [69]. The decomposition of $BaSO_4$ on the other hand has started slowly at temperature above 950 ˚C when mixtures of $BaSO_4$, CuO and SiO_2 (1:1:2 or 1:1:4 stoichiometry for Ba:Cu:Si) were heated [69]. The catalytic effect of Pb-additives such as PbO was suggested based on **Reaction 2-1** [22]. $PbSO_4 \cdot 2PbO$ has been suggested by Wiedemann and Berke to be likely to form from the decomposition of $PbSO_4$ at ~1000 ˚C, which will reintroduce PbO into the decomposition of $BaSO_4$ while BaO is continuously removed to form $BaCuSi_4O_{10}$ or $BaCuSi_2O_6$ [22]. In other studies, it has been shown that pure $PbSO_4$ can start to decompose around ~800 to 900 ˚C or 880 ˚C, with PbO being the final non-volatile product [74-76], which gives support to the catalytic effect of PbO on the decomposition of $BaSO_4$ (**Reaction 2-1**).

Reaction 2-1. Reaction between PbO and $BaSO_4$:

$$PbO + BaSO_4 \leftrightarrow BaO + PbSO_4$$

The role of Pb-additives as catalyst in promoting decomposition of $BaSO_4$ was indicated by the TG/DTG analysis [8, 71]. Pure $BaSO_4$ decomposes at 1560 ˚C, but with the addition of either SiO_2 (of stoichiometric ratio of Ba:Si=1:2) or PbO (of stoichiometric ratio of

Ba:Pb=1:0.5), it starts to decompose at 1127 ˚C and 1142 ˚C, respectively [71]. When both SiO_2 and PbO were added (Ba:Si:Pb=1:2:0.5), the decomposition temperature of $BaSO_4$ decreases to 1088 ˚C [71]. When malachite was added into the mixture (with Ba:Cu:Si:Pb=1:1:2:0.5), the synthesis of Chinese purple started at 866 ˚C [71]. Furthermore, it was demonstrated that when $BaSO_4$, malachite, and SiO_2 were mixed in stoichiometric ratios of 1:1:2 and 1:1:4 for Ba:Cu:Si, with the addition of PbO (of amounts not specified in the paper), formation of $BaCuSi_2O_6$ and $BaCuSi_4O_{10}$ started at 865 ˚C and 948 ˚C, respectively [71]. Similarly, TG/DTG analysis has shown that the addition of 10 wt% of PbO, PbS, or $PbCO_3$ can have the same catalytic effect in mixtures of $BaCO_3$, malachite, and SiO_2 (Ba:Cu:Si=1:1:2) [48, 72]. Under such experimental conditions, the formation of $BaCuSi_4O_{10}$ and $BaCuSi_2O_6$ starts at temperatures of 866 ˚C (with PbO), 876 ˚C (with PbS) and 848 ˚C (with $PbCO_3$) [48, 72]. In addition to TG/DTG analysis, powder XRD coupled with high temperature experiment has been applied to investigate the catalytic effect of Pb flux [48]. 10 wt% of $PbCO_3$ was added to $BaSO_4$ or $BaCO_3$, and the mixtures were heated at 200 ˚C, 300 ˚C, 400 ˚C, 500 ˚C, 600 ˚C, 700 ˚C, or 800 ˚C for 5 hours then cooled to room temperature, and the end-products were characterized by powder XRD. While $BaSO_4$ did not decompose within this temperature range and heat treatment time, $BaCO_3$ started to decompose at 600 ˚C, forming $BaPbO_3$ with orthorhombic PbO, which was the decomposition product of $PbCO_3$ at 600-700 ˚C.

One study has also employed high temperature XRD to monitor in situ phase

transformations [77]. $BaCO_3$ was pre-heated at 950 ˚C for 12 hours before mixing with CuO and SiO_2 with stoichiometric ratio of Ba:Cu:Si = 1:1:2, and high temperature XRD characterization was performed at 25 ˚C, 700 ˚C, 800 ˚C and 900 ˚C, when the mixture was heated at these temperatures for certain time duration that was not specified in the paper. $BaCuSi_2O_6$ diffraction peaks started to appear at 700 ˚C.

2.3 Current hypotheses on production technology of Chinese blue and Chinese purple

With no written records on the manufacturing process of Chinese blue and purple, nor any known sites of ancient production centers, our knowledge on the possible operational steps for the production of these pigments is based mainly on characterization studies of archaeological samples and laboratory-based reproduction experiments. Research on other contemporary pyrotechnological industries such as the making of pottery, Cu-Sn-Pb bronze and PbO-BaO-SiO_2 glass, has also contributed in developing some hypotheses on ancient production technology of Chinese blue and Chinese purple, raw materials selection and synthesis conditions.

2.3.1 Possible sources for raw materials

2.3.1.1 Pb-source

China has a long history of mining Pb-containing minerals and extraction of metallic Pb

in early metallurgy such as bronze production. For example, based on previous chemical analyses on properly-provenanced Chinese bronze objects, Pb was intentionally added to the Cu-Sn alloy before casting from ca. 1100 B.C. onward [78]. As an abundant Pb-containing mineral, galena (PbS) is generally considered a common source of Pb in antiquity [78], from which one does not require sophisticated roasting and smelting technique to be able to extract Pb [79]. In ancient China, before being processed, galena was called "生铅" ('raw lead'), and the metallic Pb obtained after roasting and smelting was referred to as "熟铅" ('cooked lead') [80]. Two other common Pb-containing minerals, cerussite ($PbCO_3$) and anglesite ($PbSO_4$), do not require roasting and can be smelted directly [81].

The use of lead in ancient China was also closely related to alchemical activities and medicinal practices. Ancient Chinese alchemists favored metallic Pb because varying the processing methods, they could obtain Pb-compounds of different colors, ranging from white ($PbCO_3$, $Pb_3(CO_3)_2(OH)_2$, or $Pb(C_2H_3O_2)_2$), yellow (orthorhombic PbO), to red (tetragonal PbO, or Pb_3O_4) [80]. The detailed making and application of these Pb-compounds as "丹" ('dan', i.e. elixir), cosmetics, and Chinese medicines have been recorded in significant amounts of ancient Chinese manuscripts and texts since as early as Warring States period [80].

It is therefore possible that the Pb-source used in production of Chinese blue and Chinese purple could have come from natural Pb-containing minerals, metallic Pb after extraction, or Pb-compounds artificially made from alchemical or medicinal practices.

2.3.1.2 Ba-source

The most abundant and commonly available Ba-containing mineral in China is barite ($BaSO_4$). Witherite ($BaCO_3$) is a rare mineral, with the largest supply found in China. About 40 witherite deposits have been identified, which are confined by northern Daba Mountains and southern Qinling Mountains, in the region between Sichuan and Shaanxi provinces, constituting a witherite belt of about 300 km [82-84]. These deposits are about 200-500 km from the various important sites where abundant archaeological artefacts containing Chinese blue and Chinese purple have been recovered. If witherite was indeed the Ba-source in ancient production, it may suggest either a long-distance travel to obtain witherite to produce the pigments locally, or a long-distance inter-regional exchange of witherite.

The Ba-source, whether barite or witherite, employed in the production of Chinese blue and Chinese purple has been a major dispute in the published literature. In some studies, the identification of barite ($BaSO_4$), either structurally confirmed by XRD or μRS, or stoichiometric determination by EDS or EPMA in the archaeological Chinese blue and Chinese purple samples and the abundance of barite ores in China, suggested the use of this mineral as the Ba-containing precursor [9, 47, 50, 51]. In another study, the absence of S in Chinese blue faience beads, pointed to the use of witherite ($BaCO_3$) mineral [46]. In all other scientific studies, the source of Ba is either not discussed, or suggested to be either barite or witherite.

The identification of $BaSO_4$ in archaeological samples, however, should be considered carefully, as $BaSO_4$ may be reaction residue due to the use of barite, or may be reaction

byproduct resulting from the use of witherite together with S introduced via other raw materials as for example the Pb precursor. Therefore, microstructural information such as particle size, morphology, abundance of the $BaSO_4$ crystals, as well as the location where the $BaSO_4$ crystals are identified (outer layer, inner core, etc.) should also be taken into consideration.

The disparity on the Ba-source is also seen in studies focusing on laboratory-based reproduction experiments. Two studies, indicated $BaCO_3$ to be chemically more reactive at producing Chinese blue and Chinese purple whereas attempts in the direct use of $BaSO_4$ or its calcined dust have failed in producing the pigments [48, 73]. The latter resulted in unreacted $BaSO_4$ in great amounts under various experimental conditions despite the catalytic effect of PbO in promoting decomposition of $BaSO_4$ at lower temperatures, as demonstrated by thermal analysis [8, 71]. In only one study, the successful syntheses of Chinese blue and Chinese purple with the direct use of $BaSO_4$ has been reported, with $BaSO_4$ identified as one of the major phases besides $BaCuSi_4O_{10}$ or $BaCuSi_2O_6$ [71].

Similarly, previous experiments for the reproduction of ancient Chinese glass of the PbO-BaO-SiO_2 system, indicated that $BaSO_4$ is chemically less reactive than $BaCO_3$ and less likely to have been used as the Ba source [70, 85]. It has shown that based on a formula of 45% PbO, 14% BaO, 38% SiO_2 and 3% Na_2O, the use of $BaSO_4$ produced poorly melted glass with much unreacted $BaSO_4$ even after 6 hours of heating at 1200 ˚C. Conversely, the use of $BaCO_3$ resulted in a well melted, transparent and homogeneous glass [70]. In another study for the reproduction of two archaeological PbO-BaO-SiO_2 glass samples, the use of $BaSO_4$ either

directly or after calcination at 1200 ˚C for 12 hours, resulted in a partially vitrified product with residual $BaSO_4$. Under the same experimental conditions, the use of $BaCO_3$ produced a completely vitrified glass end product [85].

2.3.1.3 Cu-source

According to different studies, the source of Cu in the production of Chinese blue and Chinese purple include Cu-containing minerals, metallic copper, or reused ancient bronzes [22, 71]. In most scientific analyses of archaeological samples, Cu was the major element detected, suggesting Cu-containing minerals or metallic Cu for the production of the pigment. The absence of Sn or arsenic (As) excluded the use of Cu from bronzes [57]. In only two archaeological Chinese purple samples, significant amounts of Sn ranging from ~5 wt% to ~20 wt% were detected, pointing to Cu-deriving from reused bronze (Cu-Sn alloy) for the production of the pigment [45, 47]. In these two cases, the samples were taken from a painted decoration depicting an umbrella covering an iron chariot [45] and from a polychrome figurine [47]. Both samples were recovered from tombs dated to the Western Han Dynasty in Shandong Province.

Written records of copper mining and smelting from the Shang Dynasty (ca. 1600-1046 BC) to the Warring States Period (475-221 BC), can be found in many ancient texts, manuscripts, as well as inscription on bronze objects from the Zhou Dynasties (1046-476 BC) [86]. Based on geological surveys, Cu-containing ores such as native copper, cuprite (Cu_2O),

malachite ($Cu_2CO_3(OH)_2$), azurite ($Cu_3(CO_3)_2(OH)_2$) and chalcopyrite ($CuFeS_2$) are widely located in China. Mining holes from ancient or historical times can also be found in almost all the Cu-containing ores still mined today. This may suggest a continuous use of these Cu-containing ores [86]. The four major mining areas with the richest reservoirs of Cu ores are located in 1) the middle and lower reaches of the Changjiang Rivier, including the Hubei, Jiangxi, and Anhui provinces; 2) the Zhongtiao Mountain in Shanxi Province; 3) the Dongchuan and Yimen mines in Sichuan and Yunnan provinces; and 4) the Jinchuan and Baiyinchang mines in Gansu Province [86]. Over 100 ancient mining and/or smelting sites of Cu ores dated to the Xia Period, the Shang Period and the Zhou Period have been excavated [86]. Many of the sites are near areas where archaeological Chinese blue and Chinese purple samples have been recovered. As such, the abundance and variety of Cu ore deposits utilized for bronze production in ancient China should have provided sufficient Cu raw material for the making of these high-valued barium copper silicate pigments.

2.3.1.4 Si-source

In antiquity, vitreous materials such as faience and glass were produced with SiO_2 usually in the form of quartz or sand [87, 88]. This was likely also the Si-source for the production of Chinese blue and Chinese purple [22, 71, 73]. Minor or trace elements such as Fe, Al, Na, K, Zr, Ti, as well as rare earth elements (REEs) could have been introduced into the final products as impurities in the quartz or sand [73, 89]. For example, Qin et al. identified the use of quartzite

from the Tonlushan Mine of Daye County of Hubei Province, which contains 95.2% of SiO_2 with minor amounts of Al, Fe, K and Na [73]. These elements (or some of them) have been commonly detected in minor amounts in archaeological Chinese blue and Chinese purple [9, 22, 39, 41, 44-47, 49-51]. While the presence of these minor and trace elements may point to a particular source in antiquity, similar elements could also be introduced into the pigments as impurities associated with other raw materials. For example, both a witherite ore from Chengkou Mine of Chongqing City and a barite ore from Zhuans County of Hubei Province contains ~5% of CaO [73, 85]. A tenorite ore from Tonlushan Mine has minor amounts of Fe, and Al [73]. A malachite ore from the Tonglushan Mine contains minor amounts of Na, Ca, K, Fe, and Al [73, 85]. A galena ore from Zhuans County contains ~1% of Fe_2O_3, and a cerussite ore from Tongling County of Anhui Province contains minor amounts of Na, Ca, K, Al and S [85]. Also, besides from raw materials, some of these minor or trace elements can also be introduced from the burial environment or contamination from the crucibles and fuel during high temperature heat treatment.

2.3.2 Possible synthesis conditions

The synthesis of Chinese blue and Chinese purple can be written as **Reaction 2-2** and **Reaction 2-3**, respectively. Pb-additives has a dual role, both as a flux to reduce the melting temperature of SiO_2, and as a catalyst to promote the decomposition of Ba-containing minerals and the synthesis of the pigments.

Reaction 2-2. Formation of Chinese blue ($BaCuSi_4O_{10}$):

$$BaO + CuO + 4SiO_2 \xrightarrow{Pb\text{–}source,\ high T} BaCuSi_4O_{10}$$

Reaction 2-3. Formation of Chinese purple ($BaCuSi_2O_6$):

$$BaO + CuO + 2SiO_2 \xrightarrow{Pb\text{–}source,\ high T} BaCuSi_2O_6$$

During and prior to the occurrence of Chinese blue and Chinese purple, kilns that could sustain high temperature of firing were already available in other pyrotechnological industries, such as in pottery/ceramics. Thermal analysis on grey and red pottery sherds dated to the Neolithic Age in China showed that they were originally fired in the range of 950-1050 ˚C [90]. Additional pottery sherds dated to the Shang Dynasty (ca. 1600 BC-1046 BC) and Western Zhou Dynastry (1046-771 BC) were originally fired in the range of 950-1200 ˚C, and 'proto-porcelain' sherds dated to the Eastern Zhou and Han Dynasties were originally fired in the range of ~1150-1250 ˚C, with one sample fired to as high as 1310±20 ˚C [90, 91]. The achievable firing temperature in the production of contemporary pottery or porcelain are in general comparable to the temperature range suggested by previous researches on the making of Chinese blue and Chinese purple, providing support for the technological possibility to produce these pigments at high temperature firing conditions.

2.4 Current knowledge gap and challenges on the study of production technology of Chinese blue and Chinese purple

In most published communications, the identification of archaeological Chinese blue and Chinese purple has been mainly confirmed with the detection of the principle crystalline phases,

$BaCuSi_4O_{10}$ and $BaCuSi_2O_6$, and main phases of other reaction residues and synthesis byproducts. However, very few have focused on analyzing the microstructure and relative distribution of main and minor phases, which are important to reverse engineer the production technology including formation mechanisms and boundary conditions of heat treatment, and derive raw material selection and the operational sequence (chaîne opératoire) for the synthesis of these highly heterogeneous and complex ancient frits. In addition, data on the distribution and density of the various phases and microstructural characteristics from archaeological samples serves as the one of the bases to guide the design of modern reproduction experiments. Out of all published literature, only six studies [41, 44, 47-50] integrate information on the pigments' microstructure and none of the laboratory-based re-created Chinese blue or Chinese purple has been analyzed with BSE-SEM to reveal characteristics of the microstructure and distribution of the phases present in the end-product, thus hindering a more comprehensive comparison with the archaeological samples.

Another challenge in the characterization of the pigments is the detection limits of traditional bench analytical techniques such as SEM-EDS/EPMA, μRS and μXRD, commonly employed in the study of archaeological Chinese blue and Chinese purple samples. These have lateral resolution at the micron scale and fail to detect sub-micron crystallites and other important particles related to the raw materials used and production technology of the pigments. This was demonstrated in a previous study, where μRS with lateral resolution of about 1 μm, failed to isolate the $PbO\text{-}BaO\text{-}SiO_2$ glass from surrounding $\alpha\text{-}SiO_2$ and $BaCuSi_4O_{10}$ crystals,

resulting in Raman mixed spectra of these individual components [57]. Therefore, characterization techniques with high specificity and high lateral resolution need to be applied for the comprehensive analysis of archaeological Chinese blue and Chinese purple pigments. The heterogeneity of the microstructure at micron to sub-micron scale and variability in the chemistry and phases reported in literature on archaeological Chinese blue and Chinese purple samples pose another challenge in the reverse engineering of the technology and the successful reproduction of these pigments. The synthesis of the pigments requires raw materials providing at least four components (BaO, CuO, SiO_2 and PbO), or five components (BaO, CuO, SiO_2, PbO and SO_3) based on the variability of chemistry in archaeological samples. However, phase transformations and chemical reactions in these sintered polycrystalline systems are highly complicated, with many variables requiring consideration including:

- the identities and relative proportions of different raw materials;
- the heat treatment temperature and time, whether it is a single-step or multi-step;
- and the furnace redox atmosphere.

As it is extremely difficult to address all variables at once, various reproduction experiments can be designed by changing a single parameter at a time, while keeping the others unchanged. The limited number of such systematic studies and the lack of microstructural comparison with archaeological samples to evaluate any similarity and difference not just the chemistry, has thus far hindered our understanding in production technology of Chinese blue and Chinese purple.

2.5 Visible light (Vis)-induced near infrared (NIR) photoluminescent property of the Chinese blue, Chinese purple and Egyptian blue

Besides their archaeological significance, Chinese blue, Chinese purple, together with Egyptian blue, have unique photophysical properties that not only serve as the basis for non-invasive identification and mapping of the pigments on archaeological objects, but also render them suitable as novel optical materials in various fields of application other than archeological science.

Previous studies have shown that $BaCuSi_4O_{10}$, $BaCuSi_2O_6$ and $CaCuSi_4O_{10}$, the main crystalline component of Chinese blue, Chinese purple and Egyptian blue, respectively, emit radiation in the near infrared (NIR) region (800-1100 nm) of the electromagnetic spectrum when excited by the visible radiation [11], which will be termed "Vis-induced NIR photoluminescence" in this thesis. The origin of the NIR photoluminescence is attributed to the square planar symmetry (D_{4h}) of the Cu^{2+} chromophore that undergoes the $^2B_{2g} \rightarrow {}^2B_{1g}$ d-d electronic transition [11], which can be induced by excitation radiation in the visible range that correspond to the electronic transitions from the ground state to the different excited states. It has been shown that with a laser excitation at 632 nm, which is close to the maxima of the main absorption bands of these pigments, Chinese blue and Chinese purple emit strong NIR photoluminescence with a broad band centered at about 980 nm [11]. Similarly, Egyptian blue emits strong NIR photoluminescence with a broad band centered at about 950 nm [11]. Furthermore, these are the only three pigments that emit NIR photoluminescence in the 800-

1100 nm range with excitation in the range of red light among the commonly found ancient and historical blue or purple pigments [92, 93]. Therefore, since the discovery of this unique photophysical property of Chinese blue, Chinese purple and Egyptian blue, Vis-induced NIR photoluminescence photography has been applied on archaeological objects such as terracotta figurines [93], wall paintings [92, 94], and faience beads [92] to non-invasively identify the presence and to map the distribution of these three pigments.

Recent studies have shown that the crystalline phase of Egyptian blue and Chinese blue can be delaminated into monolayer nanosheets in hot water with stirring, which renders Egyptian blue and Chinese blue suitable for potential applications as 2D nanomaterials [12, 95]. In addition, Chinese blue hierarchical mesoporous microspheres consisted of $BaCuSi_4O_{10}$ nanosheets assembled with no preferred orientation has been synthesized under hydrothermal conditions [96].

The high chemical stability and strong NIR luminescent properties of $BaCuSi_4O_{10}$ and its ability to delaminate into monolayer nanosheets are major advantages for functional applications in new material innovations. More specifically, because of its visible-induced luminescence in the imaging window (650-1450 nm) where tissue penetration is greatest with the lowest absorption in tissue, Chinese blue is potentially a good candidate as fluorescent marker [97]. As particles greater than 1 μm in size however, can cause blockage at the injection site [97], it would necessitate the synthesis of nanoscale Chinese blue.

2.6 Research motivation

The invention and manufacture of the high-valued Chinese blue and Chinese purple more than 2000 years ago, represents a significant technological achievement in China's history, from the deliberate selection of specific raw materials and the careful control of heat treatment conditions, to the capability to utilize natural resources to produce the colors that met the aesthetic, philosophical and political needs at the time. The reconstruction of the production technology of these pigments is therefore important to deepen our understanding on ancient pyrotechnology and any possible inter-regional trade of technology and materials within ancient China, which reflects social organization and human agency at the time. In addition, the study of the synthesis of these two pigments may help to explain their short period of existence, as it may be related not only to political, social and religious changes, as it has been previously suggested [43], but also to limited resources and access of certain raw materials.

In addition, building on the stable chemical property and strong Vis-induced NIR photoluminescence in the imaging window, the synthesis of nanoscale Chinese blue as potential fluorescent markers in biomedical imaging is also explored in this research.

Chapter 3. New insights into the manufacturing of archaeological Chinese blue via scanning transmission electron microscopy (STEM) and transmission electron microscopy (TEM)

Scanning transmission electron microscopy (STEM)/transmission electron microscopy (TEM) coupled with energy dispersive X-ray spectroscopy (EDS) provides local information on properly prepared samples with atomic resolution and yields elemental composition of atomic and nano-scale structures. Here we demonstrate the first direct visualization of the atomic arrangement of $BaCaSi_4O_{10}$ in archaeological Chinese blue and evidence the detection and identification of sub-micron scale crystallites of $BaSO_4$, $BaSO_4$-$PbSO_4$ solid solution, Pb_3O_4, and amorphous SiO_2. The characterization of major and minor compounds and sub-micron inclusions at the atomic scale provided new insight and helped draw inferences on the raw materials used and operational sequences (*chaîne opératoire*) followed in the production of Chinese blue.

3.1 The Archaeological site of Majiayuan Cemetery, Tianshui City, Gansu Province

Located in the Taoyuan Village in the Zhangjiachuan Automous County of the Hui people, Tianshui City, Gansu Province, China, the Majiayuan cemetery consists of 59 stepped tombs and sacrifice pits and covers an area of ~20,000 m^2 [98-102]. Numerous important funerary objects of high technological importance were unearthed, among which, luxury lacquered chariots, decorated with copper and silver ornaments, faience and glass beads of different colors, as well as bronze, gold, silver, tin, bone, agate, turquoise, ceramics and other

vitreous artifacts. Great in number, were also blue, purple and white faience beads, which were recovered from burial contexts.

The discovery of valued artifacts at the site suggests that the individuals buried in the Majiayuan cemetery were nobles, belonging to the Western Rong, a cultural group in constant contact and warfare with the Qin people, until the establishment of the Qin Dynasty and the unification of ancient China. The identities of the specific tribes belonging to this group, however, have not yet been confirmed [98-102]. The material record, also infers influences from cultures from the West and the North of ancient China, as well as from the Qin culture from central China during the Late Warring States Period.

3.2 Materials and methods

3.2.1 Materials

Analyses were focused on a Chinese blue faience bead, a vitreous material that consists of a silica-rich body with varying amounts of interparticle glass, coated with a glaze that is rich in Chinese blue in this case (**Figure 3-1**(a)), recovered from Tomb M4 of the Majiayuan cemetery (together with many other similar beads) and dated to the Late Warring States Period (475-221 BC). The faience bead analyzed, has a cylindrical shape with a perforation in the center, and with an outer diameter of 2.8 mm and an inner diameter of 1.8 mm. Its ‘glazed’ surface has a smooth texture and light blue color, whereas the core has a buff color and a coarse

'sandy' appearance. Evidence of fibers adhered to the walls surrounding the perforation of the bead may suggest threading/stringing of the beads to create a necklace or another type of ornament. As a result of long-term burial and weathering, the faience bead is also very fragile and prone to delamination and fracturing under minor mechanical stresses.

Following a systematic examination of the bead using digital microscopy, a tangential cross section was prepared from the broken edge (**Figure 3-1**(b)). For the preparation of the cross section, the small fragment was embedded in Buehler EpoxiCure® epoxy resin cured with EpoxiCure® Epoxy Hardener in a Teflon mold, and ground gradually with Buehler silicon carbide grinding papers from 600 to 1200 grit. The sample was then polished on a Leco® GP-25 polishing turntable with water-based diamond suspensions of 6 μm and 1 μm over Buehler® MasterTex polishing cloths.

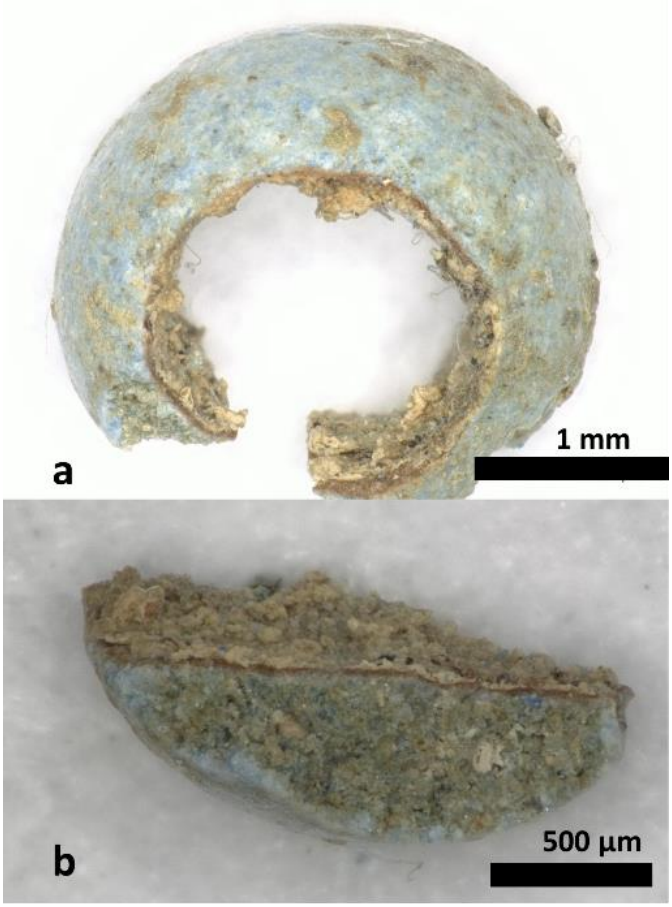

Figure 3-1. a. A digital microscopic image of the overview of a faience bead containing Chinese blue pigment from the Late Warring States Period, Tomb M4, Majiayuan Cemetery, Zhangjiachuan, Tianshui City, Gansu Province, China. b. A cross section through the faience bead, showing a glazed layer that is rich in Chinese blue pigment crystals and a core faience body that is rich in quartz.

3.2.2 Characterization methods

Digital microscopy (DM)

Initial examination of the sample was undertaken using a Keyence VHX-1000 digital microscope in the Electron and X-ray facility of the Materials Science and Engineering (MSE) Department at the University of California, Los Angeles (UCLA). Observations of the surface and core of the specimen (at magnifications between 50x and 200x) informed technical and weathering indices and exposure, and enabled to accurately record the size and color of the bead and to map surface characteristic and topography, as well as, defects and corrosion layers.

Scanning electron microscopy coupled with energy dispersive X-ray spectroscopy (SEM-EDS)

The polished cross section was analyzed using FEI Nova™ NanoSEM 230 field emission gun (FEG) scanning electron microscope (SEM) at the Molecular and Nano Archaeology (MNA) Laboratory, part of the Electron and X-ray facility at the MSE, UCLA. Compositional contrast micrographs for microstructural and phase characterization and to inform areas of interest for micro-sampling using FIB for STEM/TEM-EDS characterization were obtained by an FEI Magellan 400L SEM with backscattered electron detector (BSE) at accelerating voltage of 10.0 kV and a current of 80 pA under high vacuum at the Centre for Nanosciences and Nanotechnology (C2N), CNRS/Paris Sub University-UMR 9001. An Oxford INCASynergy 350 energy dispersive X-ray spectrometer (EDS) coupled to the SEM was used for elemental characterization and mapping.

Focused ion beam (FIB)

An FEI Dual-Beam Scios focused ion beam (FIB) with a Ga ion source at the Centre for

Nanosciences and Nanotechnology (C2N), CNRS/Paris Sud University-UMR 9001 was employed to prepare micron scale thin sections of single crystals and at grain boundaries (interface). A thin section with 2D dimensions of ~20 μm x 28 μm and thickness of about 200 nm was prepared. The FIB preparation was followed by a cleaning and final thinning by argon ion milling at low voltage (1.5 kV) and low incident angle (5°) with a PIPS (Precision Ion Polishing System) from Gatan.

Scanning transmission electron microscopy/transmission electron microscopy coupled with energy dispersive X-ray spectroscopy (STEM/TEM-EDS)

Characterization and elemental analysis of the thin section was performed using an aberration-corrected Titan Themis 200 scanning transmission electron microscopy/transmission electron microscopy (STEM/TEM) coupled with a Chemistem Super-X EDS. The accelerating voltage was 200 kV and the probe current was about 80 pA.

3.3 Results

The faience bead consists of two distinctive components with characteristic microstructures: a fine surface blue 'glaze' layer and, a buff colored coarse core (**Figure 3-2**(a)). Analysis indicated that both the 'glaze' and the faience core contain $BaCuSi_4O_{10}$ crystals and Pb/Ba-rich phases. In terms of microstructure, the faience core contains larger quartz particles and has a higher porosity than the faience 'glaze'. Characterization using the backscattered electron (BSE) detector of selected area within the blue 'glaze' (red square in **Figure 3-2**(a))

indicated a highly heterogeneous layer (**Figure 3-2**(b)). Phase and elemental characterization using BSE and EDS respectively, detected the presence of micron to submicron size inclusions, rich in lead (Pb) and barium (Ba), along with $BaCuSi_4O_{10}$ and SiO_2 crystals. To further investigate this intricate multi-phase system, an area of interest at the interface between multiple different particles was micro-sampled for the preparation of an ultra-thin section using FIB (**Figure 3-2**(b)) and analyzed by STEM-EDS.

High annular angle dark field (HAADF)-STEM analysis of the sample consistently revealed the presence of prevalent micron/sub-micron inclusions within the defects of $BaCuSi_4O_{10}$ crystals with an average dimension of ~19 μm in length, and between 6.5 μm and 12.5 μm in width (**Figure 3-2**(c)). Most submicron inclusions in the defects of the $BaCuSi_4O_{10}$ crystals are rich in Ba, Pb, S, and O (**Figure 3-2**(d)-(g)); one elliptical inclusion in an area analyzed contains, however, only Si and O (**Figure 3-2**(g), (h)). Given the importance of Pb- and Ba-rich micron/submicron-size inclusions within the $BaCuSi_4O_{10}$ crystal to resolve manufacturing processes, analyses were focused at identifying their chemical compositions and phases, and determining the mechanisms of their formation. We have overcome possible analytical artifacts such as the use of Cu-based TEM holder and the presence of heavy elements in the matrix inducing the fluorescence of Cu (**Figure 3-2**(i)) and EDS limitations in resolving

the small energy differences between the K_α line of S and M_α line of Pb by performing elemental map of Pb based on its L_α and L_β lines (**Figure 3-2**(e)).

HAADF-STEM and STEM-EDS data from these inclusions found consistently within several single crystals of $BaCuSi_4O_{10}$ (**Figure 3-3**(a)) - revealed the coexistence of two distinct

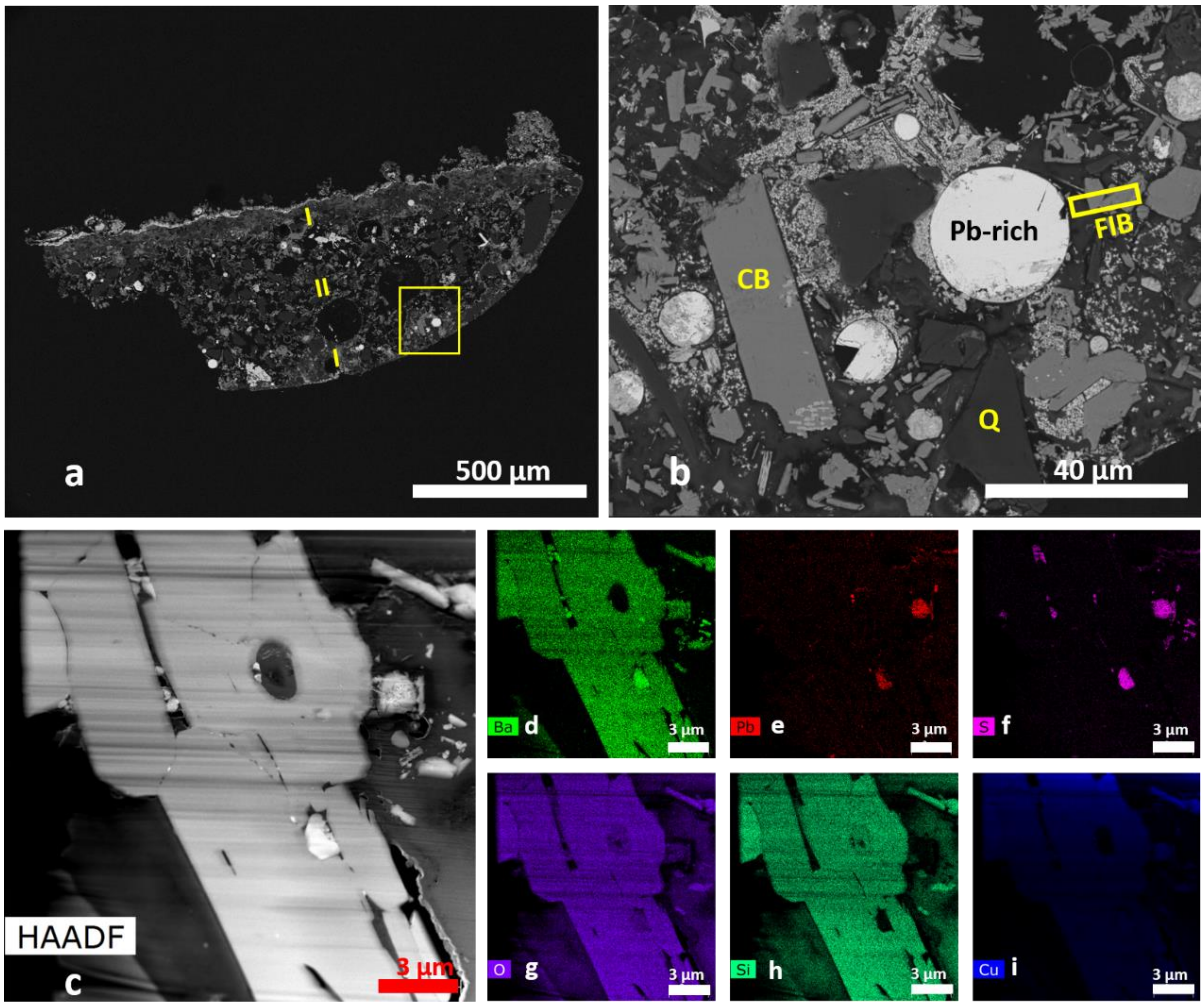

Figure 3-2. (a) BSE-SEM image of the overview of the polished cross section. Component I: a "glazed" layers that are rich in $BaCuSi_4O_{10}$ crystals (grey) with presence of Pb-rich inclusions (white). Component II: a faience body that has heterogeneous distribution of $BaCuSi_4O_{10}$ crystals, quartz (dark), Pb/Ba-rich inclusions, and high porosity (black); (b) A zoomed-in BSE-SEM image of area labeled in yellow frame in (a), showing details of the three major components-CB: $BaCuSi_4O_{10}$ crystals, Q: quartz, and Pb/Ba: Pb- or Ba-rich inclusions. The area where FIB sampling was performed is labeled in yellow; (c) High-angle annular dark field (HAADF) STEM image of a portion of the thin section prepared with FIB; (d)-(i). Elemental distribution maps of (c), showing areas where Ba, Cu, Si, O, Pb and S are concentrated within the thin section.

phases: phase I: submicron crystallites (**Figure 3-3**(a)-area 1) rich in Ba, O (**Figure 3-3**(b), (c)) that also contain S and Cu (**Figure 3-3**(d), (e)), and phase II: submicron crystallites (**Figure 3-3**(a)-area 2), rich in Pb (**Figure 3-3**(f)).

Si was only detected within the $BaCuSi_4O_{10}$ single crystal and was absent from the inter-crystal inclusions (**Figure 3-3**(g)). Quantitative elemental data of the crystallites in area 1 (phase I) indicated: 63.5 atomic% (24.7±1.1 wt%) of O, 15.2 atomic% (50.9±5.3 wt%) of Ba, 11.2 atomic% (8.7±0.4 wt%) of S, 9.6 atomic% (14.8±0.7 wt%) of Cu, 0.3 atomic% (0.2±0.1 wt%) of P, 0.1 atomic% (0.1±0.1 wt%) of Si and 0.1 atomic% (0.5±0.2 wt%) of Pb. The presence of ~10 atomic% of Cu in the inclusions area 1 is attributed to secondary fluorescence by the concentrated heavy element Ba in the inclusions, in addition to the Cu-sample holder absorption.

Quantitative EDS data in area 1 (phase I) suggest that the small crystallites are mainly composed of Ba, S, and O at a molar ratio of ~1:0.7:4.2. This ratio corresponds to $BaSO_4$,

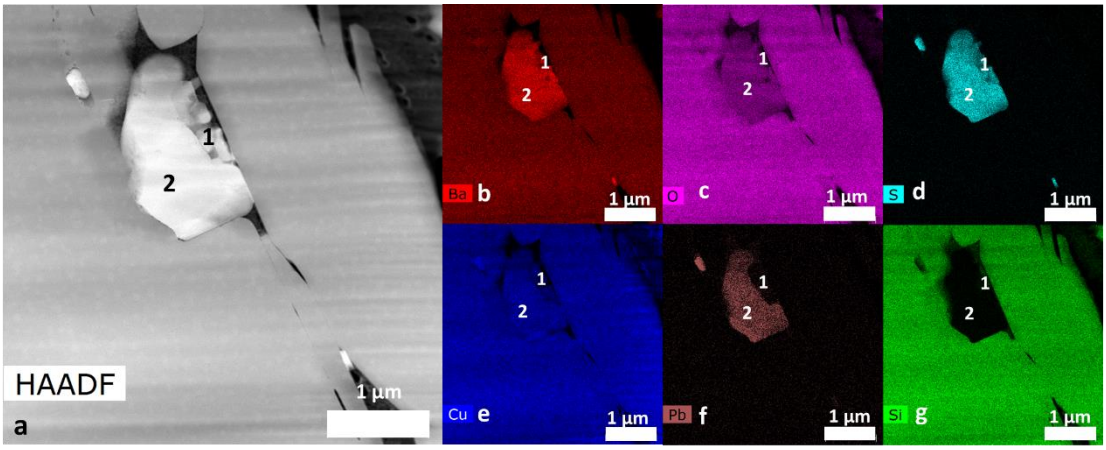

Figure 3-3. (a) An STEM-HAADF image of an inclusion of interest, showing the inclusion contains multiple sub-micron scale crystallites; (b)-(g) EDS elemental maps of Ba, O, S, Cu, Pb, and Si of this inclusion. Area 1 and Area 2 show different compositional abundance of Pb.

which has been previously confirmed by μRS in archaeological Chinese blue [9, 41, 57].

Quantitative data from the crystallites in area 2 (phase II) show a different composition from area 1, containing: 65.5 atomic% (25.2±0.8 wt%) O, 12.2 atomic% (40.3±4.1 wt%) Ba, 11.0 atomic% (16.8±0.5 wt%) Cu, 8.5 atomic% (6.6±0.2 wt%) S, 2.1 atomic% (10.5±1.1 wt%) Pb, 0.3 atomic% Si (0.2±0.0 wt%) and 0.3 atomic% (0.3±0.0 wt%) P. As in the case of area 1, the high value of atomic% Cu can be attributed to the secondary fluorescence of Cu in the presence of a high concentration of heavy elements such as Ba and Pb, as well as, the use of Cu-based sample holder. The molar ratio of (Ba+Pb):S:O is ~1:0.6:4.6, suggesting that this micron size crystallite is a solid solution of $BaSO_4$-$PbSO_4$.

To confirm the identities of these submicron phases, HAADF-STEM characterization at higher magnifications was performed on selected inclusions within the areas 1 and 2 (red frames in **Figure 3-4**(a)). An HAADF-STEM image at higher magnification of area 1 was obtained (**Figure 3-4**(b)). Based on a selected area of this image (red frame in **Figure 3-4**(b)), the Fast Fourier Transform (FFT) was indexed (**Figure 3-4**(b)), matching the orthorhombic $BaSO_4$ crystal with a zone axis of [001]: d_{010} measured on FFT is 5.464 Å, which is within 1.3% of the established reference value for d_{010} of $BaSO_4$ (5.538 Å); d_{200} is measured to be 4.396 Å, within 2.1% agreement of reference value for d_{200} of $BaSO_4$ (4.489 Å) [103-105]. Similarly, an HAADF-STEM image at higher magnification of area 2 (red frame in **Figure 3-4**(a)) was obtained (**Figure 3-4**(c)). Index result of the FFT of a selected area (red frame in **Figure 3-4**(c)) indicates this is a crystal of orthorhombic $BaSO_4$-$PbSO_4$ solid solution with a zone axis of [001].

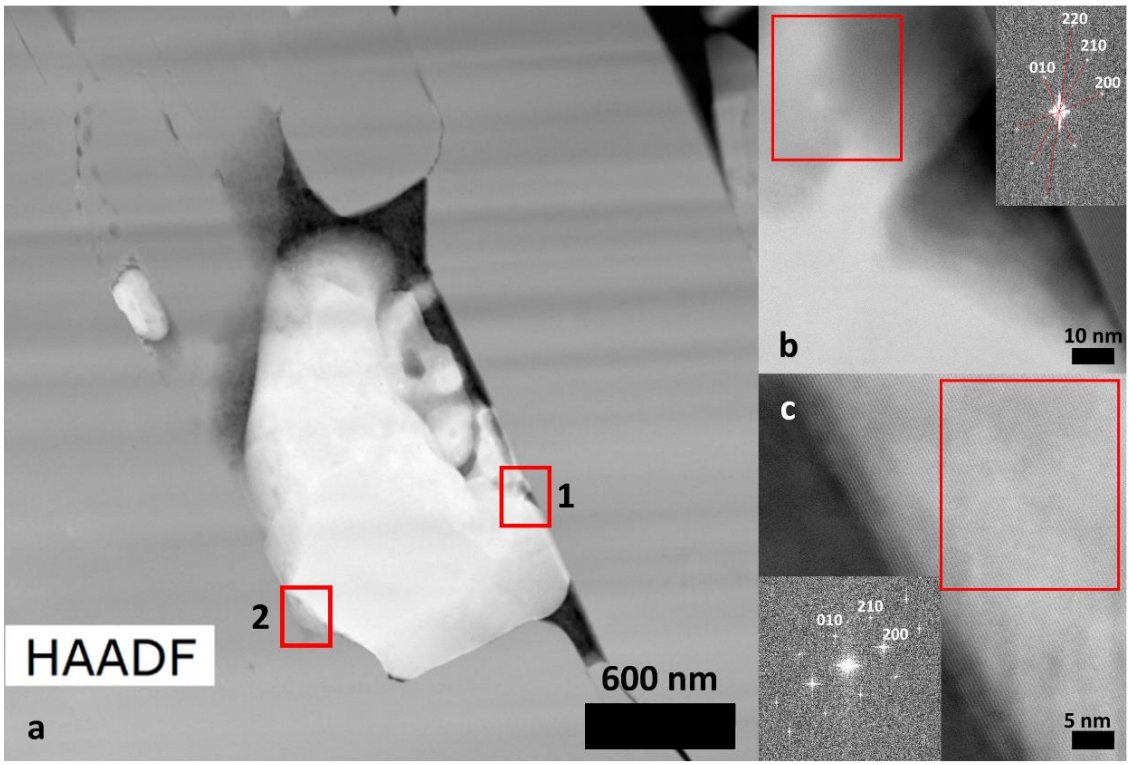

Figure 3-4. (a) An STEM-HAADF image of an inclusion. (b) An STEM-HAADF image of interface between a Ba-rich crystallite (white) and the surrounding $BaCuSi_4O_{10}$ crystal (gray) within Area 1 labeled in a, showing the detail of the atomic arrangements of these two phases. The Fast Fourier Transform (FFT) of the Ba-rich crystallite within the area enclosed (red frame) is shown in the lower left with crystallography index. (c) An STEM-HAADF image with atomic resolution of interface between a Ba- and Pb-rich crystallite (white) and the surrounding $BaCuSi_4O_{10}$ crystal (gray) within Area 2 labeled in (a). The FFT of the Ba- and Pb-rich crystallite within the area enclosed (red frame) is shown in the lower left with crystallography index.

The measured d_{010} and d_{200} are 5.333 Å and 4.246 Å, respectively. Based on EDS results for area 2, the molar ratio of Ba:Pb is close to 0.85:0.15. Compared to the d_{010} and d_{200} of $Ba_{0.85}Pb_{0.15}SO_4$,which are 5.450 Å and 4.406 Å (calculated from reference unit cell parameters [106], respectively, the measured d_{010} and d_{200} are within 2.1% and 3.6% agreement.

STEM/TEM-EDS characterization was also performed on a micron-size light elements-rich particle (appearing dark in compositional contrast images), found together with nano-size heavy-metal-containing inclusions (appearing lighter in compositional contrast images) (**Figure 3-5**(a)). The dark inter-crystal inclusion of ~1 μm x 2 μm, consists of Si and O (**Figure 3-5**(b) and (c)), whereas, the surrounding light grey matrix is of pure $BaCuSi_4O_{10}$ crystalline phase (**Figure 3-5**(b)-(e)). From the nano-size bright inclusions, only one was found to contain Ba (**Figure 3-5**(e)), an inclusion that doesn't contain Pb (**Figure 3-5**(f)) but is rich in S instead (**Figure 3-5**(g)). Pb was found in the remaining of the nano-size inclusions (**Figure 3-5**(f)).

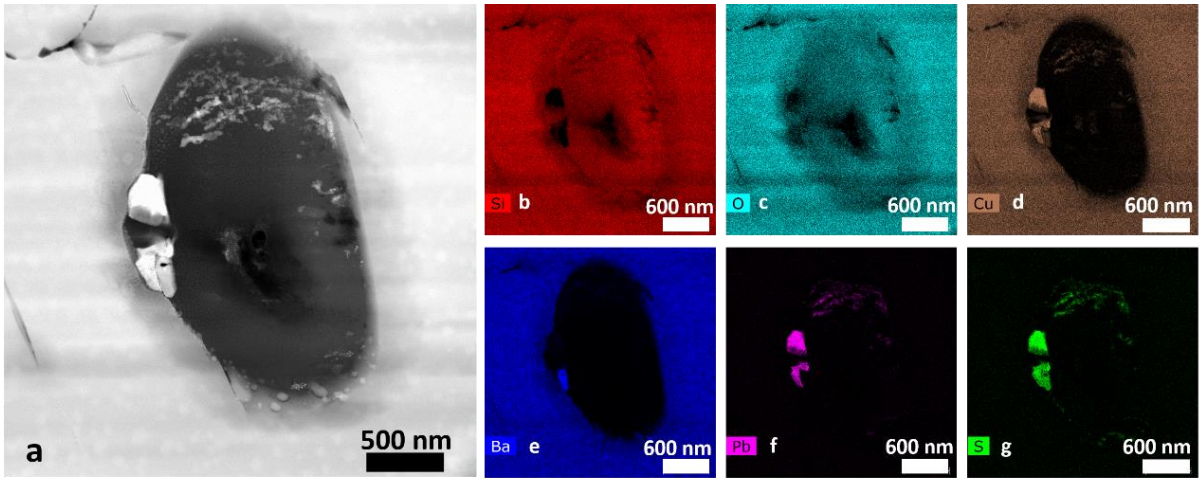

Figure 3-5. (a) An STEM-HAADF image of the micron to sub-micron size inclusions within a $BaCuSi_4O_{10}$ crystal. (b)-(g) EDS elemental maps of Si, O, Cu, Ba, Pb, and S of this area.

Further analysis to obtain structural information (**Figure 3-6**) based on STEM/TEM of three crystallites (Area 1-3 in **Figure 3-6** (a)) showed the presence of Pb-rich crystals; in Area 1 and 2 these were identified as Pb_3O_4, indexed based on FFT obtained from the corresponding high resolution TEM images of the crystalline phases (**Figure 3-6**(b) and (c)). The Ba- and S-rich crystallite in Area 3 was identified as $BaSO_4$ (**Figure 3-6**(d)). TEM images further revealed amorphous SiO_2 matrix in which the nano-size crystalline inclusions are embedded in (**Figure**

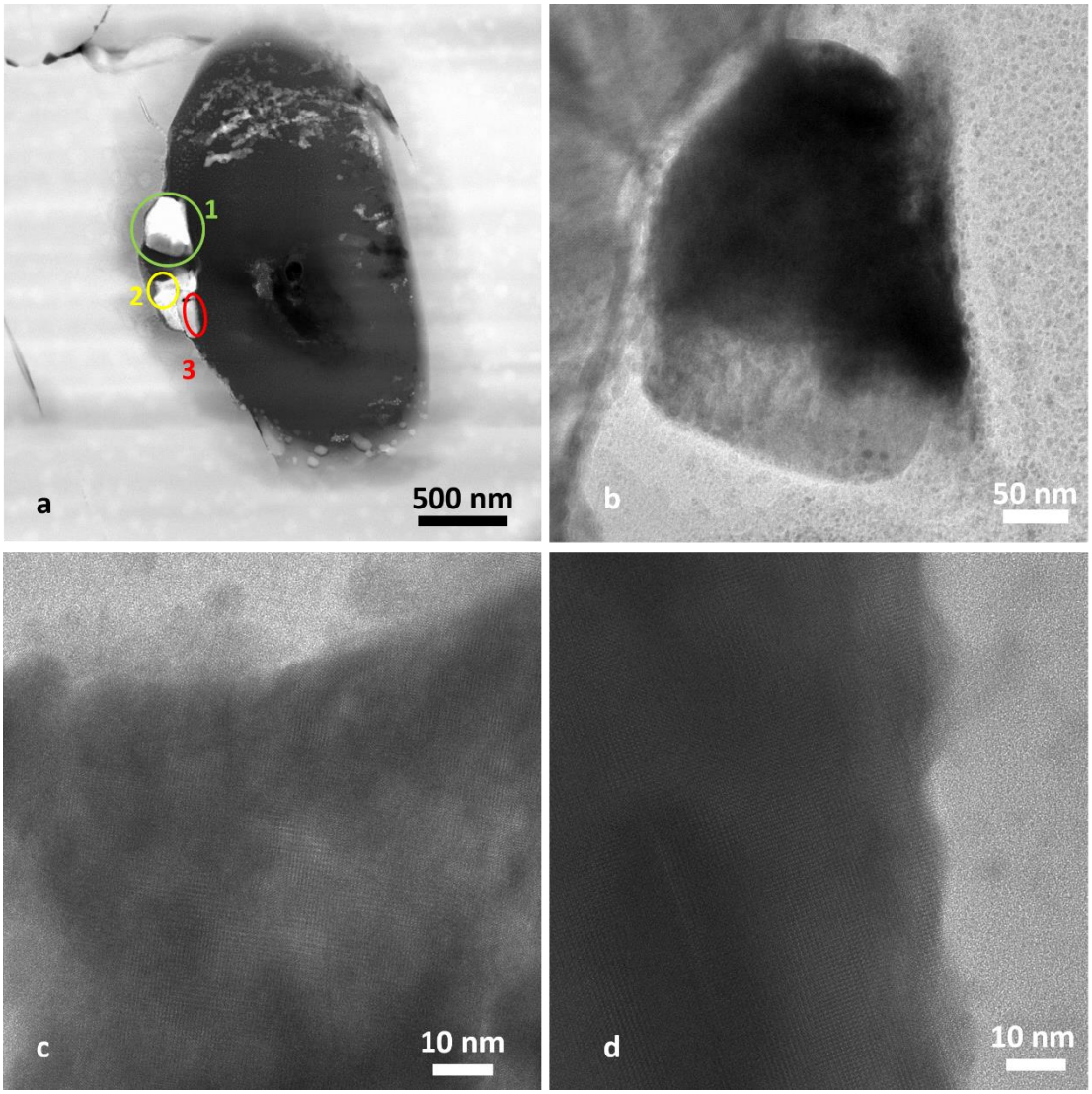

Figure 3-6. (a) An STEM-HAADF image of the area of interest, with three individual nano-size inclusions labeled. (b) A TEM image at high magnification of Area 1. (c) A TEM image at high magnification of Area 2. (d) A TEM image at high magnification of Area 3.

3-6(b)-(d)).

In addition to the characterization of micron to sub-micron inclusions within $BaCuSi_4O_{10}$ crystals, a direct observation of the silicate layer structure of $BaCuSi_4O_{10}$ crystals was made. One of the pigment crystals was oriented to the [100] direction. The atomic arrangement of rows of atoms, viewed in the HAADF-STEM image as bright spots, was inferred by the relative size of the atoms, with Ba being the largest atoms, Cu being the intermediate atoms, and Si being the smallest atoms (**Figure 3-7**(a) and (c)). The lattice constants measured on this HAADF-STEM image were a = 7.22 Å, c = 16.38 Å, indicated by the yellow arrows (**Figure 3-7**(a)). These values of 'a' and 'c' are within ~3% and ~2%, respectively, relative to the

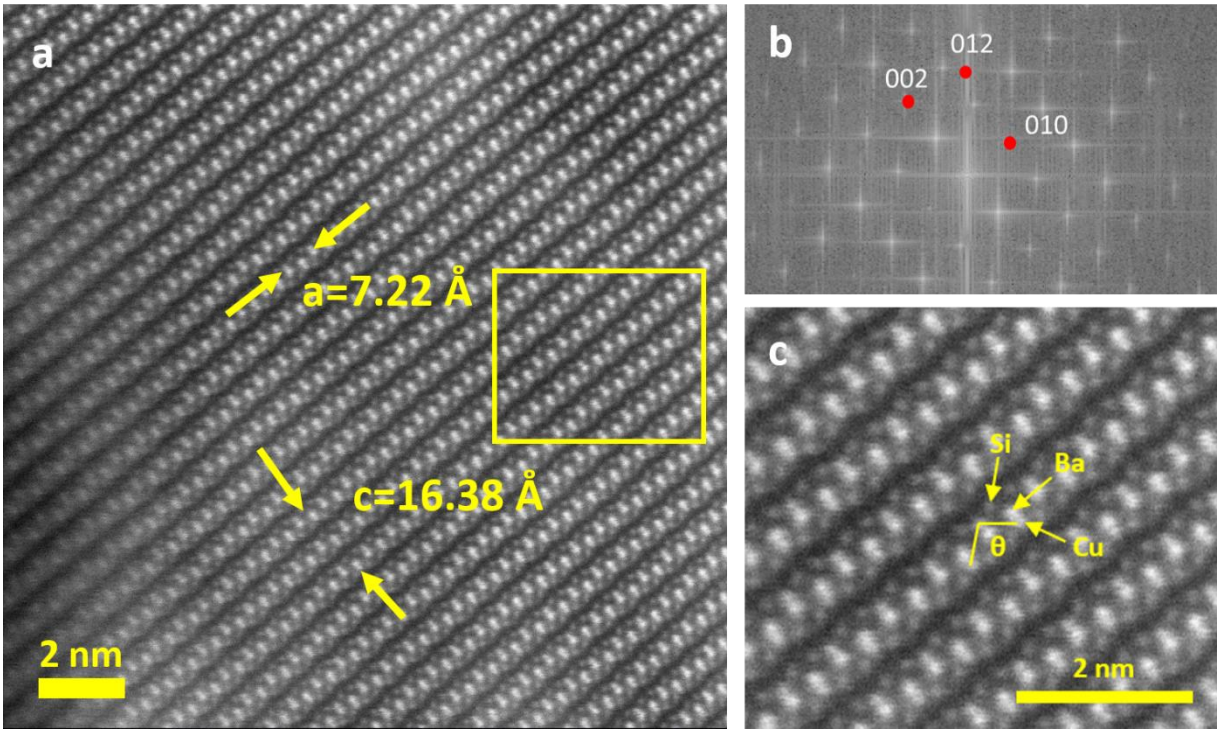

Figure 3-7. (a) An HAADF-STEM image of a $BaCuSi_4O_{10}$ single crystal oriented to the [100] zone axis, showing the atomic arrangement with direct observation of columns of Ba, Cu and Si atoms in the tetragonal crystal structure. Yellow arrows show the 'a' and 'c' lattice parameters. (b) FFT of the HAADF-STEM image shown in (a) with index. (c) A zoomed-in area (shown in yellow square in (a)), showing locations of Ba, Cu, and Si atoms, as well as the angle θ between three adjacent Cu atoms, measured to be 99.24±1.2 degree.

reported values determined by XRD on synthetic $BaCuSi_4O_{10}$ crystal or effenbergerite mineral sample (**Table 3-1**). The interplanar angles between (002) and (010), and between (012) and (010), were measured to be 89.73 degree and 42.90 degree, respectively (**Figure 3-7**(b)). These measured values are within 0.5% difference relative to their theoretical values, which are 90 degree and 42.69 degree, respectively. In addition, the angle between three adjacent Cu atoms, θ (**Figure 3-7**(c)), was measured on the HAADF-STEM image to be 99.24±1.2 degree, which is within ~1.5% difference relative to the value measured on a reference 3D molecular model of $BaCuSi_4O_{10}$ (based on the structure reported in [27]) oriented to the same zone axis, which was 100.75±0.55 degree.

Table 3-1. Lattice parameters on $BaCuSi_4O_{10}$ crystal reported in literature.

a (Å)	c (Å)	References
7.44±0.01	16.11 ± 0.02	[25]
7.440(2)	16.097(6)	[26]
7.447(1)	16.138(2)	[27]
7.4409(3)	16.1367(8)	[28]
7.442(2)	16.133(5)	[30]

3.4 Discussion

3.4.1 Structure of archaeological Chinese blue

The few percent differences in lattice parameters of $BaCuSi_4O_{10}$ crystal between values measured in this study and those reported in literature could be due to systematic error resulted from calibration of the STEM/TEM microscope. Deformation effects such as strain field induced between the sample and the thin foil could also result in such difference. This first

direct observation of the atomic arrangement of single crystal of $BaCuSi_4O_{10}$ can help to visualize its layer structure for the characterization of the exfoliated 2D nanosheets of $BaCuSi_4O_{10}$ reported in a previous study [95] in the development of novel optical materials.

3.4.2 Production technology of archaeological Chinese blue

Our research using STEM/TEM-EDS characterization of archaeological Chinese blue presents the first direct visualization of $BaCuSi_4O_{10}$ atomic arrangement and identification of sub-micron scale crystals of $BaSO_4$, solid solution of $BaSO_4$-$PbSO_4$, Pb_3O_4, and amorphous SiO_2, key features of the reverse engineering of the pigment, pointing to certain processes for the production of the Chinese blue faience bead. These data are very important as they can prove or disprove previous claims based on empirical experimentation regarding the choice of raw materials and pigment synthesis [8, 9, 41, 48, 69, 71, 73, 107].

Source(s) for barium (Ba)

Barite ($BaSO_4$), a readily available and abundant mineral in ancient China, has been previously suggested as one of the possible raw materials as a source of Ba in the production of Chinese blue, both based on raw material availability and the presence of $BaSO_4$ identified on some archaeological Chinese blue samples [9, 47, 50, 51]. However, laboratory reproduction experiments have shown that due to its high thermal decomposition temperature (1580 °C if in its pure form) and despite the catalytic effect of PbO in promoting decomposition

of $BaSO_4$ at lower temperatures [8, 71], direct use of barite resulted in large amounts of unreacted $BaSO_4$, which affected the quality and overall color of the Chinese blue pigment [9, 48, 73, 108]. Since different lead compounds are found in Chinese blue as byproducts, it has been suggested that Pb-containing minerals have been used as catalysts to increase the decomposition rates of barite [8, 9, 41, 71]. Although successful synthesis of Chinese blue using $BaSO_4$ was reported in one study, with a molar ratio of 1:1:2 for Ba:Cu:Si, unreacted $BaSO_4$ was identified as one of the major phases besides $BaCuSi_4O_{10}$ and CuO after continuous 24-hour firing at 900 °C [71]. Also, albeit the use of 25 wt% PbO as flux/catalyst and/or calcination pre-treatments of barite, a significant amount of unreacted $BaSO_4$ slags were still present after continuous 10-hour firing at 1100 °C [73]. In addition, with CuO and SiO_2 as raw materials and a Ba:Cu:Si of 1:1:4, with the addition of 20 wt% of PbO, $PbCO_3$, $PbSO_4$, or PbS, the use of barite failed to produce Chinese blue pigment as the main phase without the large amount of unreacted $BaSO_4$ or formation of Cu_2O as byproduct, under the heat treatment temperatures from 800 to 1000 °C and synthesis time of 6 hours or 24 hours [108].

Contrary, employing the same operational sequences for the pigment's production, though, substituting barite with witherite ($BaCO_3$) – another Ba-containing mineral, produces Chinese blue with higher purity [8, 9, 41, 48, 71, 73, 107, 108]. In addition, thermal analysis by TG/DTG has shown that $BaCO_3$ started to decompose at ~800 ˚C and completed at ~950 ˚C when mixtures of $BaCO_3$, CuO and SiO_2 (with either 1:1:2 or 1:1:4 stoichiometry for Ba:Cu:Si) were heated up to 1000 ˚C [69]. Thereupon, witherite was suggested as the material most likely used

in the production of these pigments based on a chemical point of view. However, witherite resources in China are much rarer than their barite counterpart, with the only known witherite deposits in China is located in the Southern Qinling, covering the southern part of the Shaan'xi province, Sichuan province and Chongqing area [82-84]. These witherite deposits are ~300-400 km away from modern day Xianyang (the capital of Qin Dynasty) and Xi'an (the capital of Western Han Dynasty), but are about 600 km away from modern day Gansu Province (the region in which a lot of Chinese blue faience beads dated to the Warring States Period have been recovered, including the sample analyzed in this study) and Luoyang (the capital of Eastern Han Dynasty), pointing to either a long distance travel to obtain witherite to produce the pigments locally, or a long distance inter-reginal exchange of pigment products, if witherite was indeed the Ba-source.

In our research, in addition to the sub-micron $BaSO_4$ crystals identified by STEM-EDS, observations of the cross section by BSE-SEM (**Figure 3-2**(a), (b)) showed that micron-scale inclusions rich in Ba are limited; large amount of unreacted $BaSO_4$ slags are not observed as it was in previous studies [48, 73]. Our microstructural data points to the higher possibility that witherite instead of barite had been used as source of Ba in the production. The sub-micron $BaSO_4$ crystallites within the $BaCuSi_4O_{10}$ crystal are likely to be reaction byproducts resulting from the manufacturing process, which suggests that the source of sulfates is most likely linked to Pb-containing and/or Cu-containing raw materials, or as impurity from the witherite source.

Source(s) for sulfur (S)

Considering that witherite rather than barite was selected as the Ba-source, the sulfur (S) in byproducts such as $BaSO_4$ and $BaSO_4$-$PbSO_4$ could have been introduced from Cu-bearing minerals such as chalcocite (Cu_2S), which can be found in many parts of China. It has been noted, however, that compared to CuO, the direct use of Cu_2S as the source of copper results in a distinct change in the tone of pigment [9]. Based on commonly known copper extraction processes, chalcocite may be pre-treated (**Reaction 3-1** and **Reaction 3-2**) [109] and converted into CuO as the Cu precursor to $BaCuSi_4O_{10}$ (**Reaction 3-3**). The SO_2 resulting from these reactions can then react with $BaCO_3$ to form $BaSO_4$ [9]. From a chemical point of view however, the thermal decomposition of malachite ($Cu_2CO_3(OH)_2$) or azurite ($Cu_3(CO_3)_2(OH)_2$) to provide CuO is much easier and simpler. Therefore, although the use of Cu-S-containing minerals such as chalcocite cannot be ruled out, it is more likely that Pb-bearing minerals such as galena (PbS) or anglesite ($PbSO_4$) provided the source of SO_4^{2-} in the formation of sub-micron $BaSO_4$ and $BaSO_4$-$PbSO_4$ inclusions in this study.

Reaction 3-1.

$$2Cu_2S + 3O_2 \rightarrow 2Cu_2O + 2SO_2$$

Reaction 3-2.

$$Cu_2S + 2Cu_2O \rightarrow 6Cu + SO_2$$

Reaction 3-3.

$$Cu + \frac{1}{2}O_2 \rightarrow CuO$$

Source(s) for lead (Pb)

If S was indeed provided by Pb-containing source in the production of the Chinese blue faience bead studied in this research, the most likely source for Pb would be galena (PbS) and/or anglesite ($PbSO_4$). Galena, an abundant Pb-containing mineral in China, has been suggested as one of the possible raw materials for the source of Pb in the manufacturing of Chinese blue and Chinese purple ($BaCuSi_2O_6$, the earliest synthetic purple pigment in China's history with contemporary production to Chinese blue) [57, 72]. It has been shown that under the same reaction conditions, with malachite ($Cu_2CO_3(OH)_2$), sand (SiO_2) and witherite ($BaCO_3$) as sources of Cu, Si, and Ba, respectively, the use of PbS with 10 wt% of PbO content, promotes the formation of Chinese blue; whereas the use of lead carbonate ($PbCO_3$), with an equal 10 wt% of PbO content, promotes the formation of Chinese purple [72]. In addition to galena, anglesite ($PbSO_4$), one of the most common secondary minerals resulting from the near-surface oxidation of galena [110], is another Pb-containing mineral that could have been used as the source of Pb and S.

Thermal oxidation of PbS in air between 600 K and 1200 K under equilibrium conditions can lead to the formation of $PbSO_4$ (**Reaction 3-4**), PbO (**Reaction 3-5**), and metallic Pb (**Reaction 3-6**) [111-113], with **Reaction 3-4** being the primary oxidation reaction and $PbSO_4$ as the most abundant oxidized product up to 870 [111, 113]. Various chemical reactions between PbS and the oxidized products ($PbSO_4$ and PbO), as well as among oxidized products can occur depending on the heat treatment temperature oxygen concentration, and remaining

oxidized products, leading to regeneration of $PbSO_4$, PbO, and/or metallic Pb and formation of intermediate products such as $PbO{\cdot}PbSO_4$ [111, 113]. These Pb-containing compounds can take part in the formation of $BaCuSi_4O_{10}$ as catalyst to increase the reaction rate, and/or can react with other raw materials to form different crystalline and amorphous by products such as $BaSO_4$-$PbSO_4$ solid solution and Pb_3O_4 inclusions, which will be discussed in more detailed in the following section.

Reaction 3-4.

$$PbS + 2O_2 \rightarrow PbSO_4$$

Reaction 3-5.

$$2PbS + 3O_2 \rightarrow 2PbO + 2SO_2$$

Reaction 3-6.

$$PbS + O_2 \rightarrow Pb + SO_2$$

At elevated temperatures, besides a polymorphic transformation from orthorhombic to monoclinic in the range of 850-865 °C [114, 115], thermal decomposition of $PbSO_4$ has been reported to be noticeable or start at different temperatures with large discrepancy in the range of 637-860 °C [74, 114, 116-118], depending on the various experimental procedures and conditions. In one study, it has been stated that $PbSO_4$ decomposes strongly at 900-1000 °C in a molten state [119]. It has also been shown that when heated for one hour at ~1000-1100 °C, the decomposition proceeds from 2.1% to 29.0% [114]. The decomposition of $PbSO_4$ leads to the formation of PbO and $PbO{\cdot}PbSO_4$, with the release of SO_2 and O_2 (**Reaction 3-7** and **Reaction 3-8**) [114], which can participate in reactions with the other raw materials and/or products of other chemical reactions occurring in the manufacturing process of Chinese blue.

Reaction 3-7.

$$PbSO_4 \rightarrow PbO + SO_2 + \frac{1}{2}O_2$$

Reaction 3-8.

$$4PbSO_4 \rightarrow 2PbO \cdot PbSO_4 + 2SO_2 + O_2$$

With the decomposition of witherite (**Reaction 3-9**) and the gradual formation of $BaCuSi_4O_{10}$ upon cooling based on nucleation and growth from a melt (or partial melt) with high temperature firing (**Reaction 3-10**), some of the BaO can react with SO_2 (resulted from chemical reactions involving PbS and/or $PbSO_4$) (**Reaction 3-11**), or with $PbSO_4$ (from the oxidation reaction of galena or from the direct use of anglesite) (**Reaction 3-12**) to form the observed sub-micron $BaSO_4$ inclusions within the large $BaCuSi_4O_{10}$ crystals).

Reaction 3-9.

$$BaCO_3 \rightarrow BaO + CO_2$$

Reaction 3-10.

$$BaO + CuO + 4SiO_2 \xrightarrow{\sim 900 - \sim 1000\,^{\circ}C\,/\,1000\,^{\circ}C - RT} BaCuSi_4O_{10}$$

Reaction 3-11.

$$BaO + SO_2 + \frac{1}{2}O_2 \rightarrow BaSO_4$$

Reaction 3-12.

$$BaO + PbSO_4 \rightarrow BaSO_4 + PbO$$

Reaction 3-13.

$$BaO + PbO + 2SO_2 + O_2 \rightarrow BaSO_4 - PbSO_4$$

The presence of sub-micron $BaSO_4$-$PbSO_4$ solid solution inclusions identified with STEM-EDS within the $BaCuSi_4O_{10}$ crystals suggests a similarly possible formation mechanism. A naturally occurring $BaSO_4$-$PbSO_4$ solid solution mineral known as Hokutolite, is found in acid hot spring deposits [120]. Evidence of Pb incorporated into barite by Ba/Pb substitution

has also been identified in waste rock piles [121]. $BaSO_4$ and $PbSO_4$ are both orthorhombic with similar unit cell parameters and the same space group Pnma [122, 123]. A series of $BaSO_4$-$PbSO_4$ solid solutions with composition across the whole range has been successfully synthesized via co-precipitation from the melt of $Ba(NO_3)_2$ and $Pb(NO_3)_2$ at temperatures between 750-850°C with $NaNO_3$ as flux [124]. It is therefore possible that also in the Chinese blue faience production, the available PbO from Pb-containing fluxes/catalysts introduced as raw materials reacts with the BaO, to form through co-precipitation of $BaSO_4$ and $PbSO_4$ from the melt during the cooling process (**Reaction 3-13**), submicron scale $BaSO_4$-$PbSO_4$ solid solution inclusions. Another possible formation mechanism of the $BaSO_4$-$PbSO_4$ solid solution via secondary formation through the incorporation of Pb^{2+} into the thermally stable $BaSO_4$ inclusions over a span of more than 2000 years of burial. However, such mechanism might be favored if the $BaSO_4$ crystals are present within a glassy matrix containing Pb^{2+} resulting from a relatively fast cooling process in which crystallization of Pb-containing inclusions are prevented. In this case, Pb^{2+} can be absorbed to the surface of $BaSO_4$ crystals to allow the displacement of Ba^{2+} with Pb^{2+} in the crystal structure via diffusion.

Possible formation mechanism of Pb_3O_4

A common formation mechanism of Pb_3O_4 is via oxidation of PbO (massicot) (**Reaction 3-14**). The direction of this solid-vapor redox reaction depends on both heating temperature and pressure [125]. It has been determined that with increasing oxygen partial pressure (pO_2)

from ~50-500 psi (~3.4-34 atm), the equilibrium temperature of this redox reaction increases from ~600 ˚C to ~750 ˚C [125]. The reduction of Pb_3O_4 to PbO was observed to proceed rapidly when Pb_3O_4 was heated to ~700 ˚C in an open crucible in air in less than 30s, and the melting curve of PbO is nearly independent of pressure, with a melting point of 887 ˚C in air (for massicot) [125].

Reaction 3-14.

$$6PbO + O_2 \leftrightarrow 2Pb_3O_4$$

Therefore, if the nano-size Pb_3O_4 inclusions were formed via the solid-vapor oxidation of PbO solid, a strong oxidizing environment would have been required during the manufacturing of Chinese blue to prevent the rapid reduction of these Pb_3O_4 crystallites back to PbO. PbO solids can be obtained with the use of PbS or $PbSO_4$ as starting materials. PbO undergoes a transformation from tetragonal litharge to orthorhombic massicot at ~489 ˚C [126]. This transformation temperature was likely to be exceeded in the production of Chinese blue and massicot was likely to be the polymorph of PbO. The synthesis temperature would therefore be lower than 887 ˚C so that PbO would not melt and remain a solid.

However, if the heat treatment temperature was higher than 750 ˚C, even with a strong oxidizing environment with pO2 as high as 34 atm (which is likely to be beyond the capability of ancient pyrotechnology), Pb_3O_4 could be easily reduced to PbO. If the heat treatment was lower than 750 ˚C, then the temperature might not be high enough for the formation of $BaCuSi_4O_{10}$ crystals, as in all previous experiments to reproduce the ancient pigment, the lower limit of firing temperature for the making of Chinese blue is ~900 ˚C. An alternative

explanation would be a two-step firing in the making of the faience bead. In a previous study, it has been stated that a successful reproduction of the same type of Chinese blue faience bead was achieved by a two-step dry glazing method [50]. However, no additional data were given. If a two-step firing was the case, the formation of Pb_3O_4 could have occurred in the second step in which a glazing material containing Pb-compounds and pre-made $BaCuSi_4O_{10}$ crystals were applied over the SiO_2-rich core and subjected to firing at a lower temperature. In this way, the reduction of Pb_3O_4 back to PbO could have been prevented if the temperature in the second step was low enough.

This alternative explanation, however, contradicts the finding of these nano-size Pb_3O_4 crystals as inclusions within $BaCuSi_4O_{10}$ crystals. If the formation of Pb_3O_4 particles occurred during the second-step of low temperature heat treatment in a mixture with pre-made $BaCuSi_4O_{10}$ crystals, it would most likely be that these would be found within the glassy matrix, rather than within a $BaCuSi_4O_{10}$ single crystal as inclusions. In addition, the amorphous SiO_2 coexisting with the Pb_3O_4 crystals suggests a partial or total melt at high temperature, in which $BaCuSi_4O_{10}$, Pb_3O_4, and $BaSO_4$ crystals were nucleated. In this scenario, the nano-size Pb_3O_4 crystals could have been trapped within the $BaCuSi_4O_{10}$ single crystal, making it very difficult to participate in further reactions, including their reduction to PbO at a temperature higher than 750 ˚C.

3.5 Conclusions

We have demonstrated the first sub-micron resolution characterization of an archaeological sample of Chinese blue faience bead from the Late Warring States Period with STEM/TEM-EDS. The first direct observation of atomic arrangement of the $BaCuSi_4O_{10}$ layer structure corroborates with previous crystallographic studies and also helps its visualization in the characterization of previously reported 2D nanosheets of $BaCuSi_4O_{10}$ in the engineering of novel optical materials.

The presence of micron or sub-micron scale $BaSO_4$, $BaSO_4$-$PbSO_4$ solid solution, Pb_3O_4 and amorphous SiO_2 inclusions were first observed and reported in this study, whose formation are closely related to raw materials selection and manufacturing process. Based on possible formation mechanisms for these two inclusions from a chemical point of view, it is likely that witherite had been used as source of Ba, and galena and/or anglesite had been used as source of Pb and S. However, the possibility that S might be also from Cu-containing minerals such as chalcocite cannot be ruled out. Based on these new insights, future work focusing on trace element identification and quantification, as well as on stable isotope analysis will be carried out to provide a better understanding of the raw materials origin.

Chapter 4. Systematic laboratory-based reproduction of Chinese blue and Chinese purple

Published data of archaeological samples of Chinese blue ($BaCuSi_4O_{10}$) and purple ($BaCuSi_2O_6$) together with previous laboratory-based reproduction experiments, suggested that Chinese blue and Chinese purple can be reproduced with selected Ba-, Cu-, and Si-containing raw materials and a Pb-salt as the flux/catalyst, and treated at different firing conditions. In the absence of surviving written sources, however, the choice of the raw materials and the manufacturing process, or steps of operational sequences for their production (*chaîne opératoire*) remained unclear. This chapter attempts to provide a new insight and fill this gap of knowledge with the systematic reproduction of Chinese blue and Chinese purple, with focus on testing the effects of different combinations of Ba:Cu:Si starting stoichiometry, Ba-sources ($BaSO_4$ and $BaCO_3$) and Pb-sources (PbO, $PbCO_3$, $PbSO_4$ and PbS) as raw materials for the synthesis of the pigments. In order to establish the boundary of synthesis conditions for each combination of raw materials, heat treatments were performed in the range of 800-1000 ˚C with every 50 ˚C increment, for 6 hours to obtain the more kinetic products, and 24 hours to obtain the more thermodynamically stable products. Visible (Vis)-induced (λ_{exc} max=600 nm) near infrared (NIR) photoluminescence (λ_{em} max= ~980 nm) imaging has been applied to assess the presence of $BaCuSi_4O_{10}$ and $BaCuSi_2O_6$. Scanning electron microscopy (SEM) coupled with energy-dispersive X-ray spectrometry (EDS) and electron probe microanalysis (EPMA) has been applied to characterize microstructure and elemental composition of various phases in the end-products. Powder X-ray diffraction (XRD) has been applied to selected

samples for phase confirmation, and color measurement has been performed using fiber optic reflectance spectrometry (FORS).

4.1 Experimental Procedures

4.1.1 Raw Materials

In this systematic reproduction experiment, all starting materials are powder chemicals of high purity. CuO (ACS reagent, 99%) was used as the Cu-source. Crystalline SiO_2 (MIN-U-SIL®40, 99.7%) was provided by US Silica Company. The Ba and Pb-containing raw materials were purchased from Sigma Aldrich: $BaSO_4$ (reagent grade, 99%) and $BaCO_3$ (ACS reagent, 99%) were chosen to represent two possible Ba-containing minerals. Orthorhombic PbO (ACS reagent, 99%), $PbCO_3$ (ACS reagent grade), $PbSO_4$ (98%) and PbS (99.9% trace metals basis) were chosen as the most common Pb-containing minerals and/or synthetic products available through alchemical processes in ancient China at the time. Specifically, orthorhombic PbO represents both mineral massicot and alchemical 黄丹, "yellow dan" (a type of elixir). $PbCO_3$ represents both the mineral cerussite and an alchemical 铅粉, "lead powder", which was used as a white pigment on polychrome figurines and mural paintings, as well as a white cosmetic powder [80]. PbS and $PbSO_4$ represent the minerals galena and anglesite, respectively.

4.1.2 Synthesis Steps

$BaSO_4$ or $BaCO_3$, CuO, and SiO_2 were mixed based on Ba:Cu:Si stoichiometric ratios of either 1:1:2 or 1:1:4, with addition of 20 wt% of one of the four chosen for testing Pb-containing compounds: PbO, $PbCO_3$, $PbSO_4$, or PbS. After mixing, powders of 1:1:4 were mixed with deionized (DI) H_2O and shaped into small pigment sticks (~2-3 cm in length and ~0.5-1 cm in diameter). Powders of 1:1:2 stoichiometry were shaped into small balls (~0.5-1 cm in diameter). Both pigment sticks and balls were dried in air before receiving heat treatment (firing).

A pigment stick and a pigment ball with the same starting materials for Ba and Pb were placed in the same porcelain crucible (American Educational Low Form Porcelain Crucible, 30 mL) and heated at the same temperature and time. Heat treatment temperatures were set to be 800 ˚C, 850 ˚C, 900 ˚C, 950 ˚C, or 1000 ˚C. Heat treatment time was set to be either 6 hours to obtain kinetic products, or 24 hours for thermodynamic products. After heat treatment, the kiln was turned off and all batches were cooled naturally to room temperature with the kiln door closed. A total of 160 samples were synthesized with systematic variations of Ba-source, Pb-source, heat treatment temperature, and heat treatment time.

4.1.3 Characterization of Raw Materials and Reproduced End-products

Visible (Vis)-induced near infrared (NIR) photoluminescence imaging was performed on all end-products before cutting to establish that complete reaction has taken place and the possible presence of Chinese blue or Chinese purple. A Mini-Crimescope MCS-400 (SPEX

Forensics) with tunable excitation light capabilities was used. For this experiment, excitation was provided with λ_{exc} max = 600 nm (50 nm bandwidth) [93] . A modified UV-IR Nikon D90 DSLR camera was used to capture images, with a longpass filter Peca 910, which allows 90% transmission above ~800 nm but filters out light with $\lambda < 800$ nm.

Polished cross sections of each sample was obtained by cutting pigment sticks or balls. Cross sections were embedded in epoxy resin and ground with silicon carbide grit paper from 600 to 1200 grit and polished with water-based diamond suspensions of 6 μm and 1μm.

Optical photomicrographs were taken using a Keyence VHX-1000 digital microscope at 20-200X magnification to document distribution of different colors of each cross section, as the first assessment of phases possibly present in the end-products.

Powder X-ray diffraction (XRD) was performed on selected samples to confirm the phases. An X'Pert PRO PANalytical powder XRD with a Cu-Kα source was applied, with a voltage of 45 kV and a current of 40 mA. The 2θ range was from 10˚ to 100˚, with a step size of 0.03˚ and count time of 41.9 s per step.

Color measurement was performed on powder samples using the FiledSpec3® from Analytical Spectral Devices Inc. (ASD), which has a spectral resolution of 3 nm at 700 nm and 10 nm at 1400/2100 nm and covers from 350 nm to 2500 nm. Based on the reflectance spectra obtained from each powder sample, color values were recorded in the L*a*b* color space defined by CIE (Commission Internationale de l'Eclairage) in 1976 [127].

Polished cross sections were coated with carbon and imaged with a Phenom G-2 ProX

desktop scanning electron microscope (SEM). The backscattered electron detector (BSE) was used under high vacuum mode to obtain electron micrographs with compositional contrast enhancing the different phases present in the sample and their distribution. BSE-SEM was mainly performed at 10 kV under high resolution. Energy dispersive X-ray spectroscopy (EDS) was performed at 15 kV with a count time of either 30 s.

A JXA 8200 SuperProbe electron probe microanalyzer (EPMA) equipped with a tungsten gun and five wavelength dispersive spectrometers (WDS) was used to confirm stoichiometry of compounds identified to be possibly present based on EDS analysis, namely, $BaCuSi_4O_{10}$, $BaCuSi_2O_6$, $BaCu_2Si_2O_7$, $BaSO_4$, $BaSi_2O_5$, CuO, Cu_2O, and SiO_2. EPMA analysis was performed at an accelerating voltage of 15 kV and a current of 15 nA. Probe diameter was set to be 1 μm. Elements analyzed included Ba, Cu, Si, Pb, and S. Detection of Cu, Si and S was based on their K_α energies while detection of Pb was based on its M_α energy and detection of Ba was based on its L_α energy. Peak positions were calibrated on standard reference minerals barite ($BaSO_4$), galena (PbS), metallic Cu tape, and anorthite ($CaAl_2Si_2O_8$) with ZAF correction applied. Counting time for each element was set to be 20 sec. Spot mode was chosen and ZAF correction was applied on all EPMA analyses. Quantification was checked against Corning B (with 61.55 wt% SiO_2 and 2.66 CuO), Corning C (with 34.76 wt% SiO_2, 1.13 wt% CuO, 11.40 wt% BaO and 36.70 wt% PbO), and Corning D (with 55.24 wt% SiO_2) archaeological reference glasses, and on standard reference mineral barite ($BaSO_4$).

4.2 Results

By systematically varying the five experimental parameters, i.e. the Ba:Cu:Si stoichiometry, Ba-source, Pb-source, heat treatment temperature, and heat treatment time, a total of 160 end-products were produced. Based on qualitative and quantitative results establishing the presence of major and minor phases for Chinese blue and purple, different sub-groups were developed mainly assessing the effects of the Ba-source, the Pb-source and stoichiometry of Ba:Cu:Si. The optimal synthesis conditions (temperature ranges and time duration) were also determined (**Figure 4-1**). Major differences were observed between the samples produced with $BaSO_4$ and those with $BaCO_3$ as the source for barium. Within the group of samples produced with the $BaSO_4$ as the starting material, variations were noticeable based on the Pb-source used, whereas, stoichiometry has shown negligible effect. The group of samples produced with $BaCO_3$ on the other hand, indicated that variations in the

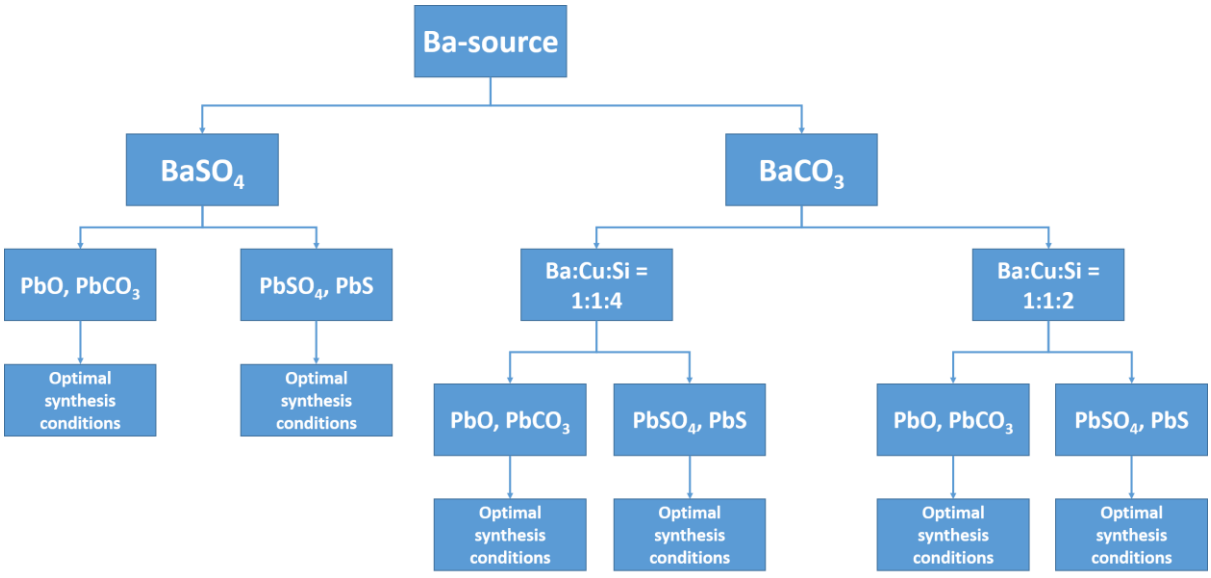

Figure 4-1. Sub-groups of end-products based on the Ba-source, Pb-source, stoichiometry of Ba:Cu:Si, and synthesis conditions (temperature range and firing time).

stoichiometry of Ba:Cu:Si played a more important role in the formation of the major pigment phases produced (**Figure 4-1**).

4.2.1 $BaSO_4$ as Ba-source

Out of 80 samples produced using $BaSO_4$ with Ba:Cu:Si of 1:1:4 and 1:1:2 under various heat treatment conditions, the majority (63 samples) have a grey, dark grey, or silvery grey exterior (**Figure 4-2**(a)), and a core (interior) consisting of grey, white, black, brownish yellow, and in some cases red particles (**Figure 4-2**(b)). These samples did not emit NIR luminescence under excitation with λ_{ex} max = 600 nm, indicating the absence of $BaCuSi_4O_{10}$ and $BaCuSi_2O_6$. Based on SEM-EDS/EPMA and XRD characterization, these end-products with vitrified and crystalline phases were further classified according to the Pb-source used.

With PbO or $PbCO_3$ as the Pb-source, the end products were identified as unreacted $BaSO_4$, CuO and SiO_2 embedded in a $PbO\text{-}SiO_2$ glass matrix with minor amounts of Cu and Ba (**Figure**

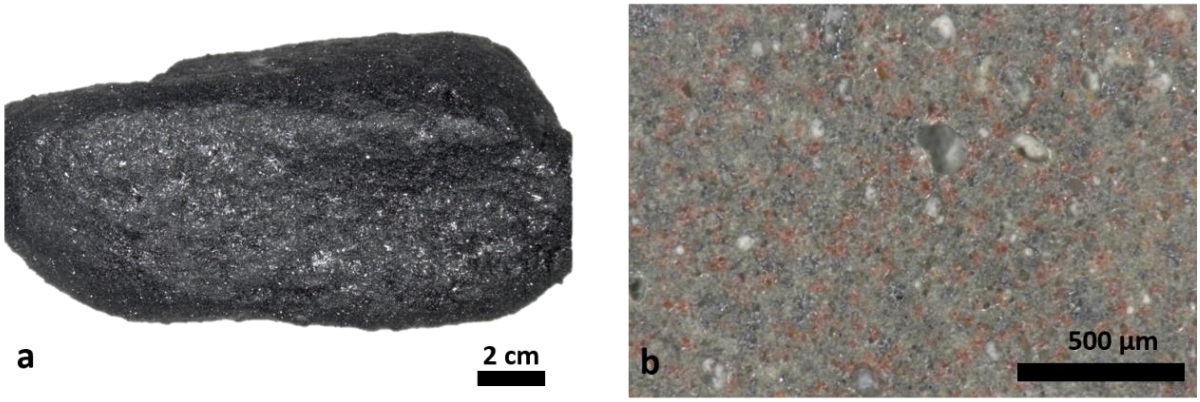

Figure 4-2. Photomicrographs of a representative pigment sample produced with $BaSO_4$ as Ba-source, showing (a) a shiny dark grey exterior, and (b) the white, grey, black, and red particles in the interior of the cross section. This sample was produced using $PbCO_3$ as Pb-source, with a Ba:Cu:Si ratio of 1:1:4, and synthesized at 950 ˚C for 6 hours.

4-3(a)). However, when $PbSO_4$ or PbS were used as the fluxes/catalysts, the end-products formed showed crystals of $(Ba,Pb)SO_4$ solid solution, unreacted CuO and SiO_2 (**Figure 4-3**(b)). These phases were confirmed by XRD (**Figure 4-4**).

In addition, when synthesis was performed at sufficiently high temperature (950 ˚C or 1000 ˚C) and/or long enough time, red Cu_2O crystals formed as one of the major phases of the end-product (**Table 4-1**). In 20 out of the 80 samples produced with $BaSO_4$, the presence of Cu_2O was recorded. During the experiments it was recorded that in the samples produced with PbO or $PbCO_3$ as the flux/catalyst, Cu_2O was starting to form at a temperature around 900 ˚C, whereas, in those produced with $PbSO_4$ or PbS, Cu_2O was formed at a higher temperature, around 1000 ˚C.

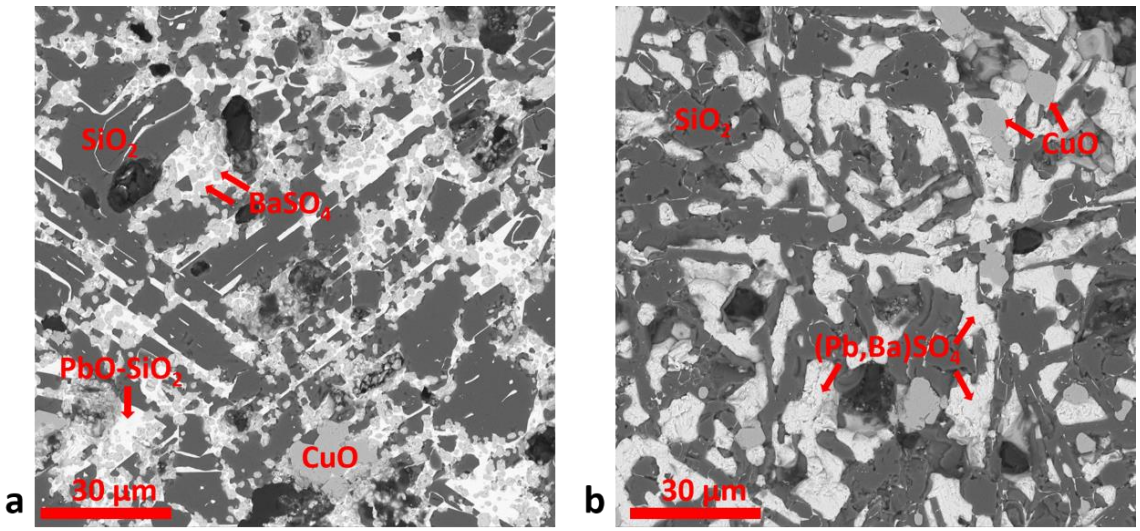

Figure 4-3. BSE micrographs of cross sections of two pigment samples produced with $BaSO_4$ as Ba-source but with different Pb-additives, with a Ba:Cu:Si ratio of 1:1:4, synthesized at 900˚C for 24 hours. (a) A cross section of a sample produced with $PbCO_3$ as the Pb-flux/catalyst, shows unreacted SiO_2 (large dark particles), $BaSO_4$ (small light grey particles), and CuO (grey particles) as the major crystalline phases, embedded in a $PbO\text{-}SiO_2$ glass matrix (white matrix). (b) A cross section of a sample produced with PbS as Pb-flux/catalyst, showing unreacted SiO_2 (large particles) and CuO (grey particles), as well as $(Pb,Ba)SO_4$ solid solution as the main phases.

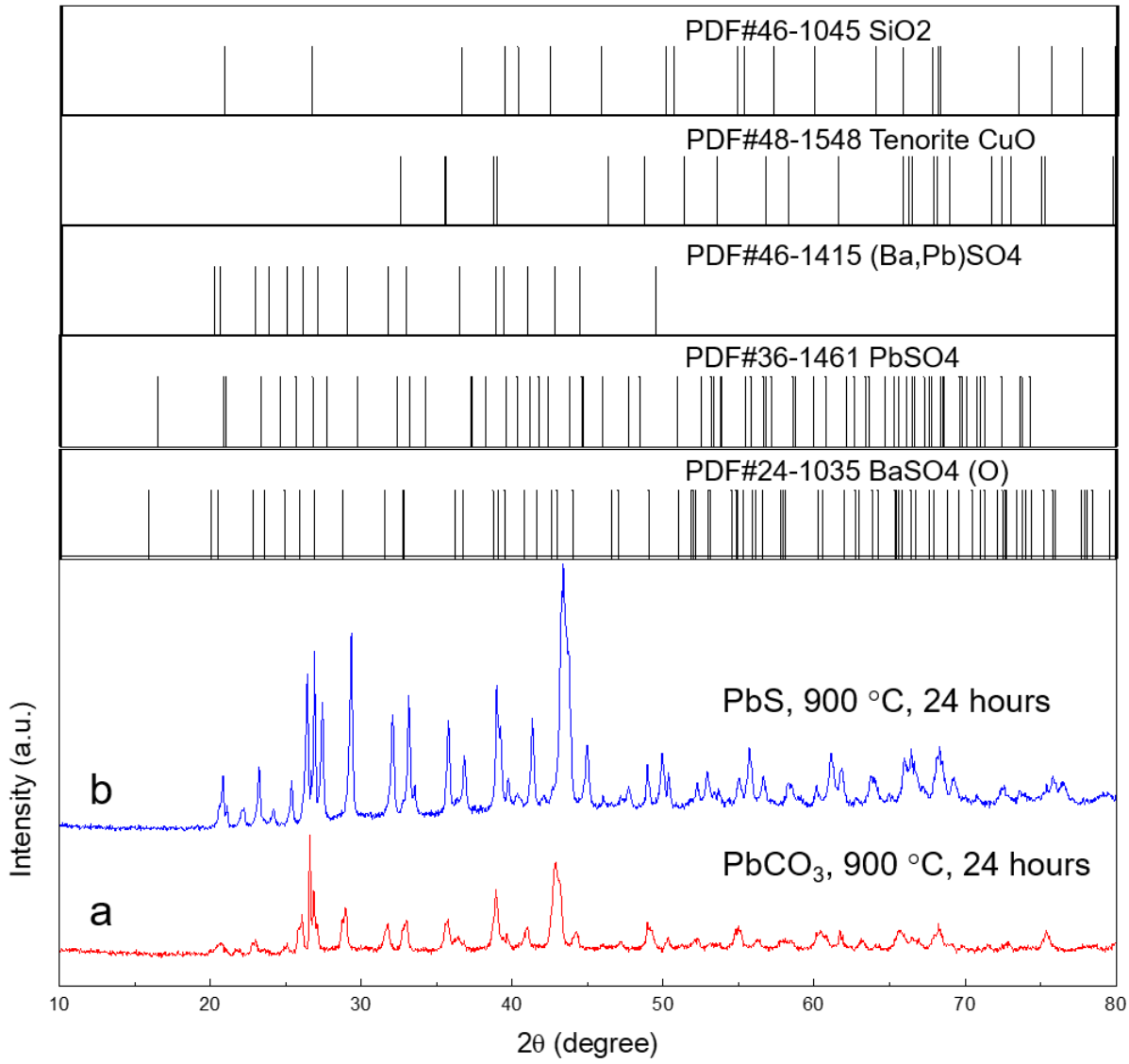

Figure 4-4. XRD diffractograms of samples shown in **Figure 4-3**, produced with $BaSO_4$ as Ba-source and with (a) $PbCO_3$, and (b) PbS, with a Ba:Cu:Si ratio of 1:1:4, synthesized at 900˚C for 24 hours.

Table 4-1. Synthesis conditions for samples produced with $BaSO_4$ with Cu_2O in the end-products. T: synthesis temperature. t: synthesis time.

Ba:Cu:Si	Ba-source	Pb-source	T (˚C)	t (hours)
1:1:4	$BaSO_4$	PbO	950	6
1:1:4	$BaSO_4$	$PbCO_3$	950	6
1:1:4	$BaSO_4$	PbO	1000	6

1:1:4	$BaSO_4$	$PbCO_3$	1000	6
1:1:4	$BaSO_4$	PbO	900	24
1:1:4	$BaSO_4$	$PbCO_3$	900	24
1:1:4	$BaSO_4$	PbO	950	24
1:1:4	$BaSO_4$	$PbCO_3$	950	24
1:1:4	$BaSO_4$	PbO	1000	24
1:1:4	$BaSO_4$	$PbCO_3$	1000	24
1:1:4	$BaSO_4$	$PbSO_4$	1000	24
1:1:4	$BaSO_4$	PbS	1000	24
1:1:2	$BaSO_4$	PbO	1000	6
1:1:2	$BaSO_4$	$PbCO_3$	1000	6
1:1:2	$BaSO_4$	$PbCO_3$	900	24
1:1:2	$BaSO_4$	PbO	950	24
1:1:2	$BaSO_4$	$PbCO_3$	950	24
1:1:2	$BaSO_4$	$PbCO_3$	1000	24
1:1:2	$BaSO_4$	$PbSO_4$	1000	24
1:1:2	$BaSO_4$	PbS	1000	24

17 out of the 80 samples produced with $BaSO_4$ showed NIR luminescence on the exterior of the pigment rods or balls (**Figure 4-5**(a), (b)), indicating the presence of $BaCuSi_4O_{10}$ and/or $BaCuSi_2O_6$. Among them, 11 samples have only a few characteristic blue spots that luminesce

(**Figure 4-5**(c)). SEM-EDS indicated that these samples contain $BaCuSi_4O_{10}$ only in the outer layer region (< 200-300 μm) but not in the core (**Figure 4-5**(d)). The main phases in the core of these samples consist of unreacted $BaSO_4$, SiO_2, and CuO. The $BaCuSi_4O_{10}$ crystals observed in the exterior region can be indication of the start of the formation reaction which will require higher synthesis temperature and/or longer synthesis time to promote the decomposition of the raw materials and formation of the pigment crystals. Also, the possibility of partial contamination from the re-use of the crucibles cannot be ruled out.

Only 6 out of the 17 luminescent samples contain $BaCuSi_4O_{10}$ crystals found both on the exterior and in the core (**Table 4-2**). However, in three of these samples the $BaCuSi_4O_{10}$ are small with length < 20 μm (**Figure 4-6**(a)), indicating the limited growth of the pigment crystals. These include samples produced with $PbO/PbCO_3$ at 1000 ˚C for 24 hours (Ba:Cu:Si = 1:1:4), and with PbO at 950 ˚C for 24 hours (Ba:Cu:Si = 1:1:2). Though present in the end-products of these formulations, $BaCuSi_4O_{10}$ is not considered to be one of the main phases in the end-products. In addition, Cu_2O is present in higher than 20% in these samples (**Figure 4-6**(b)). Based on these results, it is unlikely that this combination of raw materials and conditions were preferred for the production of $BaCuSi_4O_{10}$.

In the two samples produced with $PbCO_3/PbSO_4$ (Ba:Cu:Si = 1:1:2) at 1000 ˚C for 24 hours, although $BaCuSi_4O_{10}$ crystals have grown larger (> 50 μm) (**Figure 4-6**(c)), they remain

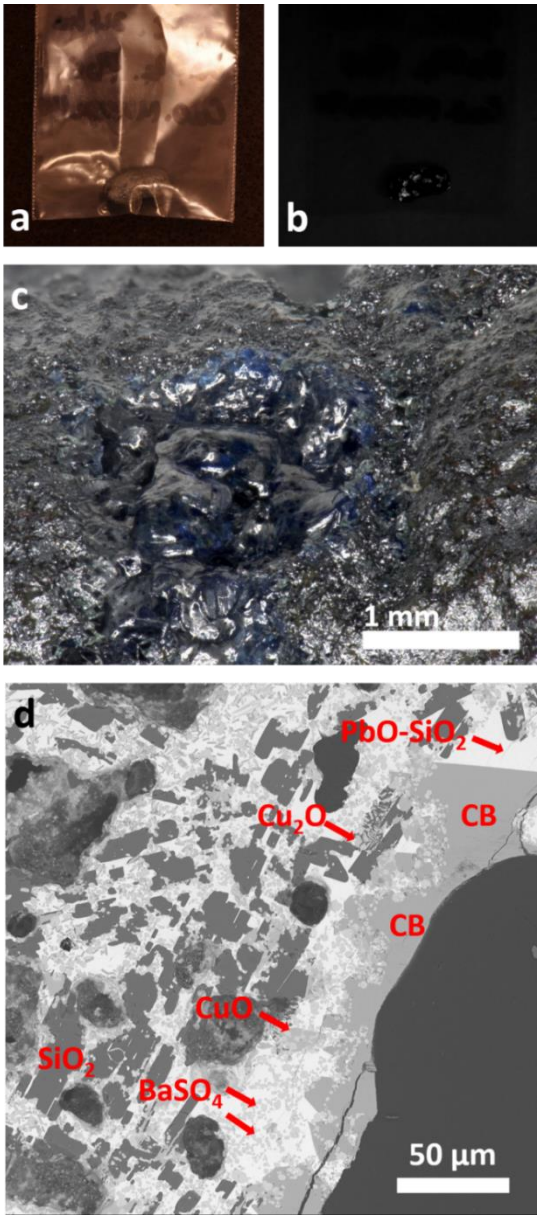

Figure 4-5. Details of pigment sample produced with $BaSO_4$ and PbO (Ba:Cu:Si = 1:1:4) at 950 ˚C for 24 hours. (a) RGB image of the sample. (b) Vis-induced NIR photoluminescent image of the sample, showing several luminescent areas, indicating the presence of $BaCuSi_4O_{10}$ and/or $BaCuSi_2O_6$. (c) Photomicrograph of the sample, showing a blue area luminescing in (b). (d) BSE micrograph of the cross section of the sample, showing the distribution of CB ($BaCuSi_4O_{10}$, dark grey) in the area that is within 50 μm from the surface, along with $BaSO_4$ (small light grey particles), CuO (grey crystals that are slightly darker than $BaSO_4$ phase), SiO_2 (dark), and Cu_2O (light grey particles), embedded in a $PbO\text{-}SiO_2$ glass matrix.

a minor phase compared to the predominant presence of red Cu_2O particles (**Figure 4-6**(d)).

These results are also inconsistent with data from the archaeological Chinese blue or Chinese

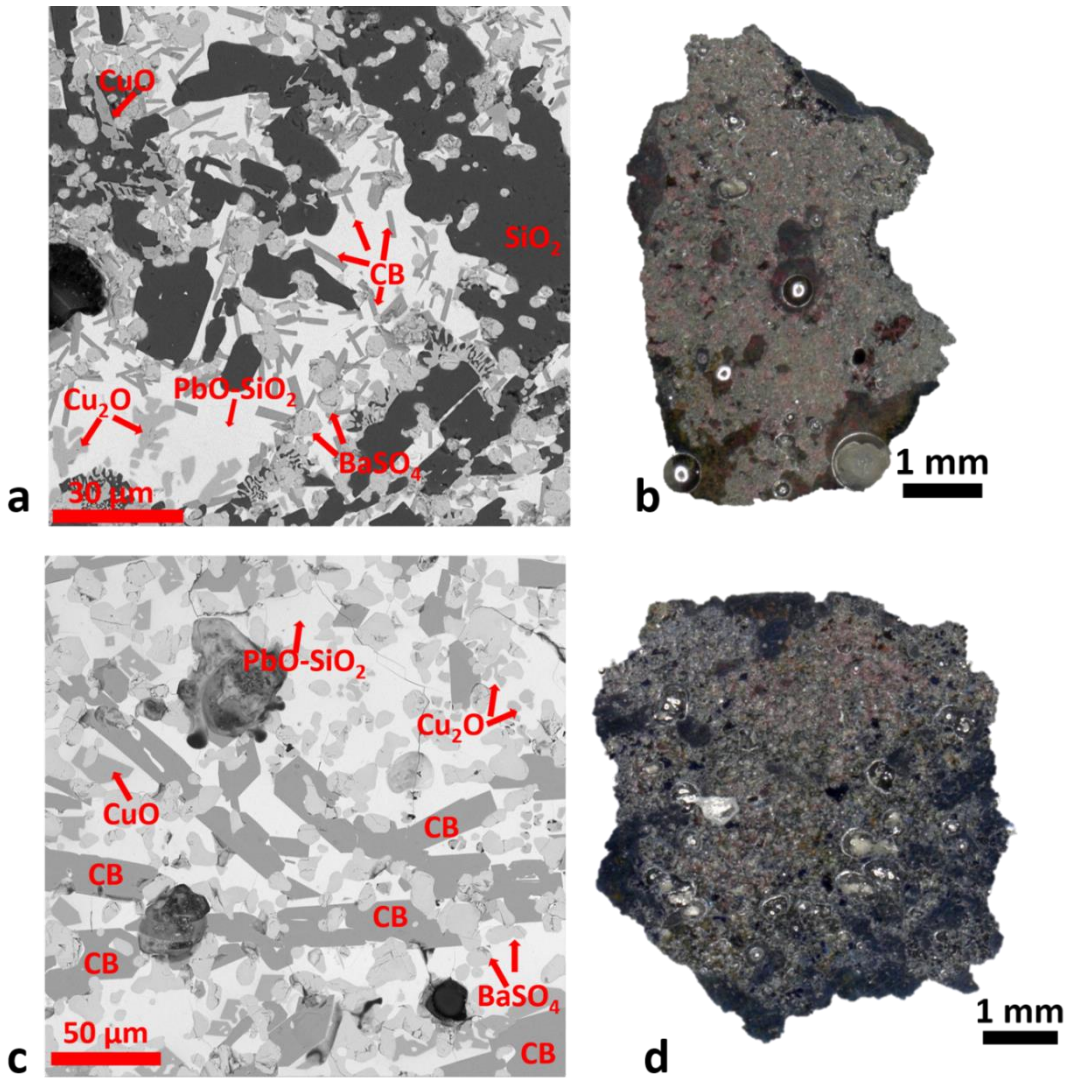

Figure 4-6. (a) BSE micrograph of a cross section of a pigment sample produced with $BaSO_4$ and PbO (Ba:Cu:Si = 1:1:4) at 1000 ˚C for 24 hours. The sample shows CB ($BaCuSi_4O_{10}$) as rectangular crystals with length < 20 µm, together with $BaSO_4$ (light grey), CuO (grey but slightly darker than $BaSO_4$ phase), SiO_2 (dark), and Cu_2O (light grey), embedded in a PbO-SiO_2 glass matrix. (b) Photomicrograph of the cross section shown in (a), showing the abundance of red Cu_2O within the cross section. (c) BSE micrograph of a cross section of a sample produced with $BaSO_4$ and $PbSO_4$ (Ba:Cu:Si = 1:1:2) at 1000 ˚C for 24 hour, showing CB ($BaCuSi_4O_{10}$) as long rectangular crystals with length > 50 µm, together with $BaSO_4$ (light grey), CuO (grey but slightly darker than $BaSO_4$ phase), and Cu_2O (light grey), embedded in a PbO-SiO_2 glass matrix. (d) Photomicrograph of the cross section shown in (c), with abundance of red Cu_2O in the core of the sample.

purple samples that show $BaCuSi_4O_{10}$ or $BaCuSi_2O_6$ as the major phase respectively.

Table 4-2. List of samples produced with $BaSO_4$ that contain $BaCuSi_4O_{10}$ crystals throughout the interior of cross sections.

Ba:Cu:Si	**Pb-source**	**T (˚C)**	**t (hrs)**	**NIR luminescence**	**Microstructure of $BaCuSi_4O_{10}$**	**Cu_2O as a major phase**
1:1:2	PbO	1000	24	Entire surface	Long rectangular crystals (>50 μm) or matrix	No
1:1:2	$PbCO_3$	1000	24	Entire surface	Long rectangular crystals (>50 μm)	Yes
1:1:2	$PbSO_4$	1000	24	Entire surface	Long rectangular crystals (>50 μm)	Yes
1:1:2	PbO	950	24	Most surface	Small rectangular crystals (<20 μm)	Yes
1:1:4	PbO	1000	24	Localized surface area	Small rectangular crystals (<20 μm)	Yes
1:1:4	$PbCO_3$	1000	24	Localized surface area	Small rectangular crystals (<20 μm)	Yes

Out of the 80 samples produced with $BaSO_4$, the only sample that contains $BaCuSi_4O_{10}$ as the major phase without formation of Cu_2O was synthesized using PbO as Pb-source, with a Ba:Cu:Si starting stoichiometry of 1:1:2 at 1000 ˚C for 24 hours (**Table 4-2**). The sample appear to be grayish blue with some yellow and dark particles (**Figure 4-7**(a)). $BaCuSi_4O_{10}$ crystals are distributed throughout the cross section either as long rectangular crystals that has length >50 μm (**Figure 4-7**(b)) or as major matrix (**Figure 4-7**(c)). Other phases in this sample include unreacted $BaSO_4$ and CuO, embedded in a $PbO\text{-}SiO_2$ glass matrix. In addition, $BaCuSi_2O_6$ crystals of minor amount are also observed (**Figure 4-7**(d)).

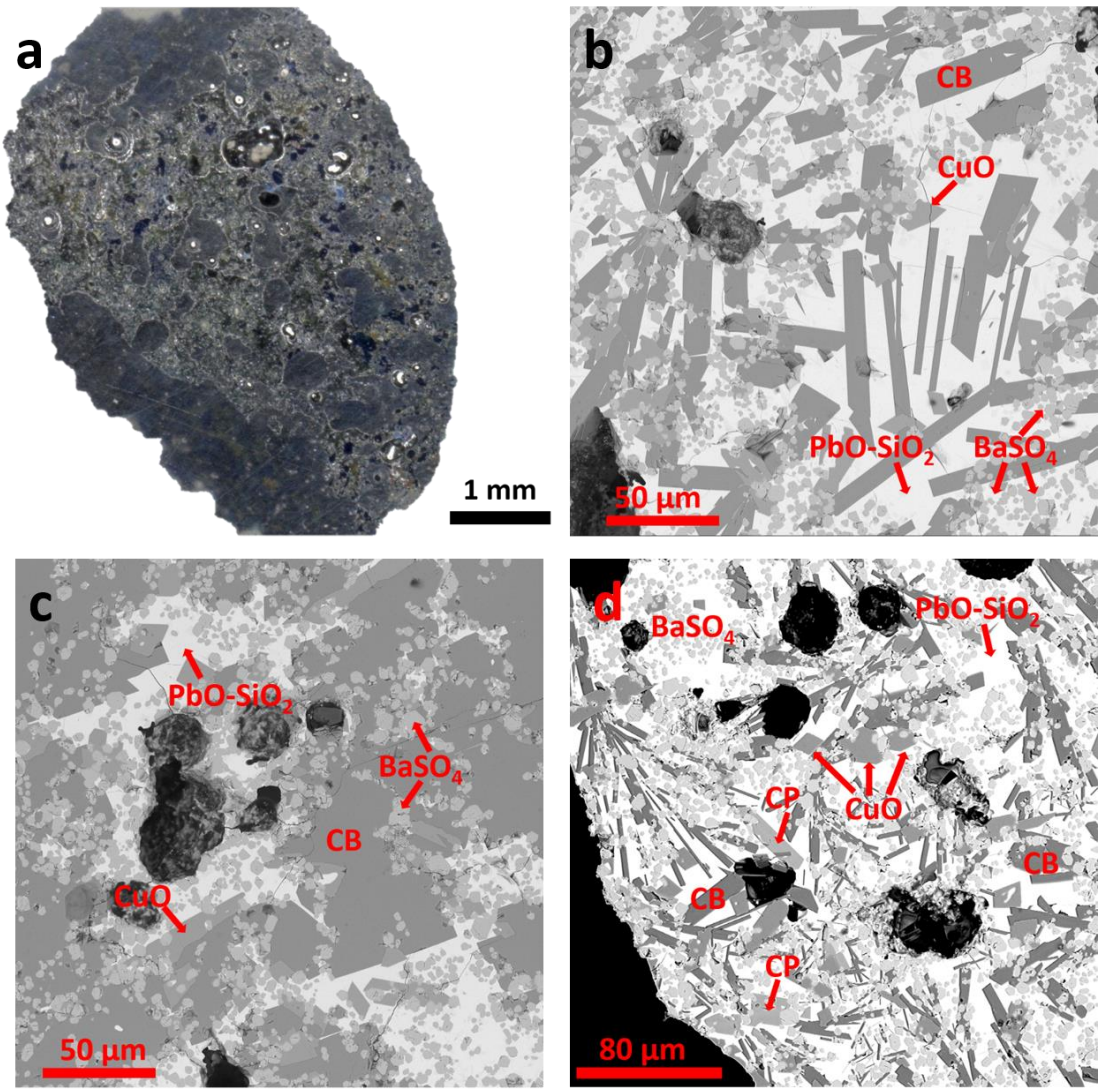

Figure 4-7. Pigment sample produced with $BaSO_4$ and PbO (Ba:Cu:Si = 1:1:2) at 1000 ˚C for 24 hours. (a) Photomicrograph of the cross section, showing a greyish blue (with some yellow and dark particles) surface of the sample. (b) BSE micrograph of an area of the cross section, showing the long rectangular (> 50 µm) CB ($BaCuSi_4O_{10}$) crystals, together with $BaSO_4$ (light grey) and CuO (grey), embedded in a PbO-SiO_2 glass matrix. (c) BSE micrograph of another area of the cross section, showing a $BaCuSi_4O_{10}$ (dark grey) and PbO-SiO_2 glass (white) matrix with interstitial $BaSO_4$ (light grey) and CuO (grey) crystals. (d) BSE micrograph of another area of the cross section, showing the presence of CP ($BaCuSi_2O_6$) crystals (light grey), with compositional contrast slightly lighter than CuO but darker than the $BaSO_4$ phase) as a minor phase, together with $BaCuSi_4O_{10}$ (dark grey), $BaSO_4$ (light grey) and CuO (grey), in a PbO-SiO_2 glass matrix.

4.2.2 $BaCO_3$ as Ba-source

All samples produced with $BaCO_3$, with Ba:Cu:Si = 1:1:4 or 1:1:2, show strong vis-

induced NIR photoluminescence (**Figure 4-8**(a), (b)) and have blue or blue to purple colors (**Figure 4-8**(c)), suggesting the strong presence of $BaCuSi_4O_{10}$ and/or $BaCuSi_2O_6$. Differences in the chemistry and microstructure of the end-products are on the basis of Ba:Cu:Si stoichiometry, identities of Pb-source, reaction temperatures and time. Among these factors, the Ba:Cu:Si stoichiometry and Pb-source play an important role in the end-products formed, whereas, the synthesis temperature and firing time affect mainly the microstructure and

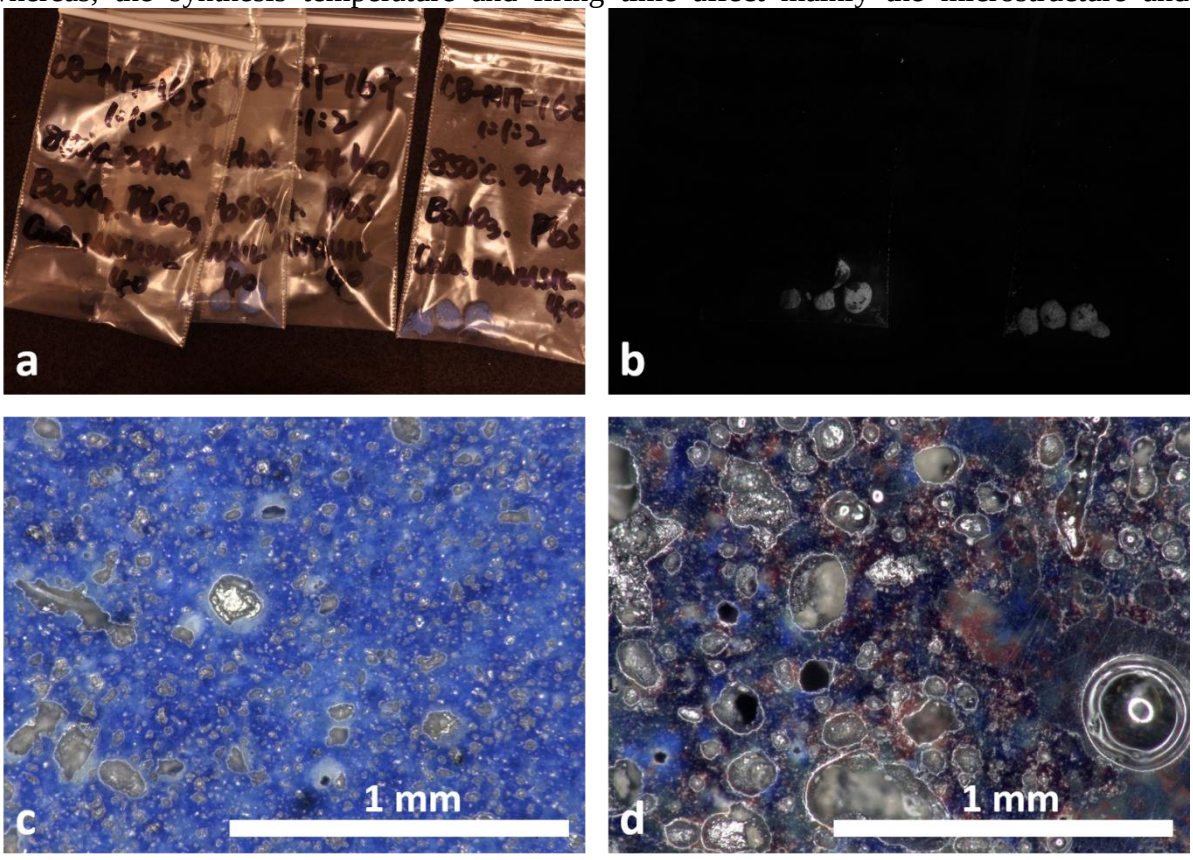

Figure 4-8. (a) RGB image of four pigment samples synthesized at 850 ˚C for 24 hour, at molar ration: Ba:Cu:Si = 1:1:2. From left to right: 1) $BaSO_4$ and $PbSO_4$ (dark blue/grey; 2) $BaCO_3$ and $PbSO_4$ (blue); 3) $BaSO_4$ and PbS (dark blue/grey) and 4) $BaCO_3$ and PbS (blue). (b) Vis-induced NIR photoluminescence image of the samples in (a). The two dark blue/grey samples (1 and 3) produced with $BaSO_4$ do not show any photoluminescence, whereas the two blue samples produced with $BaCO_3$ show strong vis-induced NIR photoluminescence. (c) Photomicrograph of a cross section of the blue sample produced with $BaCO_3$ and PbS at 850 ˚C for 24 hours, with Ba:Cu:Si = 1:1:2. (d) Photomicrograph of a cross section of a sample produced with $BaCO_3$ and PbS at 1000 ˚C for 24 hours, with Ba:Cu:Si = 1:1:2, showing the formation of red Cu_2O particles.

abundance of these phases.

Although formation of $BaCuSi_4O_{10}$ and/or $BaCuSi_2O_6$ as the major phase has been achieved using $BaCO_3$ as the Ba-source (as attested to in 14 out of 80 samples), red Cu_2O was also formed as one of the major phases (**Table 4-3**, **Figure 4-8**(d)). This was observed in samples synthesized at 950 ˚C for 24 hours, and 1000 ˚C for 6 hours or 24 hours. In general, in samples produced with PbO and PbS, Cu_2O was formed at lower temperatures than those produced with $PbCO_3$ and $PbSO_4$.

Table 4-3. Synthesis conditions for samples produced with $BaCO_3$ that have Cu_2O formed in the end-products. T: synthesis temperature. t: synthesis time.

Ba:Cu:Si	**Ba-source**	**Pb-source**	**T (˚C)**	**t (hours)**
1:1:4	$BaCO_3$	PbO	950	24
1:1:4	$BaCO_3$	PbS	950	24
1:1:4	$BaCO_3$	PbO	1000	24
1:1:4	$BaCO_3$	PbS	1000	24
1:1:2	$BaCO_3$	PbO	1000	6
1:1:2	$BaCO_3$	$PbCO_3$	1000	6
1:1:2	$BaCO_3$	PbS	1000	6
1:1:2	$BaCO_3$	PbO	950	24
1:1:2	$BaCO_3$	$PbCO_3$	950	24

1:1:2	$BaCO_3$	PbS	950	24
1:1:2	$BaCO_3$	PbO	1000	24
1:1:2	$BaCO_3$	$PbCO_3$	1000	24
1:1:2	$BaCO_3$	$PbSO_4$	1000	24
1:1:2	$BaCO_3$	PbS	1000	24

4.2.2.1 Ba:Cu:Si = 1:1:4

Based on SEM-EDS/EPMA data, $BaCuSi_4O_{10}$ is one of the major phases (>50%, estimated based on compositional contrast with ImageJ) in all samples within this group, despite the differences in Pb-source and synthesis conditions. Main differences among these samples are seen in the identities and amounts of minor phases, which can be classified into two sub-groups: samples produced with PbO/$PbCO_3$, and those with $PbSO_4$/PbS.

4.2.2.1.1 PbO or $PbCO_3$ as Pb-source

Synthesis conditions, major and minor phases, composition of glass matrix, and L*a*b* values determined on samples produced with PbO or $PbCO_3$ as Pb-source are summarized in **Table 4-4**. Pigments synthesized with these fluxes/catalysts produced mainly $BaCuSi_4O_{10}$, the main crystalline phase in Chinese blue frit, with an intense blue color under the optical microscope (**Figure 4-9** and **Figure 4-10**).

When the synthesis temperature was below 900 ˚C and synthesis time was 6 hours, besides

the presence of $BaCuSi_4O_{10}$ (CB), unreacted CuO and SiO_2 were found as major phases (**Table 4-4**). Dark areas consisting mainly of unreacted black CuO particles were also visible under the optical microscope (**Figure 4-9**(a), (f), and **Figure 4-10**(a), (f)). However, when the synthesis temperature was at 950 ˚C or 1000 ˚C for 24 hours, Cu_2O formed as one of the major phases in samples produced with PbO (**Figure 4-9**(d), (e), **Table 4-3**).

Optimal synthesis conditions are considered when $BaCuSi_4O_{10}$ is formed as the main phase without the formation of Cu_2O and without or minor amounts of CuO. Optimal conditions were therefore reached for samples produced with PbO at 850-900 ˚C for 24 hours, and at 950-1000 ˚C for 6 hours and for samples produced with $PbCO_3$ at 850-1000 ˚C for 24 hours, and at 900-1000 ˚C for 6 hours. This suggests that the use of $PbCO_3$ in the starting materials requires less strict synthesis conditions while the use of PbO requires a more sophisticated control on the synthesis temperatures and time.

Besides the presence of $BaCuSi_4O_{10}$ (CB) as the main phase in all samples within this sub-group, Chinese purple ($BaCuSi_2O_6$ (CP)) was also commonly identified as a minor phase (**Figure 4-11** and **Figure 4-12**) whereas, Chinese dark blue ($BaCu_2Si_2O_7$ (CDB)) was detected as a minor phase, mainly in samples produced at temperatures lower than 900 ˚C. Residual SiO_2 (**Figure 4-11** to **Figure 4-14**) and reaction byproducts with a stoichiometry of $BaSi_2O_5$ (**Figure 4-13** and **Figure 4-14**) were commonly found as inclusions within the $BaCuSi_4O_{10}$ crystals. A glass matrix of PbO-SiO_2 composition was also formed at optimal synthesis conditions (**Figure 4-11** to **Figure 4-14**). Glass of the PbO-BaO-SiO_2 system was only detected

in samples produced at lower temperatures and/or shorter synthesis time (**Figure 4-11** to **Figure 4-14**). The identities of these phases were confirmed by XRD (**Figure 4-15**).

Table 4-4. Summary of synthesis conditions, major and minor phases, composition of glass matrix, and L*a*b* values for samples produced with $BaCO_3$ and $PbO/PbCO_3$, with Ba:Cu:Si = 1:1:4. CB: $BaCuSi_4O_{10}$; CP: $BaCuSi_2O_6$; CDB: $BaCu_2Si_2O_7$. Syntheses in which Chinese blue was successfully reproduced are highlighted in blue.

Pb-source	t (hrs)	T (ºC)	Main phases	Minor phases	Inclusions	Glass matrix	L*	a*	b*
PbO	24	800	CB, CuO, SiO_2	CDB, Pb/Ba-silicate	-	PbO-SiO_2	54.022	-11.2	-31.0
PbO	24	850	CB	CP, CuO	SiO_2	PbO-SiO_2, PbO-BaO-SiO_2	56.471	-7.6	-19.1
PbO	24	900	CB	CP	SiO_2	PbO-SiO_2, PbO-BaO-SiO_2	44.859	-10.4	-25.0
PbO	24	950	CB	CP, Cu_2O	SiO_2	PbO-SiO_2, PbO-BaO-SiO_2	59.432	-6.3	-12.9
PbO	24	1000	CB	CP, Cu_2O	SiO_2	PbO-SiO_2	53.684	-4.9	-11.9
$PbCO_3$	24	800	CB, CuO, SiO_2	Pb/Ba-silicate	-	PbO-SiO_2	60.598	-10.4	-28.2
$PbCO_3$	24	850	CB	CP, CuO, SiO_2	SiO_2	PbO-SiO_2, PbO-BaO-SiO_2	58.113	-8.1	-27.5
$PbCO_3$	24	900	CB	CP	SiO_2, $BaSi_2O_5$	PbO-SiO_2, PbO-BaO-SiO_2	59.797	-5.7	-15.9
$PbCO_3$	24	950	CB	CP	SiO_2, $BaSi_2O_5$	PbO-SiO_2, PbO-BaO-SiO_2	54.979	-7.4	-22.2
$PbCO_3$	24	1000	CB	-	SiO_2, $BaSi_2O_5$	PbO-SiO_2, PbO-BaO-SiO_2	52.88	-9.8	-28.3
PbO	6	800	CB, CuO, SiO_2	CDB, Pb/Ba-silicate	-	PbO-SiO_2, PbO-BaO-SiO_2	60.665	-5.9	-15.1
PbO	6	850	CB, CuO, SiO_2	CDB, Pb/Ba-silicate	SiO_2	PbO-SiO_2, PbO-BaO-SiO_2	61.563	-6.1	-17.1
PbO	6	900	CB, CuO, SiO_2	CP	SiO_2	PbO-SiO_2, PbO-BaO-SiO_2	49.86	-8.2	-30.4

PbO	6	950	CB	CP	SiO_2	PbO-SiO_2, PbO-BaO-SiO_2	61.48	-5.8	-15.9
PbO	6	1000	CB	CP, CDB	SiO_2, $BaSi_2O_5$	PbO-SiO_2	57.476	-5.0	-16.8
$PbCO_3$	6	800	CB, CuO, SiO_2	CDB, Pb/Ba-silicate	-	PbO-SiO_2, PbO-BaO-SiO_2	67.366	-6.8	-15.4
$PbCO_3$	6	850	CB, CuO, SiO_2	CDB, Pb/Ba-silicate	SiO_2	PbO-SiO_2, PbO-BaO-SiO_2	58.412	-8.1	-24.6
$PbCO_3$	6	900	CB	CP, CDB	SiO_2, $BaSi_2O_5$	PbO-SiO_2, PbO-BaO-SiO_2	53.584	-12.0	-36.0
$PbCO_3$	6	950	CB	CP	SiO_2, $BaSi_2O_5$	PbO-SiO_2, PbO-BaO-SiO_2	54.531	-12.4	-26.5
$PbCO_3$	6	1000	CB	CP, CDB, CuO	SiO_2, $BaSi_2O_5$	PbO-SiO_2, PbO-BaO-SiO_2	53.225	-10.9	-34.7

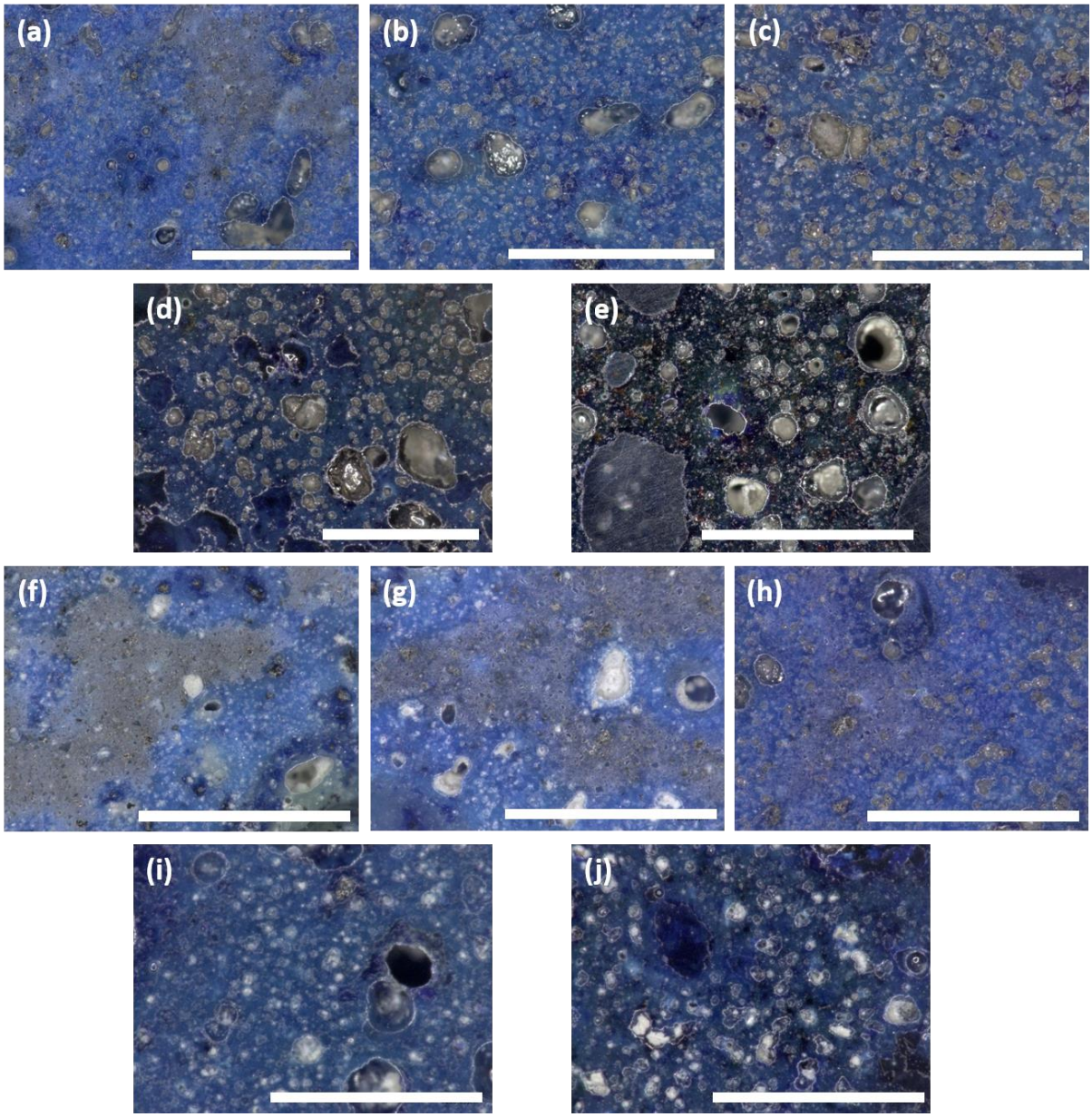

Figure 4-9. Photomicrographs of pigment samples produced with $BaCO_3$ and PbO, with starting stoichiometry of Ba:Cu:Si = 1:1:4, and heat treatment for 24 hours at (a) 800 ºC, (b) 850 ºC, (c) 900 ºC, (d) 950 ºC, and (e) 1000 ºC, and for 6 hours at (f) 800 ºC, (g) 850 ºC, (h) 900 ºC, (i) 950 ºC, and (j) 1000 ºC. Scale bar: 1 mm.

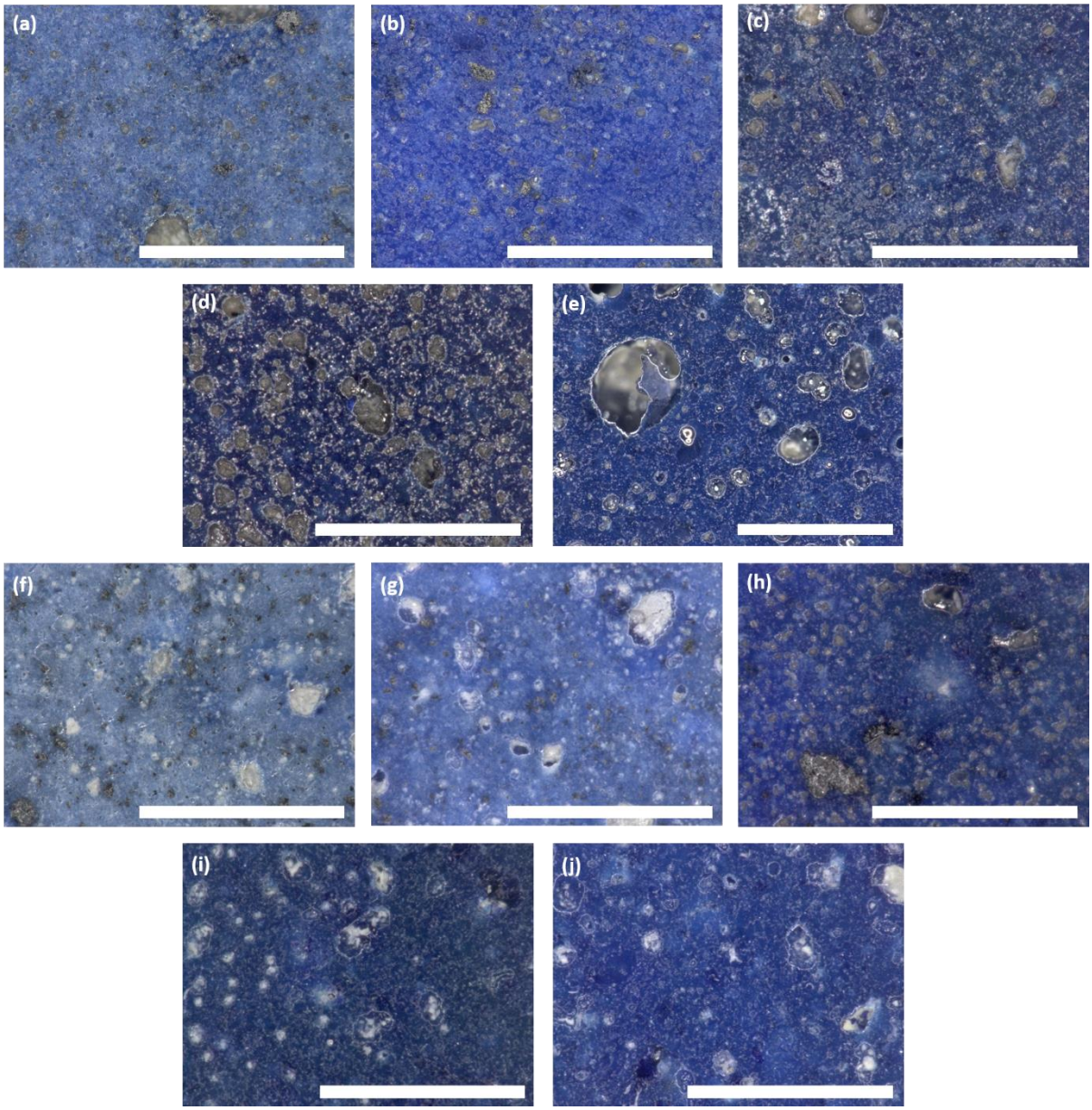

Figure 4-10. Photomicrographs of pigment samples produced with $BaCO_3$ and $PbCO_3$, with starting stoichiometry of Ba:Cu:Si = 1:1:4, and heat treatment for 24 hours at (a) 800 ºC, (b) 850 ºC, (c) 900 ºC, (d) 950 ºC, and (e) 1000 ºC, and for 6 hours at (f) 800 ºC, (g) 850 ºC, (h) 900 ºC, (i) 950 ºC, and (j) 1000 ºC. Scale bar: 1 mm.

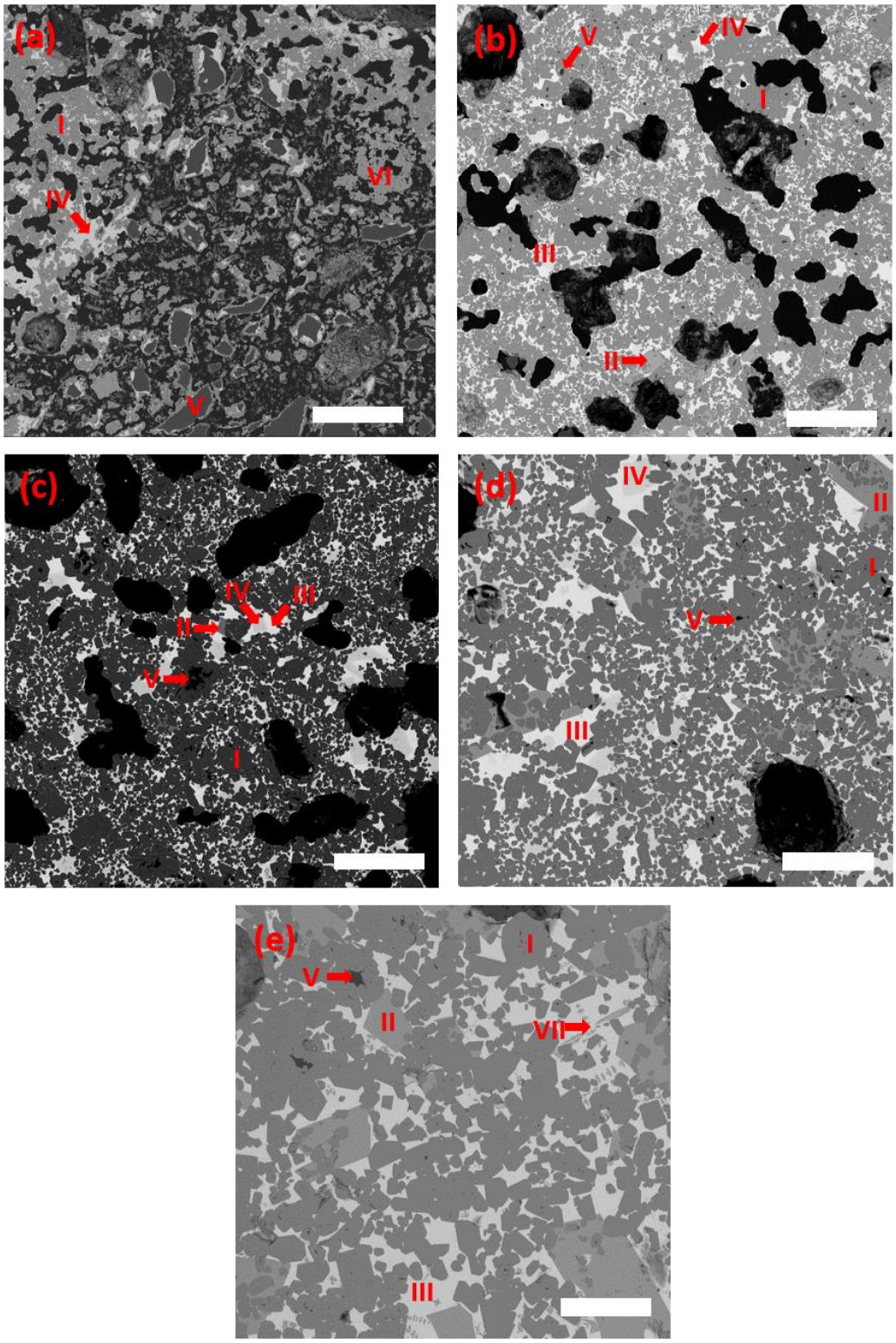

Figure 4-11. BSE micrographs of pigment samples produced with $BaCO_3$ and PbO, with starting stoichiometry of Ba:Cu:Si = 1:1:4, and heat treatment for 24 hours at (a) 800 ºC, (b) 850 ºC, (c) 900 ºC, (d) 950 ºC, and (e) 1000 ºC. I: $BaCuSi_4O_{10}$ (CB). II: $BaCuSi_2O_6$ (CP). III: PbO-SiO_2 glass. IV: PbO-BaO-SiO_2 glass. V: SiO_2. V: CuO. VII: Cu_2O. Scale bar: 50 µm.

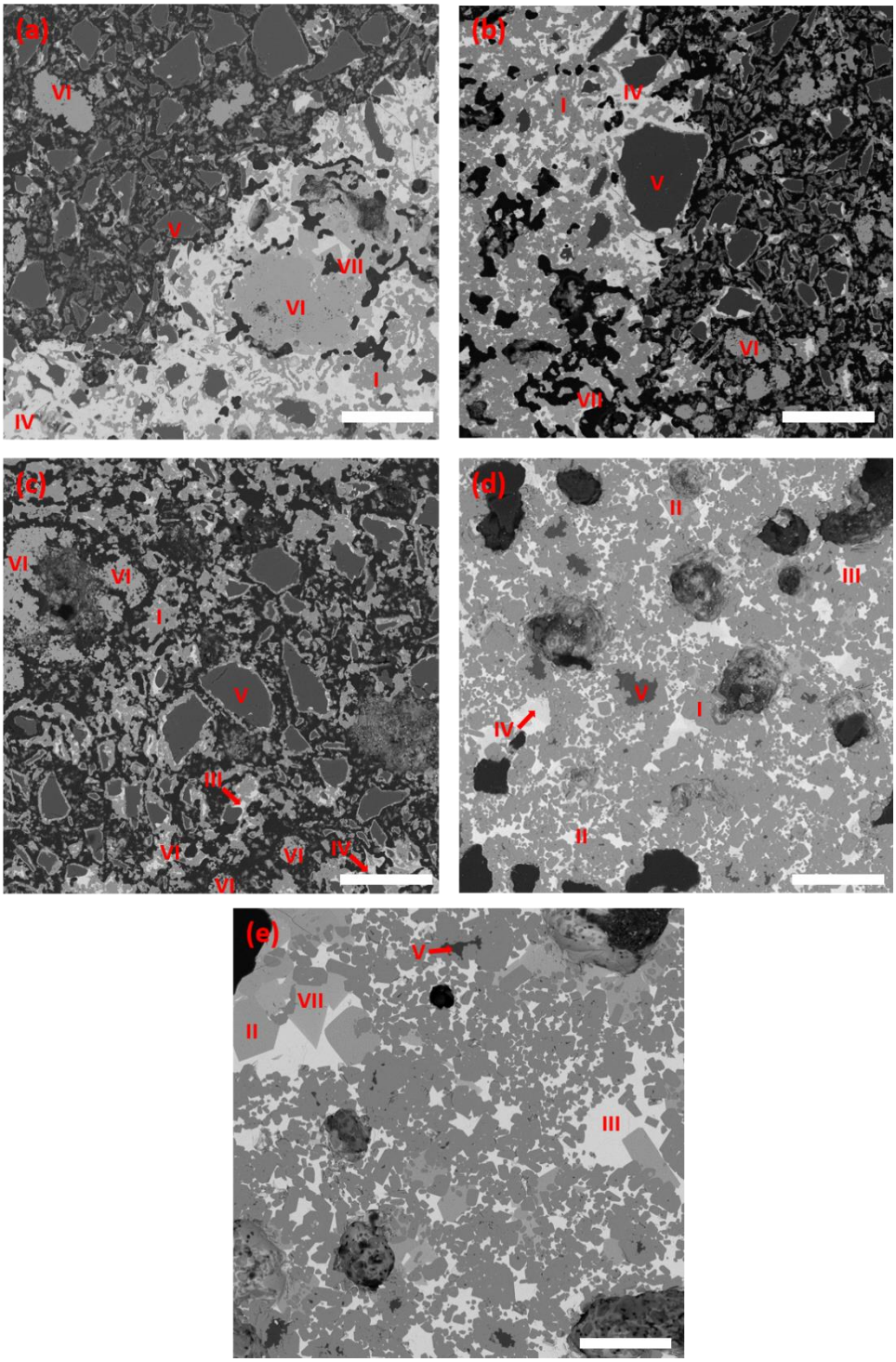

Figure 4-12. BSE micrographs of pigment samples produced with $BaCO_3$ and PbO, with starting stoichiometry of Ba:Cu:Si = 1:1:4, and heat treatment for 6 hours at (a) 800 ºC, (b) 850 ºC, (c) 900 ºC, (d) 950 ºC, and (e) 1000 ºC. I: $BaCuSi_4O_{10}$ (CB). II: $BaCuSi_2O_6$ (CP). III: PbO-SiO_2 glass. IV: PbO-BaO-SiO_2 glass. V: SiO_2. VI: CuO. VII: $BaCu_2Si_2O_7$ (CDB). Scale bar: 50 µm.

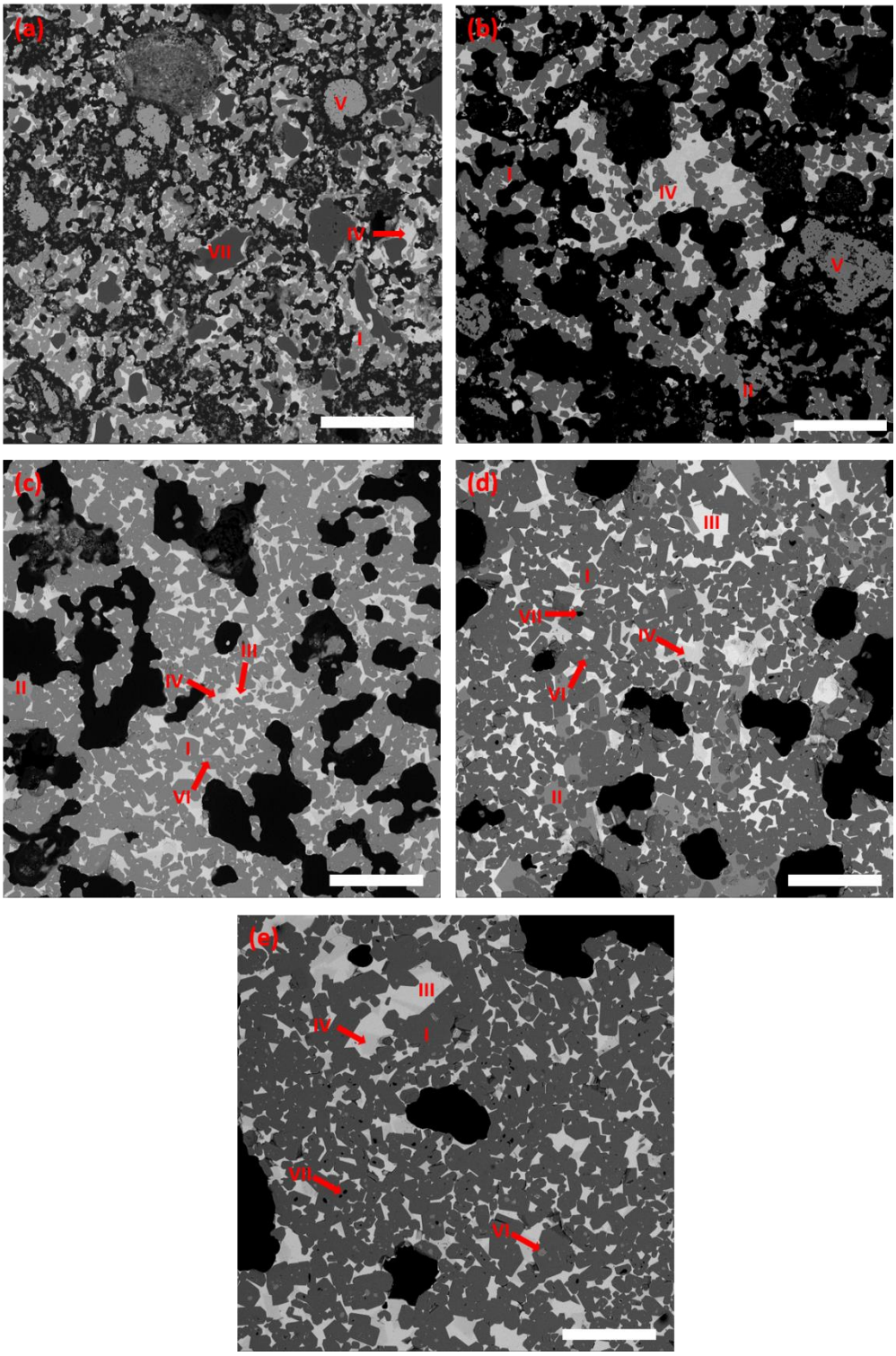

Figure 4-13. BSE micrographs of pigment samples produced with $BaCO_3$ and $PbCO_3$, with starting stoichiometry of Ba:Cu:Si = 1:1:4, and heat treatment for 24 hours at (a) 800 ºC, (b) 850 ºC, (c) 900 ºC, (d) 950 ºC, and (e) 1000 ºC. I: $BaCuSi_4O_{10}$ (CB). II: $BaCuSi_2O_6$ (CP). III: PbO-SiO_2 glass. IV: PbO-BaO-SiO_2 glass. V: CuO. VI: $BaSi_2O_5$ (inclusion). VII: SiO_2. Scale bar: 50 µm.

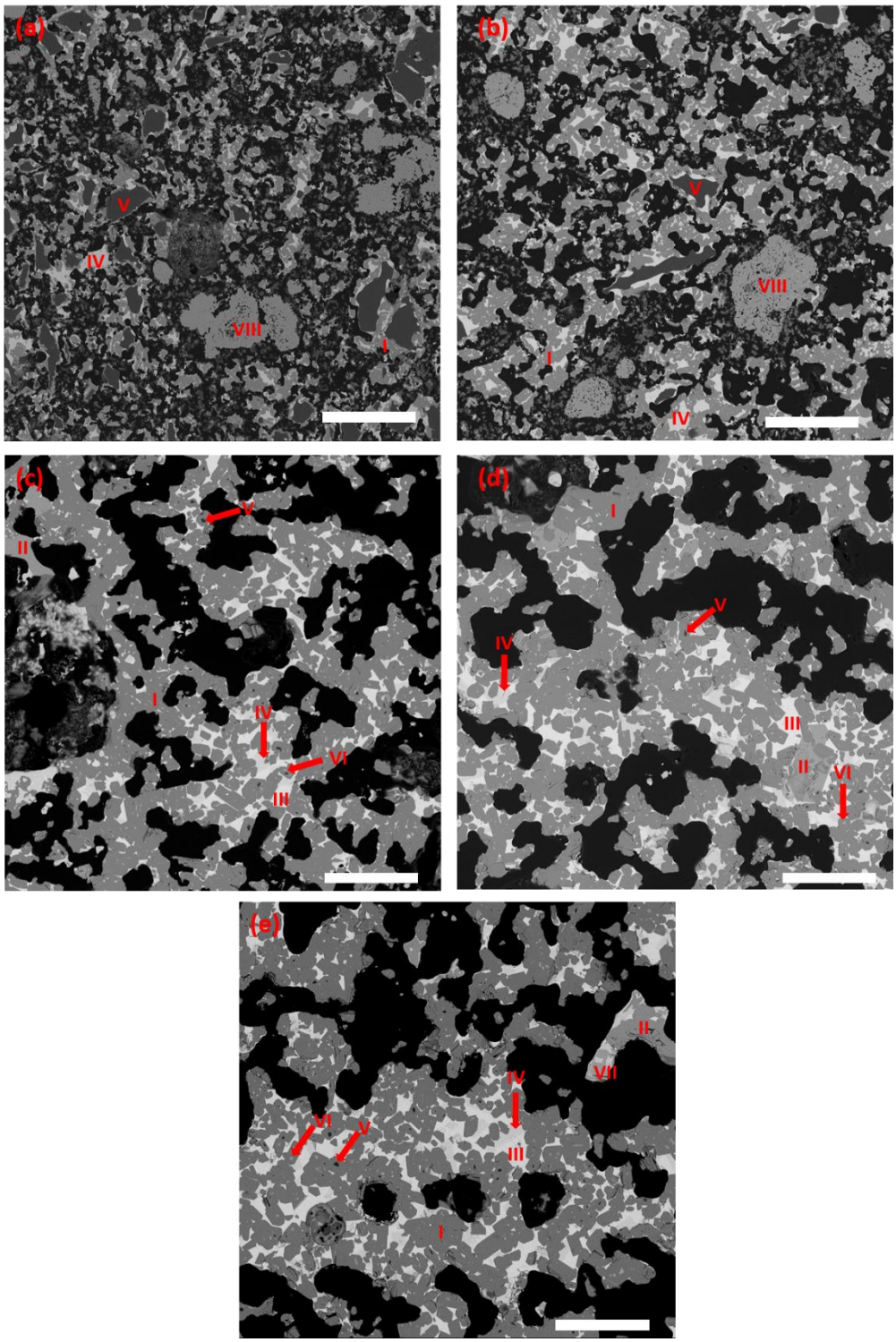

Figure 4-14. BSE micrographs of pigment samples produced with $BaCO_3$ and $PbCO_3$, with starting stoichiometry of Ba:Cu:Si = 1:1:4, and heat treatment for 6 hours at (a) 800 ºC, (b) 850 ºC, (c) 900 ºC, (d) 950 ºC, and (e) 1000 ºC. I: $BaCuSi_4O_{10}$ (CB). II: $BaCuSi_2O_6$ (CP). III: PbO-SiO_2 glass. IV: PbO-BaO-SiO_2 glass. V: SiO_2. VI: $BaSi_2O_5$ (inclusion). VII: $BaCu_2Si_2O_7$ (CDB). Scale bar: 50 µm.

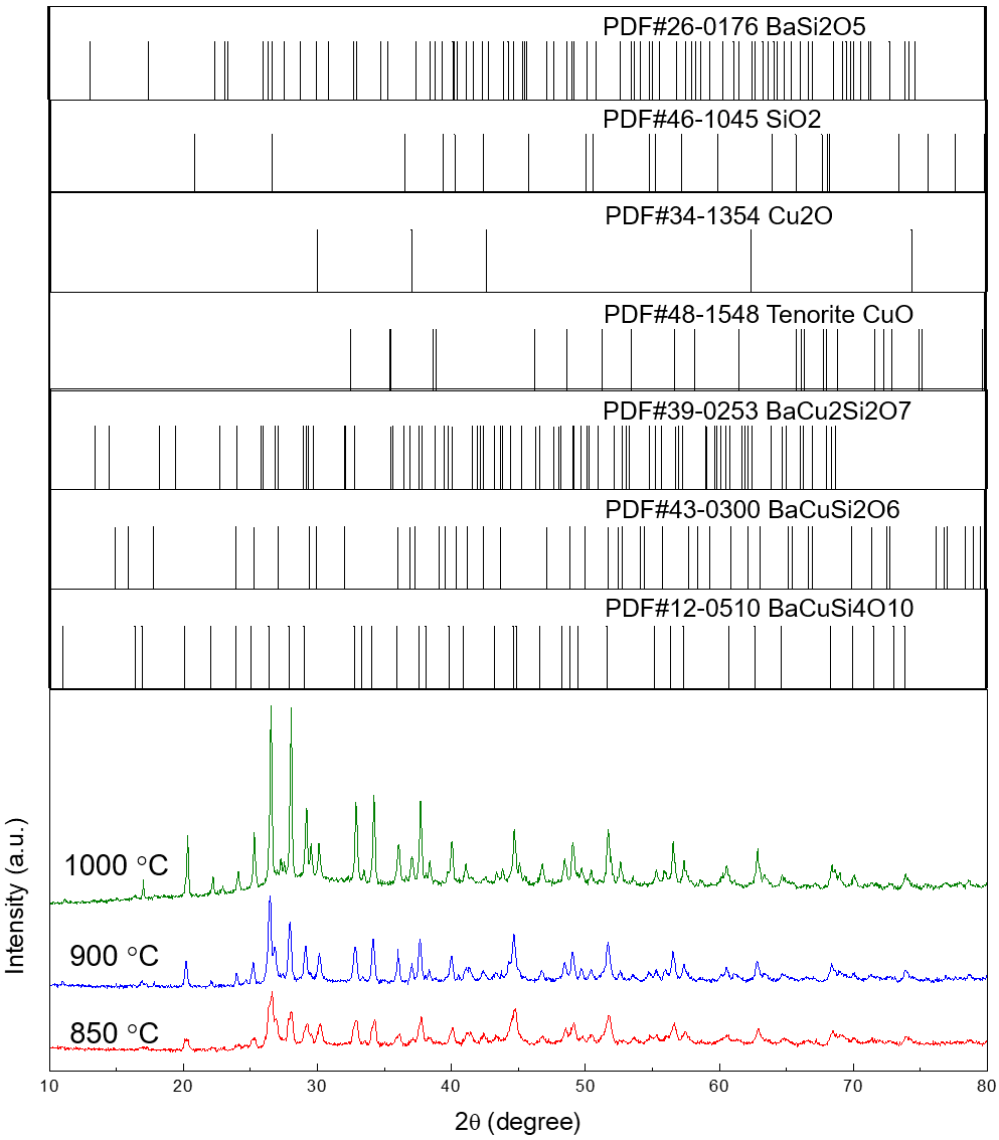

Figure 4-15. XRD diffractograms of pigment samples produced with $BaCO_3$ and PbO, with starting stoichiometry of Ba:Cu:Si = 1:1:4, and heat treatment for 24 hours at 850 ºC, 900 ºC, and 1000 ºC.

4.2.2.1.2 PbS or $PbSO_4$ as Pb-source

Synthesis conditions, major and minor phases, composition of glass matrix, and CIE L*a*b* values determined on samples produced with PbS or $PbSO_4$ as Pb-source are summarized in **Table 4-5**. In comparison to the sub-group produced with PbO or $PbCO_3$,

samples in this sub-group have a blue to greyish blue color (**Figure 4-16** and **Figure 4-17**). Pigments synthesized with $PbSO_4$ or PbS (Table 4-3) at temperature of 800 ˚C or 850 ˚C and a short heat treatment time of 6 hours, produced $BaCuSi_4O_{10}$ as the major phase with significant amounts of unreacted black CuO and SiO_2 (**Figure 4-16**(a), (f), and (g), **Figure 4-17**(a), (f), and (g)). At temperatures of 950 ˚C or 1000 ˚C for 24 hours, Cu_2O was also formed as one of the major phases. Therefore, for samples produced with $PbSO_4$, syntheses performed at 850-1000 ˚C for 24 hours, or at 900-1000 ˚C for 6 hours are optimal, while for samples produced with PbS, syntheses performed at 850-900 ˚C at 24 hours, or at 900-1000 ˚C for 6 hours are optimal to reproduce Chinese blue.

Crystalline phases in samples of the sub-group using either PbS or $PbSO_4$ as the Pb-source include $BaCuSi_4O_{10}$, unreacted SiO_2 and $BaSO_4$ as byproduct (**Figure 4-18** to **Figure 4-21**). With an increase of the synthesis temperature and time, the morphology of SiO_2 changes from separate individual angular particles to an interconnected network (**Figure 4-18** to **Figure 4-21**). Reaction byproduct $BaSO_4$ detected in all samples, show an increase in particle size as temperature and time increase (**Figure 4-18** to **Figure 4-21**). $BaCuSi_2O_6$ (CP) or $BaCu_2Si_2O_7$ (CDB) are only found as small inclusions within $BaCuSi_4O_{10}$ (CB) crystals (**Table 4-5**) in samples produced with PbS or $PbSO_4$, unlike in the case of using PbO or $PbCO_3$. Furthermore, the glass matrix identified as PbO-SiO_2, with a few wt% of Cu and Ba, however, without the presence of PbO-BaO-SiO_2 found in samples produced with PbO or $PbCO_3$. Identities of major and minor phases were confirmed with powder XRD (**Figure 4-22**).

Table 4-5. Summary of synthesis conditions, major and minor phases, composition of glass matrix, and L*a*b* values for samples produced with $BaCO_3$ and $PbSO_4$/PbS, with Ba:Cu:Si = 1:1:4. CB: $BaCuSi_4O_{10}$; CP: $BaCuSi_2O_6$; CDB: $BaCu_2Si_2O_7$. Syntheses in which Chinese blue was successfully reproduced are highlighted in blue.

Pb-source	t (hrs)	T (ºC)	Main phases	Minor phases	Inclusions	Glass matrix	L*	a*	b*
$PbSO_4$	24	800	CB, CuO, SiO_2	$BaSO_4$	CDB, CP	PbO-SiO_2	57.646	-12.5	-19.1
$PbSO_4$	24	850	CB, $BaSO_4$, SiO_2	CuO	CP, $BaSi_2O_5$	PbO-SiO_2	52.732	-12.1	-14.7
$PbSO_4$	24	900	CB, $BaSO_4$, SiO_2	CuO	-	PbO-SiO_2	59.445	-5.0	-7.0
$PbSO_4$	24	950	CB, $BaSO_4$, SiO_2	CuO	-	PbO-SiO_2	51.666	-8.5	-10.6
$PbSO_4$	24	1000	CB, $BaSO_4$, SiO_2	CuO	-	PbO-SiO_2	54.553	-7.1	-8.8
PbS	24	800	CB, CuO, SiO_2	$BaSO_4$	-	PbO-SiO_2	57.435	-13.4	-14.6
PbS	24	850	CB, $BaSO_4$, SiO_2	CuO	CP, $BaSi_2O_5$	PbO-SiO_2	57.455	-5.9	-5.4
PbS	24	900	CB, $BaSO_4$, SiO_2	CuO	-	PbO-SiO_2	57.462	-5.0	-5.7
PbS	24	950	CB, $BaSO_4$, SiO_2	CuO, Cu_2O	-	PbO-SiO_2	54.957	-5.0	-4.3
PbS	24	1000	CB, $BaSO_4$, SiO_2	CuO, Cu_2O	-	PbO-SiO_2	51.072	-6.5	-5.1
$PbSO_4$	6	800	CB, CuO, SiO_2	$BaSO_4$	CDB, CP	PbO-SiO_2	64.675	-7.8	-17.5
$PbSO_4$	6	850	CB, CuO, SiO_2	$BaSO_4$	CDB, CP	PbO-SiO_2	95.801	-7.8	-14.5
$PbSO_4$	6	900	CB, $BaSO_4$, SiO_2	CuO	-	PbO-SiO_2	56.526	-10.8	-13.8
$PbSO_4$	6	950	CB, $BaSO_4$, SiO_2	CuO	$BaSi_2O_5$	PbO-SiO_2	57.672	-7.6	-11.2
$PbSO_4$	6	1000	CB, $BaSO_4$, SiO_2	CuO	-	PbO-SiO_2	55.898	-5.3	-7.4
PbS	6	800	CB, CuO, SiO_2	$BaSO_4$	CP	PbO-SiO_2	64.607	-8.1	-10.9
PbS	6	850	CB, CuO, SiO_2	$BaSO_4$	-	PbO-SiO_2	58.847	-11.7	-12.4
PbS	6	900	CB, $BaSO_4$, SiO_2	CuO	-	PbO-SiO_2	54.093	-9.5	-10.5
PbS	6	950	CB, $BaSO_4$, SiO_2	CuO	SiO_2	PbO-SiO_2	59.551	-5.6	-6.9
PbS	6	1000	CB, $BaSO_4$, SiO_2	CuO	-	PbO-SiO_2	48.443	-5.4	-5.7

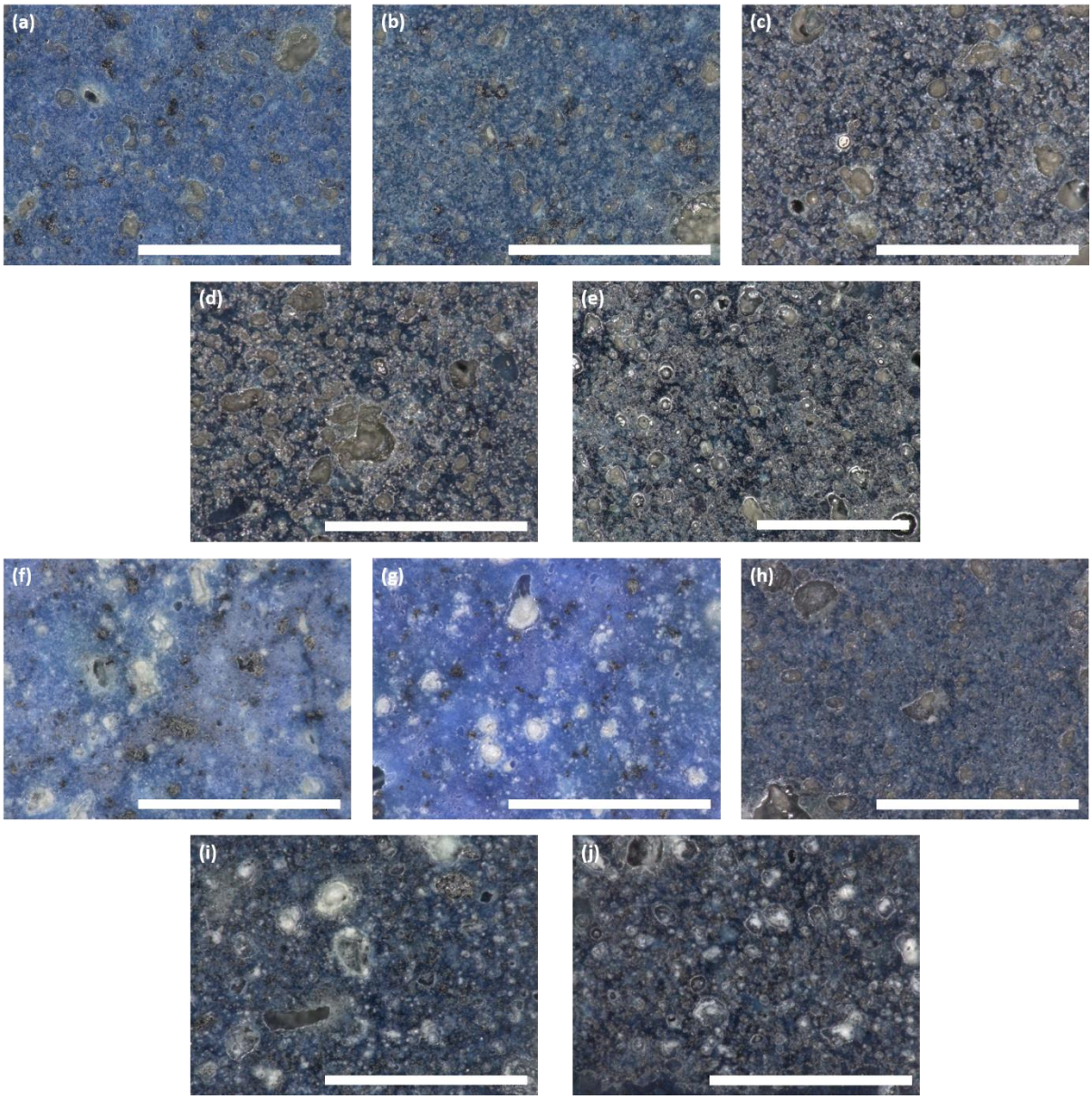

Figure 4-16. Photomicrographs of pigment samples produced with $BaCO_3$ and $PbSO_4$, with starting stoichiometry of Ba:Cu:Si = 1:1:4, and heat treatment for 24 hours at (a) 800 ºC, (b) 850 ºC, (c) 900 ºC, (d) 950 ºC, and (e) 1000 ºC, and for 6 hours at (f) 800 ºC, (g) 850 ºC, (h) 900 ºC, (i) 950 ºC, and (j) 1000 ºC. Scale bar: 1 mm.

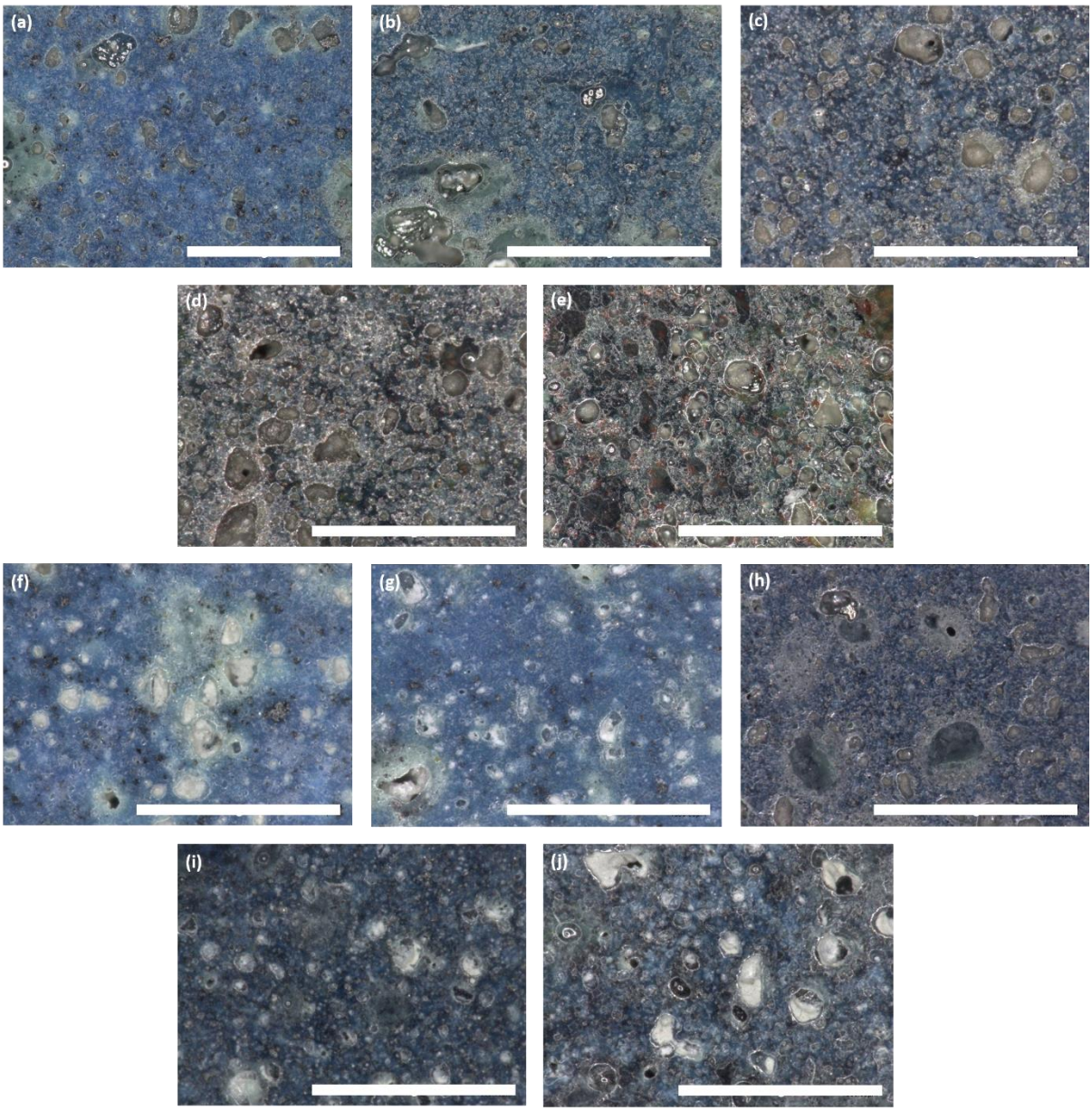

Figure 4-17. Photomicrographs of pigment samples produced with $BaCO_3$ and PbS, with starting stoichiometry of Ba:Cu:Si = 1:1:4, and heat treatment for 24 hours at (a) 800 ºC, (b) 850 ºC, (c) 900 ºC, (d) 950 ºC, and (e) 1000 ºC, and for 6 hours at (f) 800 ºC, (g) 850 ºC, (h) 900 ºC, (i) 950 ºC, and (j) 1000 ºC. Scale bar: 1 mm.

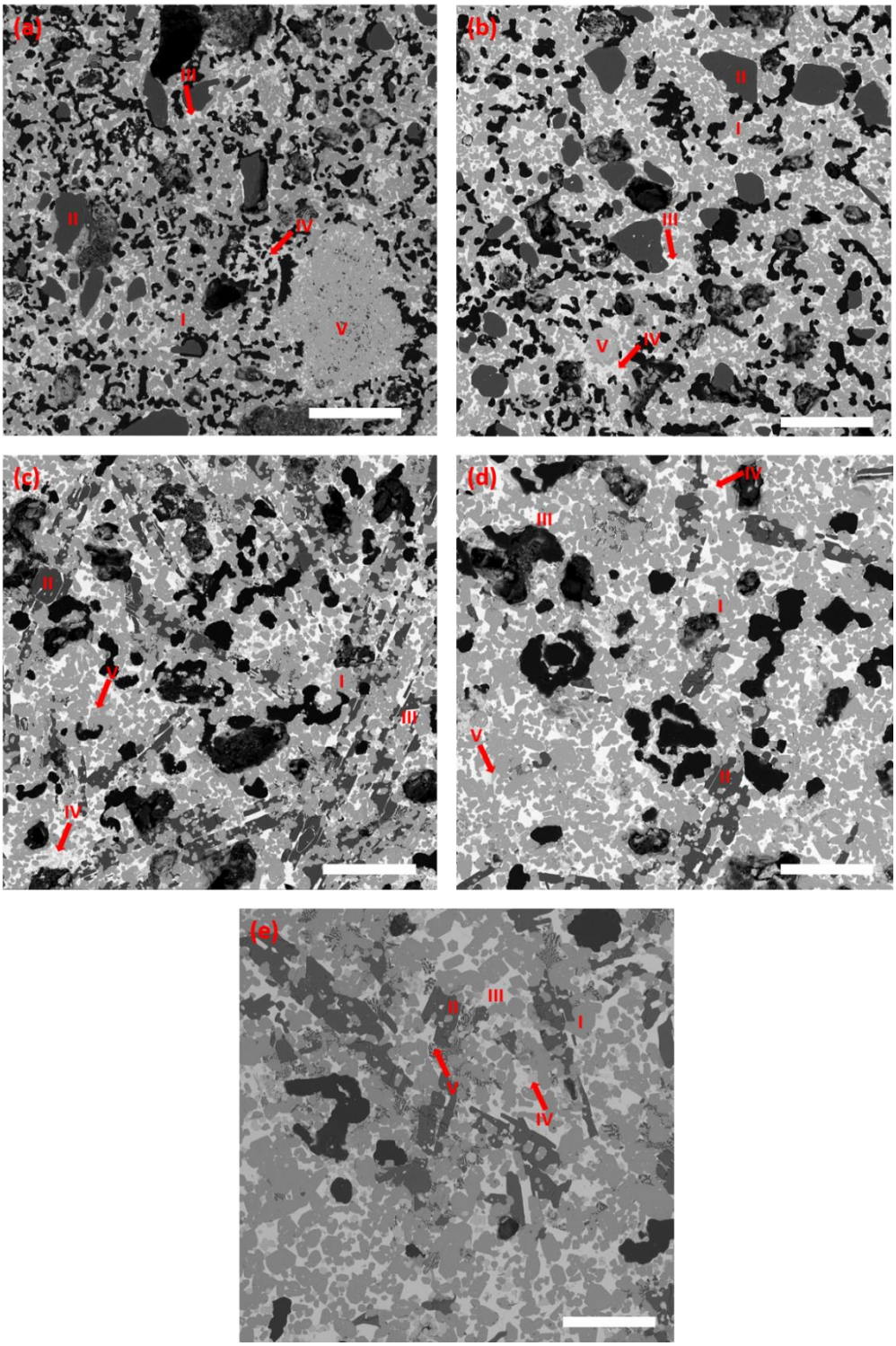

Figure 4-18. BSE micrographs of pigment samples produced with $BaCO_3$ and $PbSO_4$, with starting stoichiometry of Ba:Cu:Si = 1:1:4, and heat treatment for 24 hours at (a) 800 ºC, (b) 850 ºC, (c) 900 ºC, (d) 950 ºC, and (e) 1000 ºC. I: $BaCuSi_4O_{10}$ (CB). II: SiO_2. III: PbO-SiO_2 glass. IV: $BaSO_4$. V: CuO. Scale bar: 50 µm.

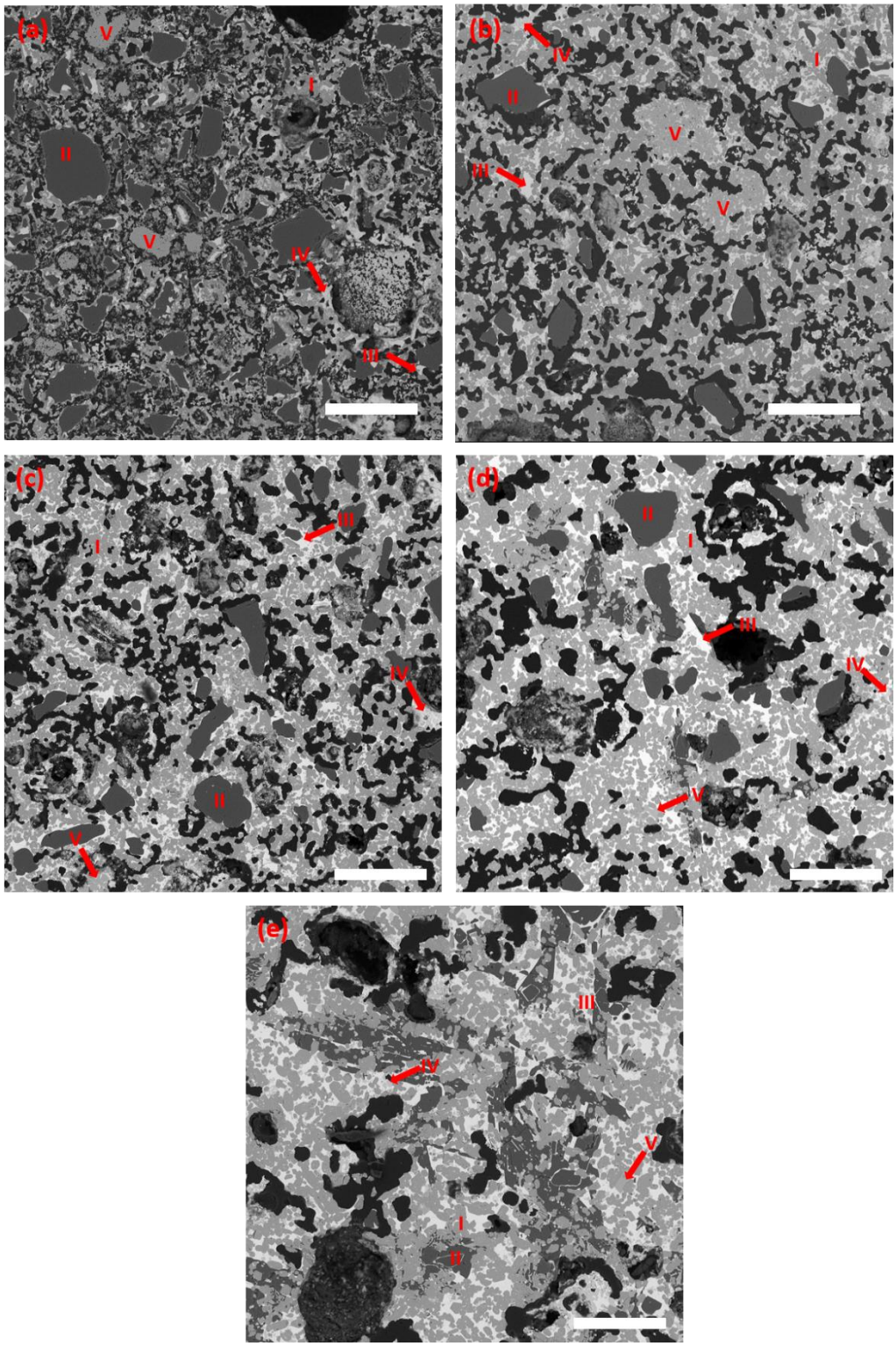

Figure 4-19. BSE micrographs of pigment samples produced with $BaCO_3$ and $PbSO_4$, with starting stoichiometry of Ba:Cu:Si = 1:1:4, and heat treatment for 6 hours at (a) 800 ºC, (b) 850 ºC, (c) 900 ºC, (d) 950 ºC, and (e) 1000 ºC. I: $BaCuSi_4O_{10}$ (CB). II: SiO_2. III: PbO-SiO_2 glass. IV: $BaSO_4$. V: CuO. Scale bar: 50 µm.

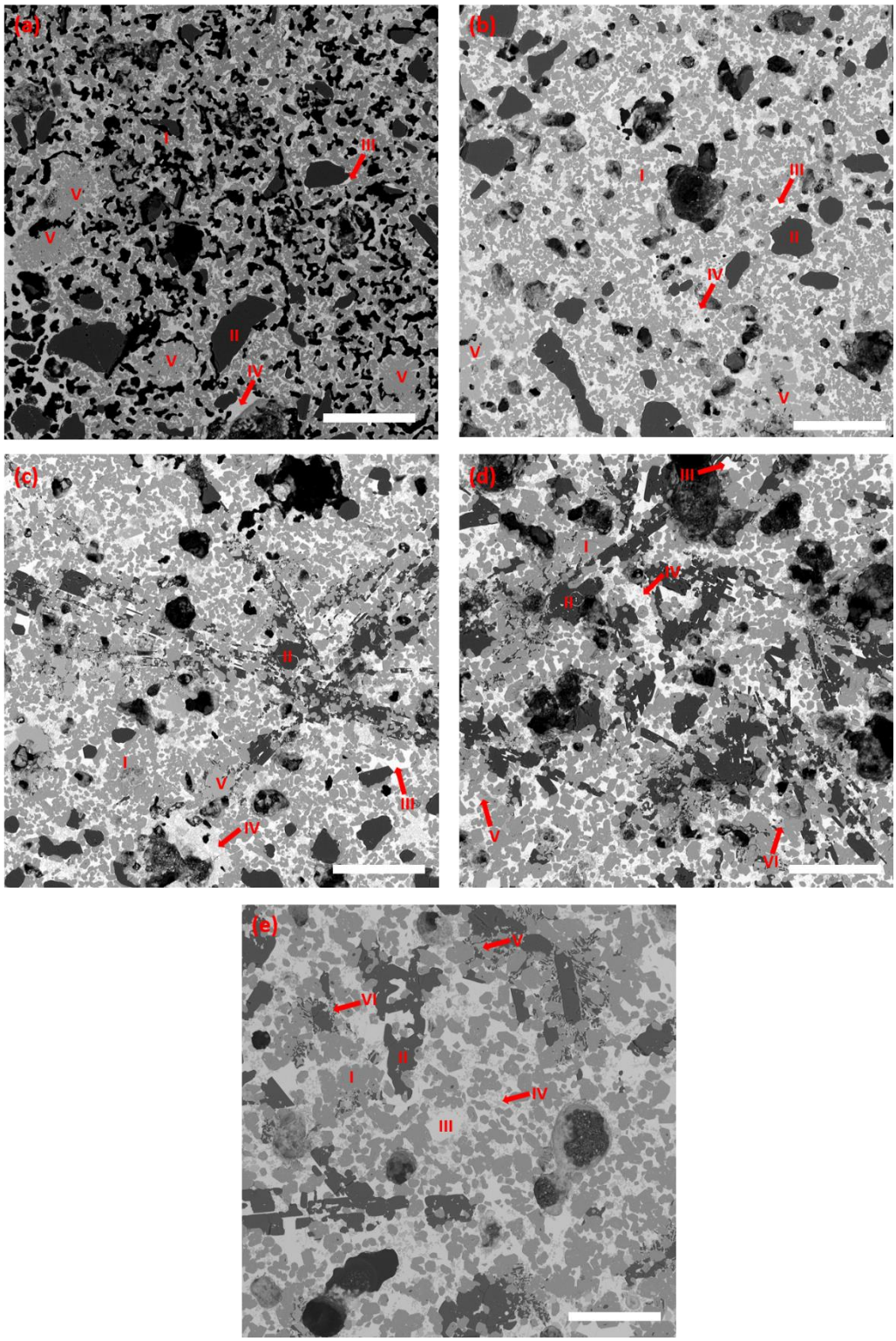

Figure 4-20. BSE micrographs of pigment samples produced with $BaCO_3$ and PbS, with starting stoichiometry of Ba:Cu:Si = 1:1:4, and heat treatment for 24 hours at (a) 800 ºC, (b) 850 ºC, (c) 900 ºC, (d) 950 ºC, and (e) 1000 ºC. I: $BaCuSi_4O_{10}$ (CB). II: SiO_2. III: PbO-SiO_2 glass. IV: $BaSO_4$. V: CuO. VI: Cu_2O. Scale bar: 50 µm.

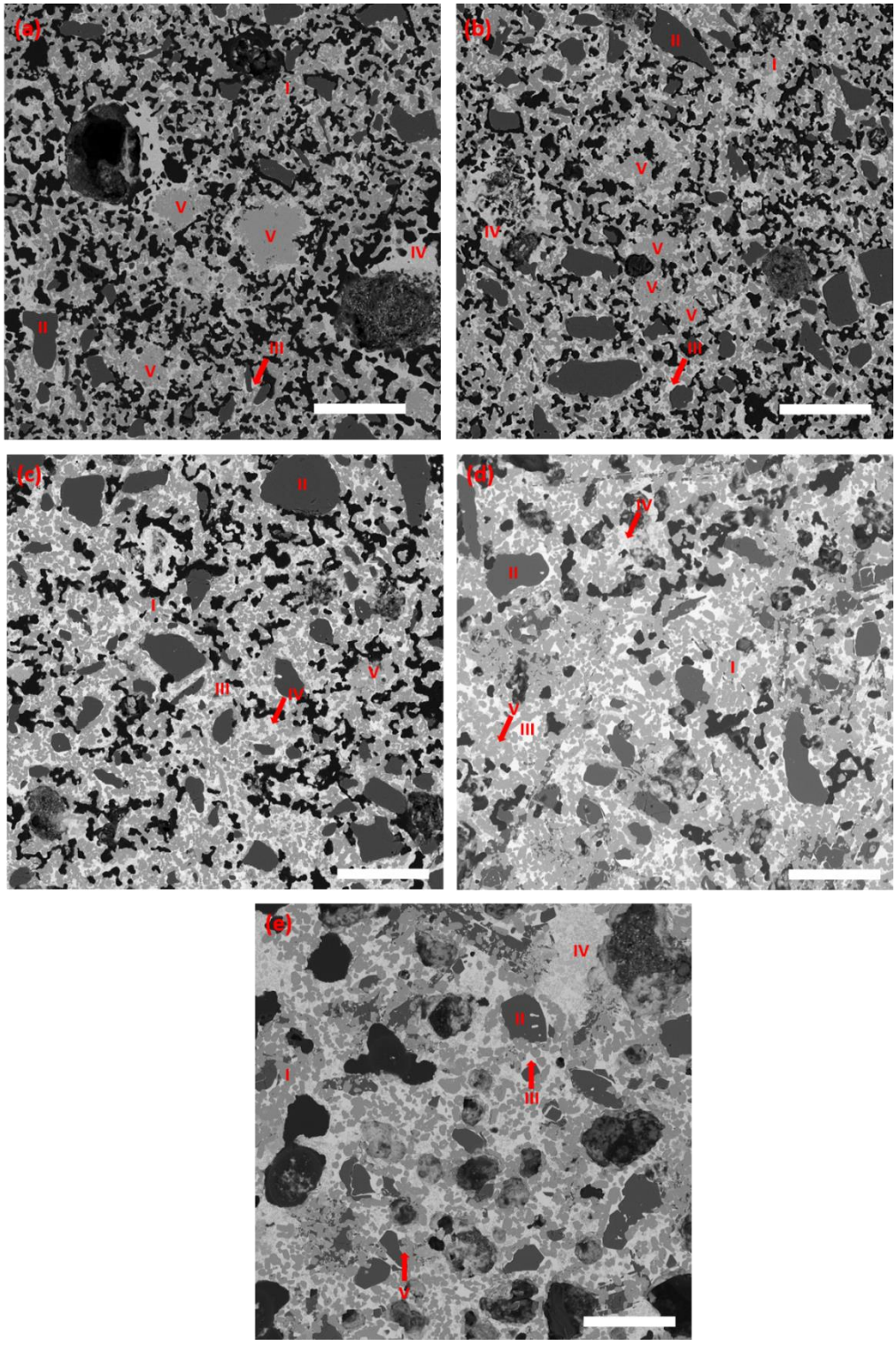

Figure 4-21. BSE micrographs of pigment samples produced with $BaCO_3$ and PbS, with starting stoichiometry of Ba:Cu:Si = 1:1:4, and heat treatment for 6 hours at (a) 800 ºC, (b) 850 ºC, (c) 900 ºC, (d) 950 ºC, and (e) 1000 ºC. I: $BaCuSi_4O_{10}$ (CB). II: SiO_2. III: PbO-SiO_2 glass. IV: $BaSO_4$. V: CuO. Scale bar: 50 µm.

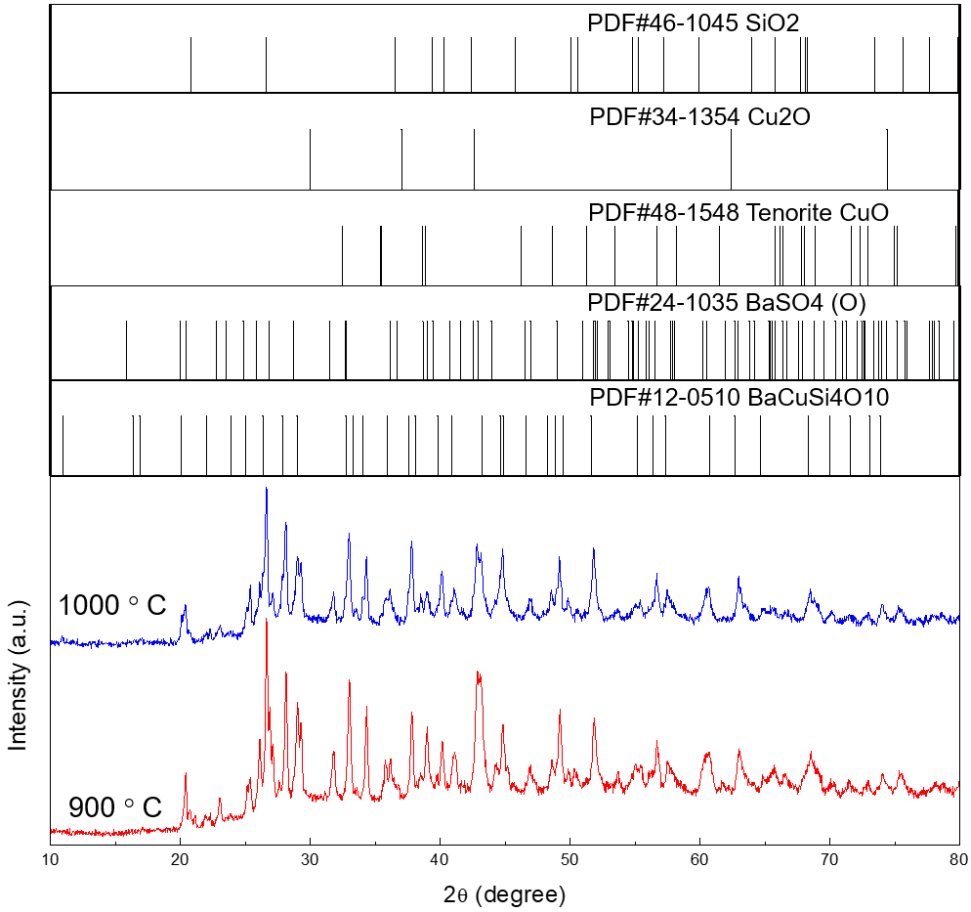

Figure 4-22. XRD diffractograms of pigment samples produced with $BaCO_3$ and PbS, with starting stoichiometry of Ba:Cu:Si = 1:1:4, and heat treatment for 24 hours at 900 ºC and 1000 ºC.

4.2.2.2 Ba:Cu:Si = 1:1:2

With the starting stoichiometry for $BaCuSi_2O_6$ (Ba:Cu: Si = 1:1:2), the major and minor phases in the end-products differ significantly based on the identities of Pb-additives and synthesis conditions. Unlike those produced with $BaCuSi_4O_{10}$ stoichiometry (Ba:Cu: Si = 1:1:2), $BaCu_2Si_2O_7$ was formed in samples produced with the starting stoichiometry for $BaCuSi_2O_6$. $BaCuSi_4O_{10}$ was identified as one of the main phases in samples produced with $PbSO_4$ or PbS.

4.2.2.2.1 PbO or $PbCO_3$ as Pb-source

Synthesis conditions, major and minor phases, the composition of glass matrix, and CIE L*a*b* values determined for pigment samples produced with PbO or $PbCO_3$ as Pb-source are summarized in **Table 4-6**. Samples in this sub-group have a blue to bluish purple color (**Figure 4-23** and **Figure 4-24**). Distinctive red Cu_2O particles were present in samples produced at 1000 ˚C for 24 hours and 6 hours, and at 950 ˚C for 24 hours (**Figure 4-23**(d), (e), and (j), **Figure 4-24**(d), (e), and (j)). When synthesis temperature was below 900 ºC for 6 hours or below 850 ºC for 24 hours, areas of unreacted black CuO can be observed (**Figure 4-23**a, f, and g, **Figure 4-24**a, f, and g). Both $BaCuSi_2O_6$ (CP) and $BaCu_2Si_2O_7$ (CDB) were detected with their relative proportions influenced by the synthesis conditions. In general, at lower synthesis temperature (800-900 or 950 ºC) and short reaction time (6 hours), the initial kinetic product $BaCu_2Si_2O_7$ (CDB) predominated, while $BaCuSi_2O_6$ (CP) was the main pigment phase in samples produced with higher synthesis temperature (950-1000 ºC) and longer reaction time (24 hours) (**Table 4-6**). The glass matrix contained PbO-BaO-SiO_2 at lower synthesis temperature (between 800 ºC and 900 ºC), whereas, at higher temperature (950-1000 ºC) a PbO-SiO_2 composition coexist with PbO-BaO-SiO_2 glass (**Table 4-6**, **Figure 4-25** to **Figure 4-28**). These phases are confirmed by powder XRD (**Figure 4-29**).

Table 4-6. Summary of synthesis conditions, major and minor phases, composition of glass matrix, and L*a*b* values for samples produced with $BaCO_3$ and PbO/$PbCO_3$, with Ba:Cu:Si = 1:1:2. CB: $BaCuSi_4O_{10}$; CP: $BaCuSi_2O_6$; CDB: $BaCu_2Si_2O_7$. Syntheses in which Chinese purple was successfully reproduced are highlighted

in blue.

Pb-source	t (hrs)	T (ºC)	Main phases	Minor phases	Inclusions	Glass matrix	L*	a*	b*
PbO	24	800	CuO, CDB	CP, CB	-	$PbO-BaO-SiO_2$	53.96	-3.5	-28.0
PbO	24	850	CDB	CP, CuO	CB	$PbO-BaO-SiO_2$	60.49	2.4	-23.6
PbO	24	900	CP	CDB, CuO	-	$PbO-BaO-SiO_2$ $PbO-SiO_2$	39.176	3.6	-39.1
PbO	24	950	CP	CDB, CuO, Cu_2O	CB	$PbO-BaO-SiO_2$ $PbO-SiO_2$	40.757	2.5	-22.4
PbO	24	1000	CP	CDB, Cu_2O	-	$PbO-BaO-SiO_2$ $PbO-SiO_2$	42.391	6.3	-19.4
$PbCO_3$	24	800	CuO, CB	CDB, CP	-	$PbO-BaO-SiO_2$	51.696	-1.2	-32.5
$PbCO_3$	24	850	CP	CDB, CuO	CB	$PbO-BaO-SiO_2$	48.036	5.2	-33.2
$PbCO_3$	24	900	CP	CDB, CuO	-	$PbO-BaO-SiO_2$ $PbO-SiO_2$	55.948	2.8	-25.3
$PbCO_3$	24	950	CP	CDB, CuO, Cu_2O	CB	$PbO-BaO-SiO_2$ $PbO-SiO_2$	37.674	3.2	-24.2
$PbCO_3$	24	1000	CP	Cu_2O	-	$PbO-BaO-SiO_2$ $PbO-SiO_2$	57.814	3.4	-12.7
PbO	6	800	CuO, SiO_2, CDB	CP	-	$PbO-BaO-SiO_2$	56.206	-3.1	-6.5
PbO	6	850	CuO, CB	CP, CDB	-	$PbO-BaO-SiO_2$	57.593	-1.0	-22.2
PbO	6	900	CDB	CP, CuO	-	$PbO-BaO-SiO_2$ $PbO-SiO_2$	52.593	1.1	-21.4
PbO	6	950	CDB	CP, CuO	CB	$PbO-BaO-SiO_2$ $PbO-SiO_2$	48.953	-0.1	-30.2
PbO	6	1000	CP	CDB, Cu_2O, $BaSiO_3$	$BaSiO_3$	$PbO-BaO-SiO_2$ $PbO-SiO_2$	51.131	1.5	-17.2
$PbCO_3$	6	800	CuO, SiO_2, CB	CP, CDB	-	$PbO-BaO-SiO_2$	62.314	-5.5	-13.3
$PbCO_3$	6	850	CuO, CB, CP	-	-	$PbO-BaO-SiO_2$	58.393	0.7	-24.4
$PbCO_3$	6	900	CDB	CP, CuO	CB	$PbO-BaO-SiO_2$	58.035	2.3	-18.0
$PbCO_3$	6	950	CDB	CP, CuO	CB	$PbO-BaO-SiO_2$ $PbO-SiO_2$	46.917	4.3	-30.6
$PbCO_3$	6	1000	CP	CDB, Cu_2O, $BaSiO_3$	$BaSiO_3$	$PbO-BaO-SiO_2$ $PbO-SiO_2$	39.646	3.7	-24.2

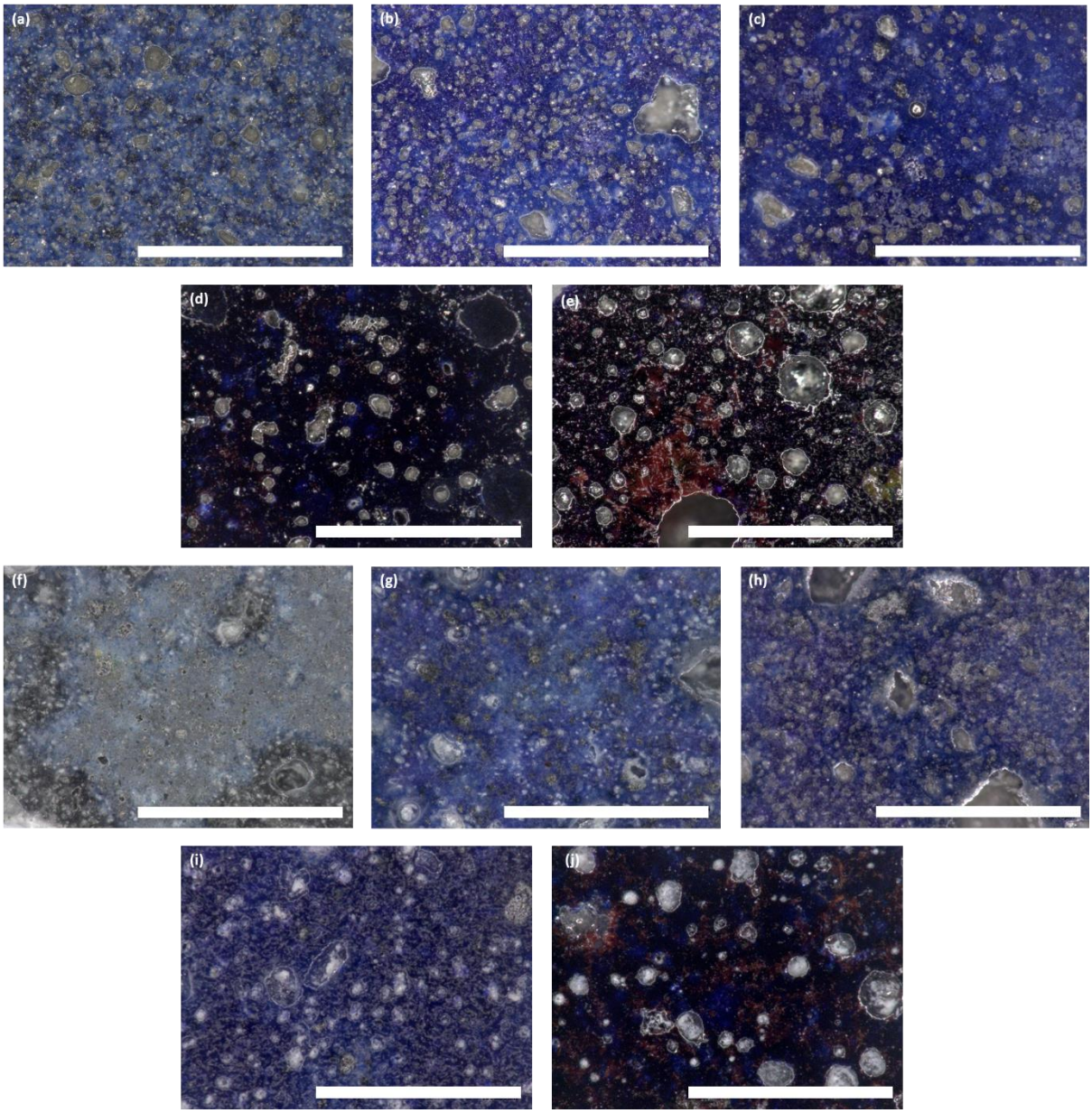

Figure 4-23. Photomicrographs of pigment samples produced with $BaCO_3$ and PbO, with starting stoichiometry of Ba:Cu:Si = 1:1:2, and heat treatment for 24 hours at (a) 800 ºC, (b) 850 ºC, (c) 900 ºC, (d) 950 ºC, and (e) 1000 ºC, and for 6 hours at (f) 800 ºC, (g) 850 ºC, (h) 900 ºC, (i) 950 ºC, and (j) 1000 ºC. Scale bar: 1 mm.

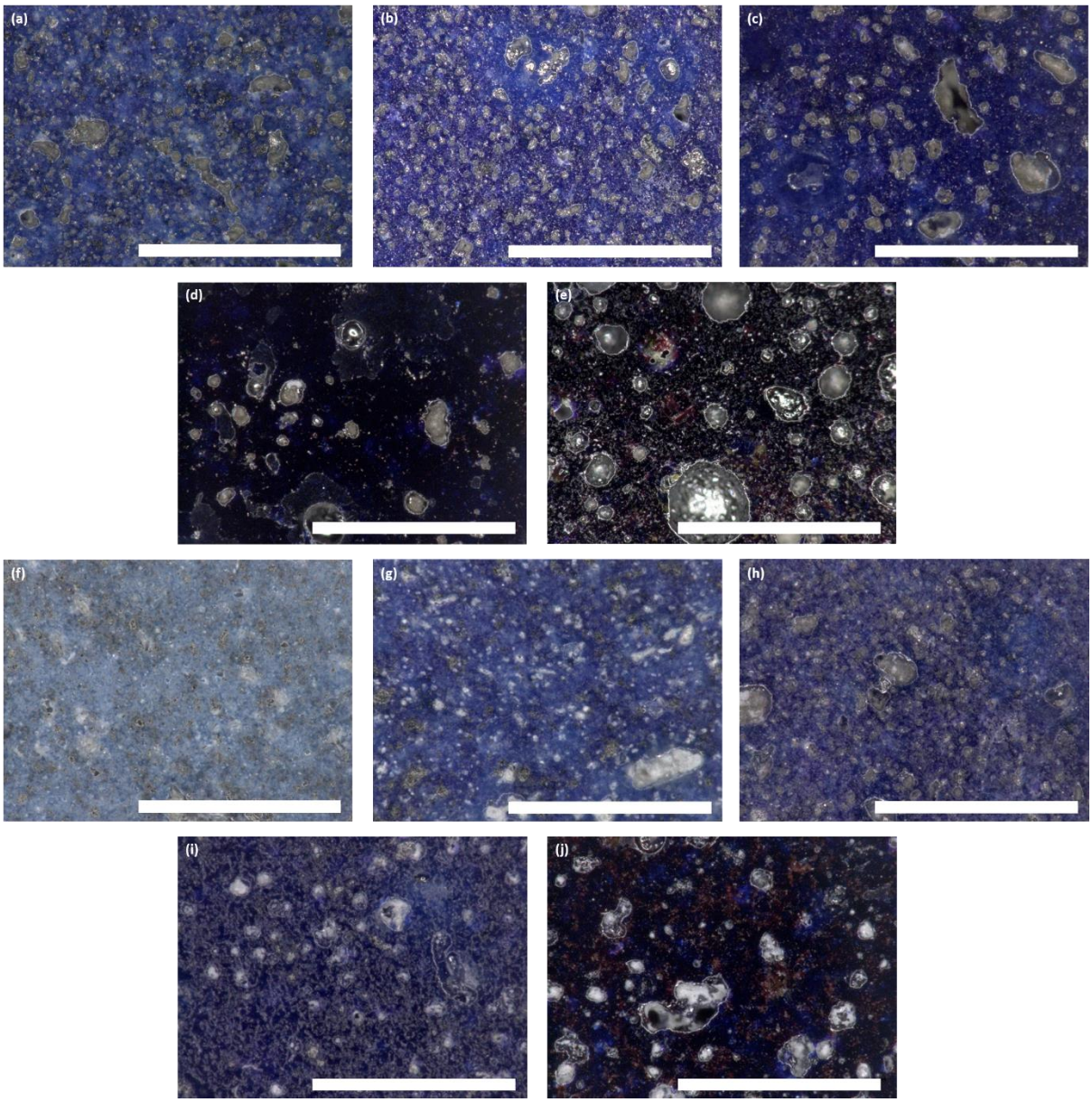

Figure 4-24. Photomicrographs of pigment samples produced with $BaCO_3$ and $PbCO_3$, with starting stoichiometry of Ba:Cu:Si = 1:1:2, and heat treatment for 24 hours at (a) 800 ºC, (b) 850 ºC, (c) 900 ºC, (d) 950 ºC, and (e) 1000 ºC, and for 6 hours at (f) 800 ºC, (g) 850 ºC, (h) 900 ºC, (i) 950 ºC, and (j) 1000 ºC. Scale bar: 1 mm.

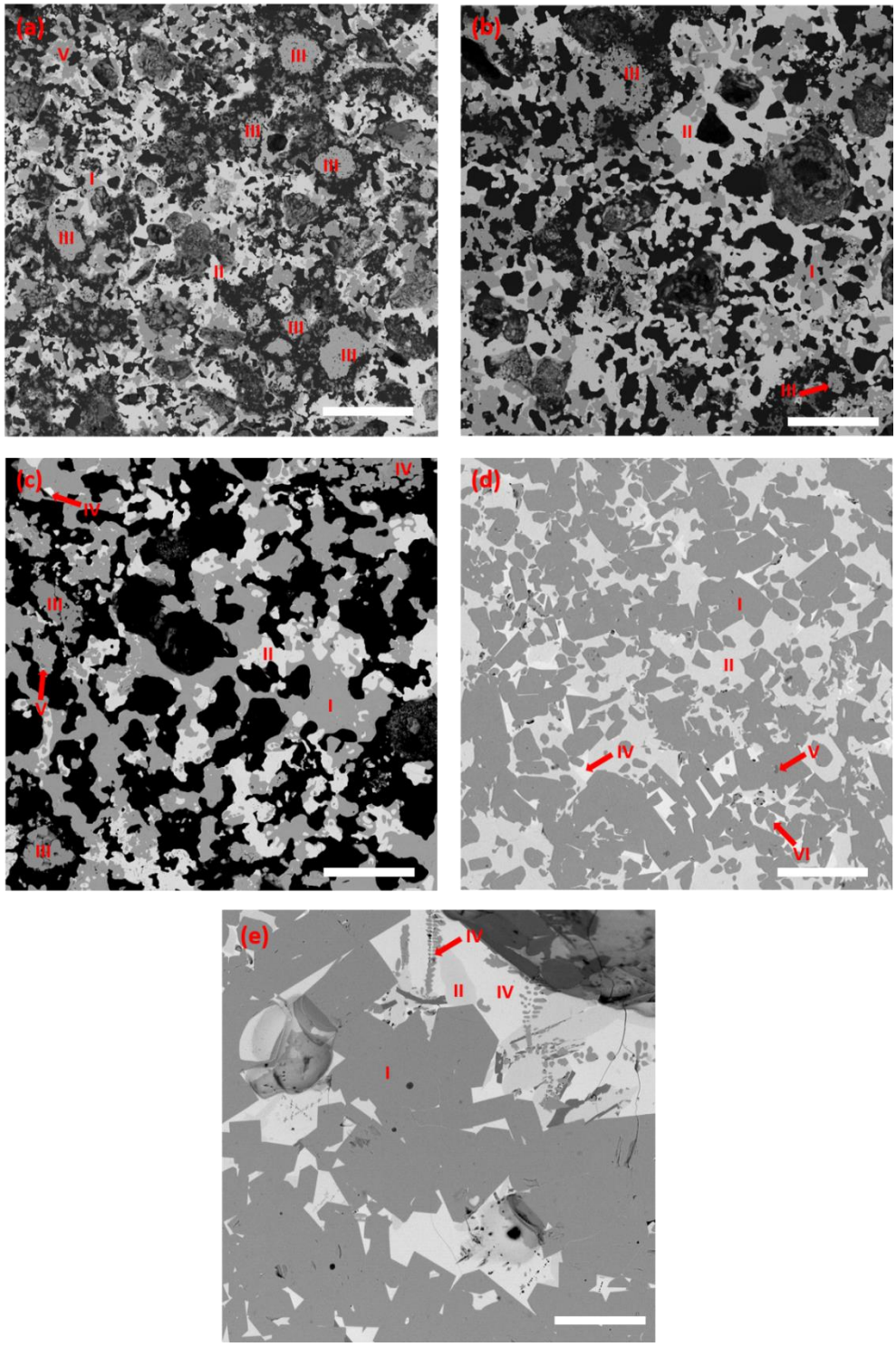

Figure 4-25. BSE micrographs of pigment samples produced with $BaCO_3$ and PbO, with starting stoichiometry of Ba:Cu:Si = 1:1:2, and heat treatment for 24 hours at (a) 800 ºC, (b) 850 ºC, (c) 900 ºC, (d) 950 ºC, and (e) 1000 ºC. I: $BaCuSi_2O_6$ (CP) or $BaCu_2Si_2O_7$ (CDB). II: PbO-BaO-SiO_2 glass. III: CuO. IV: PbO-SiO_2 glass. V: $BaCuSi_4O_{10}$ (CB). VI: Cu_2O. Scale bar: 50 µm.

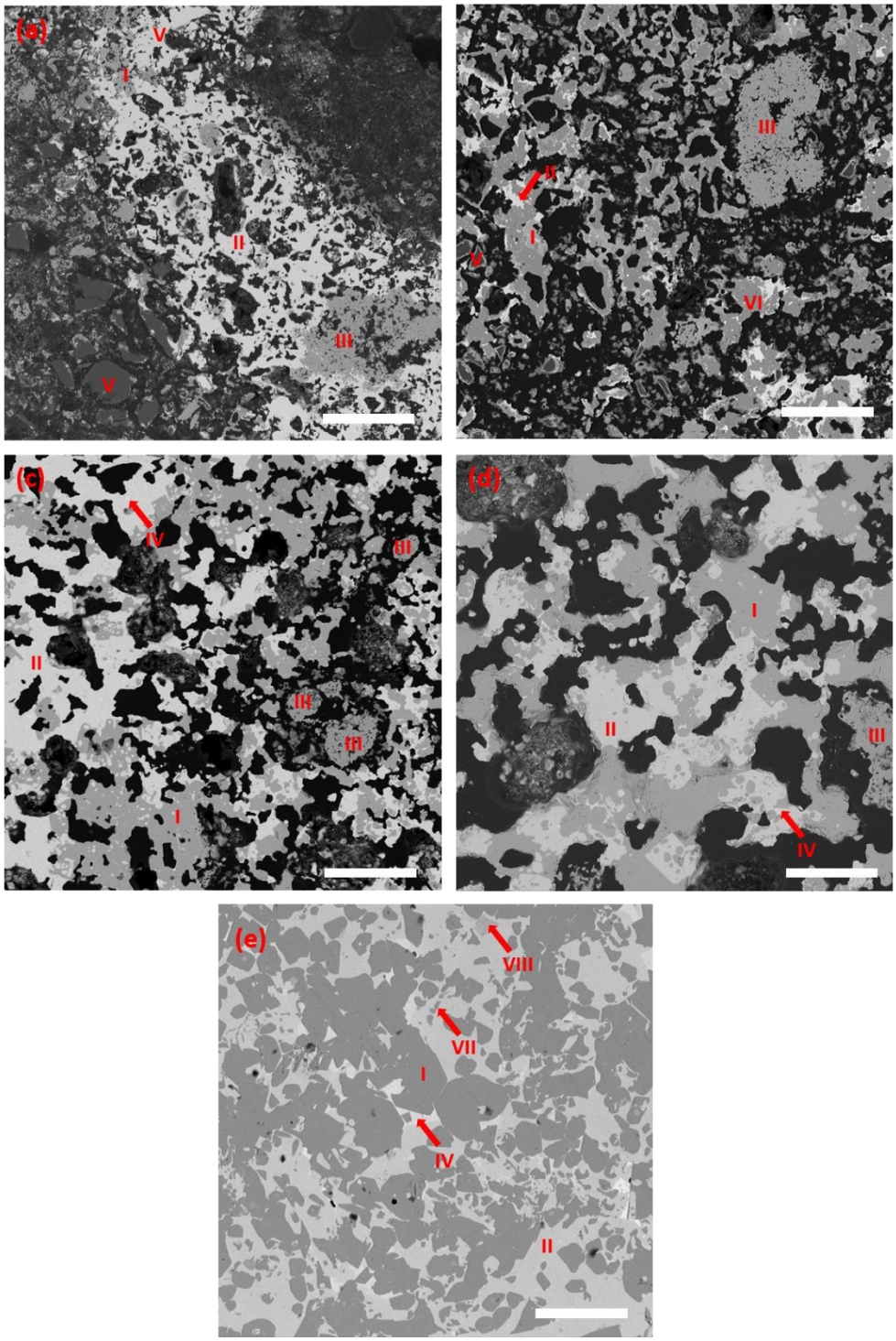

Figure 4-26. BSE micrographs of pigment samples produced with $BaCO_3$ and PbO, with starting stoichiometry of Ba:Cu:Si = 1:1:2, and heat treatment for 6 hours at (a) 800 ºC, (b) 850 ºC, (c) 900 ºC, (d) 950 ºC, and (e) 1000 ºC. I: $BaCuSi_2O_6$ (CP) or $BaCu_2Si_2O_7$ (CDB). II: PbO-BaO-SiO_2 glass. III: CuO. IV: PbO-SiO_2 glass. V. SiO_2. VI: $BaCuSi_4O_{10}$ (CB). VII: Cu_2O. VIII: $BaSiO_3$. Scale bar: 50 µm.

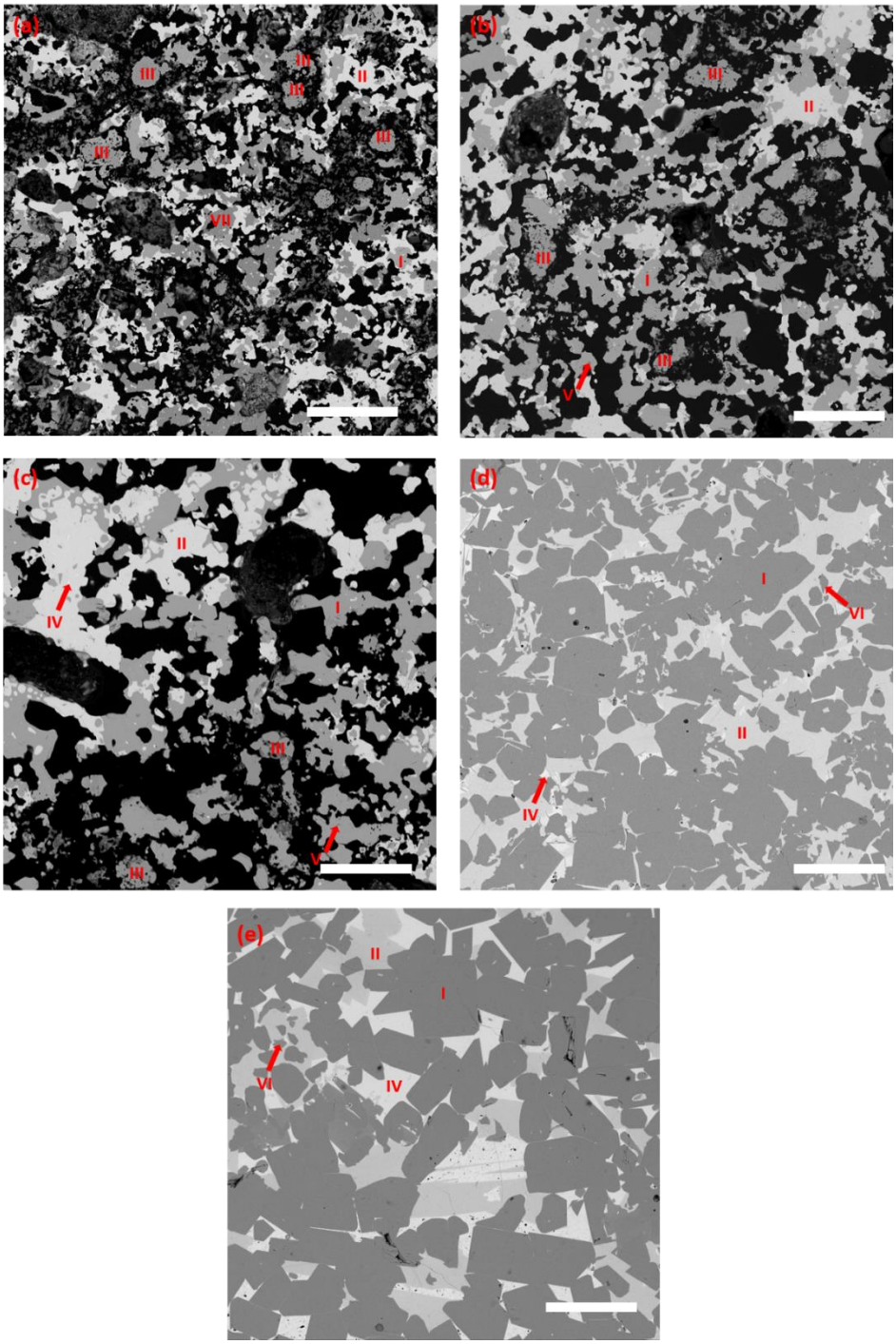

Figure 4-27. BSE micrographs of pigment samples produced with $BaCO_3$ and $PbCO_3$, with starting stoichiometry of Ba:Cu:Si = 1:1:2, and heat treatment for 24 hours at (a) 800 ºC, (b) 850 ºC, (c) 900 ºC, (d) 950 ºC, and (e) 1000 ºC. I: $BaCuSi_2O_6$ (CP) or $BaCu_2Si_2O_7$ (CDB). II: PbO-BaO-SiO_2 glass. III: CuO. IV: PbO-SiO_2 glass. V: $BaCuSi_4O_{10}$ (CB). VI: Cu_2O. VII: $BaCuSi_4O_{10}$ (CB) Scale bar: 50 µm.

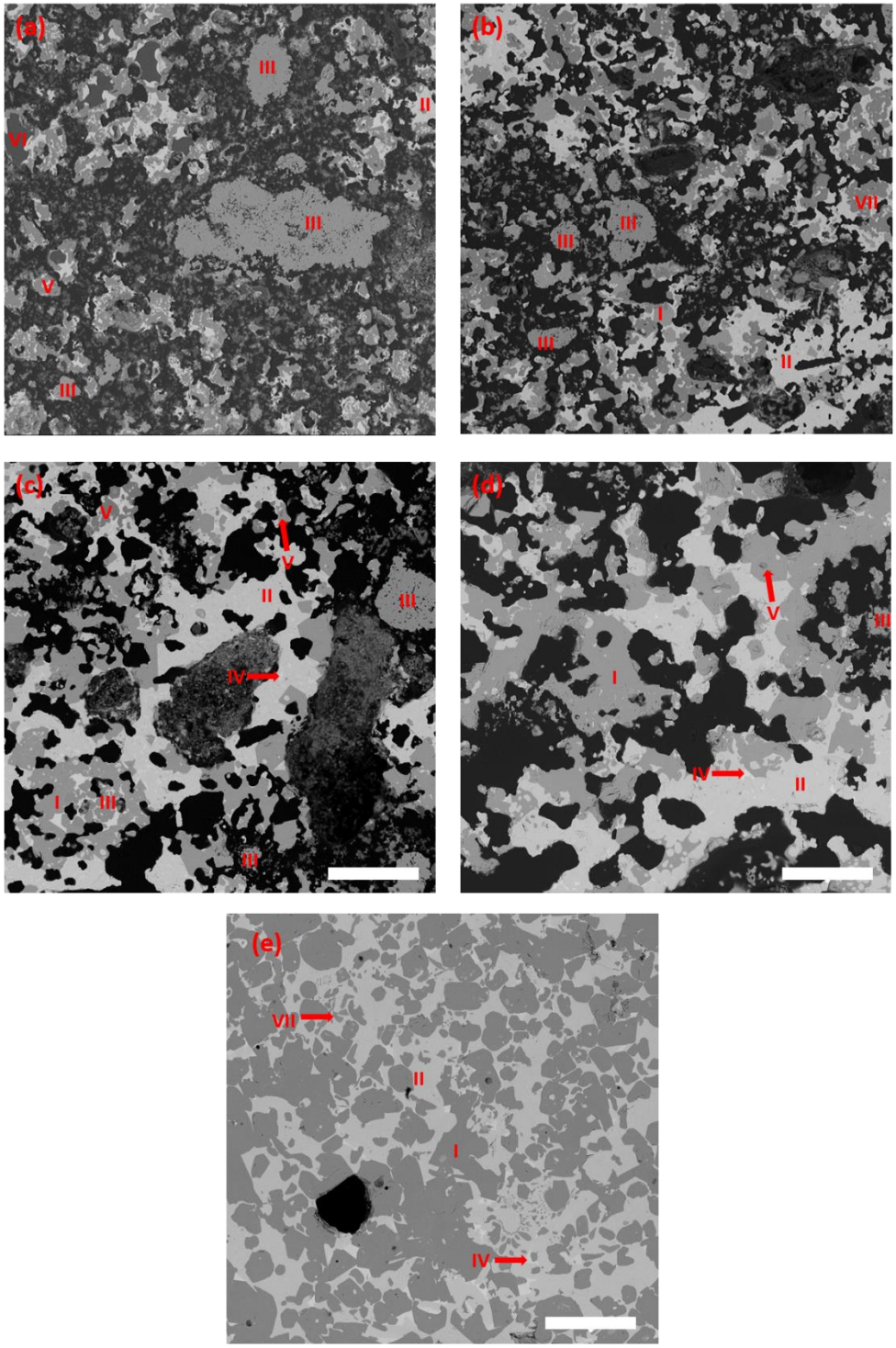

Figure 4-28. BSE micrographs of pigment samples produced with $BaCO_3$ and $PbCO_3$, with starting stoichiometry of Ba:Cu:Si = 1:1:2, and heat treatment for 6 hours at (a) 800 ºC, (b) 850 ºC, (c) 900 ºC, (d) 950 ºC, and (e) 1000 ºC. I: $BaCuSi_2O_6$ (CP) or $BaCu_2Si_2O_7$ (CDB). II: PbO-BaO-SiO_2 glass. III: CuO. IV: PbO-SiO_2 glass. V: $BaCuSi_4O_{10}$ (CB). VI: SiO_2. VII: Cu_2O. Scale bar: 50 µm.

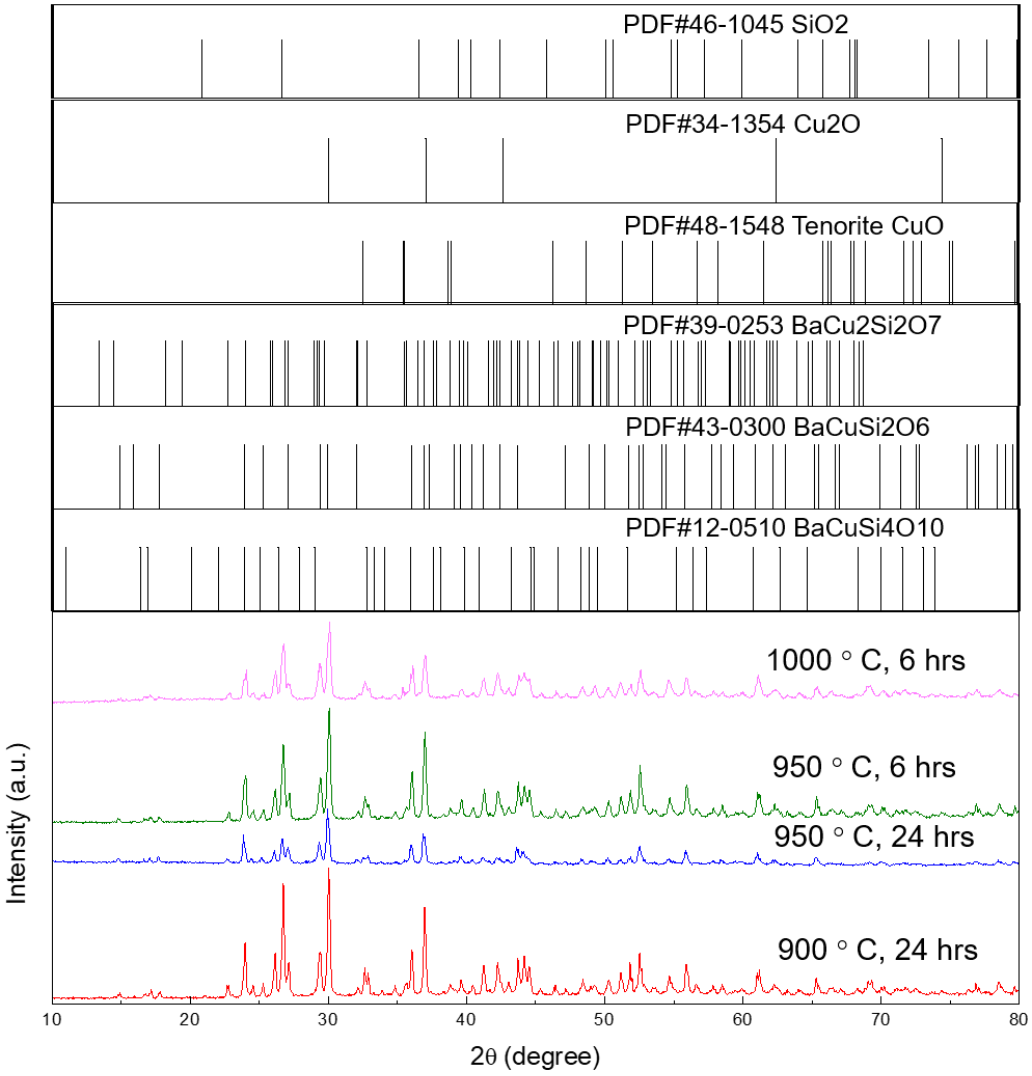

Figure 4-29. XRD diffractograms of pigment samples produced with $BaCO_3$ and $PbCO_3$, with starting stoichiometry of Ba:Cu:Si = 1:1:2, and heat treatment for 6 hours at 950 ºC and 1000 ºC, and for 24 hours at 900 ºC and 950 ºC.

4.2.2.2.2 $PbSO_4$ or PbS as Pb-source

Synthesis conditions, major and minor phases, composition of glass matrix, and CIE L*a*b* values determined for pigment samples produced with $PbSO_4$ or PbS as Pb-source are summarized in **Table 4-7**. Samples in this sub-group have a blue to bluish purple color (**Figure 4-30** and **Figure 4-31**). Red Cu_2O particles were also detected mainly in pigment samples

produced with PbS (**Figure 4-31**d, e, and j), and in one pigment sample produced with $PbSO_4$ (**Figure 4-30**e). $BaCuSi_4O_{10}$ (CB) and $BaCu_2Si_2O_7$ (CDB) are commonly found as the two main phases in samples within this sub-group, while $BaCuSi_2O_6$ (CP) is the main phase only in selected samples produced with $PbSO_4$ (**Table 4-7**, **Figure 4-32** to **Figure 4-35**). However, $BaCuSi_2O_6$ (CP) crystals are almost absent in samples produced with PbS (**Table 4-7**, **Figure 4-34** and **Figure 4-35**). Reaction byproduct $BaSO_4$ is present in all samples, and Pb/Ba-rich silicates are present in samples produced at lower synthesis temperatures (**Table 4-7**, **Figure 4-34** and **Figure 4-35**). The glass composition is of PbO-SiO_2. The phases are confirmed by powder XRD (**Figure 4-36**).

Table 4-7. Summary of synthesis conditions, major and minor phases, composition of glass matrix, and L*a*b* values for samples produced with $BaCO_3$ and $PbSO_4$/PbS, with Ba:Cu:Si = 1:1:2. CB: $BaCuSi_4O_{10}$; CP: $BaCuSi_2O_6$; CDB: $BaCu_2Si_2O_7$. Syntheses in which Chinese purple was successfully reproduced are highlighted in blue.

Pb-source	t (hrs)	T (ºC)	Main phases	Minor phases	Inclusions	Glass matrix	L*	a*	b*
$PbSO_4$	24	800	CP, CDB, CB, CuO	Pb/Ba-silicates, $BaSO_4$	-	PbO-BaO-SiO_2	50.436	-6.4	-35.5
$PbSO_4$	24	850	CDB, CB	CP, CuO, Pb/Ba-silicates, $BaSO_4$	-	PbO-SiO_2	62.053	-3.9	-23.0
$PbSO_4$	24	900	CDB, CP, CB	Pb/Ba-silicates, $BaSO_4$	-	PbO-SiO_2	48.414	-4.0	-32.4
$PbSO_4$	24	950	CP, CB	CDB, $BaSO_4$	-	PbO-SiO_2	56.818	-2.0	-18.6
$PbSO_4$	24	1000	CP, CB	CDB, Cu_2O, $BaSO_4$	-	PbO-SiO_2	43.208	1.8	-20.8
PbS	24	800	CDB, CB, CuO	Pb/Ba-silicates, $BaSO_4$	-	PbO-BaO-SiO_2	60.938	-7.5	-25.1
PbS	24	850	CDB, CB	CuO, Pb/Ba-silicates, $BaSO_4$	-	PbO-SiO_2	62.439	-4.5	-20.3
PbS	24	900	CDB, CB	CP, Pb/Ba-silicates, $BaSO_4$	-	PbO-SiO_2	46.882	-9.0	-29.4

PbS	24	950	CDB, CB	$BaSO_4$, Cu_2O	-	PbO-SiO_2	45.785	-4.0	-13.7
PbS	24	1000	CP, CB	Cu_2O	-	PbO-SiO_2	47.112	-4.2	-18.6
$PbSO_4$	6	800	CuO, CDB, CB	CP, Pb/Ba-silicates, $BaSO_4$	-	PbO-BaO-SiO_2	65.926	-4.6	-12.1
$PbSO_4$	6	850	CB, CDB, CP	Pb/Ba-silicates, $BaSO_4$	-	PbO-SiO_2	53.846	-3.8	-26.4
$PbSO_4$	6	900	CP, CB	CDB, $BaSO_4$, CuO	-	PbO-SiO_2	54.545	-1.8	-21.6
$PbSO_4$	6	950	CP, CB	CDB, $BaSO_4$, CuO	$BaSi_2O_5$	PbO-SiO_2	45.524	-3.3	-27.4
$PbSO_4$	6	1000	CP	CB, CDB, $BaSO_4$	-	PbO-SiO_2	54.43	-1.0	-23.8
PbS	6	800	CuO, CDB	CP, Pb/Ba-silicates, $BaSO_4$	-	PbO-BaO-SiO_2	61.85	-7.8	-20.3
PbS	6	850	CDB	CB, CP, Pb/Ba-silicates, $BaSO_4$	-	PbO-SiO_2	59.229	-7.3	-20.6
PbS	6	900	CDB	CB, CP, Pb/Ba-silicates, $BaSO_4$	-	PbO-SiO_2	52.45	-6.4	-22.9
PbS	6	950	CDB	Pb/Ba-silicates, $BaSO_4$, CuO, CP, CB	$BaSi_2O_5$	PbO-SiO_2	56.362	-7.6	-30.7
PbS	6	1000	CP	CDB, CB, Cu_2O, $BaSO_4$	-	PbO-SiO_2	53.96	-3.5	-28.0

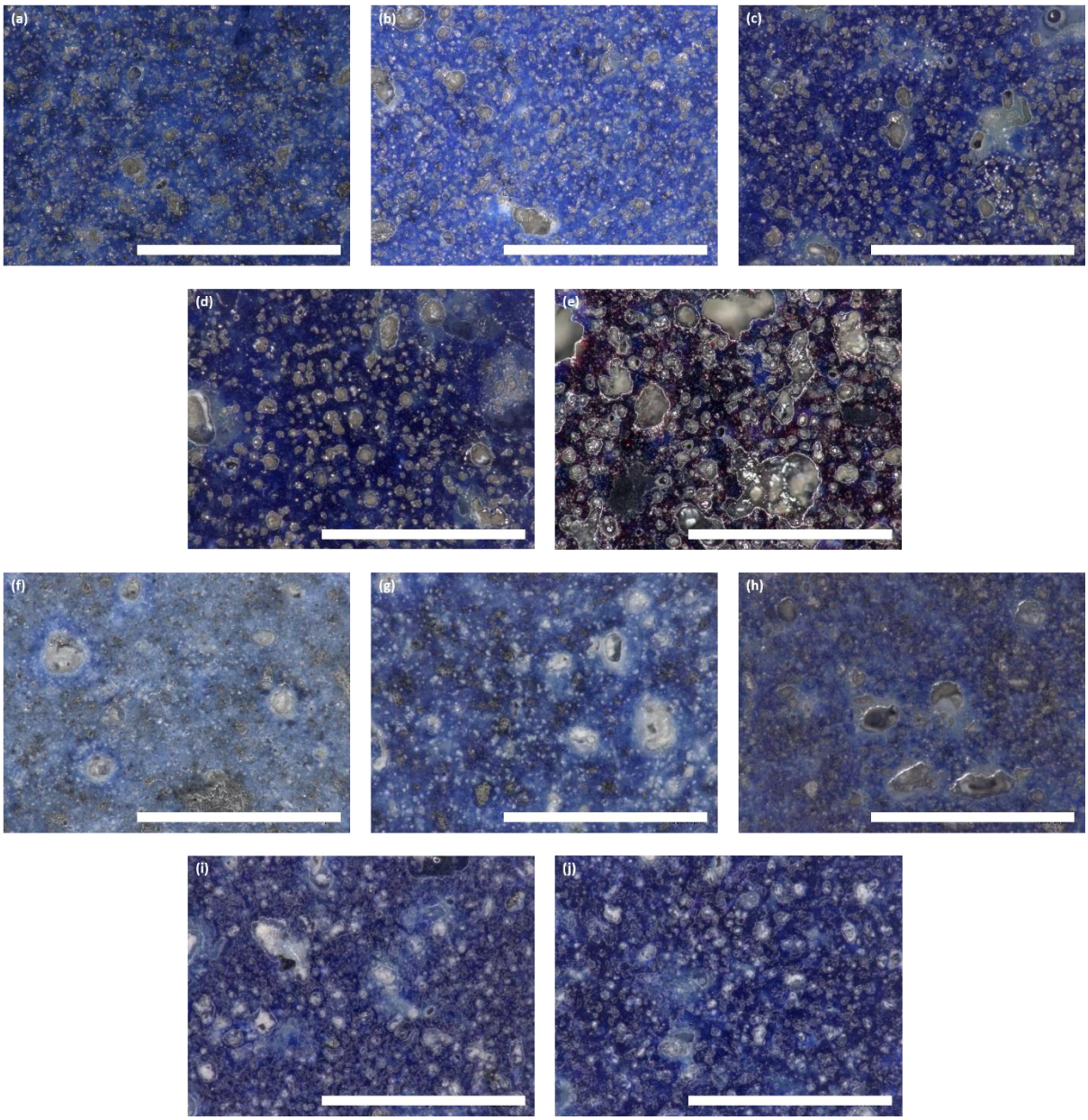

Figure 4-30. Photomicrographs of pigment samples produced with $BaCO_3$ and $PbSO_4$, with starting stoichiometry of Ba:Cu:Si = 1:1:2, and heat treatment for 24 hours at (a) 800 ºC, (b) 850 ºC, (c) 900 ºC, (d) 950 ºC, and (e) 1000 ºC, and for 6 hours at (f) 800 ºC, (g) 850 ºC, (h) 900 ºC, (i) 950 ºC, and (j) 1000 ºC. Scale bar: 1 mm.

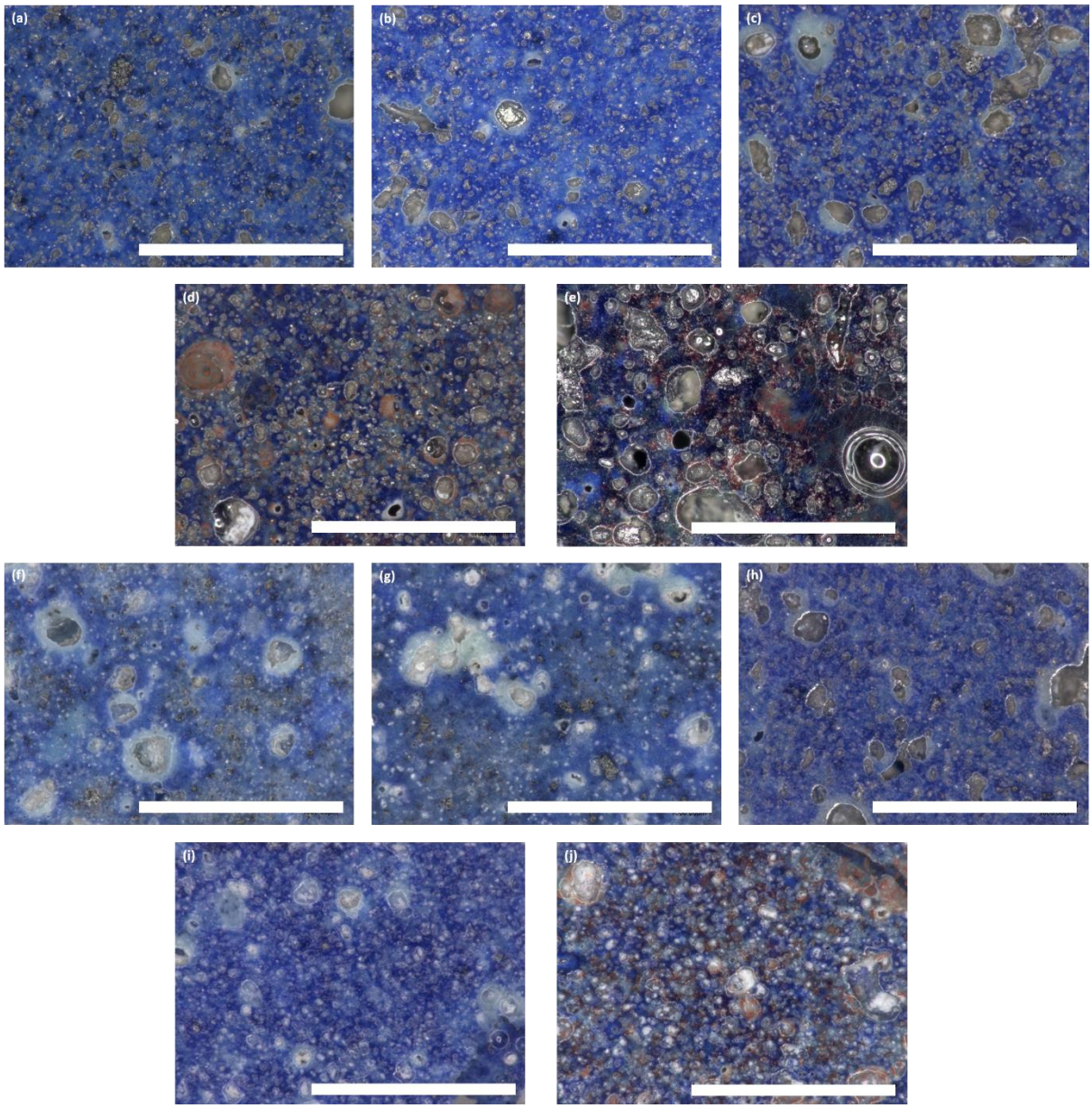

Figure 4-31. Photomicrographs of pigment samples produced with $BaCO_3$ and PbS, with starting stoichiometry of Ba:Cu:Si = 1:1:2, and heat treatment for 24 hours at (a) 800 ºC, (b) 850 ºC, (c) 900 ºC, (d) 950 ºC, and (e) 1000 ºC, and for 6 hours at (f) 800 ºC, (g) 850 ºC, (h) 900 ºC, (i) 950 ºC, and (j) 1000 ºC. Scale bar: 1 mm.

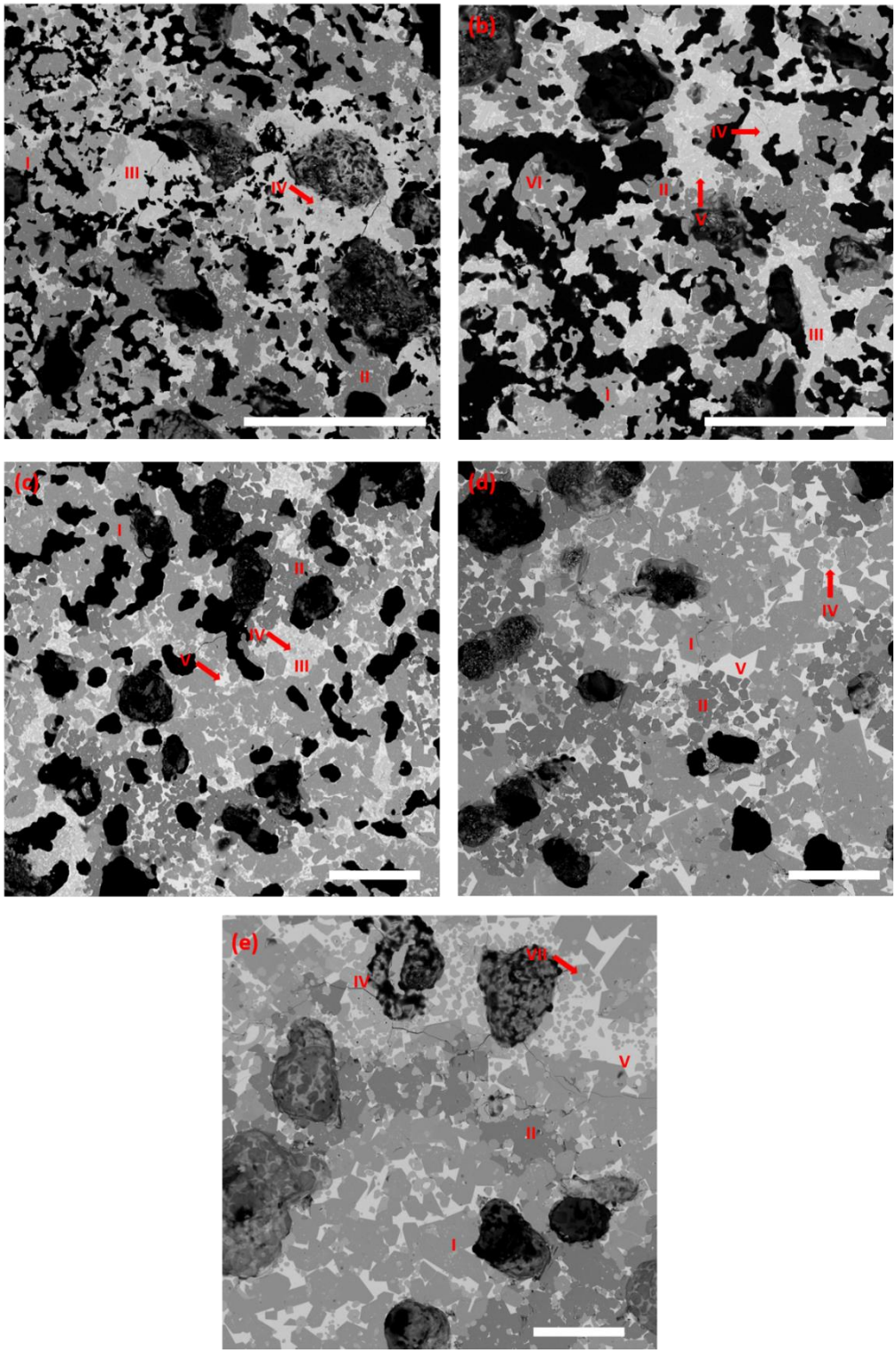

Figure 4-32. BSE micrographs of pigment samples produced with $BaCO_3$ and $PbSO_4$, with starting stoichiometry of Ba:Cu:Si = 1:1:2, and heat treatment for 24 hours at (a) 800 ºC, (b) 850 ºC, (c) 900 ºC, (d) 950 ºC, and (e) 1000 ºC. I: $BaCuSi_2O_6$ (CP) or $BaCu_2Si_2O_7$ (CDB). II: $BaCuSi_4O_{10}$ (CB). III: Pb/Ba silicate phases. IV: $BaSO_4$. V: $PbO\text{-}SiO_2$ glass. VI: CuO. VII: Cu_2O. Scale bar: 50 µm.

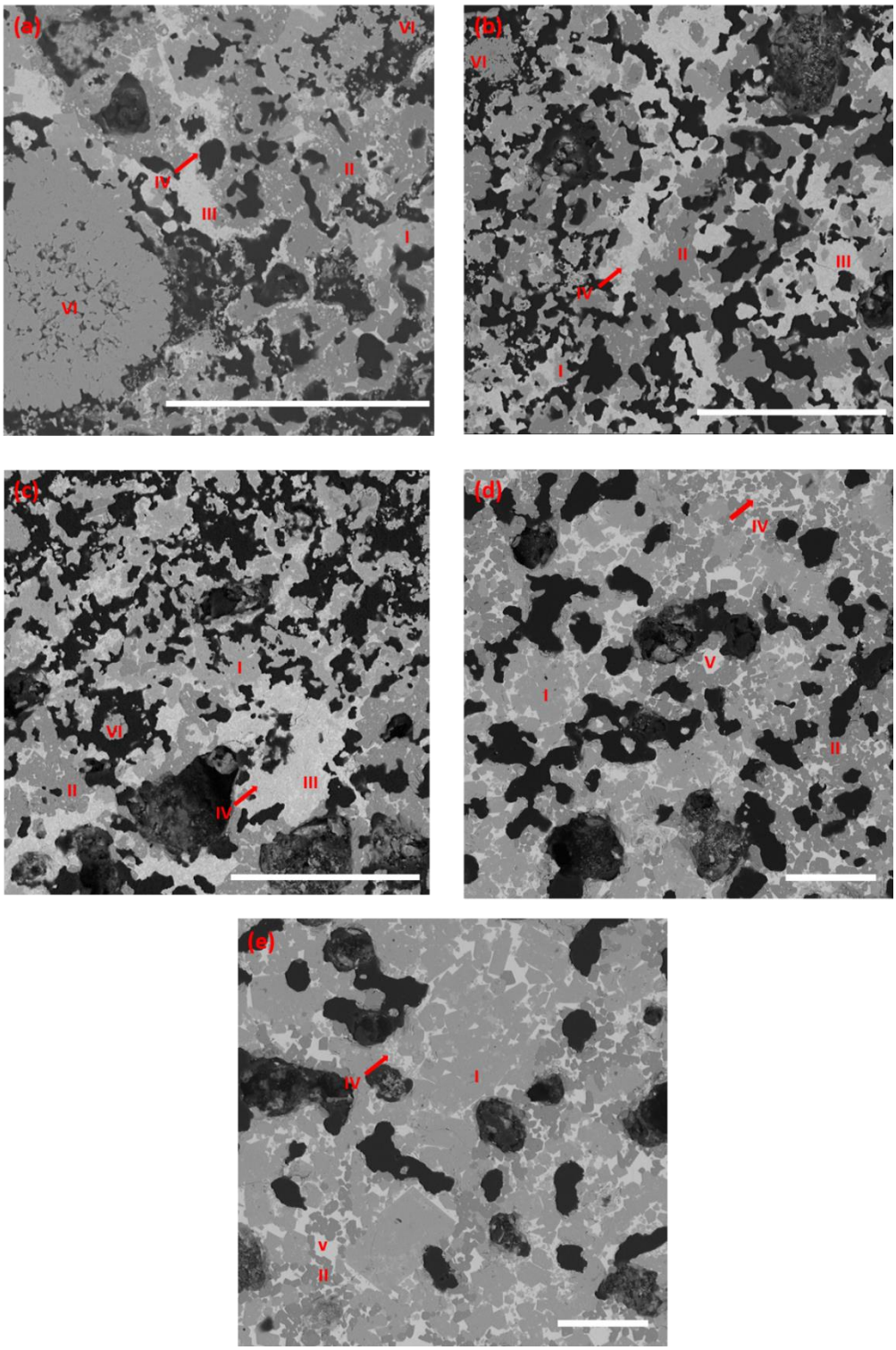

Figure 4-33. BSE micrographs of pigment samples produced with $BaCO_3$ and $PbSO_4$, with starting stoichiometry of Ba:Cu:Si = 1:1:2, and heat treatment for 6 hours at (a) 800 ºC, (b) 850 ºC, (c) 900 ºC, (d) 950 ºC, and (e) 1000 ºC. I: $BaCuSi_2O_6$ (CP) or $BaCu_2Si_2O_7$ (CDB). II: $BaCuSi_4O_{10}$ (CB). III: Pb/Ba-silicates. IV: $BaSO_4$. V: $PbO\text{-}SiO_2$ glass. VI: CuO. VII: Cu_2O. Scale bar: 50 µm.

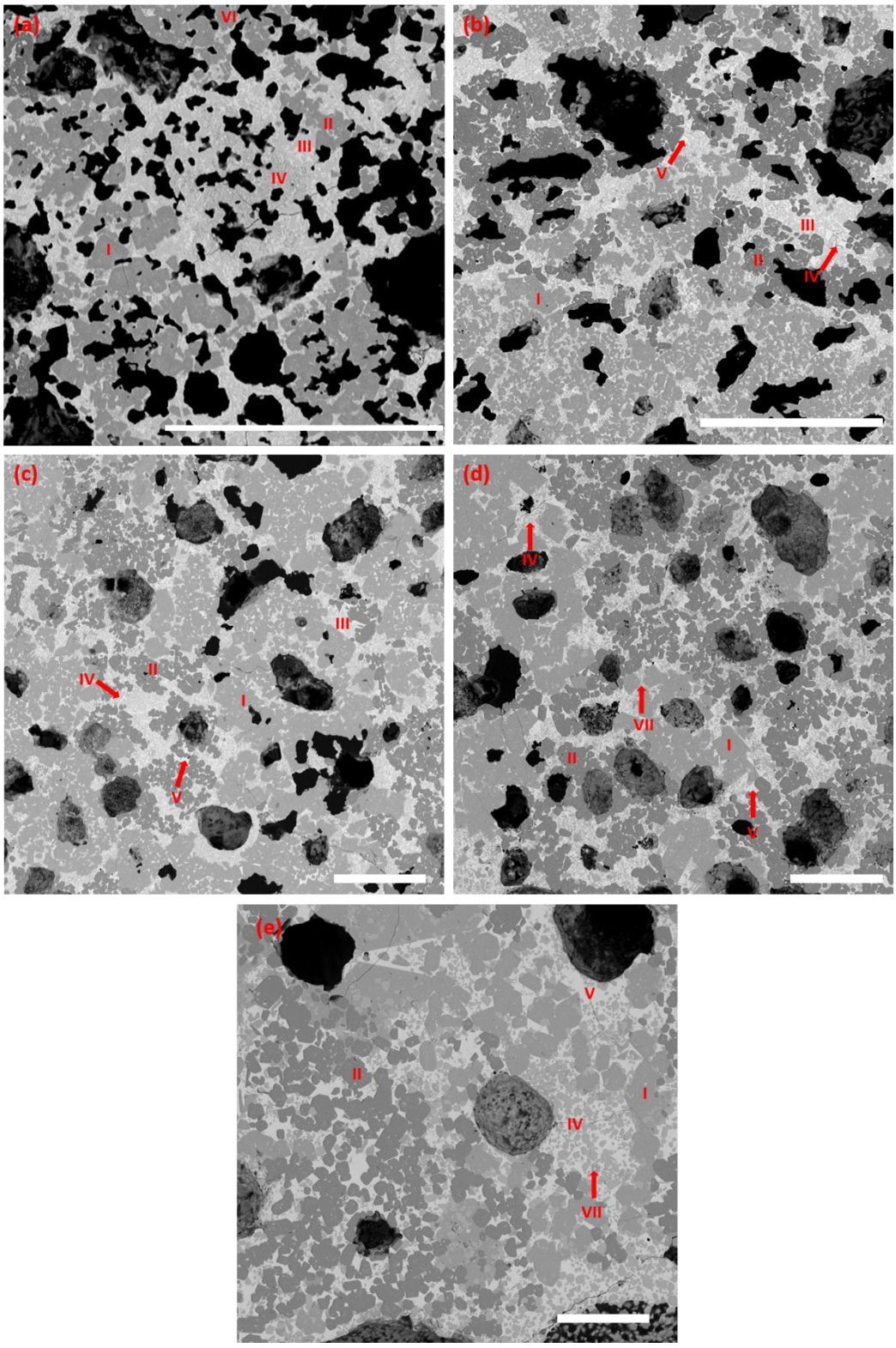

Figure 4-34. BSE micrographs of pigment samples produced with $BaCO_3$ and PbS, with starting stoichiometry of Ba:Cu:Si = 1:1:2, and heat treatment for 24 hours at (a) 800 ºC, (b) 850 ºC, (c) 900 ºC, (d) 950 ºC, and (e) 1000 ºC. I: Mainly $BaCu_2Si_2O_7$ (CDB). II: $BaCuSi_4O_{10}$ (CB). III: Pb/Ba-silicates. IV: $BaSO_4$. V: PbO-SiO_2 glass. VI: CuO. VII: Cu_2O. Scale bar: 50 µm.

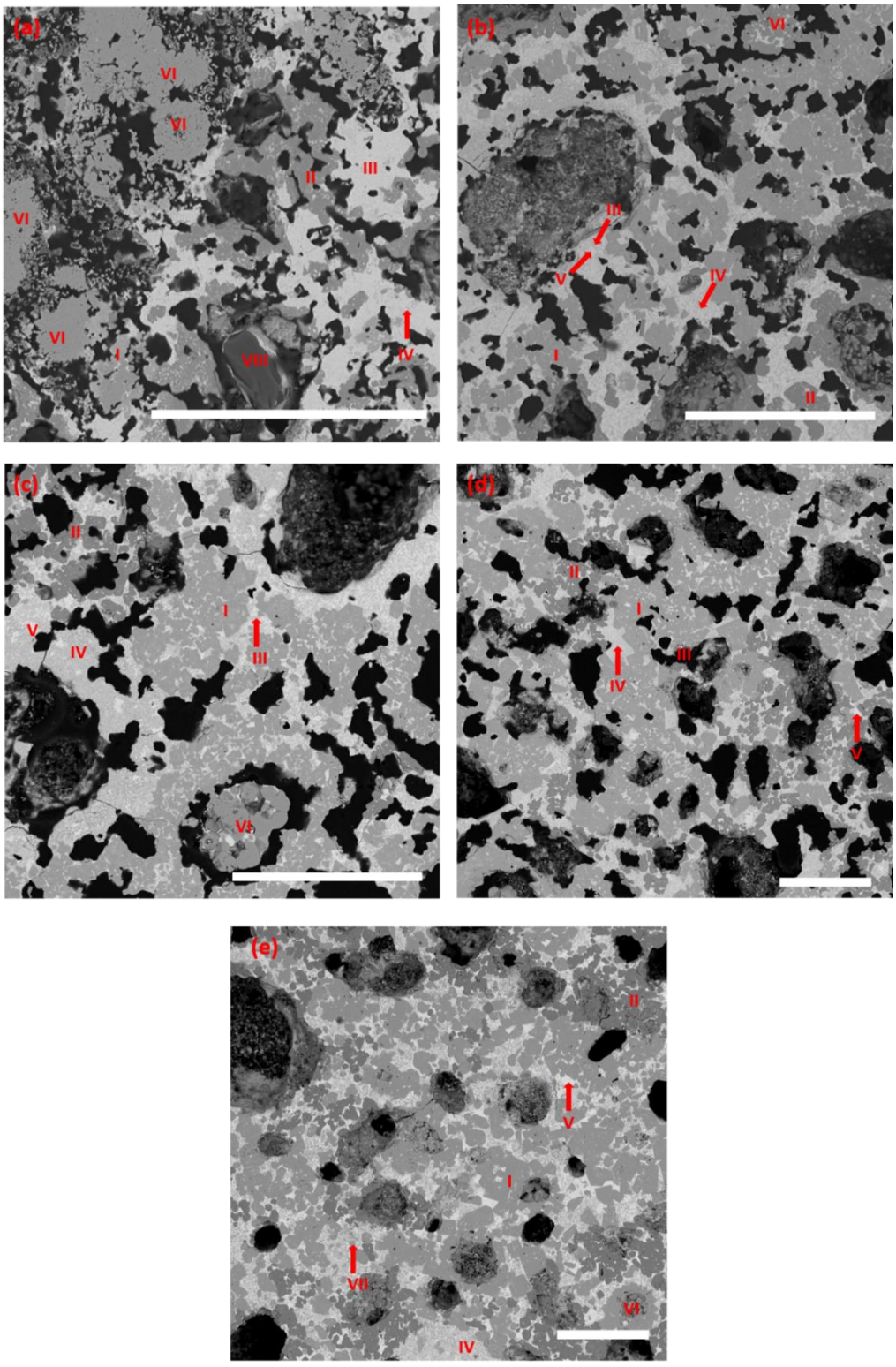

Figure 4-35. BSE micrographs of pigment samples produced with $BaCO_3$ and PbS, with starting stoichiometry of Ba:Cu:Si = 1:1:2, and heat treatment for 6 hours at (a) 800 ºC, (b) 850 ºC, (c) 900 ºC, (d) 950 ºC, and (e) 1000 ºC. I: Mainly $BaCu_2Si_2O_7$ (CDB). II: $BaCuSi_4O_{10}$ (CB). III: Pb/Ba-silicates. IV: $BaSO_4$. V: PbO-SiO_2 glass. VI: CuO. VII: Cu_2O. VIII: SiO_2. Scale bar: 50 µm.

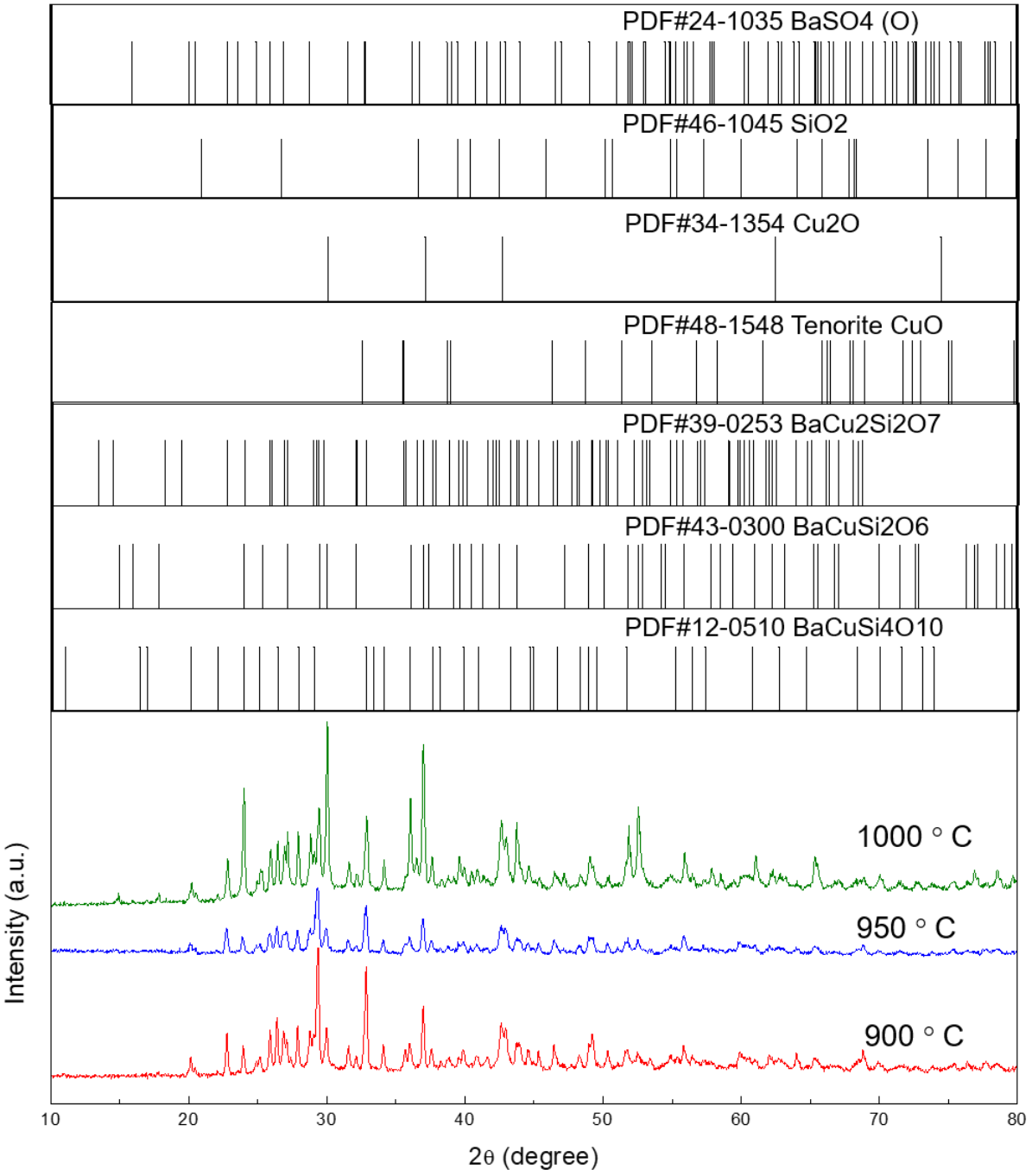

Figure 4-36. XRD diffractograms of pigment samples produced with $BaCO_3$ and $PbSO_4$, with starting stoichiometry of Ba:Cu:Si = 1:1:2, and heat treatment for 24 hours at 900 ºC, 950 ºC and 1000 ºC.

4.3 Discussion

In the systematic reproduction of Chinese blue and Chinese purple, five parameters have

been taken into consideration: the Ba-source, the Pb-source, the starting stoichiometry of Ba:Cu:Si, heat treatment temperatures and heat treatment time. The effects of these five parameters that reflect possible raw materials selection on the pigment synthesis and byproduct formation, as well as, the implications on ancient production technology of Chinese blue and Chinese purple are discussed in this session.

4.3.1 $BaSO_4$ and $BaCO_3$ as Ba-source

With CuO as the Cu-source and quartz SiO_2 as the Si-source, the direct use of $BaSO_4$ has failed to reproduce Chinese blue or Chinese purple for most of the 80 different combinations of Pb-additives. Ba:Cu:Si = 1:1:4 or1:1:2 in all heat treatment conditions set for this study produced end-products with unreacted CuO, SiO_2 and $BaSO_4$, or $(Pb,Ba)SO_4$ solid solution as the main phases (**Figure 4-2**, **Figure 4-3**, **Figure 4-4**, and **Figure 4-6**). The only successful synthesis was performed using 20 wt% of PbO with Ba:Cu:Si = 1:1:2 at 1000 ˚C for 24 hours. Using this formulation and experimental conditions, Chinese blue ($BaCuSi_4O_{10}$) was formed as one of the main phases, while Cu_2O was not a major phase (**Figure 4-7**). A successful synthesis of Chinese blue with $BaSO_4$ as the Ba source was previously reported; in this study for Ba:Cu:Si = 1:1:2, they used malachite ($Cu_2(OH)_2CO_3$) as the Cu-source and quartz SiO_2 as the Si-source, with the addition of 19 wt% of PbO, and fired at 900 ˚C for 24 hours [71]. The color of the end-product was reported to be bluish green, with main phases being identified by XRD as $BaCuSi_4O_{10}$, $BaSO_4$, and CuO [71]. The main differences between these two

successful syntheses are in the Cu-source and heat treatment temperature. Although the use of malachite as an alternative Cu-source has not been explored in this research, it can be seen that with Ba:Cu:Si = 1:1:2 stoichiometry corresponding to optimum molar ratio for the production of Chinese purple ($BaCuSi_2O_6$), synthesis with the direct use of $BaSO_4$ at high temperatures (900 ˚C for malachite and 1000 ˚C for CuO) for 24 hours results in the formation of Chinese blue ($BaCuSi_4O_{10}$). This can be attributed to the smaller wt% of SiO_2 in the starting batches with the stoichiometry of Ba:Cu:Si = 1:1:2, which makes the melting of quartz SiO_2 easier for a given heat treatment condition in comparison to the case with starting stoichiometry of Ba:Cu:Si = 1:1:4. This can be seen in four samples produced with $BaSO_4$ at Ba:Cu:Si = 1:1:2 with the formation of $BaCuSi_4O_{10}$ in the bulk and surface of the samples, whereas, only two samples with the starting stoichiometry of Ba:Cu:Si = 1:1:4 were able to produce the $BaCuSi_4O_{10}$ compound (**Table 4-2**).

All 80 samples produced with $BaCO_3$ on the other hand, produced all major crystalline compounds in Chinese blue ($BaCuSi_4O_{10}$), Chinese purple ($BaCuSi_2O_6$), and/or Chinese dark blue ($BaCu_2Si_2O_7$) as major phase(s) in the end-products, with or without significant amount of CuO or Cu_2O. With these data, it can be concluded that $BaSO_4$ is chemically less reactive than $BaCO_3$ requiring strict production conditions and operational sequences to produce the desirable pigments. It is therefore unlikely to have been deliberately selected as the raw material for the Ba-source required for the synthesis of these pigments.

This is mainly due to the higher thermal stability of $BaSO_4$ than that of $BaCO_3$. Without

the addition of flux, when heat treated for 1 hour, $BaSO_4$ undergoes slight decomposition with the evolution of SO_2 and O_2 (**Reaction 4-1**) at temperatures between 975 ˚C and 1300 ˚C [128], or up to 1500 ˚C [129]. Conversely, the thermal decomposition of $BaCO_3$ (**Reaction 4-2**), without addition of flux and after phase transformation from orthorhombic to hexagonal at 806-825 ˚C [130-135] and from hexagonal to cubic at 964-983 ˚C [130-134], starts at 1340-1357 ˚C at 1 atm CO_2 [134, 136]. Eutectic temperature of 1030 ˚C [133], 1060 ˚C [137], or 1070-1150 ˚C [130] at a pCO_2 of 0.00661 atm [137] or 0.0039-0.0066 atm [130] have been reported for a eutectic composition of $2BaCO_3 \cdot BaO$. As reproduction experiments in this study were performed in an oxidizing condition (in air), the pCO_2 should be only ~0.0004 atm. Thermal analysis by TG/DTG has shown that $BaCO_3$ started to decompose at ~800 ˚C and completed at ~950 ˚C when mixtures of $BaCO_3$, CuO and SiO_2 (with either 1:1:2 or 1:1:4 stoichiometry for Ba:Cu:Si) were heated up to 1000 ˚C [69]. With the addition of Pb-source as flux, the thermal decomposition of $BaCO_3$ is expected to have started at a temperature much lower than 1340-1357 ˚C, with BaO being the stable phase in contact with CO_2 [134]. The difference in thermal stability between $BaSO_4$ and $BaCO_3$ can be directly seen in a previous study in which thermal decomposition temperatures of mineral barite ($BaSO_4$) from the Zhuans County of Hubei Province and mineral witherite ($BaCO_3$) from the Chengkou Mine of Chongqing City are reported to be 1180 ˚C and 900 ˚C, respectively [73].

Reaction 4-1. Decomposition of $BaSO_4$:

$$2BaSO_4 \rightarrow 2BaO + 2SO_2 + O_2$$

Reaction 4-2. Decomposition of $BaCO_3$:

$$BaCO_3 \rightarrow BaO + CO_2$$

After the thermal decomposition of $BaSO_4$ or $BaCO_3$, BaO can react with CuO and SiO_2 to form $BaCuSi_4O_{10}$ (CB, **Reaction 4-3**), $BaCuSi_2O_6$ (CP, **Reaction 4-4**), and $BaCu_2Si_2O_7$ (CDB, **Reaction 4-5**), and/or it can become part of the silicate glass structure forming the PbO-BaO-SiO_2 glass, or it can participate in other side reactions such as the formation of $BaSO_4$ with S introduced with PbS or $PbSO_4$. The addition of Pb-source which serves as flux, promotes the thermal decomposition of $BaSO_4$ and $BaCO_3$ to occur at lower temperatures. However, as it is shown in this research, even with the addition of 20 wt% of PbO, $PbCO_3$, $PbSO_4$, or PbS, and with a heat treatment temperature as high as 1000 ˚C and a reaction time as long as 24 hours, the direct use of $BaSO_4$ still poses severe limitations in the reproduction of Chinese blue or Chinese purple. This result agrees with other previously published studies on reproduction experiments for the production of Chinese blue and Chinese purple in which $BaCO_3$ has also been suggested to be a more likely Ba-source under various experimental set-ups, different from this research [48, 73]. It is worth noting that the use of $BaSO_4$ after a calcination pretreatment at 1200 ˚C still failed to produce Chinese blue or Chinese purple without a large amount of $BaSO_4$ slag residues present in the end-products [73].

Reaction 4-3. Formation of $BaCuSi_4O_{10}$, the main pigment phase of Chinese blue (CB):

$$BaO + CuO + 4SiO_2 \rightarrow BaCuSi_4O_{10}$$

Reaction 4-4. Formation of $BaCuSi_2O_6$, the main pigment phase of Chinese purple (CP):

$$BaO + CuO + 2SiO_2 \rightarrow BaCuSi_2O_6$$

Reaction 4-5. Formation of $BaCu_2Si_2O_7$, the main pigment phase of Chinese dark blue (CDB):

$$BaO + 2CuO + 2SiO_2 \rightarrow BaCu_2Si_2O_7$$

Despite the much higher success rate of reproducing Chinese blue and Chinese purple with the use of $BaCO_3$ as starting material, witherite (the mineral form of $BaCO_3$), is much rarer than barite (the mineral form of $BaSO_4$) which is the most abundant and commonly available Ba-containing mineral in China. Only about 40 witherite deposits have been identified in China, within a witherite belt that is about 300 km long located between northern Daba Mountains and sourthern Qinling Mountains [82-84]. Distances between the witherite deposits and important sites where significant amounts of artifacts containing Chinese blue and Chinese purple have been recovered are estimated by measuring the direct distances (on Google Map) from the following counties near some of the richest deposits along the witherite belt as well as at the boundaries: Ziyang (紫阳) County and Zhenba (镇巴) County in Shaanxi Province, Wanyuan (万源) County in Sichuan Province, Chengkou (城口) County in Chongqing Municipality, and Zhuxi (竹溪) County in Hubei Province. The witherite deposits are thus estimated to be located 1) about 300-450 km from modern day Tianshui (天水), the city in Gansu Province where a large amount of Chinese blue and Chinese purple faience beads (including the one studied in Chapter 3 in this thesis) dated to the late Warring States Period (475-221 BC) have been recovered; 2) about 200-250 km from modern day Xianyang (咸阳), the capital of the Qin Dynasty (221-207 BC); 3) about 200-250 km from modern day Xi'an (西安), the capital of the Western Han Dynasty (206 BC-AD 8); and 4) about 350-500 km from Luoyang (洛阳), the capital of the Eastern Han Dynasty (25-220 AD).

If witherite ($BaCO_3$) was indeed the original Ba-source, with the witherite deposits located about 200-500 km from the various important sites, it may also imply a long-distance direct trade to obtain witherite or a long-distance inter-regional exchange of witherite to produce the pigments locally, or a long-distance inter-regional exchange of pigment products if the pigments were produced in areas near the witherite deposits. In any of these scenarios, a sufficient amount of labor and resource support should have required to complete the long-distance travel, which would not have been considered if it was not for the production of materials of high values and significance. Based on ancient texts, vermilion was the royal color for the kings in both the Western Zhou Dynasty (1046-771 BC) and the Eastern Zhou Dynasty (770-256 BC) [138]. During the Spring and Autumn Period (770-476 BC), which was the first half of the Eastern Zhou Dynasty, dukes and marquees of states started to wear purple color [138]. With the decline of the kings' power during this period, as dukes and marquees continued to seek rise in their political and military power, purple was intentionally promoted to be a color with social status as high as the royal color vermilion [138]. Eventually, from the beginning of the Western Han Dynasty (206 BC-AD 8), besides being a noble color, purple also became a sacred color that represented the sky [138]. With the absence of naturally occurring purple mineral in China and a demand for a purple pigment that could be applied on mural paintings in royal and noble tombs, as well as on terracotta objects of high status such as the Emperor Qinshihuang's terracotta warriors, the making of Chinese purple is believed to have been important during these time periods. Similarly, as a blue pigment that has much

higher chemical stability than azurite ($Cu_3(CO_3)_2(OH)_2$), a natural blue mineral which can easily transform into the green mineral malachite ($Cu_2(CO_3)(OH)_2$) by environmentally-induced effects, the importance of Chinese blue during these time periods in China's history can be inferred from the findings of Chinese blue pigment applied on mural paintings and the Chinese blue faience beads recovered from noble tombs. Therefore, with the high social, political and aesthetic values of Chinese purple and Chinese blue pigments, the long-distance travel and intense labor required to obtain witherite could be justified.

The deliberate selection and use of witherite as the Ba-source instead of barite despite the adverse conditions of obtaining this mineral for the production of Chinese blue and Chinese purple, may suggest that there was sufficient knowledge of the properties and chemical stability the two minerals for the production of these highly valued pigments. Such knowledge of raw materials selection may have derived from previous knowledge on the production of Chinese lead barium ($PbO\text{-}BaO\text{-}SiO_2$) glass, which appeared during the early Warring States Period. The discovery of archaeological $PbO\text{-}BaO\text{-}SiO_2$ glass in North-West China and central China dated to the late Warring States Period, as well as the Western and Eastern Han dynasties [139] suggests a close relationship with the contemporary production of Chinese blue and Chinese purple, which also required the addition of Pb-additives as flux/catalyst and the use of Ba-containing raw materials. Similarly, although $BaSO_4$ grains have been reported to be present in $PbO\text{-}BaO\text{-}SiO_2$ glass samples, in two reproduction experiments of $PbO\text{-}BaO\text{-}SiO_2$ glass, the use of $BaCO_3$ has been shown to form well-vitrified glass products while the use of $BaSO_4$ lead

to poorly vitrified products with significant amounts of residual $BaSO_4$ [70, 85]. Therefore, the BaSO4 found in archaeological samples might have come from reaction byproducts or impurity introduced with witherite or other raw materials.

4.3.2 Effects of Ba:Cu:Si starting stoichiometry on the formation of $BaCuSi_4O_{10}$ (Chinese blue, CB), $BaCuSi_2O_6$ (Chinese purple, CP), and $BaCu_2Si_2O_7$ (Chinese dark blue, CDB)

The effect of Ba:Cu:Si starting stoichiometry in the production of CB, does not seem to play a significant role when $BaSO_4$ was used as the Ba-source because the main raw materials $BaSO_4$, CuO and SiO_2 have mostly remained unchanged under various heat treatment conditions. As stated earlier, only at stoichiometry of Ba:Cu:Si = 1:1:2, high temperatures (1000 ˚C mainly) and long reaction time (24 hours) (**Table 4-2**, Figure 4-6 and Figure 4-7), conditions under which thermal decomposition of $BaSO_4$ and melting of SiO_2 can be promoted yielded $BaCuSi_4O_{10}$ crystals. This can be explained with the lower wt% of SiO_2 contained in the batches with a Ba:Cu:Si = 1:1:2 starting stoichiometry vs 1:1:4, resulting in an easier melting of SiO_2. This is also reflected in the results that $BaCuSi_4O_{10}$ is one of the main phases in four samples produced with a Ba:Cu:Si =1:1:2 starting stoichiometry versus two samples produced with a Ba:Cu:Si = 1:1:4 starting stoichiometry. Based on density functional theory (DFT) calculations, $BaCuSi_4O_{10}$ is thermodynamically the most stable of the Chinese pigments [46]. Therefore, a prolonged heat treatment time (24 hours) promotes the formation of the

stable $BaCuSi_4O_{10}$, even with a starting stoichiometry of Ba:Cu:Si = 1:1:2.

On the other hand, the Ba:Cu:Si starting stoichiometry in samples produced with $BaCO_3$ plays an important role in the production of the main pigment crystal phase(s) in the end-products. $BaCuSi_4O_{10}$ is the main pigment phase in all samples produced with starting stoichiometry of Ba:Cu:Si = 1:1:4 regardless of the differences in Pb-source and synthesis conditions, as a result of the sufficient starting SiO_2 content which promotes the progressive condensation reaction progress of silicate (**Reaction 4-6**) [9].

Reaction 4-6. The progressive condensation process of silicate compounds in the BaO-CuO-SiO_2 system:

$$SiO_4^{4-} \rightarrow Si_2O_7^{6-}(BaCu_2Si_2O_7) \rightarrow Si_4O_{12}^{8-}(BaCuSi_2O_6) \rightarrow Si_8O_{20}^{8-}(BaCuSi_4O_{10})$$

With a starting stoichiometry of Ba:Cu:Si = 1:1:2, however, SiO_2 is less sufficient to promote the formation of $BaCuSi_4O_{10}$. Instead, the initial kinetic product $BaCu_2Si_2O_7$ and the intermediate $BaCuSi_2O_6$ [9] are commonly present in various proportions, depending on the different combinations of Pb-source and synthesis conditions. However, the use of $PbSO_4$ and PbS specifically promotes the formation of $BaCuSi_4O_{10}$ (which will be discussed below). Therefore, even with a starting stoichiometry of $BaCuSi_2O_6$, the identity of the main pigment phase is strongly affected by the Pb-source and synthesis conditions, which will be discussed in the next session.

4.3.3 Effects of Pb-source and synthesis conditions on formation of pigment phases, $BaSO_4$ and Cu_2O

Most experiments for the production of the pigment indicated that the Pb-source selected

in the starting materials, plays an important role in the end-products produced. Within each of these three main sub-groups: 1) samples produced with $BaSO_4$; 2) samples produced with $BaCO_3$ and a starting stoichiometry of Ba:Cu:Si = 1:1:4; and 3) samples produced with $BaCO_3$ and a starting stoichiometry of Ba:Cu:Si = 1:1:2, differences in the main phases and in the byproducts are largely due to the different Pb-sources used: 1) Pb-sources not containing S (i.e. PbO or $PbCO_3$) and 2) S-containing Pb sources ($PbSO_4$ or PbS). The effect on the major phases produced can be explained with the differences in the temperature ranges in which thermal decomposition and/or melting of the four Pb-source occur, as well as the conditions in which complex redox reactions associated with the S content (in the form of sulfide or sulfate) occur. PbO used in this reproduction experiment is in the form of orthorhombic massicot, which melts at 887 ˚C in air in its pure form [125]. Even if the tetragonal litharge had been used, it would have been transformed into the orthorhombic massicot at ~489 ˚C [126], which is much lower than the lowest heat treatment temperature (800 ˚C) employed in this study. With the presence of other Ba-, Cu-, and Si-containing raw materials, the melting of PbO is expected to have started at temperature lower than 887 ˚C. As no residual PbO has been detected in the end-products, and owing to the presence of $PbO\text{-}SiO_2$ and/or $PbO\text{-}BaO\text{-}SiO_2$ glass coexisting with other crystalline phases (**Table 4-4** to **Table 4-7**), it can be concluded that the melting of PbO occurs at all heat treatment temperatures applied in this study (between 800 and 1000 ˚C).

Previous studies have shown that the decomposition temperature and decomposition mechanism of $PbCO_3$ highly depends on the experimental conditions such as particle pressure

of carbon dioxide (pCO_2) and heating rate [131, 132, 140-145]. When air atmosphere is applied [143], in which pCO_2 is approximately 0.0004 atm, or a CO_2 atmosphere is applied with pCO_2 controlled to be under 1 atm [144] or under 0.2 atm [145], $PbCO_3$ first decomposes to the intermediate $PbCO_3 \cdot 2PbO$ (**Reaction 4-7**) at 190 ˚C [143] or at ~200 ˚C [144]. $PbCO_3 \cdot 2PbO$ in turn decomposes to PbO (**Reaction 4-8**) at 330 ˚C [143] or at ~310 ˚C [144]. Since this reproduction experiment was performed in air, this is expected to be the decomposition mechanism applicable in this research, as well as in the ancient production of Chinese blue and Chinese purple since pCO_2 should have been very unlikely to reach a partial pressure as high as 1 atm from a pCO_2 of 0.0004 atm in air. Even though the actual decomposition temperatures of $PbCO_3$ to $PbCO_3 \cdot 2PbO$, and $PbCO_3 \cdot 2PbO$ to PbO might differ to certain extent from the temperatures reported in previous studies due to the differences in experimental conditions, with the lowest heat treatment temperature being 800 ˚C in this research, $PbCO_3$ is expected to have decomposed completely to PbO, followed by the melting of PbO and the subsequent formation of $PbO\text{-}SiO_2$ and/or $PbO\text{-}BaO\text{-}SiO_2$ glass matrix.

Reaction 4-7. Decomposition of $PbCO_3$ to the intermediate $PbCO_3 \cdot 2PbO$:

$$3PbCO_3 \rightarrow PbCO_3 \cdot 2PbO + 2CO_2$$

Reaction 4-8. Decomposition of the intermediate $PbCO_3 \cdot 2PbO$ to the final solid product PbO:

$$PbCO_3 \cdot 2PbO \rightarrow 3PbO + CO_2$$

Therefore, due to the low thermal decomposition temperature of $PbCO_3$ with PbO being the final decomposition product, samples produced with PbO and $PbCO_3$ as Pb-source in general have the same main and minor crystalline phases and glass matrix composition for the

same synthesis condition, with a few samples having differences in the formation of Cu_2O, mainly due to the self-generating CO_2 gas from decomposition of $PbCO_3$ that affects the kinetics and/or the partial pressure at the sample surface.

Thermal decomposition of $PbSO_4$ has been reported to be noticeable or to begin at various temperatures in the range of 637-895 ˚C [74, 114, 116-118, 146], depending on the different experimental procedures and conditions. The final non-volatile product is PbO [74] given sufficiently high heat treatment temperature and/or sufficiently long heat treatment time. It has been shown that under a N_2 atmosphere, the thermal decomposition of $PbSO_4$ starts at ~895 ˚C, and as temperature increases, the three basic lead sulfates that are stable at high temperature in the PbO-$PbSO_4$ system, $PbO{\cdot}PbSO_4$, $2PbO{\cdot}PbSO_4$, and $4PbO{\cdot}PbSO_4$ [147-150], progressively form, with PbO starting to appear at temperature above 1170 ˚C and being the only end-product at 1200 ˚C (mainly in the form of massicot) (**Reaction 4-9**) [146, 150]. Therefore, if the desired heat treatment conditions are met and a complete decomposition of $PbSO_4$ is achieved, the overall reaction can be written as **Reaction 4-10**.

Reaction 4-9. Progressive thermal decomposition of $PbSO_4$ to PbO:

$$PbSO_4 \rightarrow PbO \cdot PbSO_4 \rightarrow 2PbO \cdot PbSO_4 \rightarrow 4PbO \cdot PbSO_4 \rightarrow PbO$$

Reaction 4-10. Overall reaction of thermal decomposition of $PbSO_4$ to PbO:

$$2PbSO_4 \rightarrow 2PbO + 2SO_2 + O_2$$

It has been shown that pure $PbSO_4$ can partially decompose to $PbO{\cdot}PbSO_4$ after a heat treatment at 850 ˚C for 10 hours while partial decomposition occurs at 800 ˚C for 8 hours for natural anglesite (the mineral containing mainly $PbSO_4$) [150]. When heated at 950 ˚C, pure

$PbSO_4$ is decomposed to mainly $PbO{\cdot}PbSO_4$ (with minor $2PbO{\cdot}PbSO_4$) after 5 hours, $2PbO{\cdot}PbSO_4$ (with minor $PbO{\cdot}PbSO_4$) after 10 hours, and $2PbO{\cdot}PbSO_4$ (with minor $4PbO{\cdot}PbSO_4$) after 15 hours [150]. In addition, pure $PbSO_4$ has fully decomposed to $4PbO{\cdot}PbSO_4$ after a heat treatment at 1050 ˚C for 5 hours, while decomposition occurs at only 950 ˚C for 9 hours for natural anglesite [150]. The lower onset of decomposition temperatures observed in natural anglesite in comparison to pure $PbSO_4$ is likely to be due to impurities possibly present in the natural mineral. Based on these previously published data [150], raw materials and heat treatment conditions in this research, it can be derived that the thermal decomposition of $PbSO_4$ has started with the progressive reaction in the formation of $PbO{\cdot}PbSO_4$ at the lowest heat treatment temperature (800 ˚C), and in the formation of $4PbO{\cdot}PbSO_4$ (**Reaction 4-9**) at the highest heat treatment temperature in this study (1000 ˚C).

Similarly, mechanism(s) and product(s) of thermal oxidation of PbS are highly dependent on the experimental conditions [111-113, 150-153]. In general, at low temperatures, PbS in air is primarily oxidized to $PbSO_4$, which can then follow the progressive formations of $PbO{\cdot}PbSO_4$, $2PbO{\cdot}PbSO_4$, and $4PbO{\cdot}PbSO_4$ as temperature increases before the breakdown of the sulfates, resulting in the formation of PbO (**Reaction 4-11**) [111, 112, 151-153]. Therefore, if the desired heat treatment conditions are met and a complete oxidation of PbS is achieved, the overall reaction may be written as **Reaction 4-12**.

However, additional redox reactions can occur between PbS and its oxidized products ($PbSO_4$ or PbO), forming metallic Pb (**Reaction 4-13** and **Reaction 4-14**), which can undergo

further oxidation to form PbO (**Reaction 4-15** and **Reaction 4-16**) [111, 152].

Reaction 4-11. Progressive thermal oxidation of PbS:

$$PbS \rightarrow PbSO_4 \rightarrow PbO \cdot PbSO_4 \rightarrow 2PbO \cdot PbSO_4 \rightarrow 4PbO \cdot PbSO_4 \rightarrow PbO$$

Reaction 4-12. Overall reaction for thermal oxidation of PbS to PbO:

$$2PbS + 3O_2 \rightarrow PbO + SO_2$$

Reaction 4-13. Reaction between PbS and $PbSO_4$ to form metallic Pb:

$$PbS + PbSO_4 \rightarrow 2Pb + 2SO_2$$

Reaction 4-14. Reaction between PbS and PbO to form metallic Pb:

$$PbS + 2PbO \rightarrow 2Pb + SO_2$$

Reaction 4-15. Oxidation of Pb to PbO in O_2:

$$2Pb + O_2 \rightarrow 2PbO$$

Reaction 4-16. Oxidation of Pb to PbO in the presence of $PbSO_4$:

$$Pb + PbSO_4 \rightarrow 2PbO + SO_2$$

In summary, in comparison to $PbSO_4$, heat treatment of PbS is more complicated, which can involve more redox reactions. The decomposition temperatures of each step, as well as, the identities of reaction products highly depend on the experimental conditions such as heat treatment temperatures and time duration, as well as, atmosphere. For example, with a heating rate of 10 ˚C/min, the thermal oxidation of PbS in air up to 980 ˚C results in the formation of $PbSO_4$; $PbO \cdot PbSO_4$ becomes the main oxidation product at a temperature ~1075 ˚C, and the progressive formation of $2PbO \cdot PbSO_4$ and $4PbO \cdot PbSO_4$, PbO starts when temperature reaches 1170 ˚C [152]. However, when PbS is heated in air at 500 ˚C for 2 hours [111, 150] and 10 hours [150], the main oxidation product of PbS is $PbSO_4$ [111, 150], while $PbO \cdot PbSO_4$ is the main oxidation product if PbS is heated in air for 15 hours at the same temperature [111]. Since

the reproduction experiment in this research was performed between 800 and 1000 ˚C for 6 hours or 24 hours, the previously published literature in which thermal oxidation experiment of PbS has been performed at different temperatures for certain time scales represents a similar experimental condition. It has been shown that after heat treatment at 300 ˚C for 10 hours, PbS starts to oxidize to $PbSO_4$, while $PbO{\cdot}PbSO_4$ starts to form after a heat treatment of PbS at 700 ˚C for 2 hours or 10 hours, resulting in a mixture of PbS, $PbSO_4$, and $PbO{\cdot}PbSO_4$ [150]. At 800 ˚C, PbS has fully been oxidized to $PbSO_4$ and $PbO{\cdot}PbSO_4$ after 2 hours or 10 hours of heat treatment [150]. Therefore, with the lowest heat treatment temperature being 800 ˚C and a shortest heat treatment time being 6 hours, it is expected that PbS would oxidize to $PbSO_4$ and $PbO{\cdot}PbSO_4$.

$BaSO_4$ forms as a byproduct when $BaCO_3$ was used with $PbSO_4$ or PbS under all synthesis conditions (**Table 4-5** and **Table 4-7**), with an increase in particle size as heat treatment temperature and/or reaction time increase (**Figure 4-18** to **Figure 4-21**, and **Figure 4-32** to **Figure 4-35**). BaO resulting from the thermal decomposition of $BaCO_3$ (**Reaction 4-2**) can readily react either with the SO_2 and O_2 gases dissolved in the melt (**Reaction 4-17**), or with the $PbSO_4$ (**Reaction 4-18**) from the direct use of $PbSO_4$ or from the thermal oxidation of PbS, to form $BaSO_4$.

Reaction 4-17. Reaction of BaO with SO_2 and O_2 to form $BaSO_4$:

$$2BaO + 2SO_2 + O_2 \rightarrow 2BaSO_4$$

Reaction 4-18. Reaction of BaO with $PbSO_4$ to form $BaSO_4$:

$$BaO + PbSO_4 \rightarrow BaSO_4 + PbO$$

Cu_2O is an undesired byproduct observed to have formed in some end-products. The black CuO, either being unreacted residue as that in the case of end-products produced with $BaSO_4$, or being excess from the formation of the main pigment phases, can be reduced to the red Cu_2O (**Reaction 4-19**). CuO decomposes to Cu_2O in air at temperature higher than 1026 ˚C [154-157] or 1027 ˚C [158] under a partial pressure of O_2 (pO_2) of 0.21 atm [154-158]. Since the reproduction experiments in this research were also performed in air, the expected formation of Cu_2O from CuO should be around 1026 ˚C or 1027 ˚C. However, with the presence of Ba-source, Pb-source and SiO_2, as well as CO_2, SO_2, and/or additional O_2 evolved as a result of thermal decomposition or oxidation of Ba-source and/or Pb-source, the formation of Cu_2O would occur at a different temperature and a different pO_2.

Reaction 4-19. Formation of Cu_2O from CuO:

$$4CuO \rightarrow 2Cu_2O + O_2$$

In general, because of the differences in their chemical properties at high temperature, samples produced with $PbO/PbCO_3$ differ significantly from those produced with $PbSO_4$/PbS. Minor differences are also present between samples produced with PbO and $PbCO_3$, as well as between $PbSO_4$ and PbS. Side reactions such as the formation of $BaSO_4$ and Cu_2O are also related to the differences observed among samples produced with the various Pb-source within the integrated system of reactions. All these differences will be discussed based on the three different sub-groups: 1) samples produced with $BaSO_4$; 2) samples produced with $BaCO_3$ and a starting stoichiometry of Ba:Cu:Si = 1:1:4; and 3) samples produced with $BaCO_3$ and a

starting stoichiometry of Ba:Cu:Si = 1:1:2.

4.3.3.1 Effects of Pb-source on samples produced with $BaSO_4$

For samples produced with $BaSO_4$ with both Ba:Cu:Si = 1:1:2 and Ba:Cu:Si = 1:1:4, the use of $PbO/PbCO_3$ mainly resulted in the formation of $PbO\text{-}SiO_2$ glass matrix after the melting of PbO, either from the direct use of PbO or from the thermal decomposition of $PbCO_3$ (**Reaction 4-7** and **Reaction 4-8**). With the limited thermal decomposition of $BaSO_4$ (**Reaction 4-1**) due to its high thermal stability, CuO and SiO_2 remain mostly unreacted (**Figure 4-2**(a) and **Figure 4-3**(a)).

On the contrary, when $PbSO_4$ or PbS was used as Pb-source, $BaSO_4$ and $PbSO_4$ (either from the direct use of $PbSO_4$ or from the thermal oxidation of PbS) tend to form a solid solution $(Pb,Ba)SO_4$, with CuO and SiO_2 remaining unreacted (**Figure 4-3**(b)). This is mainly due to the much higher thermal stability of $PbSO_4$ in comparison to PbO and $PbCO_3$, with limited thermal decomposition of $PbSO_4$ (either from the direct use of $PbSO_4$ or from the oxidation of PbS) achieved. Therefore, no $PbO\text{-}SiO_2$ glass forms except for samples produced with Ba:Cu:Si = 1:1:2 at 1000 ˚C for 24 hours, which started with less amount of SiO_2 and was subjected to high enough heat treatment temperature for sufficient time, leading to the partial melting of PbO and formation of limited amount of $PbO\text{-}SiO_2$.

Within this sub-group, with the CuO being mostly unreacted, Cu_2O commonly forms in samples produced with heat treatment temperature at 1000 ˚C for 24 hours (**Figure 4-2**(b),

Table 4-1), mainly because at this temperature (close to the 1026 ˚C or 1027 ˚C), the decomposition of CuO occurs forming Cu_2O (**Reaction 4-19**) in air [154-158]. In addition, Cu_2O tends to form at lower heat treatment temperatures (900 ˚C or 950 ˚C) in samples produced with PbO/$PbCO_3$ than those produced with $PbSO_4$/PbS (**Table 4-1**). This could be due to the readily available PbO to form a partial melt of PbO-SiO_2 to aid the heat transport in thermal decomposition reactions, as well as to facilitate the reactions among raw materials and increase chemical activities. Also, because of the much lower thermal decomposition temperature of $PbCO_3$ into the final product PbO (at 330 ˚C [143] or at ~310 ˚C [144]), the CO_2 evolved lowers the pO_2 from 0.21 atm, which lowers the temperature at which CuO decomposes into Cu_2O. In comparison, although SO_2 and O_2 gases are expected to have been evolved in the thermal decomposition of $PbSO_4$ (**Reaction 4-9** and **Reaction 4-10**) or thermal oxidation and decomposition of PbS (**Reaction 4-11** and **Reaction 4-12**), it requires a higher heat treatment temperature than that in the case of $PbCO_3$, resulting in a pO_2 not significantly lower than 0.21 atm and thus a Cu_2O formation temperature closer to the equilibrium value.

The only successful synthesis of Chinese blue ($BaCuSi_4O_{10}$) using $BaSO_4$ was achieved with the use of PbO. This is mainly due to the readily availability of PbO in comparison to other Pb-source as a flux, which can more effectively lower the melting temperature of SiO_2. Although the starting stoichiometry is ideal for the formation of Chinese purple ($BaCuSi_2O_6$), with the starting $BaSO_4$ not having fully been decomposed (**Figure 4-7**(b)-(d)), BaO is insufficient to participate in the formation of barium copper silicates, resulting in a Ba:Cu:Si

ratio different from the 1:1:2 stoichiometry. Therefore, with a long reaction time (24 hours), $BaCuSi_4O_{10}$, the most stable compound in the BaO-CuO-SiO_2 system, forms as a main phase (**Figure 4-7**(b)-(d)) with minor amount of $BaCuSi_2O_6$ crystals (**Figure 4-7**(d)).

4.3.3.2 Effects of Pb-source on samples produced with $BaCO_3$ and a Ba:Cu:Si = 1:1:4 starting stoichiometry

With a Ba:Cu:Si = 1:1:4 starting stoichiometry and the use of $BaCO_3$ as Ba-source, the sufficient SiO_2 content promote the formation of Chinese blue ($BaCuSi_4O_{10}$) in all samples within this sub-group (**Table 4-4** and **Table 4-5**), which is the most stable compound in the BaO-CuO-SiO_2 system [46]. Due to their low thermal stability of PbO and $PbCO_3$, PbO is readily available as an effective flux to lower the melting temperature of SiO_2, forming the PbO-SiO_2 glass matrix and resulting in a more complete synthesis of Chinese blue of high purity, indicated by the minor amount of Chinese purple ($BaCuSi_2O_6$) and residual SiO_2 inclusion (**Figure 4-11** to **Figure 4-14**). A minor amount of BaO becomes part of the glass structure and form PbO-BaO-SiO_2 glass at temperature above 850 ˚C.

Owing to their much higher thermal stability and the more complicated decomposition or oxidation processes, the use of $PbSO_4$ or PbS in the starting material results in a less complete synthesis of Chinese blue, with residual SiO_2 being one of the main phases. Therefore, $PbSO_4$ and PbS are not as effective fluxes as PbO and $PbCO_3$ promoting the melting of SiO_2 and thermal decomposition of $BaCO_3$. After the decomposition of $BaCO_3$, a minor amount of BaO

forms the insoluble $BaSO_4$ with the SO_2 and O_2 gases (**Reaction 4-17**) generated from the thermal decomposition reactions of Pb-source, and/or with the $PbSO_4$ either from the direct use of $PbSO_4$ or from the thermal oxidation of PbS (**Reaction 4-18**). The formation of $BaSO_4$ as a reaction byproduct is observed in all pigment samples within this sub-group, indicating the thermal decomposition of $BaCO_3$ has started at temperature as low as 800 ˚C after 6 hours, which is much lower than the reported decomposition temperature (1340-1357 ˚C) at 1 atm CO_2 [134, 136].

Cu_2O is found in 4 samples within this sub-group, produced with PbO and PbS at 950 ˚C and 1000 ˚C for 24 hours **(Table 4-3**). With the addition of Pb-flux, the thermal decomposition of the $BaCO_3$ (equivalent to 30 wt% of the total batch mass) results in the generation of significant amount of CO_2 gas (**Reaction 4-2**) that does not participate in any further reactions in the system, though it can lower the pO_2 in the system from the 0.21 atm equilibrium pressure. The pO_2 could also have been changed by introducing materials that could have resulted in formation of other gases such as CO from the use of coal. Therefore, the formation temperature of Cu_2O can possibly be lowered from the equilibrium value (1026 ˚C or 1027 ˚C [154-158]). Under this scenario, minor differences in Cu_2O formation are still observed between PbO and $PbCO_3$, and between PbS and $PbSO_4$, in which Cu_2O only forms in samples produced with PbO and PbS.

Although the thermal decomposition of $PbCO_3$ also generates CO_2 gas that can further alter the pO_2, with 20 wt% of $PbCO_3$ in the starting materials, the CO_2 gas generated is of minor

amount, which might not be sufficient to affect the pO_2 significantly. At the same time, this additional CO_2 gas may improve the mixing and stirring in the partial melt, kinetically promoting reaction among CuO, BaO and SiO_2 to form $BaCuSi_4O_{10}$ in comparison to the use of PbO. Therefore, there can be more residual CuO in samples produced with PbO, which can form Cu_2O after 24 hours of heat treatment at 950 ˚C or 1000 ˚C while it is not the case in samples produced with $PbCO_3$ under the same synthesis conditions. Thermal oxidation of PbS to PbO (**Reaction 4-12** has more redox reactions possibly involved (**Reaction 4-13** to **Reaction 4-16**) which is more complicated than the thermal decomposition of $PbSO_4$ to PbO (**Reaction 4-9**). Therefore, PbS is a less effective flux than $PbSO_4$, resulting in more residual CuO that can form Cu_2O after 24 hours of heat treatment at 950 ˚C or 1000 ˚C.

Within this sub-group, it can be concluded that the use of PbO or $PbCO_3$ result in $BaCuSi_4O_{10}$ of higher purity and less residual SiO_2, and with $BaCuSi_2O_6$ being a common minor phase. Due to the generation of CO_2 gas that increases the kinetic rate of pigment synthesis, the optimal synthesis conditions to produce Chinese blue using $PbCO_3$ are less strict than using PbO; the use of PbO requires heat treatment at 850-900 ˚C for 24 hours or at 950-1000 ˚C for 6 hours, while the use of $PbCO_3$ requires heat treatment at 850-1000 ˚C for 24 hours or at 900-1000 ˚C for 6 hours (**Table 4-4**). The use of $PbSO_4$ or PbS result in $BaCuSi_4O_{10}$ of lower purity with more residual SiO_2, with $BaSO_4$ being a common reaction byproduct. Due to the higher redox complexity of thermal oxidation process of PbS, the optimal synthesis conditions to produce Chinese blue using $PbSO_4$ are less strict than using PbS: the use of PbS

requires heat treatment at 850-900 ˚C for 24 hours or at 900-1000 ˚C for 6 hours, while the use of $PbSO_4$ requires heat treatment at 850-1000 ˚C for 24 hours or at 900-1000 ˚C for 6 hours (**Table 4-5**).

4.3.3.3 Effects of Pb-source on samples produced with $BaCO_3$ and a Ba:Cu:Si = 1:1:2 starting stoichiometry

Although the starting Ba:Cu:Si stoichiometry is that of Chinese purple ($BaCuSi_2O_6$), the main pigment phase in the end-products in this sub-group depend strongly on the differences in Pb-source and synthesis conditions. This is mainly because in the BaO-CuO-SiO_2 system, $BaCuSi_2O_6$ is the intermediate product [9] while it is thermodynamically the least stable [46]. Therefore, it is more difficult to obtain Chinese purple of high purity, and the initial kinetic product Chinese dark blue ($BaCu_2Si_2O_7$) and the thermodynamically most stable product Chinese blue ($BaCuSi_4O_{10}$) can preferentially form with certain combinations of Pb-source and synthesis conditions.

Within this sub-group, Chinese purple ($BaCuSi_2O_6$) is the main phase in the end-products produced with PbO or $PbCO_3$ only when a heat treatment of 24 hours at 900-1000 ˚C is applied. With PbO or $PbCO_3$ being an effective flux due to the low thermal stability, under such synthesis conditions, sufficient heat treatment temperature and time can drive the silicate condensation reaction (**Reaction 4-6**) to favor the formation of intermediate product $BaCuSi_2O_6$. When synthesis time is short (6 hours), or if heat treatment temperature is low

(800-850 ˚C), the initial kinetic product $BaCu_2Si_2O_7$, which has a higher thermodynamic stability than $BaCuSi_2O_6$, forms as the main phase.

In the cases where $PbSO_4$ or PbS is used, Chinese blue ($BaCuSi_4O_{10}$) forms in all samples. This could be due to the higher thermal stability and redox complexity of $PbSO_4$ and PbS, resulting in the delay of PbO formation that is available to lower the melting temperature of SiO_2. At the same time, because $BaSO_4$ is very insoluble and thermally stable, it is precipitated from the partial melt as a byproduct, consuming some BaO from the formation of the barium copper silicates. As a result, although the starting stoichiometry of Ba:Cu:Si is 1:1:2, the actual Ba:Cu:Si is deviated from this ratio, with BaO being deficient. This is equivalent to have a sufficient SiO_2, promoting the formation of $BaCuSi_4O_{10}$. With 20 wt% of Pb-source added in this study, the result corroborates with a previous study in which 10 wt% of $PbCO_3$ promotes the formation of Chinese purple while 10 wt% of PbS promotes the formation of Chinese blue [48, 72].

The use of PbS results in the formation of $BaCu_2Si_2O_7$ as the predominant phase with almost no Chinese purple forming (**Table 4-7**). This is mainly due to the high complexity and redox reactions possibly occurring in the thermal oxidation of PbS compared to the thermal decomposition of $PbSO_4$, making PbS a less effective flux than $PbSO_4$. Being the initial kinetic product that has the smallest activation barrier, $BaCu_2Si_2O_7$ can therefore form instead of $BaCuSi_2O_6$. On the contrary, in the case of using $PbSO_4$ as Pb-source, when the synthesis temperature is not sufficiently high, $BaCu_2Si_2O_7$ forms as the main phase with $BaCuSi_2O_6$ as

the minor phase. At higher temperature (950-1000 ˚C), the sufficient thermal energy promotes the synthesis of $BaCuSi_2O_6$, driving the condensation reaction to the formation of this intermediate reaction product.

Cu_2O was detected in 10 out of the 40 samples within this sub-group (**Table 4-3**). With a higher starting CuO ratio than that of Ba:Cu:Si = 1:1:4, at temperature (950-1000 ˚C) close to the equilibrium formation temperature of Cu_2O, more residual CuO can decompose to Cu_2O. Samples produced with PbO, $PbCO_3$ and PbS have Cu_2O after heated at 950-1000 C for 24 hours, or at 1000 ˚C for 6 hours. However, samples produced with $PbSO_4$ has Cu_2O only after heated at 1000 ˚C for 24 hours. This may be due to the generation of O_2 gas in the thermal decomposition of $PbSO_4$ (**Reaction 4-10**), which increases pO_2 while the CO_2 generated from the thermal decomposition of $BaCO_3$ lowers pO_2.

It can be concluded that based on the experimental set-up in this research, Chinese purple can only be found as the main pigment phase with restricted raw materials combinations, and a narrower range of heat treatment temperature in comparison to the making of Chinese blue. Outside the optimal synthesis conditions, significant amount of unreacted residual CuO is present, or Cu_2O form, or Chinese dark blue is found to be the main pigment phase. The use of PbO or $PbCO_3$ promotes the formation of Chinese purple over Chinese dark blue and Chinese blue, given a long reaction time and high enough heat treatment temperature. The use of $PbSO_4$ or PbS promotes formation of Chinese blue, and Chinese purple can be obtained using $PbSO_4$ at 950 ˚C only. The direct use of PbS results in the formation of Chinese dark blue and Chinese

blue. This may suggest that although galena (PbS) is the major Pb-containing mineral and abundant in China, its direct use in the starting raw materials without any pre-treatment would have not provided a suitable Pb-source in the making of Chinese purple. However, pre-treatment such as roasting and smelting of galena could have been applied to transform it to PbO, $PbCO_3$, or $PbSO_4$. The processing/pre-treatment of galena was known to other contemporary pyrotechnological activities such as the production of Chinese leaded bronze objects, lead barium glass, as well as alchemical or medicinal practices. Given the affinity and intertwined knowledge among the various chemical arts of the period, transfer of knowledge for the pre-treatment of galena for the production of the high valued purple pigment cannot be excluded.

4.4 Conclusions

It can be inferred from this systematic reproduction experiment of Chinese blue and Chinese purple that the ancient manufacture of Chinese blue and Chinese purple requires not only the deliberate selection of raw materials, but also careful and controlled synthesis conditions and production operational sequences. Although barite ($BaSO_4$) is the most abundant and readily available Ba-containing mineral in China, it is less likely to be the Ba-source from a chemical point of view, whereas, the rare mineral witherite ($BaCO_3$) is chemically more likely to successfully produce Chinese blue and Chinese purple. If witherite was indeed the original Ba-source, it suggests a long-distance travel and intense labor involved

in the production of Chinese blue and Chinese purple, which can be supported by the high political, social and aesthetic values of these pigments recorded in ancient texts. A possible relationship between the manufacture of Chinese blue and Chinese purple and the contemporary production of Chinese lead barium glass may also be inferred based on the raw material selection.

In comparison to Chinese blue, the synthesis of Chinese purple has been shown to be more difficult, requiring a more careful raw materials selection and more precise control of synthesis conditions. The use of massicot (PbO) and cerussite ($PbCO_3$) given the optimal synthesis conditions result in the formation of Chinese blue and Chinese purple of higher purity. $BaSO_4$ is observed to have formed as reaction byproduct in all samples produced with $PbSO_4$ and PbS, indicating the $BaSO_4$ found in archaeological samples can possibly be obtained in a similar way. While galena (PbS) is the most abundant and widely available Pb-containing mineral in China, the direct use of galena favors the formation of Chinese dark blue and Chinese blue, making it not suitable as the Pb-source to produce Chinese purple. Pretreatment of galena to transform into PbO, $PbCO_3$, or $PbSO_4$ may have been required. The contemporary alchemical activities and medicinal practices and well-developed Chinese leaded bronze production may have provided technological basis and knowledge transfer.

Chapter 5. Geochemical analysis of a Late Warring States Chinese blue faience bead by lead isotope analysis (LIA) with laser ablation multi-collector inductively coupled plasma mass spectrometry (LA-MC-ICP/MS)

Lead isotope analysis (LIA) based on the stable isotopes of Pb (^{208}Pb, ^{207}Pb, ^{206}Pb and ^{204}Pb) has been commonly applied on Pb-containing archaeological objects such as bronzes and coins [159], as well as Pb-containing glasses and faience objects [1-6], including 8 Chinese blue/Chinese purple samples [1, 2, 6], to provenance the geological origin of the Pb-source employed in the ancient production of these artifacts. Studies applying LIA on archaeological Chinese glasses of the PbO-BaO-SiO_2 system and on Chinese blue and purple pigments have been previously performed by solution-based multi-collector inductively coupled plasma mass spectrometry (MC-ICP/MS) which requires: 1) dissolving the archaeological sample, and 2) extensive wet chemistry-based processing of the sample before the isotope analysis. In this research, however, to determine the Pb stable isotopic signatures that could help geosource (infer the geological location) of the raw materials used for the production of Late Warring States Chinese blue and purple faience beads from the Majiayuan Cemetery in Tianshui City of the Gansu Province (see also Chapter 3), a less-destructive approach was applied, employing a laser ablation (LA-) MC-ICP/MS which eliminated dissolution and pre-treatment of the sample.

5.1 Experimental procedure

A polished cross section of a Late Warring States Chinese blue faience bead from

Majiayuan Cemetery, Tianshui City, Gansu Province (see also Chapter 3) previously analyzed to establish the baseline composition and structure of the archaeological materials was 're-used' for LA-MC-ICP/MS analysis to determine the Pb stable isotopic signatures. A Chinese purple faience bead from the same site dated to the same period was also analyzed. For the analysis, a Nu032 Plasma HR laser ablation (equipped with a 213 nm laser) multi-collector inductively coupled plasma mass spectrometer (LA-MC-ICP/MS) was applied. LIA was performed with 75% laser energy, a repetition rate of 10 Hz, and dwell time of 30 s. The calibration and correction for the fractionation factor was based on the NIST SRM 610, whereas, the NIST SRM 612 and StHs6/80-G reference standards were used to cross check the calibration results. Possible interference of the ^{204}Hg isotope with the ^{204}Pb isotope was corrected based on the StHs6/80-G reference standard glass following the correction method proposed by Kent 2008 [160]. The certified Pb stable isotope ratios of the reference standard glasses are shown in **Table 5-1**. Three spots with spot size of 8 μm and one-line scan with width of 8 μm were performed on the archaeological Chinese blue faience bead. Eleven spots with spot size of 8 μm were performed on the archaeological Chinese purple faience bead.

Table 5-1. Certified Pb stable isotope ratios of reference standard glasses NIST 612, NIST 610, and StHs6/80-G.

Standards	$^{208}Pb/^{206}Pb$	$^{207}Pb/^{206}Pb$	$^{208}Pb/^{204}Pb$	$^{207}Pb/^{204}Pb$	$^{206}Pb/^{204}Pb$
NIST 612	2.1651	0.90745	37.020	15.516	17.099
NIST 610	2.1694	0.90986	36.991	15.515	17.052
StHs6/80-G	2.0379	0.82616	38.515	15.614	18.900

5.2 Results and discussion

The measured Pb isotope ratios for the standard reference glasses corrected for mass

fractionation and ^{204}Hg interference are shown in **Table 5-2**. The apparent agreement with the certified values reflects this correction procedure but note the high level of isotope ratio precision (**Table 5-1**). The average ^{208}Pb/^{206}Pb, ^{207}Pb/^{206}Pb, ^{208}Pb/^{204}Pb, ^{207}Pb/^{204}Pb, and ^{206}Pb/^{204}Pb with two standard deviations of the Chinese blue faience bead were determined to be 2.1808±0.0036, 0.8790±0.0004, 38.45±0.08, 15.50±0.00, and 17.64±0.01, respectively (**Table 5-3**). The average ^{208}Pb/^{206}Pb, ^{207}Pb/^{206}Pb, ^{208}Pb/^{204}Pb, ^{207}Pb/^{204}Pb, and ^{206}Pb/^{204}Pb with two standard deviations of the Chinese blue faience bead were determined to be 2.1896±0.0044, 0.8820±0.0014, 38.48±0.07, 15.50±0.10, and 17.57±0.03, respectively (**Table 5-4**). The relative percentage relative differences (RPD%) were below 0.20%, showing small variations among the analyses.

Table 5-2. Calibration and cross-check results based on NIST 612, NIST 610, and StHs6/80-G, with two standard deviations.

	^{208}Pb/^{206}Pb	^{207}Pb/^{206}Pb	^{208}Pb/^{204}Pb	^{207}Pb/^{204}Pb	^{206}Pb/^{204}Pb
NIST 612	2.1646±0.0009	0.90733±0.0004	36.98±0.11	15.51±0.03	17.09±0.04
NIST 610	2.1686±0.0037	0.90936±0.0019	37.00±0.05	15.52±0.02	17.06±0.04
StHs6/80-G	2.0369±0.0032	0.8256±0.0015	38.54±0.30	15.62±0.13	18.94±0.12

Table 5-3. Pb stable isotope ratios determined on the Late Warring States Chinese blue faience bead. CB: Chinese blue. 2SD: two standard deviations. RPD%: relative percentage difference, calculated by 2SD/Average×100%.

	^{208}Pb/^{206}Pb	^{207}Pb/^{206}Pb	^{208}Pb/^{204}Pb	^{207}Pb/^{204}Pb	^{206}Pb/^{204}Pb
CB_spot1	2.1813	0.8787	38.47	15.50	17.64
CB_spot2	2.1792	0.8791	38.42	15.50	17.63
CB_spot3	2.1797	0.8790	38.42	15.50	17.63
CB_line	2.1832	0.8792	38.50	15.51	17.64
Average	2.1808	0.8790	38.45	15.50	17.64
2SD	0.0036	0.0004	0.08	0.00	0.01
RPD%	0.16	0.05	0.20	0.03	0.07

Table 5-4. Pb stable isotope ratios determined on the Late Warring States Chinese purple faience bead. CP: Chinese purple. 2SD: two standard deviations. RPD%: relative percentage difference, calculated by 2SD/Average×100%.

	$^{208}Pb/^{206}Pb$	$^{207}Pb/^{206}Pb$	$^{208}Pb/^{204}Pb$	$^{207}Pb/^{204}Pb$	$^{206}Pb/^{204}Pb$
CP_spot1	2.1872	0.8809	38.47	15.50	17.59
CP_spot2	2.1914	0.8824	38.46	15.50	17.56
CP_spot3	2.1872	0.8815	38.44	15.49	17.57
CP_spot4	2.1944	0.8818	38.56	15.49	17.57
CP_spot5	2.1885	0.8814	38.47	15.50	17.58
CP_spot6	2.1893	0.8826	38.42	15.49	17.55
CP_spot7	2.1901	0.8824	38.47	15.50	17.56
CP_spot8	2.1903	0.8825	38.51	15.51	17.58
CP_spot9	2.1870	0.8811	38.49	15.51	17.61
CP_spot10	2.1907	0.8826	38.48	15.50	17.56
CP_spot11	2.1895	0.8829	38.46	15.51	17.57
Average	2.1896	0.8820	38.48	15.50	17.57
2SD	0.0044	0.0014	0.07	0.01	0.03
RPD%	0.20	0.16	0.18	0.10	0.19

Pb stable isotope ratios measured on the Chinese blue faience bead in this research have been compared to previously reported LIA data on archaeological Chinese blue/Chinese purple samples, contemporary Chinese PbO-BaO-SiO_2 glasses, as well as Pb-containing ores and minerals surveyed in China. Similar Pb isotope ratios suggest a similar geological origin of the Pb-source. However, the possible overlapping effect where Pb ores from different regions can have similar isotope ratios, as well as a mixing effect resulted from the introduction of multiple Pb sources into the same archaeological sample cannot be ruled out [1].

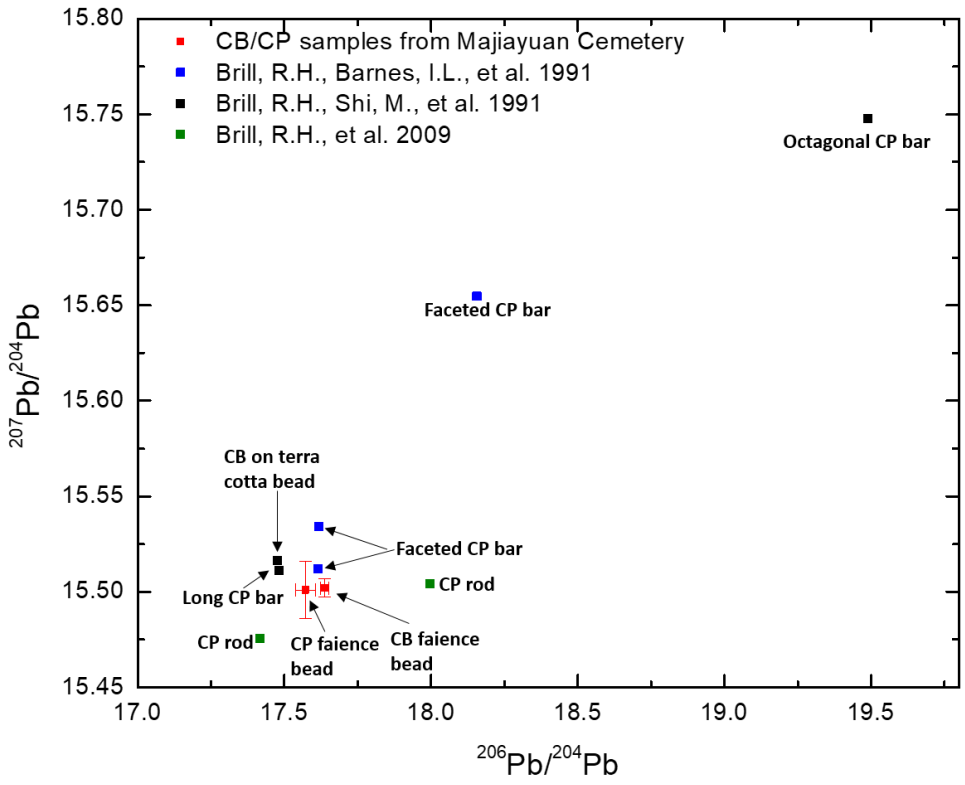

Figure 5-1. Bi-variant plot of $^{207}Pb/^{204}Pb$ and $^{206}Pb/^{204}Pb$ of Chinese blue and Chines purple faience beads analyzed in this study and eight other Chinese blue (CB) and Chinese purple (CP) samples previously reported in [1, 2, 6].

Based on $^{207}Pb/^{204}Pb$ and $^{206}Pb/^{204}Pb$ ratios, the Chinese blue and Chinese purple faience beads analyzed have isotopic signatures close to six other Chinese blue and Chinese purple samples previously reported in [1, 2, 6] (**Figure 5-1**), suggesting the same or a similar a Pb-source for their production. However, with the exception for the Chinese blue and Chinese purple faience beads analyzed in this research, all other eight samples of Chinese blue or Chinese purple lack archaeological provenance. Therefore, a comparison based on archaeological information could not be attempted.

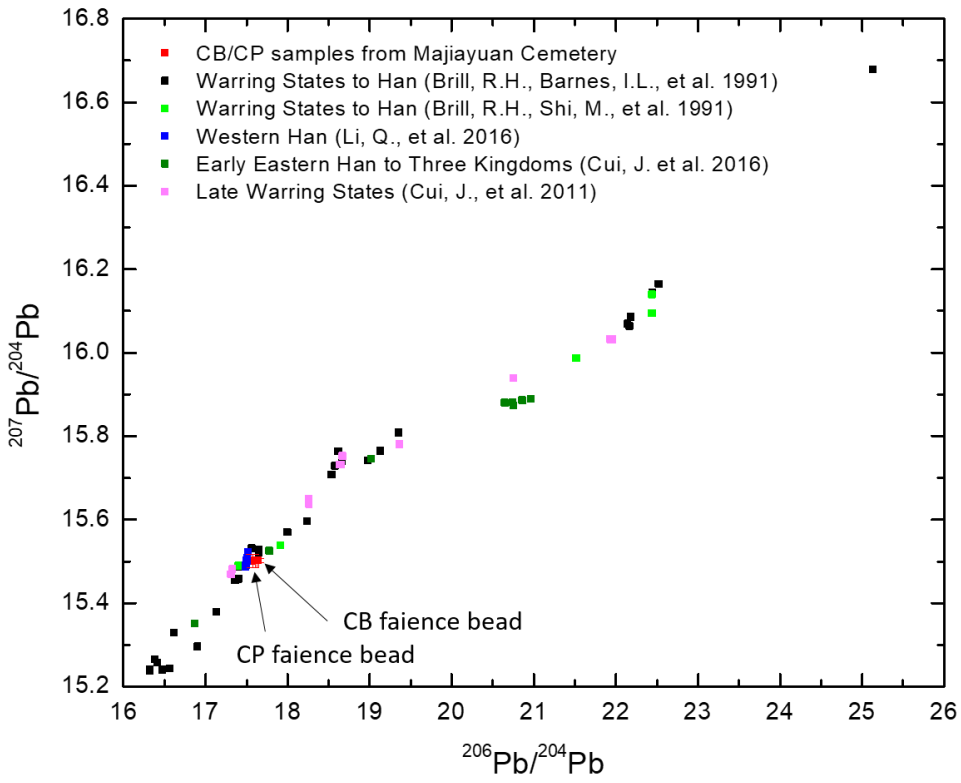

Figure 5-2. Bi-variant plot of $^{207}Pb/^{204}Pb$ and $^{206}Pb/^{204}Pb$ of Chinese blue (CB) and Chinese purple (CP) faience beads analyzed in this study and contemporary Chinese PbO-BaO-SiO_2 previously reported in [1-6].

Pb stable isotope ratios from the analysis of the Chinese blue and Chinese purple faience beads were also compared to those of contemporary Chinese PbO-BaO-SiO_2 glasses (**Figure 5-2**). The latter dataset includes Pb stable isotope ratio measurements from 36 glass samples (mainly glass beads) dated from the Warring States Period to the Han Dynasties [1, 2]. Also include in the comparison are 19 Western Han glass chimes from the Jiangdu King's Mausoleum in Xuyi County of the Jiangsu Province [3], 7 ear pendants and 1 eye bead from the Lijiaba site in Yunyang County, Chongqing City (Eastern Han Dynasty to the Three

Kingdoms Period) [5], and 11 Late Warring States glass samples from the Changde Chu tombs in the Hunan Province [4]. In general, a large variation in $^{207}Pb/^{204}Pb$ and $^{206}Pb/^{204}Pb$ ratios can be seen among the PbO-BaO-SiO_2 glasses, suggesting that either: 1) different geological deposits of Pb were used or 2) mixing of different Pb sources may have occurred.

The Pb stable isotope signature of the Late Warring States Chinese blue and Chinese purple faience beads analyzed here, lies in the region of low $^{207}Pb/^{204}Pb$ and $^{206}Pb/^{204}Pb$ ratios. In the same region, also lie the Pb stable isotope signatures of all 19 glass samples recovered from the Jiangdu King's Mausoleum dated to the Western Han Dynasty (**Figure 5-2**). These results suggest that Pb-sources of similar geological origins may have been used.

5.3 Conclusions

Pb stable isotope ratios of the Late Warring States Chinese blue and Chinese purple faience beads from the Majiayuan Cemetery found in Tianshui City in the Gansu Province, have been determined by LA-MC-ICP/MS. The isotopic signatures show close affinity to six other Chinese blue and Chinese purple samples previously reported, as well as to 19 PbO-BaO-SiO_2 glass samples from the Jiangsu Province dated to the Western Han Dynasty.

Based on the prevalent findings of contemporary Chinese leaded bronze objects and PbO-BaO-SiO_2 glasses, the ancient technology of mining and processing of Pb-ores seems to have been well-developed and applied, and therefore Pb-ores are most likely to have been mined locally for the production of ancient pigments and faience. Future research will focus on the

identification of the raw material selection and geosourcing of the Pb in the Chinese blue and Chinese purple faience beads through isotopic analysis and quantification of trace elements and rare earth elements (REEs).

Chapter 6. Hydrothermal synthesis of Chinese blue nanoscrolls

Inspired by the high NIR luminescence yield and chemical stability of the archaeological Chinese blue, here we explore the synthesis of nanoscale $BaCuSi_4O_{10}$ (the main component of Chinese blue) as a novel optical material. The experimental procedure was based on hydrothermal synthesis of $BaCuSi_4O_{10}$ nanoscrolls and focused: 1) on the effects of heat treatment temperature and time on the formation of $BaCuSi_4O_{10}$ nanoscrolls (Phase I), and 2) the effects of the pH of the precursors (Phase II).

6.1 Experimental procedure

6.1.1 Hydrothermal synthesis

Ba, Cu, and Si-compounds as precursors for hydrothermal synthesis of $BaCuSi_4O_{10}$ included $BaCl_2{\cdot}2H_2O$ (ACS reagent, ≥99%), $Cu(NO_3)_2{\cdot}2.5H_2O$ (ACS reagent, 98%), and sodium silicate solution ($Na_2O(SiO_2)_x{\cdot}xH_2O$, reagent grade, containing ~10.6% of Na_2O and ~26.5% SiO_2). All precursors were purchased from Sigma-Aldrich. NH_4OH (28-30%) was used as mineralizer and to adjust the pH to the desired values. The starting stoichiometry of Ba:Cu:Si was 1:1:6, with excess in the silicate precursor. Parr™ general purpose acid digestion vessels (maximum 250 ºC and 1800 psig) with PTFE cups were used as reaction containers in all trails of the hydrothermal synthesis.

In Phase I, hydrothermal synthesis was performed at the Laboratoire d'Archéologie Moléculaire et Structurale (LAMS) at Sorbonne Universités. Syntheses were performed with

either a 45 mL or a 23 mL cup. $BaCl_2 \cdot 2H_2O$ and $Cu(NO_3)_2 \cdot 2.5H_2O$ powder was first dissolved in deionized (DI) water (30 mL for a 45 mL synthesis, or 10 mL for a 23 mL synthesis). Sodium silicate solution was added to the solution drop by drop with stirring. NH_4OH was then added to the mixture to adjust final pH to be ~12 with the use of pH test strips. The final mixture was transferred to a PTFE-lined cup and sealed inside the acid digestion vessel, which was placed in a Memmert UF 110 Plus oven. Synthesis temperature was set to be 160, 180, or 220 ºC with synthesis time ranging from a few hours up to a few days. After the synthesis, the vessel was naturally cooled to room temperature. Solid end-products were washed thoroughly in DI water, centrifuged and dried before subjected to characterization. In Phase II, hydrothermal synthesis was performed at the Dunn's Laboratory at UCLA. Syntheses were performed with 45 mL reaction containers. The preparation of the precursor mixture was the same as that in Phase I, except that final pH of the mixture was measured with calibrated pH meter. Final pH was varied from ~11.0 to ~12.0 for a given heat treatment condition. A Quincy Lab Model 10 oven was used, and syntheses were performed at 160 ºC for 2 days or 3 days, or at 180 ºC for 3 days.

6.1.2 Characterization of end-products from hydrothermal synthesis

Visible (Vis)-induced near infrared (NIR) photoluminescence imaging was performed on all end-products as the first characterization step to survey the possible presence of $BaCuSi_4O_{10}$, or $BaCuSi_2O_6$ (the main component of Chinese purple that has similar characteristic NIR photoluminescence as Chinese blue under the current imaging set-up) as a possible impurity.

A Mini-Crimescope MCS-400 (SPEX Forensics) with tunable excitation light capabilities was used for the imaging. For this experiment, excitation was provided with λ_{exc} max = 600 nm (50 nm bandwidth) [93]. A modified UV-IR Nikon D90 DSLR camera was used to capture images, with a longpass filter Peca 910, which allows 90% transmission above ~800 nm but filters out light with $\lambda < 800$ nm.

Secondary electron (SE) imaging was performed to characterize and observe the morphology of the end-products. Powder samples were deposited onto carbon tape on top of the aluminum stub, and sputtered with gold before subjected to SEM analysis. SEM analysis using the SE detector was performed with a Hitachi SU-70 field emission gun (FEG) SEM at the Sorbonne Universités, and with an FEI Nova™ NanoSEM 230 FEG SEM at the Molecular and Nano Archaeology (MNA) Laboratory, UCLA.

Scanning transmission electron microscopy (STEM) and transmission electron microscopy (TEM) coupled with EDS was performed on selected end-products to characterize the inter-layered structure and the electron diffraction pattern of the nanoscrolls, as well as the elemental composition of the nanoscrolls. Powder samples were dispersed in ethanol with ultrasonicator prior to being deposited onto the carbon TEM grids. An aberration-corrected Titan Themis 200 STEM/TEM coupled with a Chemistem Super-X EDS was applied, with an accelerating voltage of 200 kV and a probe current of about 80 pA.

X-ray diffraction (XRD) analysis confirmed the presence of $BaCuSi_4O_{10}$ and/or $BaCuSi_2O_6$. Powder samples from end-products from Phase I were first pressed into thin pellets

and taped onto a glass slide vertical to the X-ray beam. Transmission mode was applied and an in-housed built portable XRD with Cu $K\alpha_1$ radiation was used. The 2θ scan range was from 15° to 55° with a step size of 0.042°. Powder samples from end-products from Phase II were characterized with an X'Pert PRO PANalytical powder XRD equipped with a Cu-Kα source, with a voltage of 45 kV and a current of 40 mA. The 2θ range was from 10˚ to 70˚, with a step size of 0.03˚ and count time of 41.9 s per step.

6.2 Results and Discussion

6.2.1 Phase I: Effect of heat treatment temperature and time on formation of $BaCuSi_4O_{10}$ nanoscrolls

All end-products produced in Phase I have light blue to blue, to purplish blue color (**Figure 6-1**(a)). Vis-induced NIR photoluminescence imaging (between 800 and 1000 nm) with excitation at ~600 nm of all samples show NIR luminescence yield (**Figure 6-1**(b, c)), indicating the presence of $BaCuSi_4O_{10}$ and/or $BaCuSi_2O_6$. XRD data identified $BaCuSi_2O_6$ as impurity in some end-products (with $BaCuSi_4O_{10}$ being the predominant phase), formed as an intermediate compound in the progressive silicate condensation reaction in the BaO-CuO-SiO_2 system (**Reaction 6-1**) [9]. With reaction temperature at 160 ºC, and reaction time of 7 days, $BaCuSi_2O_6$ was still present (**Figure 6-2** (a)). With reaction temperature at 180 ºC, only $BaCuSi_4O_{10}$ was present in the end-product if synthesis time was 8.5 days (**Figure 6-2** (b)).

With reaction temperature at 220 ºC, $BaCuSi_2O_6$ was still present as impurity with a reaction time up to 3 days (**Figure 6-2** (c)). The oxidation state of Cu was determined on nanoscrolls produced at 180 ºC for 8.5 days to be 2+ by STEM coupled with electron energy loss spectroscopy (EELS).

Reaction 6-1. The progressive condensation process of silicate compounds in the BaO-CuO-SiO_2 system:

$$SiO_4^{4-} \rightarrow Si_2O_7^{6-}(BaCu_2Si_2O_7) \rightarrow Si_4O_{12}^{8-}(BaCuSi_2O_6) \rightarrow Si_8O_{20}^{8-}(BaCuSi_4O_{10})$$

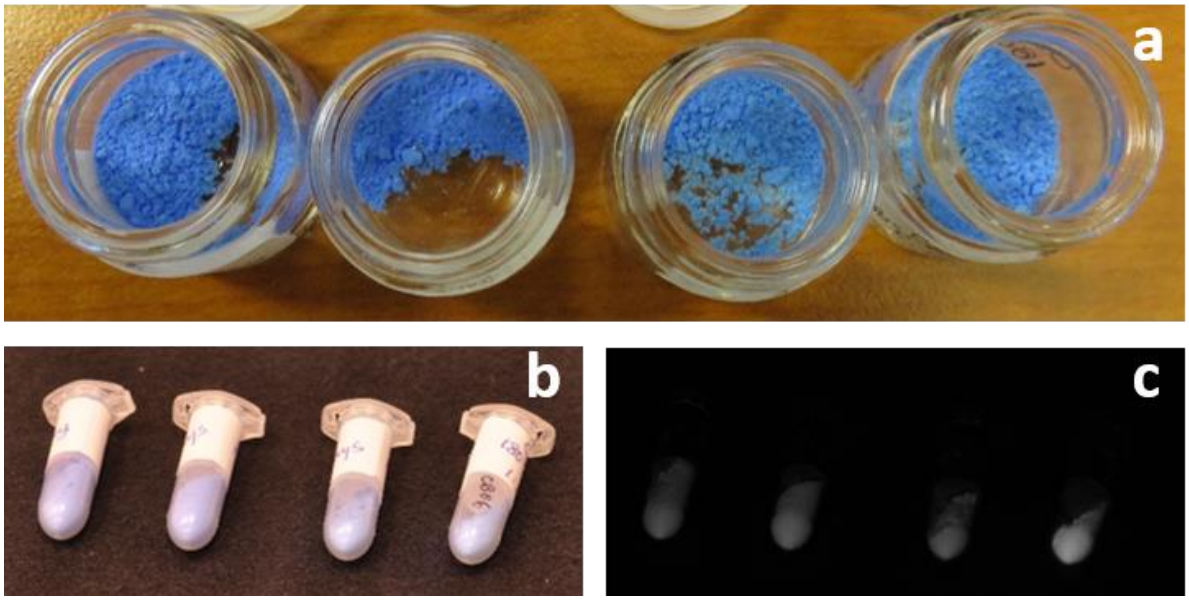

Figure 6-1. (a) RGB image of 4 representative end-products produced during Phase I, which were synthesized at 180 ºC. (b) RGB image and (c) a Vis-induced NIR photoluminescence image of the 4 samples shown in (a). Samples from left to right were synthesized with heat treatment time of 1 day, 2 days, 3 days, and 8.5 days respectively.

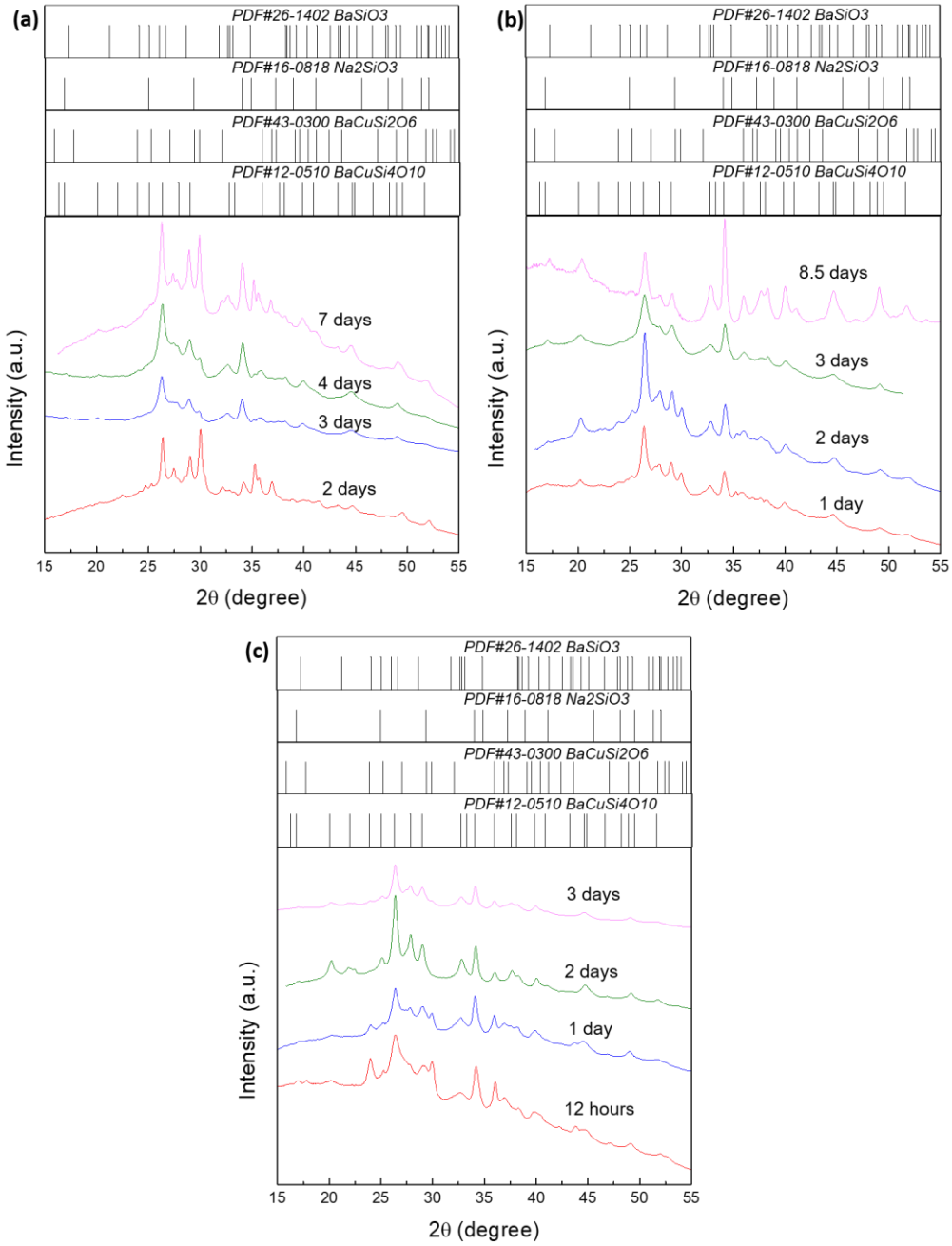

Figure 6-2. XRD diffractograms of powder samples produced at (a) 160 ºC, (b) 180 ºC, and (c) 220 ºC for various synthesis time.

Synthesis time affected not only the composition and phase of the end-products, but also the morphology of the $BaCuSi_4O_{10}$ crystals. At a temperature of 160 ºC and with synthesis time of 2 days the end-products resulted in hierarchical microspheres of $BaCuSi_4O_{10}$ nanosheets (**Figure 6-3**(a)) with nanoscrolls as a minor phase/morphology (**Figure 6-3**(b)). As synthesis

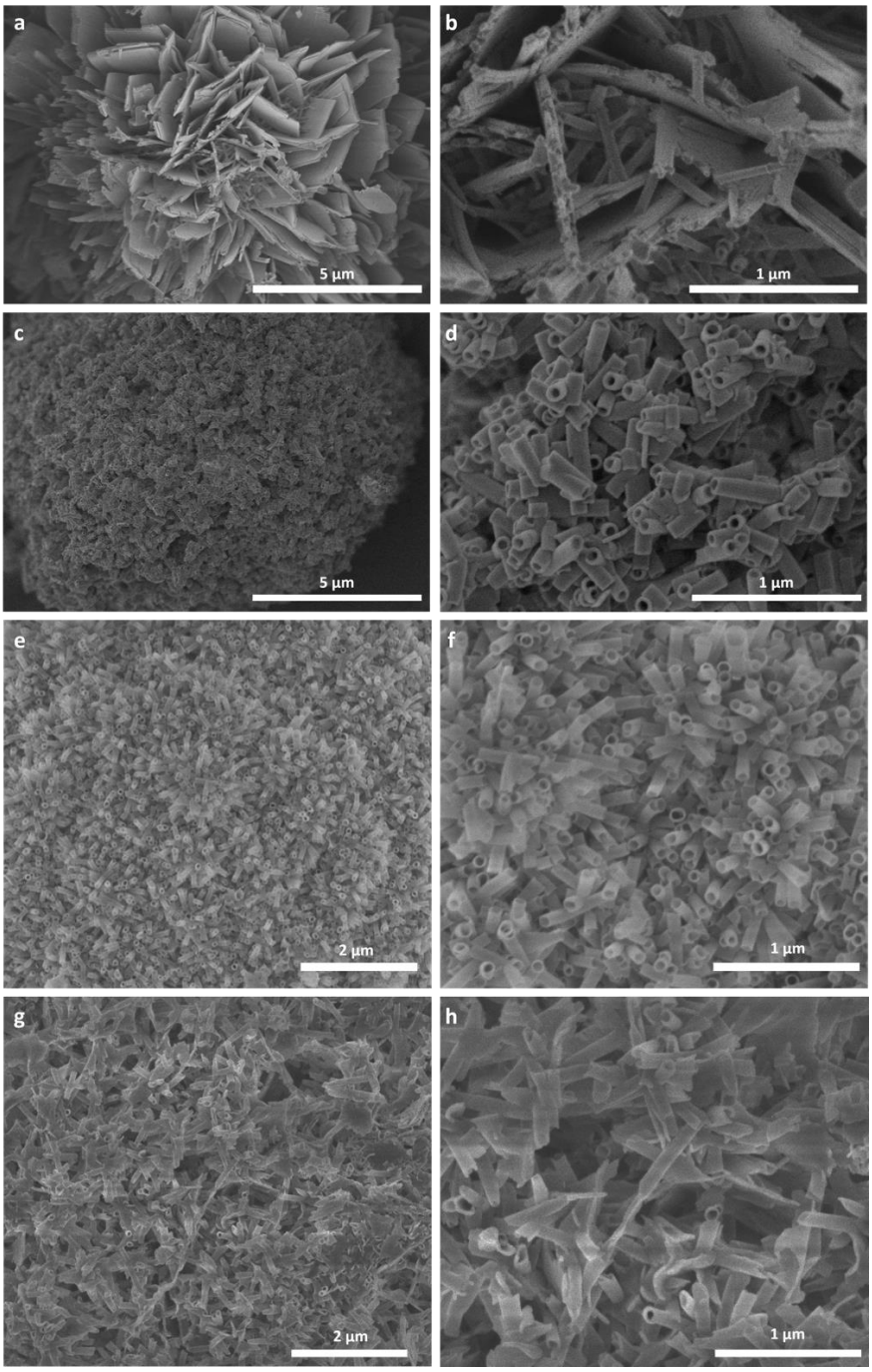

Figure 6-3. Secondary electron (SE) micrographs showing morphologies of hydrothermal synthesis end-products produced at 160 ºC for (a-b) 2 days, (c-d) 3 days, (e-f) 4 days, and (g-h) 7 days.

time increased to 3 days or 4 days, microspherical aggregates of $BaCuSi_4O_{10}$ nanoscrolls (**Figure 6-3**(c-f)) were synthesized. With synthesis time of 7 days, $BaCuSi_4O_{10}$ distorted nanoscrolls and half-rolled nanosheets with broken edges were formed (**Figure 6-3**(g-h)). End-

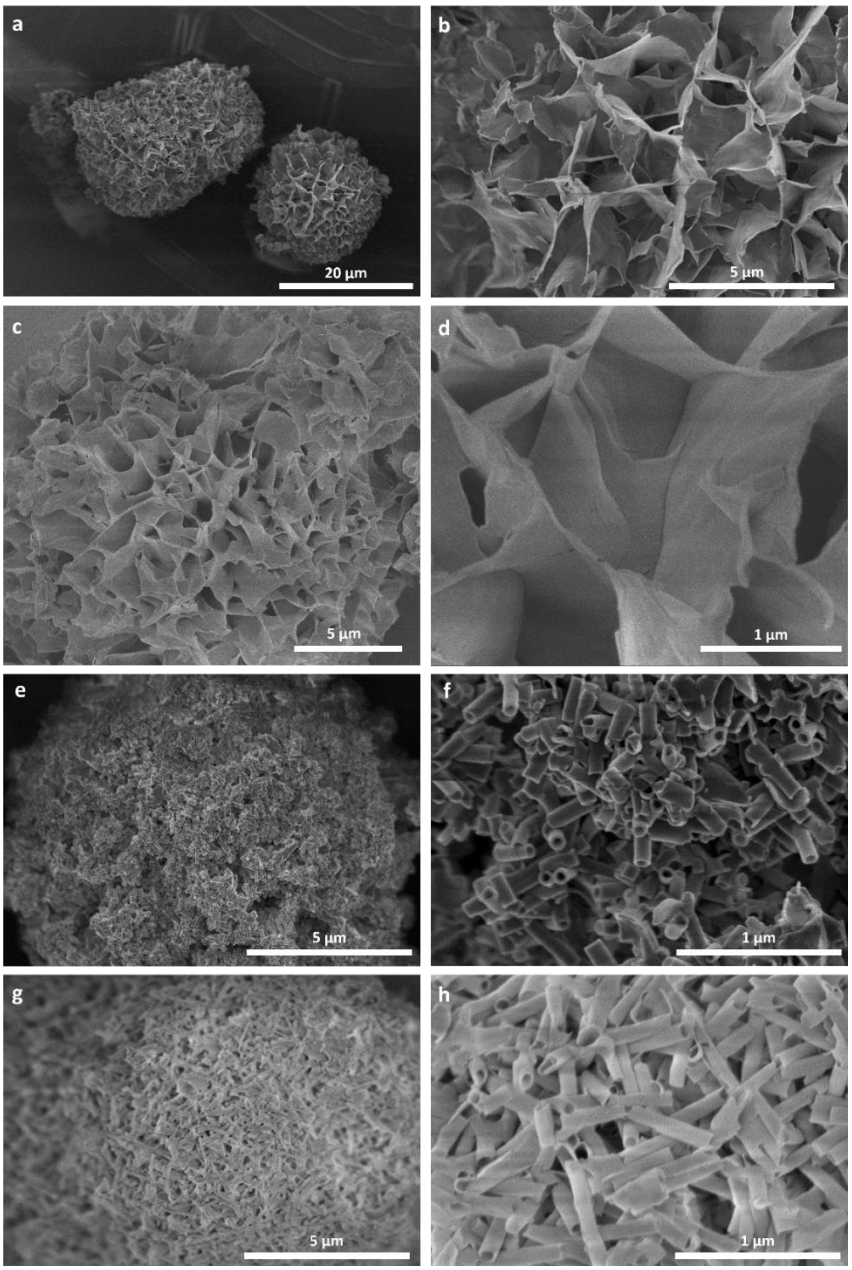

Figure 6-4. SE-SEM micrographs showing morphologies of hydrothermal synthesis end-products produced at 180 ºC for (a-b) 1 day, (c-d) 2 days, (e-f) 3 days, and (g-h) 8.5 days.

products synthesized at 180 ºC with reaction time of 1 day or 2 days, produced inter-connected $BaCuSi_4O_{10}$ nanosheets (**Figure 6-4**(a-d)). At the same synthesis temperature and with synthesis time of 3 or 8.5 days, nanoscrolls of $BaCuSi_4O_{10}$ were produced (**Figure 6-4**(e-f)) and (**Figure 6-4**(g-h)). Deformation of nanoscrolls was also observed in the end-product

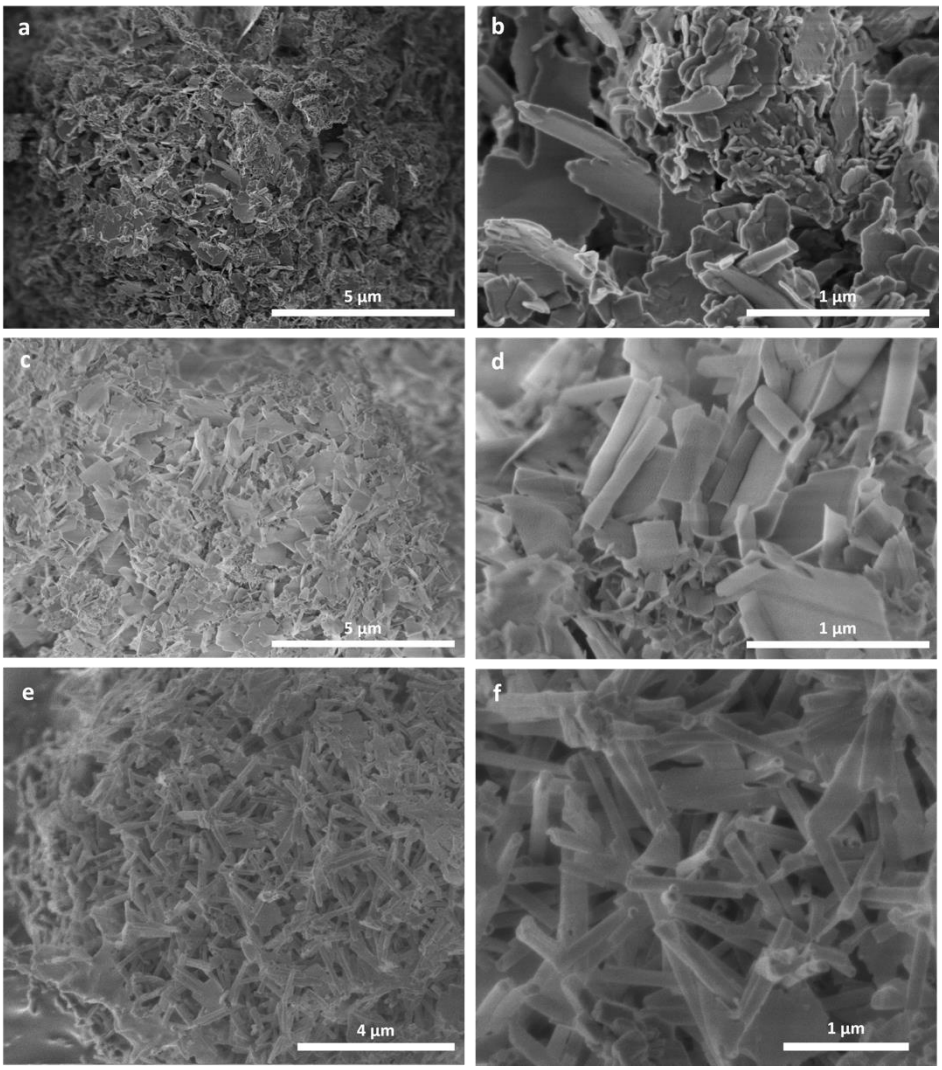

Figure 6-5. Secondary electron (SE) micrographs showing morphologies of hydrothermal synthesis end-products produced at 220 ºC for (a-b) 1 day, (c-d) 2 days, and (e-f) 3 days.

produced with synthesis time of 8.5 days (**Figure 6-4**(h)). A temperature of 220 ºC of synthesis and 1-day synthesis time led to the formation of nanolayers of $BaCuSi_4O_{10}$ with broken and un-defined shapes (**Figure 6-5**(a-b)), while nanoscrolls and half-rolled nanosheets of $BaCuSi_4O_{10}$ were synthesized with reaction time of 2 days (**Figure 6-5**(c-d)). With synthesis time being 3 days, nanoscrolls of $BaCuSi_4O_{10}$ crystals were formed.

The size of $BaCuSi_4O_{10}$ nanoscrolls was strongly affected by the synthesis temperature. For end-products synthesized with reaction time of 3 days and at increasing reaction

temperature, the length of the nanoscrolls increased from ~200 to 400 nm (160 ºC (**Figure 6-3**(c-d)) and 180 ºC (**Figure 6-4**(e-f)) to ~700-900 nm (220 ºC, **Figure 6-5**(e-f)).

Differences in the structure of the walls of $BaCuSi_4O_{10}$ nanoscrolls were also observed. High angle annular dark field (HAADF) STEM micrographs of representative $BaCuSi_4O_{10}$ nanoscrolls (of which elemental composition and stoichiometry were confirmed by EDS) synthesized at 160 ºC for 2 days, revealed that the walls were consisted of one or multiple two-monolayered Ba^{2+} ions with high compositional contrast (**Figure 6-6**(a)). As the nanoscrolls were, however, susceptible to beam-induced damage, direct observation of the atomic arrangement of Cu^{2+} or Si^{4+} ions in the structure was not achievable. It is worth noting that the gap with dark compositional contrast between the neighboring 2-monolayered Ba^{2+} ions (**Figure 6-6**(a)) or the neighboring 3-monolayered Ba^{2+} ions (**Figure 6-6**(b-c)) may be due to intra-layer or inter-layer hydration with water molecules, or may be due to the possible presence of double silicate layers. Given the severe beam damage experienced by the $BaCuSi_4O_{10}$ nanoscrolls and the difficulty to directly observe atomic arrangement of Cu^{2+} or Si^{4+} ions as a result, alternative techniques would be required to investigate the possible types of structure and bonding in the gap between the neighboring 2-monolayered Ba^{2+} ions or the neighboring 3-monolayered Ba^{2+} ions. The average thickness of the two-monolayer Ba atoms was measured to ~1.1 nm. Conversely, $BaCuSi_4O_{10}$ nanoscrolls synthesized at 160 ºC for 3 days (**Figure 6-6**(b)) and at 180 ºC for 8.5 days (**Figure 6-6**(c)) have walls consisting of one or multiple layers of three-monolayer Ba atoms, with average thickness of ~2.3 nm and ~1.9

nm, respectively.

Fast Fourier Transform (FFT) were obtained on the selected areas on the surface of the $BaCuSi_4O_{10}$ nanoscrolls synthesized at 160 ºC for 2 days (**Figure 6-7**(a-b)) and at 180 ºC for 8.5 days (**Figure 6-7**(c-d)). Electron diffraction patterns were indexed, showing that the length of the nanoscrolls was aligned to either the (200) reflections (**Figure 6-7**(b)) or the (020)

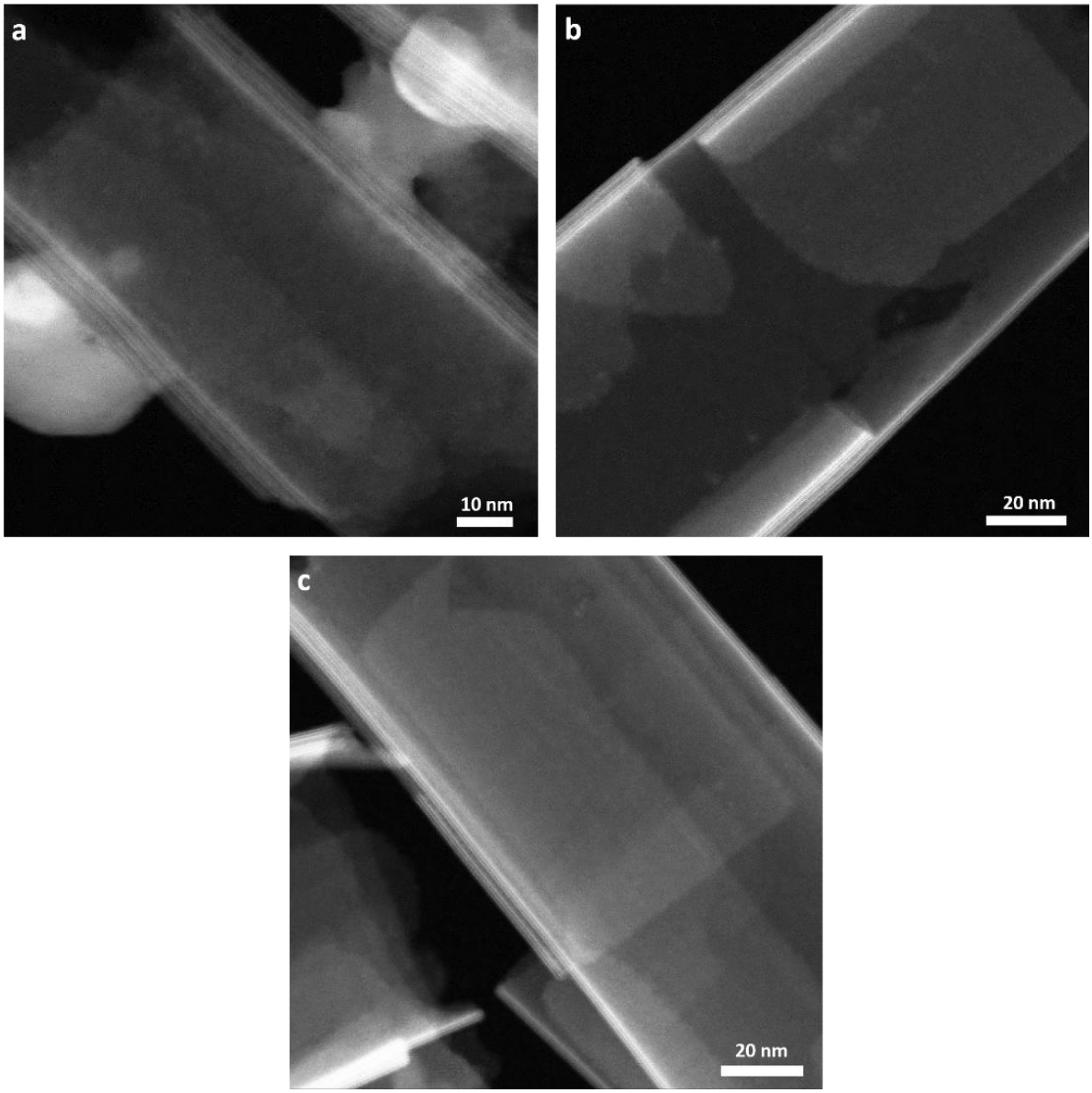

Figure 6-6. HAADF-STEM micrographs of details of representative $BaCuSi_4O_{10}$ nanoscrolls synthesized (a) at 160 ºC for 2 days, (b) at 160 ºC for 3 days, and (c) at 180 ºC for 8.5 days.

reflections (**Figure 6-7**(d)), and that the curvature of the surface of nanoscrolls was perpendicular to the [001] zone axis (**Figure 6-7**(b, d)).

Exfoliation of bulk $CaCuSi_4O_{10}$ has been reported to result in nanosheets with zone axis of [001] [12]. Since the isomorphic $MCuSi_4O_{10}$ family (M = Ba, Sr, or Ca) has perfect cleavage along the {001} family of planes in their sheet silicate structure [25], and based on the various morphologies of end-products observed in this experiment (**Figure 6-3** to **Figure 6-6**), it is likely that the $BaCuSi_4O_{10}$ nanosheets with zone axis of [001] formed first, which were then rolled into $BaCuSi_4O_{10}$ nanoscrolls via some rolling mechanism(s). In this case, the nanoscrolls should have a curvature of surface perpendicular to the <001> direction, which corresponds to the [001] zone axis indexed on the experimentally produced nanoscrolls (**Figure 6-7**(b, d)). In addition, since the length of the nanoscrolls is along the direction of the equivalent <h00> or <0k0> (**Figure 6-7**(b, d)), the rolling of the nanosheets should have taken place along either the equivalent x- or y-direction of the tetragonal unit cell. Therefore, the values of thickness of the two-monolayer Ba atoms observed in **Figure 6-6**(a) and of the three-monolayer Ba atoms observed in **Figure 6-6**(b-c) are expected to correspond to half of the lattice constant c (~0.8 nm) and the lattice constant c (~1.6 nm) [25-28], respectively. However, the values of thickness measured in this study were ~20-40% higher than the theoretical values. Such discrepancy may have been resulted from: 1) the softness of the $BaCuSi_4O_{10}$ nanoscrolls such that STEM images

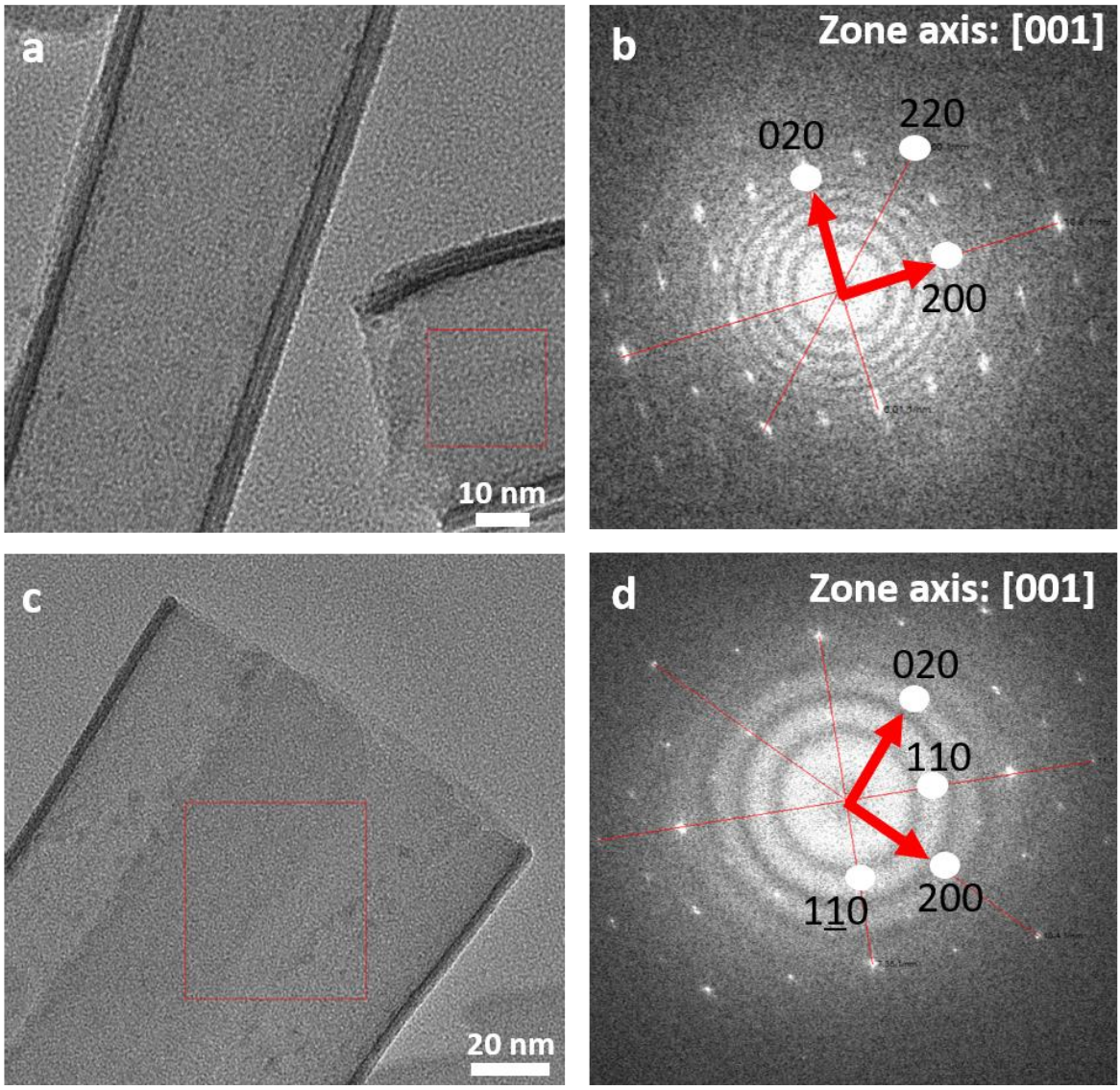

Figure 6-7. (a) A TEM micrograph of two $BaCuSi_4O_{10}$ nanoscrolls synthesized at 160 ºC for 2 days, and (b) a Fast Fourier Transform (FFT) of the area labeled with the red square in (a). (c) A TEM image of two $BaCuSi_4O_{10}$ nanoscrolls synthesized at 180 ºC for 8.5 days, and (d) a FFT of the area labeled with the red square in (c).

of higher magnifications were difficult to obtain to have a more accruement measurement; 2) calibration of the STEM/TEM microscope, and/or 3) from hydration, which has been observed in thickness measurement of the delaminated monolayers of $CaCuSi_4O_{10}$ [12].

Based on such possible formation mechanism of $BaCuSi_4O_{10}$ nanoscrolls, the effects of heat treatment temperature and time on the morphology of $BaCuSi_4O_{10}$ crystals detected in

Phase I may have been related to the quality and size of the nanosheets before rolling. A higher reaction temperature and an optimal reaction time not only drove the formation of $BaCuSi_4O_{10}$ to be more complete with less amount of the intermediate $BaCuSi_2O_6$ as impurity, but also led to formation of $BaCuSi_4O_{10}$ nanosheets with larger sizes and well-defined shapes before rolling into nanoscrolls.

In summary, in Phase I, nanoscrolls of $BaCuSi_4O_{10}$ were successfully produced, with the characteristic Vis-induced NIR photoluminescent property of the bulk $BaCuSi_4O_{10}$ preserved at this nano-scale. A reaction time shorter than 3 days tends to yield broken nanosheets of un-defined shapes as the major morphology (**Figure 6-3**(a-b), **Figure 6-4**(a-d), and **Figure 6-5**(a-d)), whereas, a prolonged heat treatment of 7 days (**Figure 6-3**(g-h)) or 8.5 days (**Figure 6-4**(g-h)) results in nanoscrolls with deformation. In order to optimize the synthesis conditions to produce $BaCuSi_4O_{10}$ nanoscrolls with higher purity and to further investigate other possible factors that may have related to the formation mechanism of the nano-scroll, in Phase II, final pH of the precursor mixture was introduced as the third experimental parameter besides reaction temperature and time.

6.2.2 Phase II: Effect of pH of the precursor mixture on the formation of $BaCuSi_4O_{10}$ nanoscrolls

Since nanoscrolls of $BaCuSi_4O_{10}$ have been successfully synthesized in Phase I at temperatures as low as 160 ºC for 2 or 3 days, during Phase II, the heat treatment temperature

was set to either 160 ºC for 2 or 3 days or at 180 ºC for 3 days partly to conserve energy, and partly to produce nanoscrolls of shorter length (200-400 nm) that can be at dimensions acceptable as luminescent markers in biomedical imaging. It has been reported that with a starting stoichiometry of Ba:Cu:Si = 1:1:4 and with $BaCl_2 \cdot 4H_2O$ solution, CuO powder and $Na_2SiO_3 \cdot 9H_2O$ solution being the Ba, Cu, and Si precursors, a pH value of 12 of the precursor mixture was required to obtain single phase $BaCuSi_4O_{10}$ mesoporous microspheres with reaction temperature of 250 ºC for 48 hours [96]. With pH of the precursor solution below 11, no $BaCuSi_4O_{10}$ was formed in the end-products [96]. With the pH ~11.5, $BaCuSi_2O_6$ was formed as an impurity, whereas at a pH higher than 12, CuO was found as impurity in the end-products [96]. Although the identities and stoichiometry of precursors as well as reaction conditions in this research were different from the previously reported hydrothermal synthesis of $BaCuSi_4O_{10}$ mesoporous microspheres [96], in Phase II, the pH of the precursor mixture was varied in three ranges (~11.0, ~11.5, and ~12.0) to investigate the possible pH effects on the purity of the end-products, as well as, on morphology of nanoscrolls. With the use of a calibrated pH meter instead of pH test strips, the pH values were more precisely controlled in this phase.

XRD results on samples produced at 160 ºC for 2 days indicate at low pH (~11), $BaCuSi_2O_6$ is present as an impurity, and $BaSiO_3$ was found in samples produced at low pH (11.0 and 11.3) as well (**Figure 6-8**(a)). $BaCuSi_4O_{10}$ was found as the single phase in the sample produced at high pH (~11.9) (**Figure 6-8**(a)). However, for samples produced at 160 ºC for 3

days, all three pH's resulted in samples having $BaCuSi_4O_{10}$ as the predominant phase with $BaCuSi_2O_6$ and $BaSiO_3$ as impurities (**Figure 6-8**(b)). With synthesis temperature at 180 ºC for 3 days, for all three pH's, $BaCuSi_4O_{10}$ was found as the predominant phase with $BaSiO_3$ as reaction impurity (**Figure 6-8**(c)).

Secondary electron micrographs show that the pH of the precursor mixture affects strongly the morphology of $BaCuSi_4O_{10}$ crystals in the end-products. With hydrothermal reaction temperature at 160 ºC for 2 days and a precursor mixture with final pH ~11.0 resulted in the formation of microspheres assembled by stacking of $BaCuSi_4O_{10}$ nanolayers with no preferred orientation (**Figure 6-9**(a-b)). When the final pH of the precursor mixture was increased to ~11.3, $BaCuSi_4O_{10}$ nanoscrolls, as well as, partially rolled nanolayers were formed (**Figure 6-9**(c-d)). At a pH of the precursor mixture of ~11.9, the major morphology of observed was

$BaCuSi_4O_{10}$ nanoscrolls with a length < 500 nm (**Figure 6-9**(e-f)).

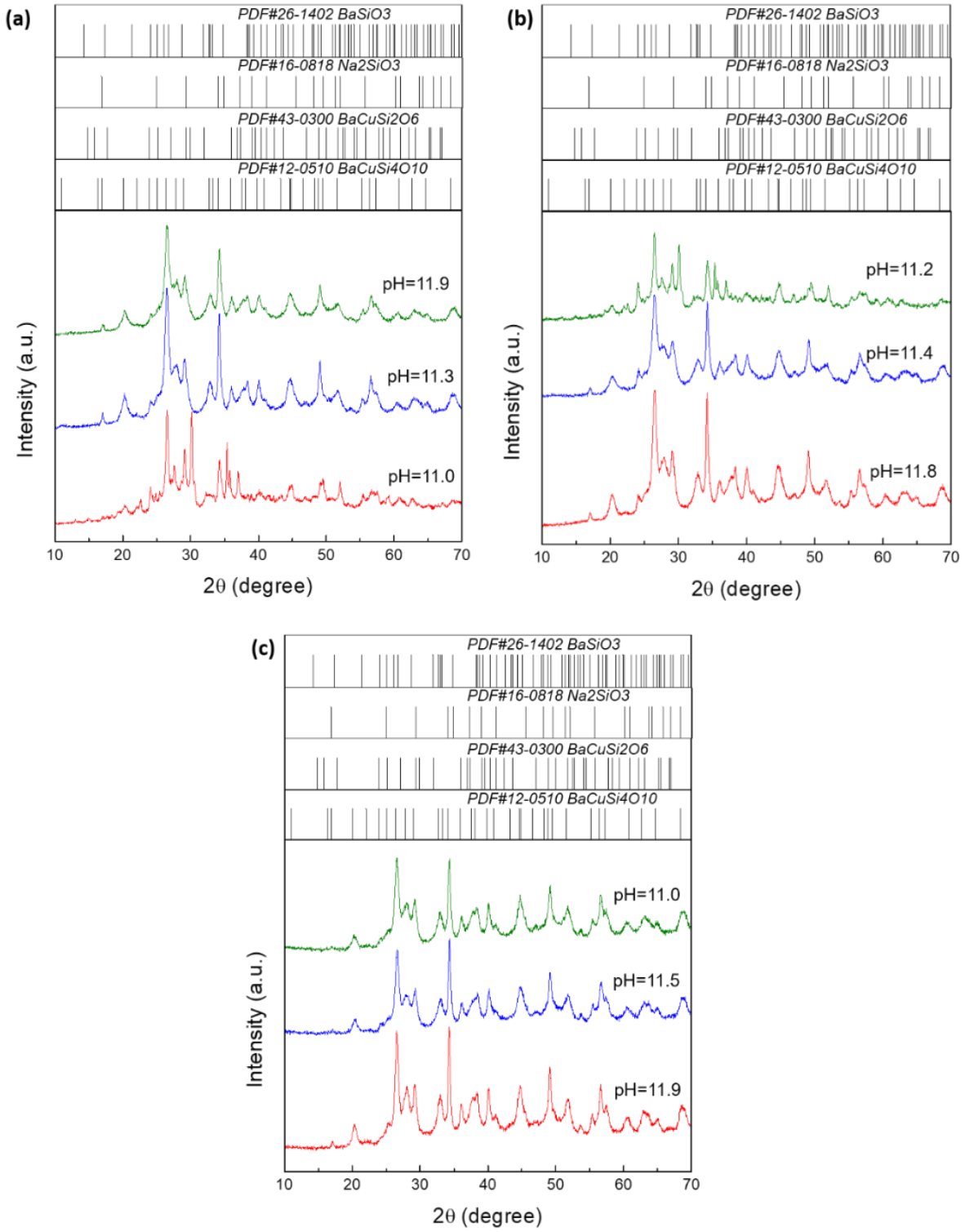

Figure 6-8. XRD diffractograms of powder samples produced (a) at 160 ºC for 2 days, (b) at 160 ºC for 3 days, and (c) at 180 ºC for 3 days, with various pH of the precursor mixture.

The optimal pH of the precursor mixture was different for end-products produced with reaction time of 3 days at 160 ºC. With a pH ~11.2, inter-connected $BaCuSi_4O_{10}$ layers of no defined shapes were formed (**Figure 6-10** (a-b)). With an increase of the pH to ~11.4, inter-connected $BaCuSi_4O_{10}$ layers of no defined shapes predominated (**Figure 6-10** (c-d)). Aggregates of $BaCuSi_4O_{10}$ nanoscrolls were found to be the minor morphology (**Figure 6-10**

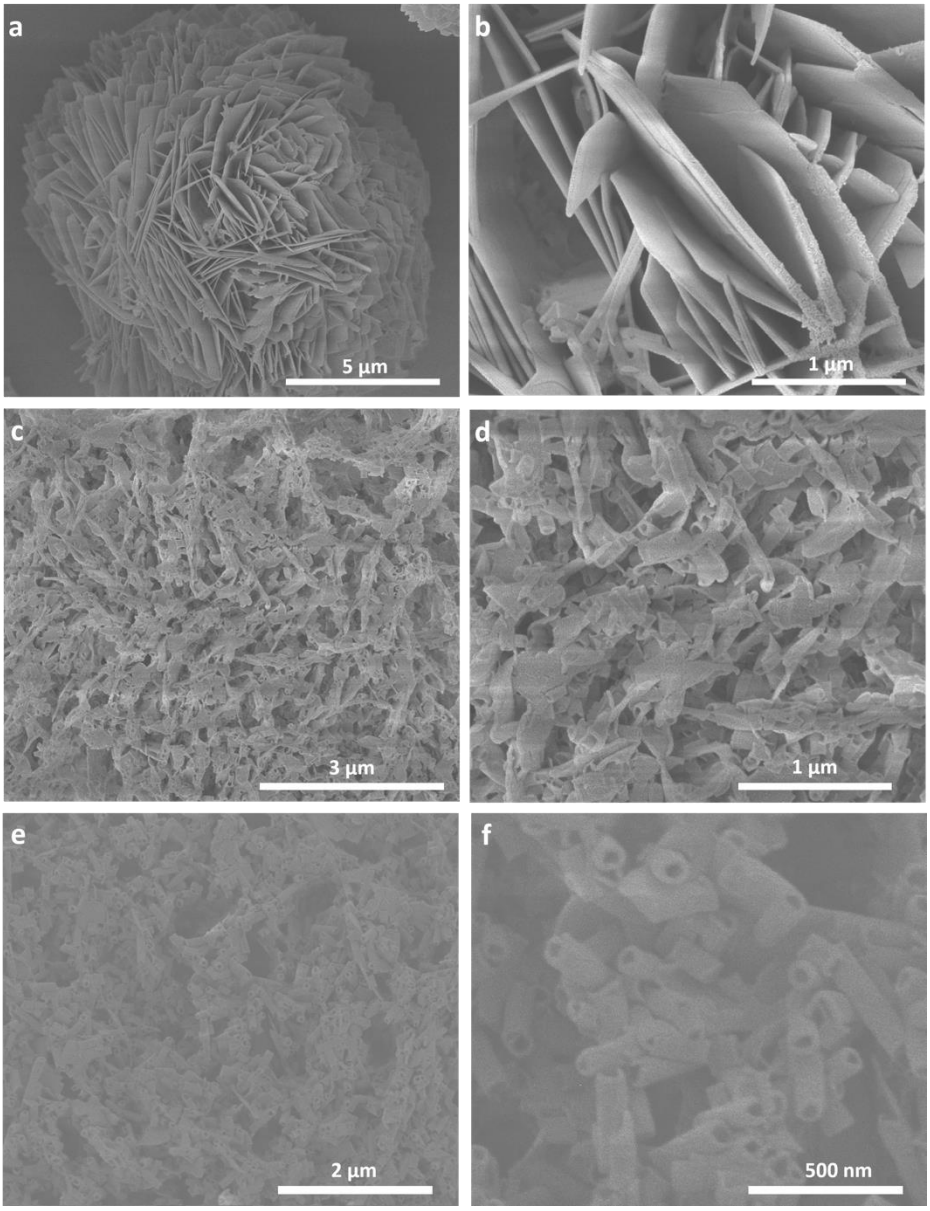

Figure 6-9. Secondary electron (SE) micrographs of hydrothermal synthesis of $BaCuSi_4O_{10}$ at 160 ºC for 2 days, with final pH of the precursor mixture being (a-b) 11.0, (c-d) 11.3, and (e-f) 11.9.

(e-f)). When the pH was increased to ~11.8, $BaCuSi_4O_{10}$ microspheres of interconnected nanolayers were synthesized (**Figure 6-10** (g-h)). At a hydrothermal synthesis temperature of

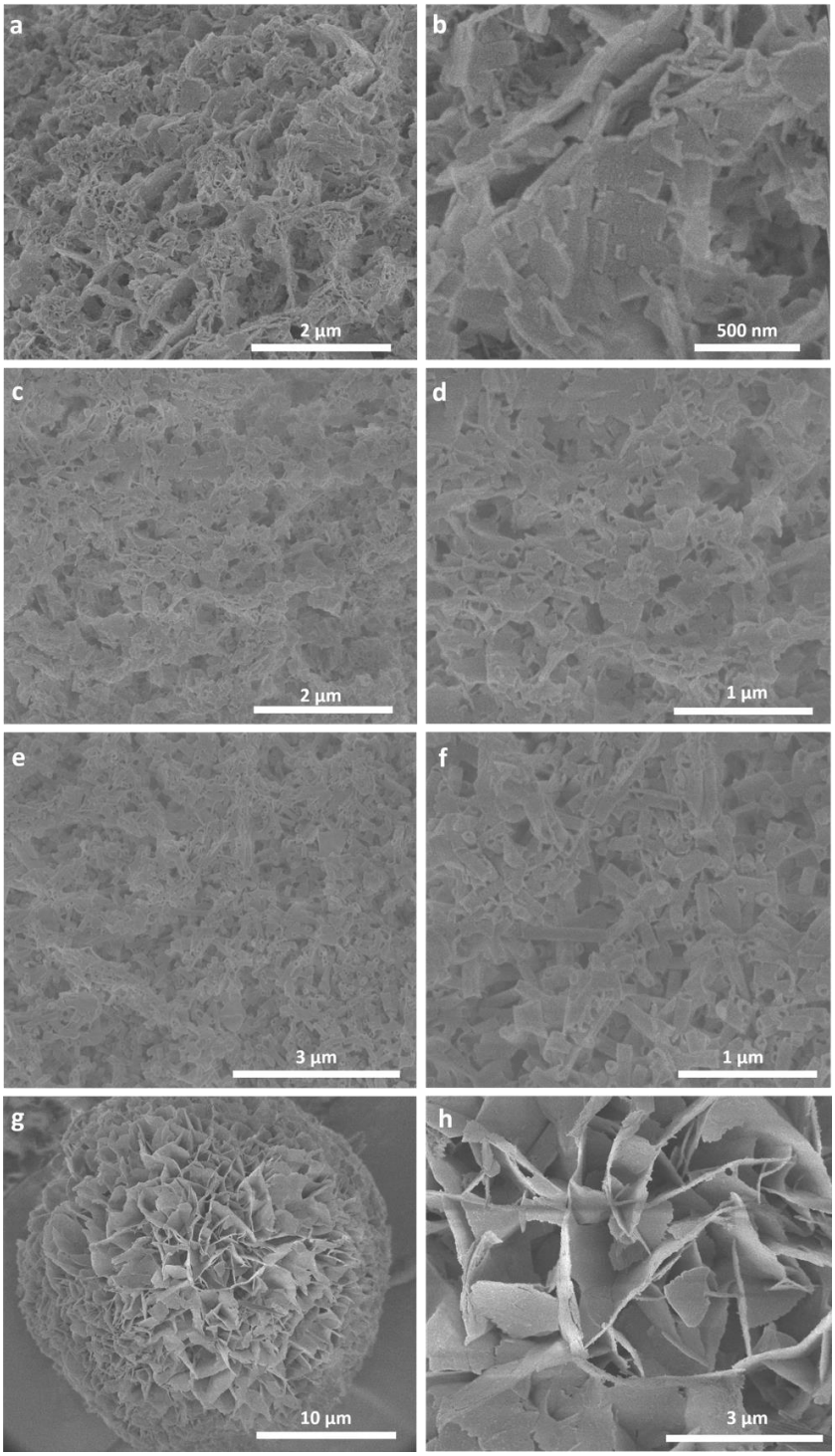

Figure 6-10. Secondary electron (SE) micrographs of hydrothermal synthesis of $BaCuSi_4O_{10}$ at 160 ºC for 3 days, with final pH of the precursor mixture being (a-b) 11.2, (c-f) 11.4, and (g-h) 11.8.

180 ºC, reaction time of 3 days, and pH of ~11.0, the major phase formed was $BaCuSi_4O_{10}$ microspheres of inter-connected layers with no defined shapes (**Figure 6-11**(a-b)). When pH was increased to ~11.5, the major phase consisted of rolled nanolayers of $BaCuSi_4O_{10}$ (**Figure**

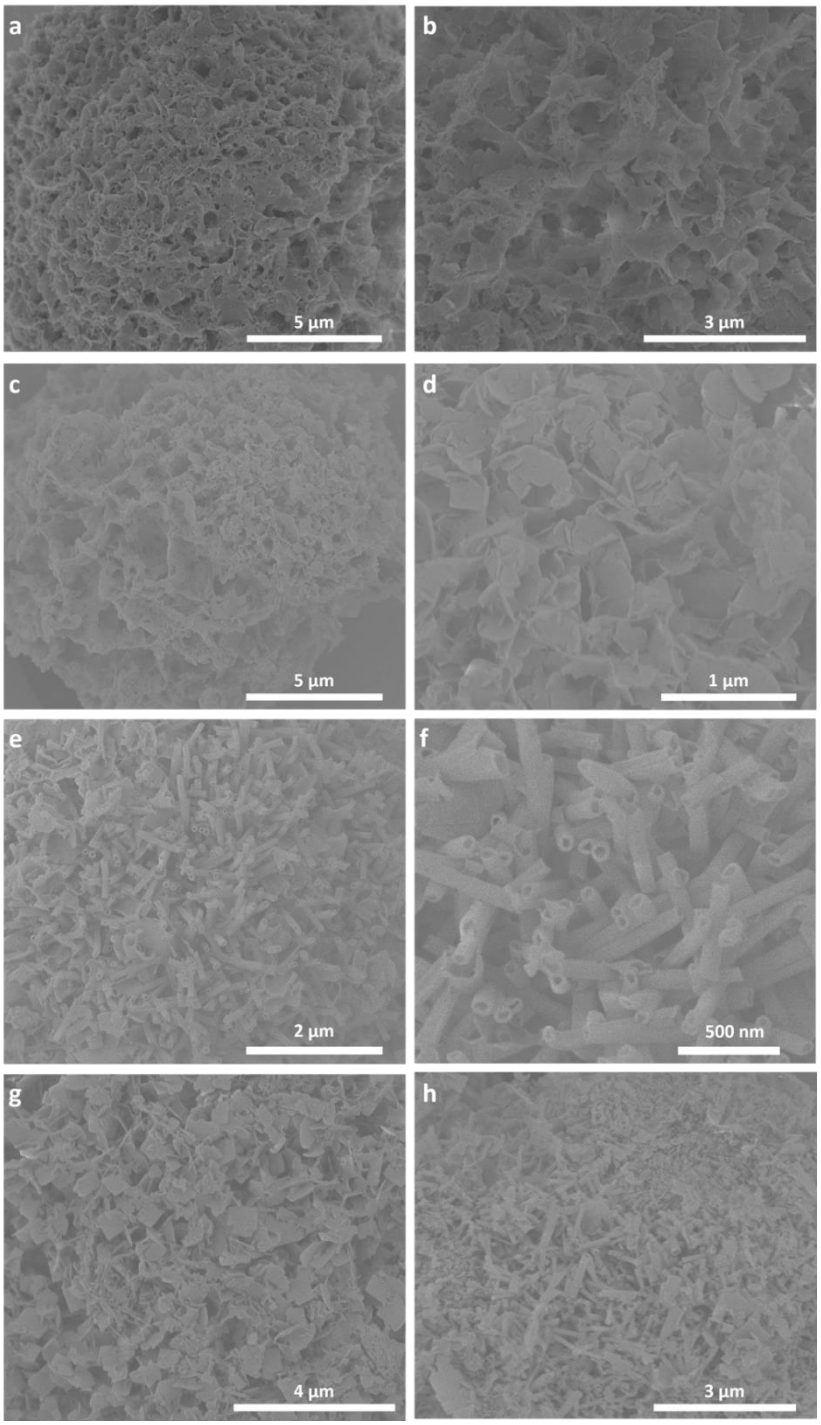

Figure 6-11. SE-SEM micrographs of hydrothermal synthesis of $BaCuSi_4O_{10}$ at 180 ºC for 3 days, with final pH of the precursor mixture being (a-b) 11.0, (c-f) 11.5, and (g-h) 11.9.

6-11(c-d)), with nanoscrolls being the minor phase (**Figure 6-11**(e-f)). When pH was increased to ~11.9, both phases could be seen in the end-products (**Figure 6-11**(g-h)). Nanoscrolls, however, were deformed and broken (**Figure 6-11**(h)).

From these experiments, it can be concluded that the pH of the precursor mixture strongly affects the morphology of the $BaCuSi_4O_{10}$ crystals for a given synthesis temperature and time. In an alkaline environment with pH in the range between 11 and 12, any silicates on the surface are expected to remain as deprotonated with negative charge. If both surfaces of the nanosheets were predominated by silicate layers, these nanosheets would remain stable and suspended in the solution from neighboring nanosheets of the same type due to charge repulsion. If such stable state was disturbed by factors such as pH of the solution, the nanosheets would be destabilized and tend to twist, bend and roll into more stable forms, a similar conformational change that has been observed in the rolling of 2D graphene nanosheets into nanoscrolls [161]. Once the new bonds between the Ba^{2+} or Cu^{2+} and the SiO_4^{4-} tetrahedra or between the two silicate layers are established, the as-rolled $BaCuSi_4O_{10}$ nanosrcolls would be stabilized in such morphology. If the two surfaces of the nanosheets were not of the same type and after the lateral growth of the nanosheets reaching a certain size, the intrinsic tension resulting from the asymmetric nanosheets could have also induced curling and rolling of the nanosheets into nanoscrolls in order to lower the strain energy, based on a rolling mechanism that has been previously proposed for the formation of TiO_2 nanotubes from nanosheets [162, 163]. The possible bonding and intra-layer structure between the neighboring 2-monolayered Ba^{2+} ions

(**Figure 6-6**(a)) or the neighboring 3-monolayered Ba^{2+} ions (**Figure 6-6**(b-c)) suggested in the Phase I experiments, would, however, require further investigation.

In summary, with pH being one of the parameters in Phase II of exploration, the optimal conditions of synthesis of $BaCuSi_4O_{10}$ nanoscrolls was determined to be at 160 ºC for 2 days, with pH~11.9. It has been previously reported that mesoporous microspheres assembled by $BaCuSi_4O_{10}$ nanosheets instead of nanoscrolls have been produced via hydrothermal synthesis at 250 ºC for 2 days, with starting stoichiometry of Ba:Cu:Si being 1:1:4 and final pH of the precursor mixture being 12 [96]. Although in this experimental research, the initial purpose to start with excess silicate was to promote the formation of $BaCuSi_4O_{10}$, the possible effects of excess silicate on formation and morphology of $BaCuSi_4O_{10}$ nanoscrolls will be explored in the future.

6.3 Conclusions

This research synthesized nanoscrolls of $BaCuSi_4O_{10}$ via a one-step hydrothermal method for the first time, with the characteristic intrinsic Vis-induced NIR photoluminescence observed on the bulk $BaCuSi_4O_{10}$. The purity and morphology of the $BaCuSi_4O_{10}$ nanoscrolls was strongly dependent on the synthesis temperature and time, as well as the pH of the precursor mixture. The optimal synthesis conditions to form $BaCuSi_4O_{10}$ nanoscrolls has been determined at a heat treatment of 160 ºC for 2 days, at a pH of the precursor mixture ~11.9.

Results from Phase I and Phase II, indicated that $BaCuSi_4O_{10}$ nanoscrolls were likely to

have formed via a rolling mechanism of the $BaCuSi_4O_{10}$ nanosheets. After the formation of the nanosheets, destabilization may have occurred, leading to the rolling of the nanosheets into nanoscrolls to lower surface stress and/or energy. Once rolled, nanoscrolls may have been stabilized by forming new intra-layer bonds on the overlaps between the as-rolled nanosheets, and aggregated into microspheres with no preferred orientation. Experimental parameters that seem to affect the formation mechanism include hydrothermal synthesis temperature and time, as well as final pH of the precursor mixture.

In order to further investigate the formation mechanism and to optimize the morphology and purity of $BaCuSi_4O_{10}$ nanoscrolls, a more systematic study will be performed in the next phase. Besides varying the heat treatment conditions and the pH of the precursor mixture in a systematic way, the possible effects of the starting stoichiometry of Ba:Cu:Si on the formation of $BaCuSi_4O_{10}$ nanoscrolls will also be explored.

Chapter 7. Conclusions and future work

This research based on materials science methods and principles shed new light on the production technology and raw material selection for the manufacture of Chinese blue, a sintered polycrystalline material (frit) and imaged for the first time, the atomic arrangement of its major silicate phase, $BaCuSi_4O_{10}$ corresponding to effenbergerite mineral. The characterization of ancient Chinese blue at the micron to submicron level with scanning transmission electron and transmission electron microscopy coupled with energy dispersive X-ray spectroscopy (STEM/TEM-EDS) revealed the presence of micron or submicron-sized $BaSO_4$, $(Ba,Pb)SO_4$ solid solution, Pb_3O_4, and amorphous SiO_2 inclusions whose formation are closely related to the raw materials and manufacturing process (operational sequence and conditions). From a chemical point of view and from the possible formation mechanisms it is most likely that the natural mineral witherite ($BaCO_3$) was preferred over the most abundant $BaSO_4$ as the source for Ba, though $BaSO_4$ might have been introduced in the pigment as an impurity of the witherite deposits. Galena (PbS) and/or anglesite ($PbSO_4$) were the possible mineral resources for Pb and S. The systematic laboratory-based reproduction experiment of Chinese blue and Chinese purple substantiated the hypothesis of the use of the scarcely occurring witherite mineral in the single-step processing experiments. Experiments also indicated that the direct use of galena (PbS) for the production of Chinese purple was challenging. Ancient contemporary bronzes, $PbO\text{-}BaO\text{-}SiO_2$ system glasses, and medicinal Pb-containing compounds may have provided the technological bases for the possible pre-

treatment of galena into a Pb-compound. The pre-treatment helps produce Chinese blue and Chinese purple with high purity. Pb stable isotope analysis with laser ablation inductively multi-collector coupled plasma mass spectrometry (LA-MC-ICP/MS) suggested that the Pb-source used in the production of the Chinese blue and Chinese purple faience beads from the Majiayuan Cemetery has its origin to the same or similar source as six other Chinese blue and Chinese purple samples, and to 19 PbO-BaO-SiO_2 glass samples from the Jiangsu Province dated to the Western Han Dynasty.

Research applying materials engineering processing for the modern reproduction of $BaCuSi_4O_{10}$ using hydrothermal synthesis produced $BaCuSi_4O_{10}$ nanoscrolls with length < 500 nm. The purity and morphology of the $BaCuSi_4O_{10}$ nanoscrolls was strongly dependent on the synthesis temperature and time, as well as the pH of the precursor mixture. Visible light induced near infrared (Vis-induced NIR) imaging has shown that the $BaCuSi_4O_{10}$ nanoscrolls preserved the characteristic NIR photoluminescence of the bulk materials. The nanoscrolls are likely to have formed from the rolling of $BaCuSi_4O_{10}$ nanosheets during the hydrothermal synthesis, with the rolling mechanism affected by the heat treatment conditions and the pH of the precursor mixture.

Future work on the reconstruction of ancient production technology of Chinese blue will be focused on trace elemental analysis and rare earth elemental analysis to compliment the Pb stable isotope analysis for geosourcing of the Pb-source. Trace and rare earth elemental analyses on both archaeological Chinese blue and mineral samples from the witherite belt in

China will also be performed and compare, to prove or disprove the hypothesis that witherite was the Ba-source in ancient production. Additional experimental parameters such as different starting stoichiometry of Ba:Cu:Si as well as different amounts of Pb-source will be introduced in the next phase reproduction experiment, in order to evaluate their effects on the production of Chinese blue and Chinese purple to gain a better insight in the original raw materials selection and synthesis conditions. Specifically, pre-treatment of $BaSO_4$ will be explored based on the modern thermal reduction industrial processing to further evaluate the possibility that whether barite can be made chemically suitable as the Ba-source through pre-treatment that can be reasonably achieved in the ancient times.

The next phase on the manufacture of $BaCuSi_4O_{10}$ nanoscrolls will be focused on a systematic synthesis to further investigate the formation mechanisms and to optimize the morphology and purity of the nanoscrolls. Future work will also be focused on the evaluation of photophysical properties and thermal and mechanical stability of the $BaCuSi_4O_{10}$ nanoscrolls to investigate their performance in as optical materials and in biomedical applications.

Bibliography

1. Brill, R.H., I.L. Barnes, and E.C. Joel, *Chapter 5 Lead isotope studies of early Chinese glasses*, in *Scientific Research in Early Chinese Glass: Proceedings of the Archaeometry of Glass Sessions of the 1984 International Symposium on Glass, Beijing, September 7, 1984, with Supplementary Papers*, R.H. Brill and J.H. Martin, Editors. 1991, The Corning Museum of Glass: Corning, New York. p. 65-91.
2. Brill, R.H., et al., *Addendum to Chapter 5*, in *Scientific research in early Chinese glass*, R.H. Brill and J.H. Martin, Editors. 1991, The Corning Museum of Glass: Corning, New York. p. 84-89.
3. Li, Q., Z. Li, and D. Gu, *Archaeological and technical study of Western Han dynasty lead barium glass chimes (Bian Qing) unearthed from the Jiangdu King's mausoleum*, in *Recent advances in the scientific research on ancient glass and glaze*. 2016, World Scientific. p. 113-127.
4. Cui, J., X. Wu, and B. Huang, *Chemical and lead isotope analysis of some lead-barium glass wares from the Warring States Period, unearthed from Chu tombs in Changde City, Hunan Province, China.* Journal of Archaeological Science, 2011. **38**(7): p. 1671-1679.
5. Cui, J., et al., *Chemical and Lead Isotope Analysis of Glass Wares Found in Lijiaba Site, Yunyang County, Chongqing City*, in *Recent Advances in the Scientific Research*

on Ancient Glass and Glaze. 2016, World Scientific. p. 179-192.

6. Brill, R.H. and H. Shirahata, *The second Kazuo Yamasaki TC-17 lecture on Asian glass: recent lead-isotope analyses of some Asian glasses with remarks on strontium-isotope analyses*, in *Ancient glass research along the Silk Road*. 2009, World Scientific. p. 149-164.

7. Xia, Y., et al., *Development of Chinese barium copper silicate pigments during the Qin Empire based on Raman and polarized light microscopy studies.* Journal of Archaeological Science, 2014. **49**: p. 500-509.

8. Berke, H., *The invention of blue and purple pigments in ancient times.* Chemical Society Reviews, 2007. **36**(1): p. 15-30.

9. Berke, H. and H.G. Wiedemann, *The chemistry and fabrication of the anthropogenic pigments Chinese blue and purple in ancient China.* East Asian Science, Technology, and Medicine, 2000(17): p. 94-120.

10. Wiedemann, H.G. and H. Berke. *Chemical and physical investigations of Egyptian and Chinese blue and purple*. in *The polychromy of antique sculptures and the terracotta army of the first Chinese emperor: studies on materials, painting techniques and conservation. International conference in Xi'an, Shaanxi History Museum, March 22-28, 1999*. 2001. Lipp.

11. Pozza, G., et al., *Photoluminescence of the inorganic pigments Egyptian blue, Han blue and Han purple.* Journal of Cultural Heritage, 2000. **1**(4): p. 393-398.

12. Johnson-McDaniel, D., et al., *Nanoscience of an ancient pigment.* Journal of the American Chemical Society, 2013. **135**(5): p. 1677-1679.

13. Laurie, A.P., W.F.P. Mclintock, and F. Miles, *Egyptian blue.* Proc. R. Soc. Lond. A, 1914. **89**(612): p. 418-429.

14. Riederer, J., *Recently identified Egyptian pigments.* Archaeometry, 1974. **16**(1): p. 102-109.

15. Tite, M., M. Bimson, and N. Meeks, *Technological characterisation of Egyptian blue.* ArchéoSciences, revue d'Archéométrie, 1981. **1**(1): p. 297-301.

16. Tite, M., M. Bimson, and M. Cowell, *Technological examination of Egyptian blue.* Advances in chemistry series, 1984. **205**: p. 215-242.

17. Tite, M.S., *Characterisation of early vitreous materials.* Archaeometry, 1987. **29**(1): p. 21-34.

18. Pradell, T., et al., *Physical processes involved in production of the ancient pigment, Egyptian blue.* Journal of the American Ceramic Society, 2006. **89**(4): p. 1426-1431.

19. Hatton, G.D., A.J. Shortland, and M.S. Tite, *The production technology of Egyptian blue and green frits from second millennium BC Egypt and Mesopotamia.* Journal of Archaeological Science, 2008. **35**(6): p. 1591-1604.

20. Kakoulli, I., *Greek painting techniques and materials from the fourth to the first century BC*. 2009: Archetype Publications.

21. Kakoulli, I., *Egyptian blue in Greek painting between 2500 and 50 BC*. 2009: na.

22. Wiedemann, H.-G. and H. Berke, *Chemical and physical investigations of Egyptian and Chinese blue and purple.* Monuments and Sites, 1999. **3**: p. 154-171.

23. Ullrich, D. *Egyptian blue and green frit: characterization, history and occurrence, synthesis*. in *Pact*. 1987.

24. Le Chatelier, A.F., *Verfahren zur Herstellung von grünen, blauen und violetten Mineralfarben aus Kieselsäure und Baryum un Kupferverbindungen, D. R. P. 112761,* in *Deutsches Reichspatent*. 1899: Germany.

25. Pabst, A., *Structures of some tetragonal sheet silicates.* Acta crystallographica, 1959. **12**(10): p. 733-739.

26. Lin, H., F. Liao, and S. Wang, *Structure of BaCuSi4O10.* Acta Crystallographica Section C: Crystal Structure Communications, 1992. **48**(7): p. 1297-1299.

27. Janczak, J. and R. Kubiak, *Refinement of the structure of barium copper silicate BaCu [Si4O10] at 300 K.* Acta Crystallographica Section C: Crystal Structure Communications, 1992. **48**(7): p. 1299-1301.

28. Chakoumakos, B.C., J.A. Fernandez-Baca, and L.A. Boatner, *Refinement of the structures of the layer silicates MCuSi4O10 (M= Ca, Sr, Ba) by Rietveld analysis of neutron powder diffraction data.* Journal of Solid State Chemistry, 1993. **103**(1): p. 105-113.

29. Bayer, G. and H. Wiedemann, *Bildung und Stabilität von Ägyptisch Blau (Cuprorivait).* Naturwissenschaften, 1975. **62**(4): p. 181-182.

30. Giester, G. and B. Rieck, *Effenbergerite, BaCu [Si_4O_{10}], a new mineral from the Kalahari Manganese Field, South Africa: description and crystal structure.* Mineralogical Magazine, 1994. **58**(393): p. 663-670.

31. Sheng, Z. and A. Hermann, *Superconductivity in the rare-earth-free Tl–Ba–Cu–O system above liquid-nitrogen temperature.* Nature, 1988. **332**(6159): p. 55-58.

32. Sheng, Z. and A. Hermann, *Bulk superconductivity at 120 K in the Tl–Ca/Ba–Cu–O system.* Nature, 1988. **332**(6160): p. 138.

33. Hazen, R., et al., *100-K superconducting phases in the Tl-Ca-Ba-Cu-O system.* Physical Review Letters, 1988. **60**(16): p. 1657.

34. Finger, L., R. Hazen, and R. Hemley, *BaCuSi 2 O 6; a new cyclosilicate with four-membered tetrahedral rings.* American Mineralogist, 1989. **74**(7-8): p. 952-955.

35. Janczak, J. and R. Kubiak, *Structure of the cyclic barium copper silicate Ba2Cu2 [Si4O12] at 300 K.* Acta Crystallographica Section C: Crystal Structure Communications, 1992. **48**(1): p. 8-10.

36. Rieck, B., H. Pristacz, and G. Giester, *Colinowensite, BaCuSi2O6, a new mineral from the Kalahari Manganese Field, South Africa and new data on wesselsite, SrCuSi4O10.* Mineralogical Magazine, 2015. **79**(7): p. 1769-1778.

37. Britvin, S., et al., *New minerals and nomenclature modifications approved in 2012 and 2013.* Mineralogical Magazine, 2013. **77**(1): p. 1-12.

38. Rieck, B., *Colinowensite, IMA 2012-060. CNMNC Newsletter No. 15, February 2013,*

page 6. 2013.

39. FitzHugh, E.W. and L.A. Zycherman, *An early man-made blue pigment from China—barium copper silicate.* Studies in Conservation, 1983. **28**(1): p. 15-23.

40. FitzHugh, E.W. and L.A. Zycherman, *A purple barium copper silicate pigment from early China.* Studies in conservation, 1992. **37**(3): p. 145-154.

41. Ma, Q., et al., *Raman and SEM studies of man-made barium copper silicate pigments in ancient Chinese artifacts.* Studies in conservation, 2006. **51**(2): p. 81-98.

42. Cheng, X., et al., *Three fabricated pigments (Han purple, indigo and emerald green) in ancient Chinese artifacts studied by Raman microscopy, energy‐dispersive X‐ray spectrometry and polarized light microscopy.* Journal of Raman Spectroscopy, 2007. **38**(10): p. 1274-1279.

43. Liu, Z., et al., *Influence of Taoism on the invention of the purple pigment used on the Qin terracotta warriors.* Journal of Archaeological Science, 2007. **34**(11): p. 1878-1883.

44. 马清林, 张治国, and 高西省, *洛阳战国墓出土八棱柱中的中国蓝和中国紫研究.* 文物, 2008(8): p. 83-88.

45. 夏寅, et al., *山东危山西汉墓出土陶器彩绘颜料研究*. 2008.

46. Berke, H., et al., *Man-made ancient Chinese Blue and Purple pigments.* 文博, 2009. **6**: p. 251-265.

47. 张治国, 马., Heinz Berke, *山东青州西汉彩绘陶俑紫色颜料研究.* 文物, 2010(9):

p. 87-93.

48. 李沫, *战国秦汉时期费昂斯制品的制备及铅钡玻璃研究*. 2014, 北京化工大学.

49. Ma, Q., et al., *Microstructure and Composition of Ancient Chinese Octagonal Sticks from the Warring States Period (475–221 BC)*, in *Recent Advances in the Scientific Research on Ancient Glass and Glaze*. 2016, World Scientific. p. 455-488.

50. 林怡娴, et al., *张家川马家塬战国墓地出土玻璃与相关材料研究*. 文物, 2018(3): p. 71-83.

51. Sun, F., M.-l. Sun, and X.-c. Zhao, *Technological Analyses of the Violet Pigments in the Site of Eastern Gate Tower of Han Yang Mausoleum (in Chinese).* SPECTROSCOPY AND SPECTRAL ANALYSIS, 2018. **38**(5): p. 1588-1591.

52. Koezuka, T. *Investigation of ancient glasses found in Japan - Historical evolution of ancient glass systems*. in *Proceedings: Internatoinal Congress on the Conservation and Restoration for Archaeological Objects, 2002*. 2002. Nara: Independent Administrative Institution, Nara National Research Institute for Cultural Properties.

53. 徐军平, et al., *东平汉墓壁画制作工艺初探*. 文博, 2009. **2009**(6): p. 211-215.

54. 冯健, 夏., Catharina Blaensdorf, Susana Greiff, *西安理工大学曲江校区西汉壁画墓颜料分析研究*. 西北大学学报: 自然科学版, 2012. **42**(5): p. 771-776.

55. 付强, et al., *河南宝丰和新郑出土硅酸盐制品的无损分析研究*. 光谱学与光谱分析, 2014. **34**(01): p. 257-262.

56. 黄晓娟, 严静, and 王辉, *甘肃马家塬战国墓地 M4 出土硅酸盐珠饰的科学分析*

研究. 光谱学与光谱分析, 2015. **35**(10): p. 2895-2900.

57. Li, Q., et al., *Identification of the man-made barium copper silicate pigments among some ancient Chinese artifacts through spectroscopic analysis.* Spectrochimica Acta Part A: Molecular and Biomolecular Spectroscopy, 2015. **138**: p. 609-616.

58. 王雪培, et al., *古代多色硅酸盐制品的光谱学分析及方法学研究.* 光谱学与光谱分析, 2016. **36**(12): p. 4045-4051.

59. Fenn, P.M., R.H. Brill, and M. Shi, *Addendum to Chapter 4*, in *Scientific Research in Early Chinese Glass: Proceedings of the Archaeometry of Glass Sessions of the 1984 International Symposium on Glass, Beijing, September 7, 1984, with Supplementary Papers.* , R.H. Brill and J.H. Martin, Editors. 1991, The Corning Museum of Glass: Corning, New York. p. 59-64.

60. Bouherour, S., H. Berke, and H.-G. Wiedemann, *Ancient man-made copper silicate pigments studied by Raman microscopy.* Chimia International Journal for Chemistry, 2001. **55**(11): p. 942-951.

61. Zuo, J., et al., *Analysis of the pigments on painted pottery figurines from the Han Dynasty's Yangling Tombs by Raman microscopy.* Journal of Raman Spectroscopy, 2003. **34**(2): p. 121-125.

62. Thieme, C., et al. *Research on paint materials, paint techniques and conservation experiments on the polychrome terracotta army of the First Emperor Qin Shi Huang*. in *The ceramics cultural heritage: proceedings of the international symposium*. 1995.

TECHNA.

63. Herm, C., et al. *Analysis of painting materials of the polychrome terracotta army of the first Emperor Qin Shi Huang*. in *The ceramics cultural heritage: proceedings of the international symposium*. 1995. TECHNA.

64. Janczak, J., R. Kubiak, and T. Głowiak, *Structure of barium copper pyrosilicate at 300 K.* Acta Crystallographica Section C: Crystal Structure Communications, 1990. **46**(8): p. 1383-1385.

65. Tsukada, I., et al., *$BaCu_2Si_2O_7$: A quasi-one-dimensional S=1/2 antiferromagnetic chain system.* Physical Review B, 1999. **60**(9): p. 6601.

66. Yang, H., et al., *Scottyite, the natural analog of synthetic BaCu2Si2O7, a new mineral from the Wessels mine, Kalahari Manganese Fields, South Africa.* American Mineralogist, 2013. **98**(2-3): p. 478-484.

67. Malinovskij, Y.A. *Crystal structure of Ba2CuSi2O7*. in *Soviet Physics Doklady*. 1984.

68. Du, J., et al., *Synthesis and structure of a new polymorph Ba2CuSi2O7.* Chinese Journal of Structural Chemistry, 2003. **22**(1): p. 33-36.

69. Wiedemann, H.G. and G. Bayer. *Formation and stability of Chinese barium copper-silicate pigments*. in *Conservation of ancient sites on the Silk Road: proceedings of an international conference on the conservation of grotto sites..., Dunhuang, the People's Republic of China, 3-8 October 1993*. 1997. Getty Conservation Institute.

70. Brill, R.H., S.S. Tong, and D. Dohrenwend, *Chapter 4 Chemical analyses of some*

early Chinese glasses, in *Scientific Research in Early Chinese Glass: Proceedings of the Archaeometry of Glass Sessions of the 1984 International Symposium on Glass, Beijing, September 7, 1984, with Supplementary Papers.* , R.H. Brill and J.H. Martin, Editors. 1991, The Corning Museum of Glass: Corning, New York. p. 31-58.

71. Zhang, Z., et al., *Simulation Synthesis of Ancient Chinese Artificial Barium Copper Silicate Pigments.* Journal of National Museum of China, 2012. **2**: p. 013.

72. Li, M., J. Wang, and Q. Ma, *The effect of lead additives on ancient Chinese Purple pigment synthesis.* Journal of Cultural Heritage, 2015. **16**(4): p. 575-578.

73. Qin, Y., et al., *A Discussion on the Emergence and Development of Ancient Chinese Artificial Barium Copper Silicate Pigments from Simulation Experiments.* Archaeometry, 2016. **58**(5): p. 796-806.

74. Ostroff, A. and R. Sanderson, *Thermal stability of some metal sulphates.* Journal of Inorganic and Nuclear Chemistry, 1959. **9**(1): p. 45-50.

75. Sajadi, S.A.A., *A comparative investigation of lead sulfate and lead oxide sulfate study of morphology and thermal decomposition.* American Journal of Analytical Chemistry, 2011. **2**(02): p. 206.

76. Kolta, G. and M. Askar, *Thermal decomposition of some metal sulphates.* Thermochimica Acta, 1975. **11**(1): p. 65-72.

77. 陈茜, 秦颖, and 李小莉, *天然矿物合成“中国紫”过程中的变温 XRD 分析.* 光谱学与光谱分析, 2012. **32**(04): p. 1111-1113.

78. Barnard, N. and S. Tamotsu, *Alloy constituents and ore distribution*, in *Metallurgical remains of ancient China*. 1975, Nichiosha: Tokyo. p. 16-27.

79. Tylecote, R.F., *Metallurgy in archaeology: A prehistory of metallurgy in the British Isles*. 1962, London: E. Arnold.

80. 赵匡华, 张清健, and 郭保章, *中国古代的铅化学.* 自然科学史研究, 1990(3): p. 248-257.

81. Rosenfeld, A., *The inorganic raw materials of antiquity*. 1965, New York: Praeger.

82. 陈有年, *陕南寒武系下统鲁家坪组毒重石矿产出的基本特性.* 陕西地质科技情报, 1989(3): p. 28-38.

83. 孙兴文 and 李瑞贞, *陕西紫阳黄柏树湾毒重石矿床地质特征.* 陕西地质, 1990(A01): p. 77-88.

84. Wang, Z. and G. Li, *Barite and witherite deposits in Lower Cambrian shales of South China; stratigraphic distribution and geochemical characterization.* Economic Geology, 1991. **86**(2): p. 354-363.

85. Qin, Y., et al., *The research of burning ancient Chinese lead-barium glass by using mineral raw materials.* Journal of Cultural Heritage, 2016. **21**: p. 796-801.

86. 魏国锋, *古代青铜器矿料来源与产地研究的新进展.* 合肥: 中国科技大学出版社, 2007.

87. Tite, M., A. Shortland, and P. Vandiver, *Raw materials and fabrication methods used in the production of Faience.* Tite, MS y Shortland, A. J., Production Technology of

Faience and Related Early Vitreous Materials, Oxford, 2008: p. 37-55.

88. Henderson, J., *The raw materials of early glass production.* Oxford Journal of Archaeology, 1985. **4**(3): p. 267-291.

89. Brems, D. and P. Degryse, *Trace Element Analysis in Provenancing Roman Glass‐Making.* Archaeometry, 2014. **56**(S1): p. 116-136.

90. 李家治, *我国古代陶器和瓷器工艺发展过程的研究.* 考古, 1978(3): p. 179-188.

91. 李家治, *我国瓷器出现时期的研究.* 硅酸盐学报, 1978. **6**(3): p. 190-198.

92. Verri, G., *The spatially resolved characterisation of Egyptian blue, Han blue and Han purple by photo-induced luminescence digital imaging.* Analytical and bioanalytical chemistry, 2009. **394**(4): p. 1011-1021.

93. Kakoulli, I., et al., *Application of forensic photography for the detection and mapping of Egyptian blue and madder lake in Hellenistic polychrome terracottas based on their photophysical properties.* Dyes and Pigments, 2017. **136**: p. 104-115.

94. Accorsi, G., et al., *The exceptional near-infrared luminescence properties of cuprorivaite (Egyptian blue).* Chemical Communications, 2009(23): p. 3392-3394.

95. Johnson-McDaniel, D. and T.T. Salguero, *Exfoliation of Egyptian blue and Han blue, two alkali earth copper silicate-based pigments.* Journal of visualized experiments: JoVE, 2014(86).

96. Chen, Y., et al., *Hydrothermal synthesis, hierarchical structures and properties of blue pigments SrCuSi 4 O 10 and BaCuSi 4 O 10.* CrystEngComm, 2014. **16**(24): p. 5418-

5423.

97. Pansare, V.J., et al., *Review of long-wavelength optical and NIR imaging materials: contrast agents, fluorophores, and multifunctional nano carriers.* Chemistry of materials, 2012. **24**(5): p. 812-827.

98. 周广济, et al., *2006 年度甘肃张家川回族自治县马家塬战国墓地发掘简报.* 文物, 2008. **9**: p. 003.

99. 王辉, *发现西戎——甘肃张家川马家塬墓地.* 中国文化遗产, 2007. **6**: p. 015.

100. 周广济, et al., *张家川马家塬战国墓地 2007~ 2008 年发掘简报.* 文物, 2009. **10**: p. 002.

101. 王辉, et al., *张家川马家塬战国墓地 2008~ 2009 年发掘简报.* 文物, 2010. **10**: p. 003.

102. 谢焱 and 刘兵兵, *张家川马家塬战国墓地 2010~ 2011 年发掘简报.* 文物, 2012. **8**: p. 003.

103. Pauling, L. and P.H. Emmett, *The crystal structure of barite.* Journal of the American Chemical Society, 1925. **47**(4): p. 1026-1030.

104. Colville, A. and S. K, *A refinement of structure of barite*. 1967, MINERALOGICAL SOC AMER 1015 EIGHTEENTH ST, NW SUITE 601, WASHINGTON, DC 20036. p. 1877-&.

105. Hill, R., *A further refinement of the barite structure.* The Canadian Mineralogist, 1977. **15**(4): p. 522-526.

106. Lee, J.-S., et al., *Crystal structure and Raman spectral studies of BaSO4—PbSO4 solid solution.* Zeitschrift für Kristallographie-Crystalline Materials, 2005. **220**(1): p. 1-9.

107. Berke, H., *Chemistry in ancient times: the development of blue and purple pigments.* Angewandte Chemie International Edition, 2002. **41**(14): p. 2483-2487.

108. Lin, Y., et al., *Systematic laboratory-based reproduction of Chinese blue to reveal raw materials selection and synthesis conditions (Presentation)*, in *42,d International Symposium on Archaeometry (ISA 2018)* 2018: Merida, Yucatan, Mexico.

109. Rostoker, W., V.C. Pigott, and J.R. Dvorak, *Direct reduction to copper metal by oxide-sulfide mineral interaction.* Archaeomaterials, 1989. **3**(1): p. 69-87.

110. Huff, L.C. and T. Lovering, *Migration of lead during oxidation and weathering of lead deposits.* Geological Survey Professional Paper, 1976. **957**: p. 21-24.

111. Ponsot, B., J. Salomon, and P. Walter, *RBS study of galena thermal oxidation in air with a 6-MeV 16O3+ ion beam.* Nuclear Instruments and Methods in Physics Research Section B: Beam Interactions with Materials and Atoms, 1998. **136**: p. 1074-1079.

112. Martinetto, P., et al., *In situ RBS study of the kinetics of galena thermal oxidation by means of 4He external micro-beam.* Nuclear Instruments and Methods in Physics Research Section B: Beam Interactions with Materials and Atoms, 2001. **181**(1-4): p. 703-706.

113. Sadovnikov, S., N. Kozhevnikova, and A. Rempel, *Oxidation of nanocrystalline lead sulfide in air.* Russian Journal of Inorganic Chemistry, 2011. **56**(12): p. 1864-1869.

114. Jaeger, F. and H. Germs, *III. Über die binären Systeme der Sulfate, Chromate, Molybdate und Wolframate des Bleies.* Zeitschrift für anorganische und allgemeine Chemie, 1921. **119**(1): p. 145-173.

115. Schenck, R. and W. Rassbach, *Über die chemischen Gleichgewichte bei der Reaktion zwischen Bleisulfid und seinen Oxydationsprodukten III.* Berichte der deutschen chemischen Gesellschaft, 1908. **41**(2): p. 2917-2925.

116. Hofman, H. and W. Wanjukow, *The decomposition of metallic sulphates at elevated temperatures in a current of dry air.* Bull. Am. Inst. Min. Eng, 1912. **77**: p. 889.

117. Nichols, M. and B. White, *Decomposition Temperatures of Some Analytical Precipitates: Calcium Carbonate and Lead Sulfate.* Industrial & Engineering Chemistry Analytical Edition, 1941. **13**(4): p. 251-256.

118. Malinowski, C., *Analysis of the chemical reaction between PbSO4 and PbS.* Thermochimica acta, 1987. **119**(2): p. 329-336.

119. Grahmann, W., *Vergleich der Sulfate der Erdalkalien und des Bleis in den Temperatur‐Konzentrationsdiagrammen mit Kaliumsulfat unter besonderer Berücksichtigung der Dimorphie von Anhydrit, Cölestin, Baryt und Anglesit.* Zeitschrift für anorganische Chemie, 1913. **81**(1): p. 257-314.

120. Okamoto, Y., *Report on the survey of hokutolite.* Publication of the Productive

Bureau, Government-General of Taiwan, 1916. **115**.

121. Courtin-Nomade, A., et al., *Evidence for the incorporation of lead into barite from waste rock pile materials*. Environmental science & technology, 2008. **42**(8): p. 2867-2872.

122. James, R.W. and W. Wood, *The crystal structure of barytes, celestine and anglesite.* Proc. R. Soc. Lond. A, 1925. **109**(752): p. 598-620.

123. Dove, P.M. and C.A. Czank, *Crystal chemical controls on the dissolution kinetics of the isostructural sulfates: Celestite, anglesite, and barite.* Geochimica et Cosmochimica Acta, 1995. **59**(10): p. 1907-1915.

124. Wang, H.-R., J.-S. Lee, and S.-C. Yu, *Synthesis of zoning-free BaSO4-PbSO4 solid solution and its structural characterizations.* Zeitschrift für Kristallographie-Crystalline Materials, 2002. **217**(4): p. 143-148.

125. White, W.B. and R. Roy, *Phase Relations in the System Lead—Oxygen.* Journal of the American Ceramic Society, 1964. **47**(5): p. 242-249.

126. Risold, D., J.-I. Nagata, and R. Suzuki, *Thermodynamic description of the Pb-O system.* Journal of phase equilibria, 1998. **19**(3): p. 213-233.

127. McLaren, K., *XIII—The development of the CIE 1976 (L* a* b*) uniform colour space and colour‐difference formula.* Journal of the Society of Dyers and Colourists, 1976. **92**(9): p. 338-341.

128. Russell Jr, R., C. Valencia, and H. Emrich, *Barite in Ceramic Whitewares.* Journal of

the American Ceramic Society, 1956. **39**(2): p. 73-82.

129. Gruver, R., *Differential Thermal‐Analysis Studies of Ceramic Materials: III, Characteristic Heat Effects of Some Sulfates.* Journal of the American Ceramic Society, 1951. **34**(11): p. 353-357.

130. Hackspill, L. and G. Wolf, *Sur la décomposition thermique des carbonates de baryum.* Comptes rendus hebdomadaires des séances de l'Académie des sciences, 1937. **204**: p. 1820-1822.

131. Cuthbert, F. and R.A. Rowland, *Differential thermal analysis of some carbonate minerals.* American Mineralogist: Journal of Earth and Planetary Materials, 1947. **32**(3-4): p. 111-116.

132. Gruver, R., *Differential Thermal‐Analysis Studies of Ceramic Materials: I, Characteristic Heat Effects of Some Carbonates.* Journal of the American Ceramic Society, 1950. **33**(3): p. 96-101.

133. Lander, J., *The Phase System BaO-BaCO3.* Journal of the American Chemical Society, 1951. **73**(12): p. 5893-5894.

134. Arvanitidis, I., D. Siche, and S. Seetharaman, *A study of the thermal decomposition of BaCO 3.* Metallurgical and materials transactions B, 1996. **27**(3): p. 409-416.

135. Antao, S.M. and I. Hassan, *BaCO 3: high-temperature crystal structures and the Pmcn→ R3m phase transition at 811 C.* Physics and Chemistry of Minerals, 2007. **34**(8): p. 573-580.

136. Birch, F., J.F. Schairer, and H.C. Spicer, *Handbook of physical constants*. Vol. 36. 1942: Geological Society of America.

137. Baker, E., *137. The barium oxide–carbon dioxide system in the pressure range 0.01—450 atmospheres.* Journal of the Chemical Society (Resumed), 1964: p. 699-704.

138. 张治国, et al., *中国古代人造硅酸铜钡颜料研究进展.* 中国文物科学研究, 2011. **4**: p. 012.

139. Henderson, J., J. An, and H. Ma, *The archaeometry and archaeology of ancient Chinese glass: a review.* Archaeometry, 2018. **60**(1): p. 88-104.

140. Peretti, E.A., *Thermal decomposition of lead carbonate.* Journal of the American Ceramic Society, 1957. **40**(5): p. 171-173.

141. Ball, M.C. and M.J. Casson, *Thermal studies on lead (II) salts—I: Stoichiometry of lead carbonate decomposition at 1 atm. pressure.* Journal of Inorganic and Nuclear Chemistry, 1975. **37**(12): p. 2253-2255.

142. Sarig, S. and F. Kahana, *Thermal decomposition of basic lead carbonate.* Thermochimica Acta, 1976. **14**(3): p. 263-268.

143. Živković, Ž., *Kinetics and mechanism of thermal decomposition of lead carbonate.* Journal of Thermal Analysis and Calorimetry, 1979. **16**(1): p. 3-11.

144. Yamaguchi, J., et al., *Thermal decomposition of cerussite (PbCO3) in carbon dioxide atmosphere (0–50 ATM).* Thermochimica Acta, 1980. **35**(3): p. 307-313.

145. Criado, J., M. Gonzalez, and M. Macías, *Influence of CO2 pressure on the kinetics of*

thermal decomposition of PbCO3. Thermochimica acta, 1987. **113**: p. 39-47.

146. Ahmed, M., H. Fjellvåg, and A. Kjekshus, *On synthesis, structure, and thermal stability of mercury and lead sulfates and oxide sulfates.* Thermochimica acta, 2002. **390**(1-2): p. 113-121.

147. Lander, J.J., *The basic sulfates of lead.* Journal of The Electrochemical Society, 1949. **95**(4): p. 174-186.

148. Esdaile, J., *The Lead Oxide‐Lead Sulfate System.* Journal of The Electrochemical Society, 1966. **113**(1): p. 71-75.

149. Billhardt, H., *New data on basic lead sulfates.* Journal of The Electrochemical Society, 1970. **117**(5): p. 690-692.

150. Hoschek, G., *Die thermische Zersetzung von PbS in Luft.* Neues Jahrbuch für Mineralogie. Monatshefte, 1962(3/4): p. 68-76.

151. Hoschek, G., *Die thermische Zersetzung der Sulfide und Sulfate zweiwertiger Kationen in Luft: Cu-, Zn-, Cd-, Hg-, Sn-und Pb-Verbindungen.* Monatshefte für Chemie und verwandte Teile anderer Wissenschaften, 1962. **93**(4): p. 826-840.

152. Abdel-Rehim, A., *Thermal and XRD analysis of Egyptian galena.* Journal of thermal analysis and calorimetry, 2006. **86**(2): p. 393-401.

153. Di Febo, R., et al., *The production of a lead glaze with galena: Thermal transformations in the PbS–SiO2 system.* Journal of the American Ceramic Society, 2018. **101**(5): p. 2119-2129.

154. Roberts, H. and F.H. Smyth, *THE SYSTEM COPPER: CUPRIC OXIDE: OXYGEN.* Journal of the American Chemical Society, 1921. **43**(5): p. 1061-1079.

155. Gadalla, A., W. Ford, and J. White, *Equilibrium relationships in the system CuO–Cu2O–SiO2.* Trans. Brit. Ceram. Soc, 1963. **62**(1): p. 45-66.

156. Eric, H. and M. Timucin, *Equilibrium relations in the system nickel oxide-copper oxide.* Metallurgical Transactions B, 1979. **10**(4): p. 561-563.

157. Boudene, A., et al., *Experimental investigation and thermochemical assessment of the system Cu-O.* Zeitschrift für Metallkunde, 1992. **83**(9): p. 663-668.

158. Hallstedt, B., D. Risold, and L.J. Gauckler, *Thermodynamic assessment of the copper-oxygen system.* Journal of phase equilibria, 1994. **15**(5): p. 483-499.

159. Stos-Gale, Z.A. and N.H. Gale, *Metal provenancing using isotopes and the Oxford archaeological lead isotope database (OXALID).* Archaeological and Anthropological Sciences, 2009. **1**(3): p. 195-213.

160. Kent, A.J., *In-situ analysis of Pb isotope ratios using laser ablation MC-ICP-MS: Controls on precision and accuracy and comparison between Faraday cup and ion counting systems.* Journal of Analytical Atomic Spectrometry, 2008. **23**(7): p. 968-975.

161. Shin, Y.-E., et al., *An ice-templated, pH-tunable self-assembly route to hierarchically porous graphene nanoscroll networks.* Nanoscale, 2014. **6**(16): p. 9734-9741.

162. Wei, M., et al., *Formation of nanotubes TiO 2 from layered titanate particles by a soft*

chemical process. Solid State Communications, 2005. **133**(8): p. 493-497.

163. Zhang, S., et al., *Formation Mechanism of H 2 T i 3 O 7 Nanotubes.* Physical review letters, 2003. **91**(25): p. 256103.